LABORATOIRE DE GLACIOLOGIE
ET GEOPHYSIQUE DE L'ENVIRONNEMENT
UMR 5183
Centre National de la Recherche Scientifique
Université Joseph Fourier
54, rue Molière- Domaine Universitaire BP 96
38402 – St Martin d'Hères Cedex (France)

UNIVERSITA DEGLI STUDI DI SIENA
SCUOLA DI DOTTORATO DI RICERCA IN SCIENZE POLARI
XX CICLO
Dipartimento di Scienze della Terra dell Università di Siena
Via del laterino 8
53100 – Siena (Italia)

UNIVERSITA CA'FOSCARI DI VENEZIA
Dipartimento di Scienze Ambientali/CNR
Dorsoduro
2137- Venezia (Italia)

EVOLUTION NATURELLE DES ELEMENTS PRESENTS A L'ETAT DE TRACES (METAUX LOURDS, METALLOIDES,TERRES RARES (REE) ET ISOTOPES DU PLOMB DANS LA CAROTTE DE GLACE EPICA/DOME C (ANTARCTIQUE DE L'EST) DE 263,000 A 671,000 ANS AVANT NOS JOURS

NATURALI CAMBI PASSATI IN ELEMENTI DI TRACCIA, DI TERRE RARE (REE), MERCURIO E GLI ISOTOPI DEL PIOMBO NELL'EPICA/DOME C GHIACCO (ANTARTIDE ORIENTALE) DA 263,000A 671,000 ANNI FA

PAST NATURAL CHANGES IN TRACE ELEMENTS, RARE EARTH ELEMENTS (REE), MERCURY AND PB ISOTOPES IN THE EPICA/DOME C ICE CORE (EAST ANTARCTICA) FROM 263,000 TO 671,000 YRS BP

Alexandrine MARTEEL

Thèse de doctorat de l'Université Joseph Fourier (Grenoble1)

(Arrêtés ministériels du 5 juillet 1984 et 30 mars 1992)

en co-tutelle avec l'Università degli Studi di Siena (Italia) et l'Università Ca'Foscari di Venezia (Italia)

Spécialité: Sciences de la Terre, de l'Univers et de l'Environnement
Specialità : Scienze Polari

Date de soutenance : 14 décembre 2007

Compositon du jury :

M. John PLANE	Rapporteur
M. Jozef PACYNA	Rapporteur
M. Claude BOUTRON	Examinateur
M. Carlo BARBANTE	Examinateur

Università degli Studi di Siena
Scuola di Dottorato di Ricerca in Scienze Polari

XX Ciclo

Past natural changes in Trace element, Rare Earth Elements (REE), mercury and Pb isotopes in the EPICA/Dome C ice core (East Antarctica) from 263,000 to 671,000 yrs BP

Candidata: dott. Alexandrine MARTEEL

Dipartimento di Scienze della Terra, Università degli Studi di Siena
Laboratoire de Glaciologie et Géophysique de l'Environnement, Université Joseph Fourier, Grenoble

Tutore: prof. Claude Boutron
Laboratoire de Glaciologie et Géophysique de l'Environnement, Université Joseph Fourier, Grenoble

prof. Carlo Alberto Ricci
Dipartimento di Scienze della Terra, Università degli Studi di Siena

Co-Tutore : prof. Carlo Barbante
Dipartimento di Scienze Ambientali, Ca'Foscari Università di Venezia

Università degli Studi di Siena
Scuola di Dottorato di Ricerca in Scienze Polari

XX Ciclo

Collegio dei docenti

Carlo Baroni
Riccardo Cattaneo-Vietti
Mariachiara Chiantore
Simonetta Corsolini
Silvano Focardi
Luigi Folco
Francesco M. Faranda
Roberto Frache
Francesco Francioni
Giovanna Giorgetti
Marcello Mellini
Rosaria Palmeri
Paolo Povero
Carlo Alberto Ricci (Coordinatore)
Giancarlo Spezie
Franco M. Talarico
Sergio Tucci
Patrizia Vigni

Data dell'esame finale

14 Dicembre 2007

Commissione giudicatrice

Prof. Josef Pacyna - Department of Center for Ecological Economics, Norwegian Institute for Air Research, Kjeller

Prof. John Plane – School of Chemistry, University of Leeds

Prof. Carlo Barbante – Dipartimento di Scienze Ambientali, Ca'Foscari Università di venezia

Prof. Claude Boutron – Laboratoire de Glaciologie et Géophysique de l'Environnement, Université Joseph Fourier, Grenoble

« Freedom is not worth having if it does not include the freedom to make mistakes »
Mahatma Gandhi

« Every day I remind myself that my inner and outer life are based on the labors of other men, living and dead, and that I must exert myself in order to give in the same measure as I have received and am still receiving »
Albert Einstein

« Every day you may make progress. Every step may be fruitful. Yet there will stretch out before you an ever-lengthening, ever-ascending, ever-improving path. You know you will never get to the end of the journey. But this, so far from discouraging, only adds to the joy and glory of the climb »
Sir Winston Churchill

« If you would be a real seeker after truth, it is necessary that at least once in your life you doubt, as far as possible, all things »
René Descartes

ACKNOWLEDGEMENTS

Writing is not solitary work, and it is not stationary business. This text has taken me to many places and has put me in touch with many people. The journey undertaken when pursuing a Ph.D. is a long and arduous one. Fortunately those who provide support, motivation, knowledge, friendship and love, make the trip through the long research and writing process more bearable and very rewarding. It is to these remarkable people I welcome the opportunity to give thanks.

I am very grateful for the support of Prof. Claude Boutron, one of mine supervisor who encouraged me to embark on this journey. He has been a great teacher and initiator.

For his easy-going attitude, yet thorough professionalism, I thank Prof. Carlo Barbante for his supervision, adding skilled guidance and bright ideas on many levels to this work.

I wish to thank the University of Siena by the way of Carlo Alberto Ricci for granting me the opportunity to conduct my research within this prestigious institution. I would also like to acknowledge the many people in the doctoral school of Siena and particularly Mrs Jacqueline Müller who have shown great kindness and support, both academically and administratively over the years.

Prof. John Plane and Prof. Jozef Pacyna are thanked for accepting of being part of my PhD commission.

Hearty thanks go to Prof. Christophe Ferrari, Dr. Aurélien Dommergue, Prof. Dominique Raynaud and Prof. Jean-Robert Petit of the Laboratory of Glaciology and Geophysics of the Environment at the University Joseph Fourier of Grenoble for who are great persons to work with and an inspiration in this lab. Very little of this work would have been possible without the assistance of Jean Francois Chemin for the maintaining cold room and clean lab in good state.

Many thanks go also to Dr. Paolo Gabrielli, Dr.Vania Gaspari and Dr. Guilio Cozzi, who are components of the laboratory of˙Pr. Paolo Cescon at the University Ca'Foscari of Venice, for giving generously of their knowledge and time and for keeping the ICP-SFMS going consistently and reliably. While Dr. Warren Cairns also falls in this category, he is

additionally acknowledge for his obscure humour at times which has kept my head in the right place when it needed to be and prevented me from taking life too seriously with his impromptu comic relief.

In kind, I wish to thank the staff and students of the Department of Applied Physics at Curtin University of Technology (Perth, Australia), particularly Prof. John De Laeter, Prof. Kevin Rosman, Dr. Paul Vallelonga, PhD student Graeme Burton and PhD student Laurie Burn for their knowledge, support and guidance for making Perth a nice place to visit. Particularly, Prof. Kevin Rosman has been a keen motivator and supporter of my research interests. I aspire to develop my career as well as he has his own.

This work is a contribution to the ‘‘European Project for Ice Coring in Antarctica’’ (EPICA), a joint ESF (European Science Foundation)/EC scientific programme, funded by the European Commission and by national contributions from Belgium, Denmark, France, Germany, Italy, the Netherlands, Norway, Sweden, Switzerland and the United Kingdom. I wish to thank all the scientific and logistic personnel working at Dome C, Antarctica.

I wish to express my gratitude to Mélanie Baroni and Laetitia Loulergue who are never far away and always helpful, supportive, full of energy and joy, in anything from accommodating the cats to stirring up a good stew and a good laugh, thank you for everything.

I want to thank also all the other friends and colleagues of the LGGE, and in particular, Hélène Brunjail, Maxime Debret, Raphaëlle Hennebelle, Anna Lourantou, Martina Shaefer, Gregory Teste, Olivier Magand, Markus Frey, Michelle Poinsot and Michel Fily. I wish also express my gratitude to Dr. Didier Voisin whose friendship and in-depth chats have helped me to pace myself during my research process.

I would like to thank all my family for supporting me and for accepting my extended absence.

Lastly, I want to thank Alec Scott for his immense patience and support in this project which has been very helpful with last minute proofreading.

ACRONYMS

AAS: ATOMIC ABSORPTION SPECTROMETER

ACR: ANTARCTIC COLD REVERSAL

ACAP: ARCTIC COUNCIL ACTION PL ZN

AMAP: ARCTIC MONITORING AND ASSESSMENT PROGRAM

AMDES: ATMOSPHERIC MERCURY DEPLETION EVENTS

BP: BEFORE PRESENT

CIA: CHEMICAL INDEX OF ALTERATION

CFA: CONTINUOUS FLOW ANALYSIS

COS: CARBONYL SULPHIDE

CS2: CARBON DISULPHIDE

CUT: CURTIN UNIVERSITY OF TECHNOLOGY

DEP: DIELECTRIC PROFILING

DES: DEPARTMENT OF ENVIRONMENTAL SCIENCES

DMS: DIMETHYLSULFIDE

ECM: ELECTRICAL CONDUCTIVITY METHOD

EDC: EPICA DOME C

EDML: EPICA DRONNING MAUD LAND

EFC: CRUSTAL ENRICHMENT FACTOR

EPICA: EUROPEAN PROJECT FOR ICE CORING IN ANTARCTICA

ESA: ELECTRIC SECTOR ANALYSIS

ETV: ELECTRO-THERMAL VAPORISATION

GEM: GASEOUS ELEMENTAL MERCURY

GFAAS: GRAPHITE FURNACE ATOMIC ABSORPTION SPECTROMETER

GRIP: GREENLAND ICE CORE PROJECT

HEPA: HIGH EFFICIENCY PARTICULATE

Hg_T: TOTAL MERCURY

Hg^{2+}: INORGANIC MERCURY

ICV: INDEX OF COMPOSITIONAL VARIABILITY

ICP-QMS: INDUCTIVELY COUPLED QUADRUPOLE MASS SPECTROMETER

ICP-SFMS: INDUCTIVELY COUPLED PLASMA SECTOR FIELD MASS SPECTROMETER

ICP-TOFMS: INDUCTIVELY COUPLED PLASMA TIME OF FLIGHT MASS SPECTROMETER

IDMS: ISOTOPE DILUTION MASS SPECTROMETRY

IPCC: INTERNATIONAL PANEL ON CLIMATE CHANGE

IPICS: INTERNATIONAL PARTNERSHIPS IN ICE CORE SCIENCES

ITCZ: INTERTROPICAL CONVERGENCE ZONE

LDPE: LOW DENSITY POLYETHYLENE

LGA : LAST GLACIAL AGES

LGGE: LABORATOIRE DE GLACIOLOGIE ET GEOPHYSIQUE DE L'ENVIRONNEMENT

LGM: LAST GLACIAL MAXIMUM

MeHg: METHYL MERCURY

Me_2Hg: DIMETHYL MERCURY

MBE: MID-BRUNHES EVENT

MC-ICP-MS: MULTI COLLECTOR INDUCTIVELY COUPLED MASS SPECTROMETER

MCGC : MULTICAPILLARY GAS CHROMATOGRAPHY

MIS: MARINE ISOTOPIC STAGE

MDL: METHOD DETECTION LIMIT

MPR: MID-PLEISTOCENE REVOLUTION

MSA: METHANESULFONIC ACID

NIST: NATIONAL INSTITUTE OF STANDARDS AND TECHNOLOGY

NMHC: NON-METHAN HYDROCARBONS

nssSO_4: NON SEA SALT SULFATE

PAHs: POLYAROMATIC HYDROCARBONS

PCFA: PRINCIPAL COMPONENTS FACTORS ANALYSIS

PFA: POLYFLUOROACETATE

PGEs: PLATINUM GROUP ELEMENTS

PSAs: POTENTIAL SOURCE AREAS

PVC: POLYVINYLCHLORIDE

REE: RARE EARTH ELEMENTS

LREE: LIGHT RARE EARTH ELEMENTS

MREE: MIDDLE RARE EARTH ELEMENTS

HREE: HEAVY RARE EARTH ELEMENTS

RGM: REACTIVE GASEOUS MERCURY

RSD: RELATIVE STANDARD DEVIATION

SEM: SECONDARY ELECTRON MULTIPLIER

ssNa: SEA SALT SODIUM

THC: THERMOHALINE CIRCULATION

TIMS: THERMAL IONISATION MASS SPECTROMETER

TOMS AAI FoO: TOTAL OZONE MAPPING SPECTROMETER ABSORBING AEROSOL INDEX FREQUENCY OF OCCURENCE

TPM: TOTAL PARTICULATE MERCURY

UCC: UPPER CONTINENTAL CRUST

RIASSUNTO

Lo studio del sistema climatico coinvolge necessariamente la raccolta ed il processamento di un'enorme quantità di dati ottenuti dall'analisi di archivi climatici, quali le carote di ghiaccio. Questo lavoro presenta i più lunghi record stratigrafici di elementi in traccia crostali, di metalli e di metalloidi, mai ottenuti in passato dall'analisi ci carote di ghiaccio. Si sono inoltre studiate le variazioni di concentrazione delle terre rare, degli isotopi del piombo e del mercurio, grazie ai campioni prelevati nell'ambito del progetto EPICA a Dome C (3270m) nell'Antartide Orientale. I campioni di ghiaccio disponibli coprono un periodo di tempo da 263,000 a 671,000 anni fa.

La determinazione analitica degli elementi crostali, metalli, metalloidi, terre rare e mercurio è stata condotto mediante spettrometria di massa ad alta risoluzione con sistema di ionizzazione al plasma accoppiato induttivamente, mentre la caratterizzazione degli isotopi del piombo è stata effettuata mediante spettrometria di massa con sistema di ionizzazione termica e la determinazione degli metilmercurio ed degli mercurio inorganico mediante della spettrometria di massa a tempo di volo accopiata induttivamente ad una sorgente al plasma. Le analisi chimiche sono state effettuate in laboratori a contaminazione controllata.

Lo studio degli elementi di origine crostale (V, Cr, Mn, Fe, Co, Rb, Ba and U) ha consentito di quantificare le variazioni naturali nel flusso di questi elementi nell'arco di tempo tra 263,000 a 671,000 anni fa. Noi mostriamo che le concentrazioni erano estremamente variabili, con valori bassi durante i caldi periodi (interglaciali) e valori molto più alti durante i palcoscenici più freddi (massimi glaciali). L'awezione degli elementi di origine crostale al plateau antartico orientale è trovata per accadere quando un valore critico ben definito δD (~ - 430%) è stato raggiunto.

Le terre rare di provenienza continentale, trasportate dal vento verso l'Antartide Orientale sono state impiegate per studiare la provenienza delle polveri crostali giunte in Antartide durante questo periodo di tempo. In questo modo la provenienza degli elementi di origine crostale durante i periodi glaciali ed interglaciale è stata identificata attraverso il confronto dei dati ottenuti con quelli relativi a potenziali aree sorgenti dell'emisfero sud. Durante i massimi glaciali meno segnati (MIS 12.2, 12.4 e 14.2) a Dome C nell'Antartide Orientale, l'esposizione di REE che impolvera materiali viene da 50% in Australia ed a 50% alla provincia di Córdoba mentre durante

i massimi glaciali più segnati (MIS 8.2, MIS 10.2, 10.4 e 16.2) vengono da 90 - 80% alla provincia di Córdoba ed a 10 - 20% in Australia. Inoltre, la polvere antartica durante i periodi interglaciali consiste di una miscela del Sud America (Argentina del sud, Argentina centrale e forse Patagonia), delle montagne di Transantarctic (ghiacciaio di Koettkitz) e dei materiali australiani.

Le concentrazioni dei metalli e dei metalloidi sono state quantificate in campioni databili tra 263,000 a 671,000 anni fa, allo scopo di studiare la variabilità a lungo termine e di ottenere importanti informazioni sul contributo delle diverse sorgenti ai meccanismi di trasporto. Le concentrazioni erano altamente variabili con i valori bassi durante i periodi caldi e gli alti valori durante i periodi freddi. Tuttavia, l'ampiezza massima delle variazioni contrassegnato differisce da da un elemento ad un altro.In particolare, i dati relativi agli isotopi del piombo, forniscono un importante contributo allo sviluppo della comprensione dei fenomeni che regolano le variazioni di composizione della polvere continentale in Antartide.

Per concludere, per la prima volta, il mercurio totale, il metilmercurio ed il mercurio inorganico sono stati misurati in un nucleo profondo del ghiaccio. Può essere osservato che i valori di concentrazione hanno variato considerevolmente, con i valori bassi durante i interglacials e gli più alti valori durante i periodi più freddi. La quantificazione del mercurio totale e delle specie di mercurio presenti cerca di spiegare le possibili variazioni nella prodittiviatà oceanica e dei meccanismi di deposizione del mercurio nel corso degli ultimi 671,000 anni.

RESUME

L'étude du climat implique nécessairement la collecte et le traitement d'une grande quantité de données obtenues par l'analyse d'archives climatiques telle que les carottes de glace. Dans ce contexte, ce travail présente le plus long enregistrement jamais obtenu d'éléments crustaux, métaux, métalloïdes, terres rares, mercure et isotopes du plomb. Cet enregistrement a été possible grâce à un forage récent réalisé en Antarctique de l'Est permettant d'obtenir une carotte de glace profonde (EPICA/Dome C, 3270 m). Ces éléments ont été étudiés dans de nombreuses sections de la carotte de glace EPICA/Dome C de 263 000 à 671 000 ans avant nos jours.

L'analyse d'éléments crustaux, métaux, métalloïdes, terres rares, mercure ont été réalisées grâce à un spectromètre de masse à secteur magnétique couplé à un plasma induit. La caractérisation des isotopes du plomb et l'analyses de methylmercure et mercure inorganique ont quant à elles étaient rendues possible par l'utilisation d'un spectromètre de masse à ionisation thermique et d'un spectromètre de masse à temps de vol couplé à un plasma induit. Ces analyses ont toutes été effectuées en salle blanche.

L'étude des éléments crustaux (V, Cr, Mn, Fe, Co, Rb, Ba et U) a permis de quantifier les variations naturelles des flux de ces éléments dans les glaces de l'Antarctique de l'Est de 263 000 à 671 000 ans avant nos jours. On a remarqué de fortes variations naturelles de concentration et de flux au cours de ces 6 cycles climatiques, avec des flux de retombées plus faibles pendant les périodes chaudes (interglaciaires) et des flux plus fort pendant les périodes froides (maxima glaciaires). De plus, ces apports augmentent brutalement en Antarctique de l'Est quand $\delta D \leq -430‰$.

Pour la première fois, les terres rares ont pu être analysées dans une carotte de glace profonde. Les variations temporelles et la provenance des terres rares, d'origine crustale, dans l'Antarctique de l'Est ont été étudiées de 263 000 à 671 000 ans avant nos jours. Ainsi, l'origine géographique des éléments crustaux pendant les périodes glaciaires et interglaciaires a été précisée grâce à la comparaison de données de terres rares obtenues dans la carotte EPICA/Dome C et celles provenant de régions potentielles d'origine des aérosols de l'hémisphère austral. L'Australie et la province de Córdoba apparaissent comme étant les sources dominantes à part égales sur le plateau de

l'Antarctique de l'Est au cours des maxima glaciaires peu prononcés (MIS 12.2, 12.4 et 14.2). Différemment, les maxima glaciaires plus prononcés (MIS 8.2, MIS 10.2, 10.4 et16.2) montrent des ratios différents : ces éléments crustaux proviennent à 80-90% de la région de Cordoba et à 20-10% de l'Australie. Pendant les périodes interglaciaires, l'Amerique du Sud (Argentine du Sud, Argentine Centrale, et peut-être la Patagonie), les montagnes Transantarctiques (glacier Koettkitz) et l'Australie apparaissent comme étant les sources dominantes au Dome C.

Les concentrations des métaux et des métalloïdes ont été mesurées de 263 à 671 ka BP afin d'examiner la variabilité à long-terme de ces éléments, d'évaluer les contributions de sources naturelles et les modes de transport. De fortes variations naturelles de concentration et de flux au cours de ces 6 cycles climatiques ont été observées, avec des flux de retombées plus faibles pendant les périodes chaudes (interglaciaires) et des flux plus fort pendant les périodes froides (maxima glaciaires). Cependant, certains métaux varient plus que d'autres. En particulier, l'approche isotopique du plomb apporte une contribution importante dans l'interprétation des variations de compositions de poussières d'origine crustale en Antarctique.

Finalement, pour la première fois, le mercure total, le methylmercure et le mercure inorganique ont été mesurés dans une carotte de glace profonde. Cette analyse montre des concentrations qui varient considérablement au cours des derniers 671 000 ans, avec de faibles valeurs pendant les interglaciaires et de fortes valeurs pendant les périodes les plus froides. L'analyse de ces éléments a permis de déterminer les variations en paleoproductivité océanique et de mieux comprendre les procédés de dépôts de mercure au cours des derniers 671 000 ans.

ABSTRACT

The study of climate necessarily involves the collection and processing of large amounts of data gathered from polar ice cores which are an excellent way of finding how the climate has changed. In this context, I provide the longest records of crustal elements, metals, metalloids, rare earth elements, lead isotopes and mercury taking advantage of the 3270m EPICA/Dome C ice core located in East Antarctica. These elements have been studied in various sections of the EPICA/Dome C deep ice core from 263 ky to 671 ky BP.

For crustal elements, metals, metalloids, rare earth elements and mercury, the analyses were performed by Inductively Coupled Plasma Sector Field Mass Spectrometry whilst the analyses of lead isotopes were performed by Thermal Ionization Mass Spectrometry and the analyses of mercury species (methylmercury and inorganic mercury) by Inductively Coupled Plasma Time of Flight Sector Field Mass Spectrometry, in clean room conditions.

The study of crustal trace elements (V, Cr, Mn, Fe, Co, Rb, Ba and U) allowed to document large natural variations in the occurrence of several crust derived elements in Antarctic ice from 263 to 671 ky BP. I show that the concentrations were highly variable, with low values during warm periods (interglacials) and much higher values during the coldest stages (glacial maxima). The advection of crustal trace elements to the East Antarctic plateau is found to occur when a well-defined critical δD value (~ - 430‰) was reached.

For the first time, the rare earth elements (REE) were analyzed in a deep ice core. The REE of continental origin windblown to the East Antarctica have been studied for their geographical provenance during this time period. In this way, crustal trace elements provenance in glacial and interglacials epochs has been identified through the rare earth elements signature and sediments from Potential Source Areas (PSA) of the Southern Hemisphere. During less pronounced glacial maxima (MIS 12.2, 12.4 and 14.2) at Dome C in East Antarctica, REE show that dust materials come from at 50% to Australia and at 50% to Córdoba province whilst during more pronounced glacial maxima (MIS 8.2, MIS 10.2, 10.4 and 16.2) they come from at 90 to 80% to Córdoba province and at 10 to 20% to Australia. Moreover, Antarctic dust during interglacial periods

consist of a mixture of South America (South Argentina, Central Argentina and perhaps Patagonia), the Transantarctic Mountains (Koettkitz glacier) and Australian materials.

Metals and Metalloids concentrations have been performed from 263 to 671 ky BP in order to examine the long-term variability, from which important information about the contribution of various sources and the transport patterns can be inferred. The concentrations were highly variable with low values during warm periods and high values during cold periods. However, the maximum amplitude of the variations markedly differs from one element to another. In particular, lead isotopes data provide an important contribution to the developing understanding of the variation of continental dust compositions present across Antarctica.

Finally, for the first time, total mercury, methylmercury and inorganic mercury have been measured in a deep ice core. It can be observed that concentration values varied considerably, with low values during interglacials and higher values during the coldest periods. The determination aimed at determining possible variations in oceanic paleoproductivity and Hg deposition processed over 671 ky BP.

CONTENTS

Chap. 3- IDENTIFICATION OF CRUSTAL TRACE ELEMENTS ORIGIN THROUGH THE RARE EARTH ELEMENTS (REE). LEAD ISOTOPE SIGNATURE

Chap. 4- MERCURY, TODAY AND IN THE PAST

Chap. 5- ANALYTICAL TECHNIQUES, MATERIALS AND METHODS

Chap. 6- RESULTS AND DISCUSSION ABOUT CRUSTAL TRACE ELEMENTS VARIABILITY IN EAST ANTARCTICA OVER THE LATE QUATERNARY

INTRODUCTION

Presentation of the work

Human activities perturb the atmosphere and thereby influence the global climate. Prominent examples are eolian mineral dust originating from changes in land use and land cover which affect the radiative balance at the surface of the Earth. Given these ongoing anthropogenic changes, understanding the past record of atmospheric composition is important. Over the past hundred years it is not always an easy task to separate atmospheric changes induced by human activities from those related to natural variability. Only the longer term past record provides the context of natural variability within which recent anthropogenic perturbation has taken place. In this respect, ice cores are an extraordinarily valuable proxy for past climatic, environmental and atmospheric conditions.

Among the wealth of information provided by ice cores, trace elements present in these very valuable samples at extremely low concentration levels are very interesting. Among these trace elements, some of them (V, Cr, Mn, Fe, Co, Rb, Ba, U and rare earth elements) are mainly derived from the continental crust.

Great efforts have been devoted during the last thirty years to assessing the occurrence of toxic metals such as Pb, Hg, Cd, As, Cu and Zn in the successive well-preserved snow and ice layers deposited in the central areas of the large Greenland and Antarctic ice caps, in order to try to obtain historical records of atmospheric concentrations of these elements in the remote polar areas of both hemispheres from prehistoric times to present. Due to the extreme purity of polar snow and ice, it is extremely difficult to collect the samples in the field and to analyze them for these elements in the laboratory without introducing contamination. Moreover, during the drilling operation of deep ice cores, wall retaining fluids with which the drilling hole must be filled to counterbalance the enormous pressure encountered at great depths and prevent rapid closure of the hole is used and contaminate greatly the ice core. Thanks to Patterson and co-workers, a cleaning procedure was successfully developed for the decontamination of the highly contaminated ice core sections.

This cleaning procedure was applied for the analysis of various elements in the EPICA/Dome C (EDC) ice core. Two broad objectives of EPICA (European Project for Ice Coring in Antarctica) are firstly to obtain a full documentation of the Antarctic climate record and then to compare this as optimally as possible with the Greenland record. To do this two more cores are needed to cover the extremes of time scale, with one at a site of higher annual snowfall to provide a detailed record of events over the last glacial cycle (so-called EDML ice core), and the other in a region of low snow accumulation to allow changes over several glacial cycles to be recorded at a lower resolution (so-called EDC ice core). So, the second core, named EDC, from Dome C, discussed here, is aimed at producing a record of the longest time period possible (~ 800 ky BP, 3270m).

In a previous work (Gabrielli et al., 2005a; 2005b; see chapter 2 for references), various sections of the upper part of the EPICA/Dome C, down to the depth of 2193m were analysed and thus covered a time period of two climatic cycles. In this work, it was decided to study to measure various trace elements and Pb isotopes in various sections of the EPICA/Dome C ice core dated from 263 ky BP (depth of 2368 m; Marine Isotopic Stage 8.2) to 671 ky BP (depth of 3062 m; Marine Isotopic Stage 16.2). The time period studied covers 6 glacial/interglacial cycles.

Each section was decontaminated using a cleaning procedure which was initially described by Candelone and co-workers (Candelone et al., 1994; see chapter 5 for references) and then analyzed by Inductively Coupled Plasma Sector Field Mass Spectrometry, Thermal Ionization Mass Spectrometry and Inductively Coupled Plasma Time of Flight Sector Field Mass Spectrometry, in clean room conditions.

One of the key objectives of this research work is to decipher the origin and the variability of the crustal trace elements windblown to Antarctica from 263 to 671 kyr BP through analysis of the EPICA/Dome C ice core. The crustal trace elements variability has been investigated through the measurement of 8 crustal trace elements (V, Cr, Mn, Fe, Co, Rb, Ba and U), each of these indicators keeping information about the paleo cycle of this elements (changes in sources of crustal trace elements, processes of transport and deposition of Tropospheric aerosol to the East Antarctic plateau). The crustal trace elements origin has been investigated following a

geochemical approach, using Rare Earth Elements which their patterns generally reflect the average compositions of the provenance.

The second objective of this study is the determination of six metals and metalloids (Cu, Zn, As, Cd, Pb and Bi) in the EPICA/Dome C ice core from 263 to 671 kyr BP in order to study the different natural sources of these elements and the processes of transport and deposition of Tropospheric aerosol to the East Antarctic plateau.

A particular attention was devoted to the study of lead isotopes. The isotopic approach could allow to evaluate changes over various climatic cycles and to better identify sources areas for aeolian particles. Moreover, it could help to distinguish different kinds of natural sources by discriminating between crustal and volcanic contributions.

Finally, the evaluation of mercury aims at determining the importance of the contribution of the Southern Ocean to the mercury budget at Dome C.

Here below is reported the general structure of this work.

Chapter 1- LATE QUATERNARY ENVIRONMENTAL CHANGES AND THE CLIMATE SYSTEM

The first chapter includes an overview of the Quaternary climate changes characterized by their forcing factors, the timescale involved and their principal environmental effects. A general inventory of the different types of natural archives of paleoclimate history is summarised. The chapter is concluded with a summary of the climatic tales from the EPICA/Dome C ice core for the last eight glacial/interglacial cycles.

Chapter 2- TRACE ELEMENTS, TODAY AND IN THE PAST

Introductory information about the history of trace elements production and their use is reported in this chapter. The definition, the nature and the climatic role of various aerosols are considered. The chapter contains also a synthesis of all natural and anthropogenic emissions of trace elements into the atmosphere and a literature review of the studies of these elements in snow and ice at Greenland and Antarctica.

Chapter 3- IDENTIFICATION OF CRUSTAL TRACE ELEMENTS ORIGIN THROUGH THE RARE EARTH ELEMENTS (REE). LEAD ISOTOPE SIGNATURE

The chapter contains a synthesis of all the most recent issues about the present-day atmospheric dust load and an overview of the principal dust source regions with particular focus on the Southern Hemisphere. The dust provenance to the East Antarctic plateau in glacial and interglacial times is also discussed. A review of REE properties and their geochemical behaviour are presented. The chapter discusses the usefulness of REE signature for crustal trace elements as tracer for provenance. The $^{206}Pb/^{207}Pb$ and $^{208}Pb/^{207}Pb$ isotopic systems and their geochemical behaviour are also presented here. Their links with volcanic and crustal aerosols are discussed here.

Chap. 4- MERCURY, TODAY AND IN THE PAST

Introductory information about mercury properties is reported in this chapter. The chapter contains a synthesis of all natural and anthropogenic emissions of mercury into the atmosphere and a literature review of the studies of this element in snow and ice in the Arctic and Antarctica. The biogeochemical cycle of mercury is also considered.

Chap. 5- ANALYTICAL TECHNIQUES, MATERIALS AND METHODS

A presentation of the European Project for Ice Coring in Antarctica (EPICA) and the ice core samples analyzed in this study is given in this chapter. Samples preparation, analytical techniques used for trace elements, REE, mercury and lead isotopes are also described.

Chap. 6- RESULTS AND DISCUSSION ABOUT CRUSTAL TRACE ELEMENTS VARIABILITY IN EAST ANTARCTICA OVER THE LATE QUATERNARY

The results of the measurements of V, Cr, Mn, Fe, Co, Rb, Ba and U in the EPICA/Dome C ice core were presented here. When combined with the data previously obtained by Gabrielli and co-workers for the upper 2193 m of the core, it gives a detailed record for these elements during a 671 ky period from the Holocene back to Marine Isotopic Stage (MIS) 16.2. Concentrations, fallout fluxes, rock and soil dust contributions are discussed here.

Chap. 7- CHANGES IN ATMOSPHERIC HEAVY METALS AND METALLOIDS IN DOME C (EAST ANTARCTICA) ICE BACK TO 671 KY BP

The results of the measurements of Cu, Zn, As, Cd, Pb and Bi on the EPICA/Dome C ice core were presented here. When combined with data previously obtained for the upper part of the core, it gives detailed record of past natural variations in the concentrations of these metals and metalloids during the last eight climatic cycles from the Holocene back to Marine Isotopic Stage (MIS) 16.2. Concentrations, fallout fluxes and contribution of various sources for these elements are discussed in this chapter.

Chap. 8- CRUSTAL TRACE ELEMENTS PROVENANCE TROUGH THE REE SIGNATURE FROM 263 TO 671 KY BP IN THE EPICA DOME C ICE CORE

The purpose of this chapter is to present the first dataset of REE (La, Ce, Pr, Nd, Sm, Eu, Gd, Tb, Dy, Ho, Er, Tm, Yb and Lu) in the EPICA/Dome C ice core during the period from 263 to 671 ky BP and to extract characteristic features from them. The crustal trace elements provenance to the East Antarctica in glacial and interglacial times is discussed.

Chap. 9- EIGHT GLACIAL CYCLES OF PB ISOTOPIC COMPOSITIONS IN THE EPICA DOME C ICE CORE

Here I present new data extending the existing Pb isotope record at Dome C from 263 to 671 ky BP. The new data enable the confirmation of climatic features observed in the most recent glacial cycle, in addition to characterising the variation of Pb isotopes over the past six glacial/interglacial cycles. The data also provide an important contribution to the developing understanding of the variation of continental dust compositions present across Antarctica.

Chap. 10- INTENSE MERCURY SCAVENGING FROM THE DUST AND SALT LADEN ANTARCTIC ATMOSPHERE DURING THE GLACIAL AGES

Here the first determination of mercury species was determined in different ice core sections over 220 ky BP and the first determination of total mercury over 671 ky BP. Total mercury and mercury species shows much stronger mercury deposition during the coldest climatic stages. This occurred in close concurrence with the highest atmospheric dust load.

Chapter 1- LATE QUATERNARY ENVIRONMENTAL CHANGES AND THE CLIMATE SYSTEM

1.1 The originality of Quaternary climate variability

The interaction between natural processes and human activities is complex. Moreover, the balance between the two has shifted dramatically (Vitousek et al., 1997; Meybeck et al., 2001), for the effects of human activities, especially during the last two centuries, have led to transformations much more significant than those resulting from natural climate change over the same period.

They have brought us into what may realistically be termed the "Anthropocene" (Crutzen, 2002) and in so doing, endowed us with a 'no-analogue' biosphere as the canvas upon which future climate changes and human activities will interact.

The Anthropocene is marked by greenhouse gas levels well outside the range of at least 650,000 years (**Figure 1.1.1**). The measured concentrations of CO_2, CH_4 and N_2O greenhouse gases fluctuated only slightly (within 4% for CO_2 and N_2O and within 7% for CH_4) over the past millennium prior to the industrial era, and also varied within a restricted range over the late Quaternary. Within the last 200 years, the late Quaternary natural range has been exceeded by at least 25% for CO_2, 120% for CH_4 and 9% for N_2O. All three records show effects of the large and increasing growth in anthropogenic emissions during the industrial era (Jansen et al., 2007).

Temperature is a more difficult variable to reconstruct than CO_2 (a globally well-mixed gas), as it does not have the same value all over the globe, so that a single record (e.g., an ice core) is only of limited value. Local temperature fluctuations, even those over just a few decades, can be several degrees celsius, which is larger than the global warming signal of the past century of about 0.7°C. The United Nations Intergovernmental Panel on Climate Change (IPCC) declared in 2007 that the understanding of anthropogenic warming and cooling influences on climate has improved since the Third Assessment Report (TAR), leading to very high confidence that the globally averaged net effect of human activities since 1750 has been one of warming, with a radiative forcing of + 1.6 [+ 0.6 to +2.4] Wm^{-2}.

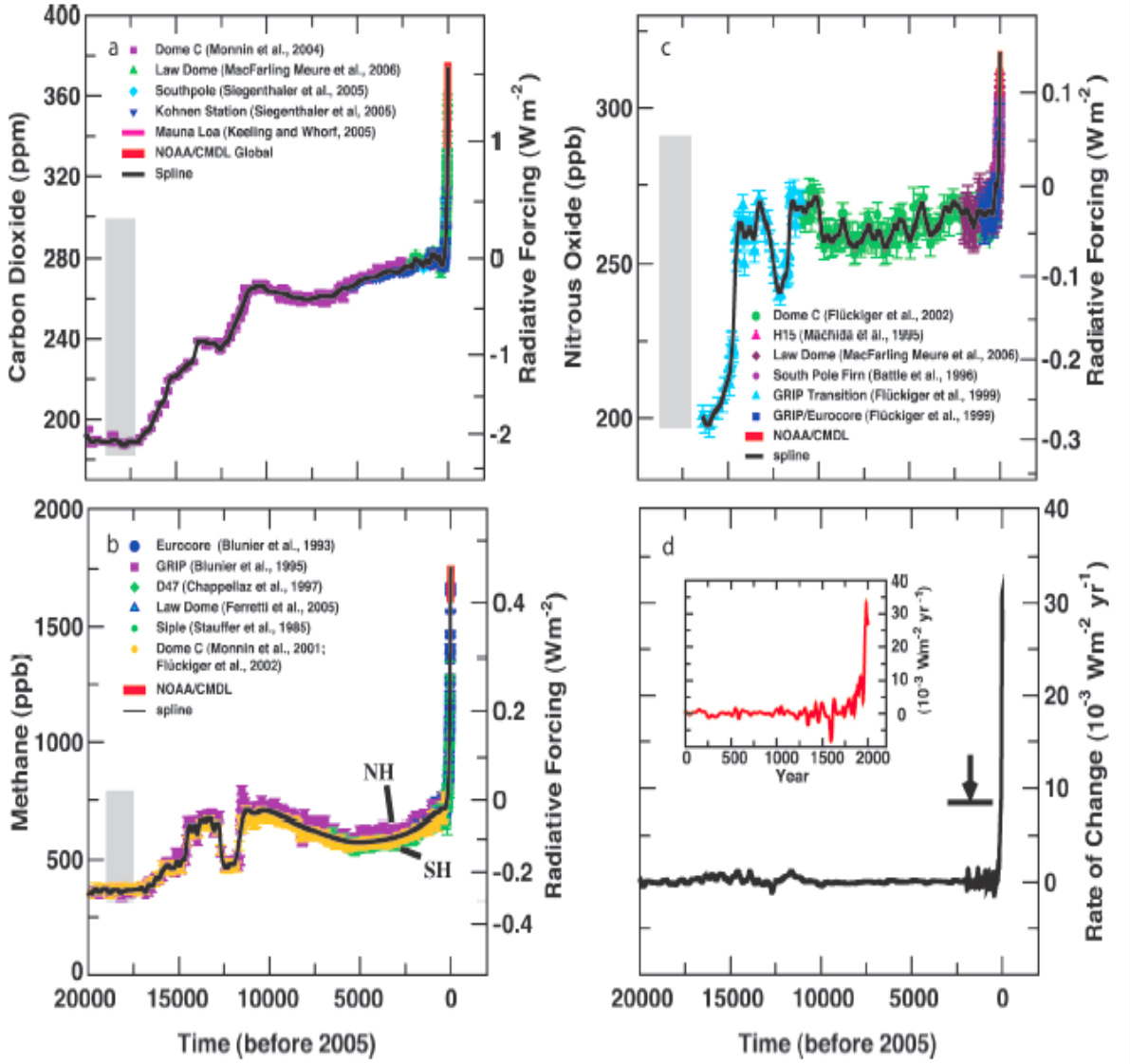

Fig. 1.1.1: *The concentrations and radiative forcing by (a) CO_2, (b) CH_4 and (c) nitrous oxide (N_2O), and (d) the rate of change in their combined radiative forcing over the last 20 kyr reconstructed from antarctic and Greenland ice and firn data (symbols) and direct atmospheric measurements (red and magenta lines). The grey bars show the reconstructed ranges of natural variability for the past 650 kyr (from Jansen et al., 2007). Variations in atmospheric CO_2 dominate the radiative forcing by all three gases.*

The Quaternary is subdivided into two epochs: the Pleistocene (roughly from two million years to ten thousand years ago) and the Holocene (about the last ten thousand years to the present day). In turn, the Pleistocene is conventionally subdivided in three parts: the lower Pleistocene (1.8-0.75 Ma), the Middle Pleistocene (750-125 kyr B.P.) and the Upper Pleistocene (125-10 kyr B.P.).

The "Anthropocene" era covers only about 2% of the whole Holocene, the present interglacial period, climatically relatively warm and stable. The Holocene constitutes only about the 0.5% of the Quaternary age that, in turn, is only the terminal, thin slice of the geological time bar represented in **Figure 1.1.2** reported by Wilson et al. (2000) in their book "The Great Ice Age". Why is the Quaternary, so-called "Great Ice age"[1], so important? Because studying it helps us understanding our past and future.

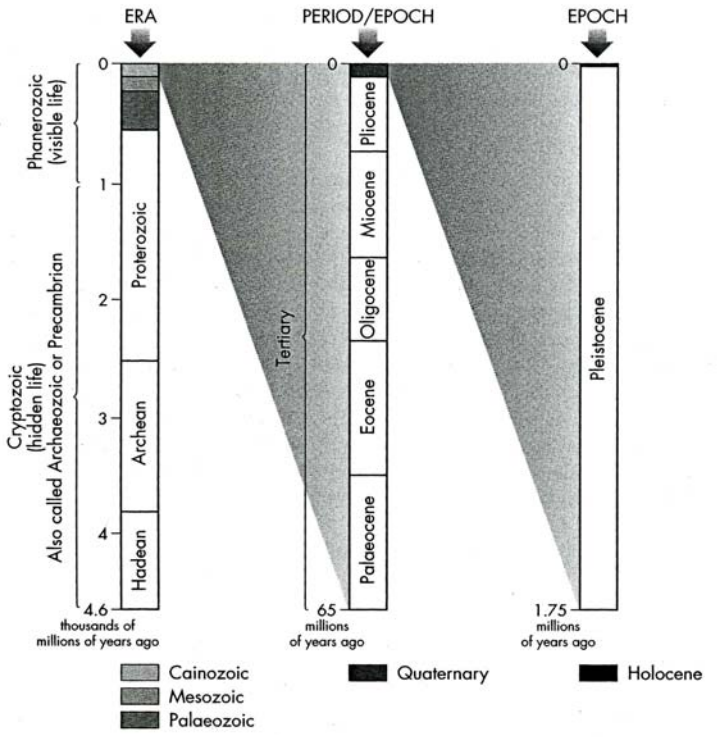

Fig. 1.1.2: *Major divisions of geological time during the last 4600 millions of years*

It is a unique period of time in the Earth's history, mainly because of its features:

1. Quaternary climatic changes can be studied with a relatively higher temporal resolution than any other period of the geological time;
2. it is characterized by repeated, and relatively regular, patterns of climate change over time scales ranging from hundreds of thousands to less than 100 years[2];
3. during the Great Ice Age, both poles were perennially covered by ice sheets, introducing a basic constituent on the climatic system;
4. humans evolved during this period, and they started to affect the natural course of climate.

[1] The Great Ice Age: describe the period during which major glaciers and ice sheets regularly advanced and retreated across the Northern Hemisphere. This 1.8 million year time interval spans the Pleistocene and Holocene epochs of the Quaternary period; the Holocene began only 10,000 years ago.

[2] Quaternary periods can be distinguished into:
Glacials: Protracted cold stages with major expansions of ice sheets and glaciers
Interglacials: Warm intervals in which temperatures were equal or higher than during the Holocene.
Stadials: Shorter episodes during which local ice advances may have occurred
Interstadials: Short-lived periods of thermal improvement during a glacial phase

To develop a world-wide accepted strategy leading to sustainability of ecosystems against human induced stresses will be one of the great future tasks of mankind, requiring intensive research efforts and wide application of the knowledge thus acquired in the noösphere (the world of thought, nickname given by the French Jesuit priest P.Teilhard de Chardin and E. Le Roy in 1924), now better known as knowledge or information society.

1.2 Introduction to the climate system

Climate is a term used across a range of spatial scales. It can be used to describe the 'average weather' for a given region over decades or more, or be used to refer to conditions across the entire planet. Climate is the result of a wide-range of interactions between several different subsystems –atmosphere, hydrosphere (mainly the oceans), cryosphere, biosphere and lithosphere- all driven by the uneven heating of the planet by solar radiation (**Figure 1.2.1**, from Wilson et al., 2000).

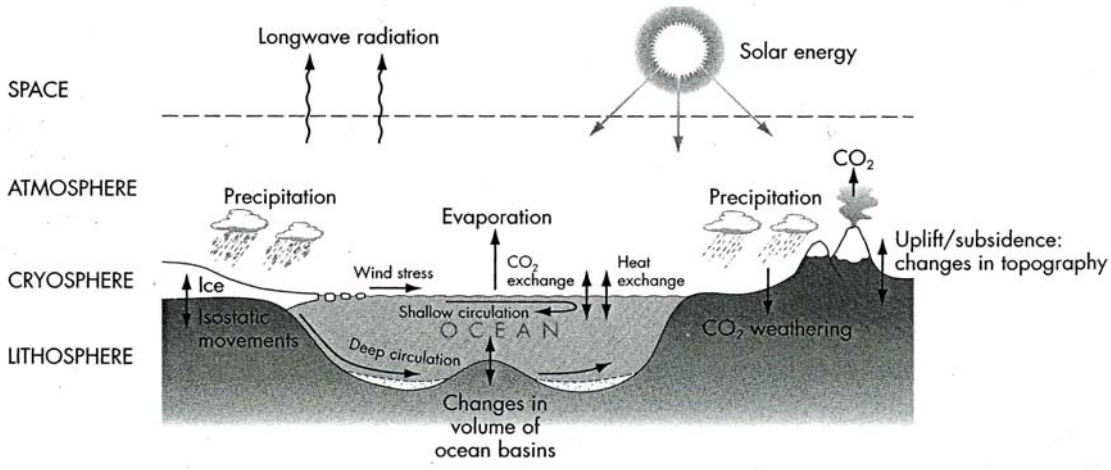

Fig. 1.2.1 : *Diagram showing the major components of the Earth's climate system and the links between them*

It tends to keep the Earth's radiation budget in balance globally so that incoming radiation is equalled by outgoing radiation (**Figure 1.2.2**). This balance was not maintained during periods when the Earth cooled and warmed into and out of glacial periods.

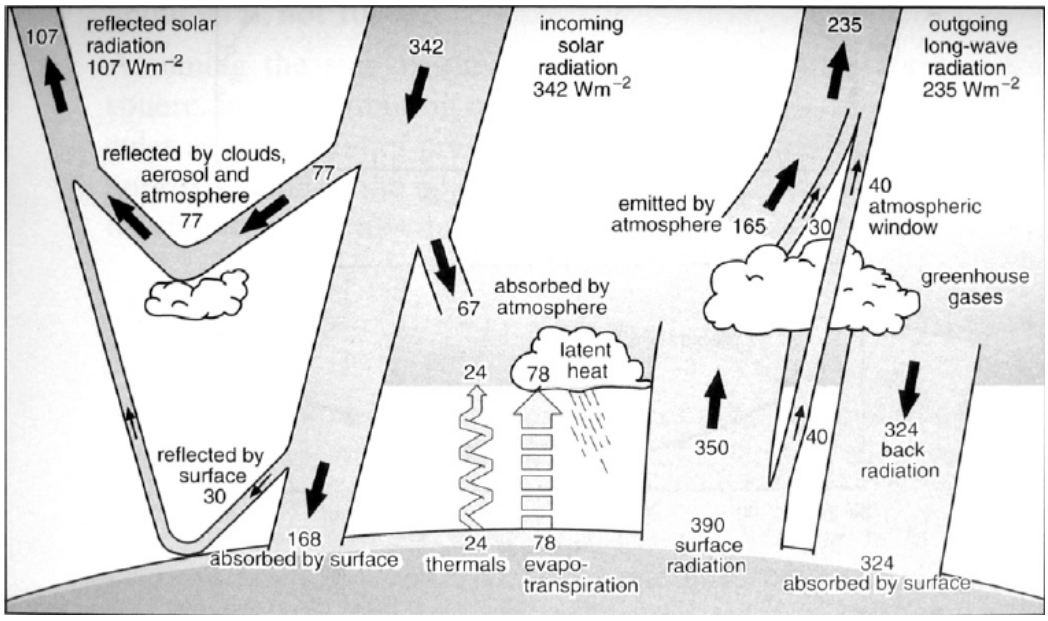

Fig. 1.2.2 : *The solar radiation balance and the energy balance of the Earth (Kiehl and Trenberth, 1997; Houghton, 2005). The net incoming solar radiation of 342Wm^{-2} is partially reflected by clouds and the atmosphere, or at the surface where 49% is absorbed. That heat is returned to the atmosphere, some as sensible heat but most from evaporation and transpiration (taken together these are known as evapotranspiration), which is later released as latent heat of condensation within the atmosphere. The rest is radiated as thermal radiation from the surface much of which is absorbed by the atmosphere or by clouds that also emit radiation both upwards and downwards. Part of the infrared radiation that is lost to space comes from cloud tops and parts of the atmosphere that are much colder than the surface.*

It is clear that the Earth's climate system must behave differently during glacial episodes to how it behaves during interglacials. The fact that both interglacial and glacial conditions persisted for thousand of years suggests not only that the climate system can exist in at least two equilibrium states, but also that one or more factors have causes it to changes states.

Table 1.2.1 (Wilson et al., 2000) summarises the factors that may contribute to climate changes, and indicates the timescales over which they operate. **Figure 1.2.3** (Wilson et al., 2000) adds the spatial dimension to this information by plotting the time scales and area extent of different climatic related phenomena on logarithmic scales. This illustrates an important point. This is that longer term changes in climate probably involve progressively more components of the Earth system.

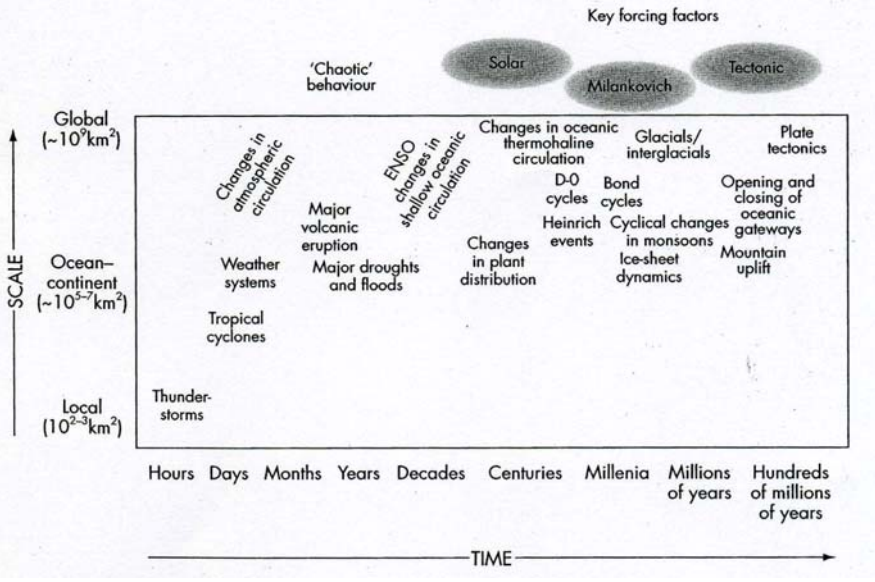

Fig. 1.2.3: *The spatial and time dimensions of the Earth's climate system plotted on logarithmic scales. The possibly role of a variety of forcing functions is also shown (from Wilson et al., 2000)*

All the components of the climate system are closely linked or coupled among them, so that a change in one sub-system can involve linked changes throughout the whole climatic system. These changes can both amplify or dampen the effect of the initial event. Positive feedbacks tend to increase the initial effects, causing an increasing destabilization of the climate system in the time. Vice versa, negative feedbacks provide a stabilizing influence on the system.

Major 'sphere' in which factors occur	*Individual factors*	*Time scales over which factors operate*
Astronomical	Changing solar flux:	
	long term	10^9 years
	short term	10–200 years
	Changes in the Earth's orbit and orientation of its axis of rotation (astronomical, or Milankovich cycles)	
	eccentricity	10^5 years
	obliquity	4×10^4 years
	precession	2×10^4 years
	harmonics of the above	Few thousand years
Lithosphere	Continental drift/plate tectonics	10^{6-8} years
	Uplift/mountain building (modifies atmospheric circulation and weathering rates affecting atmospheric CO_2 levels)	10^{6-8} years
	Isostatic response to loading by:	
	mountain building	10^{5-8} years
	ice sheet growth/melting	10^{4-5} years
	Ocean ridge growth:	
	global sea-level change	10^{6-8} years
	Volcanism (atmospheric CO_2, aerosols)	<1 year–10^8 years
Cryosphere	Ice sheet growth and melting	10^{2-5} years
Ocean	Global sea-level changes due to land ice formation and melting	10^{2-5} years
	Deep water circulation	~10^3 years
	Surface water circulation	10^{1-2} years
	Upwelling	1–10 years
	CO_2 content	~10^2 years
Atmosphere	Composition of greenhouse gases	
	Long term	10^{7-8} years
	Glacial/interglacial	10^{3-5} years
	Circulation	<1–10 years
Biosphere	Forest growth, swamp and peat bog formation	10^2 years
Human activities	Fossil fuel burning, land use	10^{1-2} years

Table 1.2.1 : *Factors that may contribute to climate change and the time scales over which they operate (Wilson et al., 2000)*

Once the climate system response is amplified or dampened by such additional feedback controls, we define such climate response as non-linear. In a linear response the rate of the climate system response at any instants is directly proportional to the magnitude of the input signal. Conversely, a non-linear response to a perturbation is reflected in a lagged response.

Solar energy is the predominant source of energy. Although the total quantity of solar radiation reaching the Earth varies little, the distribution of that radiation with latitude and season over the Earth's surface changes considerably. The changes are especially large in Polar Regions where the variations in summer sunshine, for instance, reach about 10% (Houghton, 2005). The Quaternary climatic variations have frequencies corresponding to the periodicities of three known astronomical parameters (Berger, 1978; Imbrie et al., 1992; Tzedakis et al., 1997)[3] :

1- the *eccentricity* of the Earth's orbit around the Sun (~ 400 kyr and ~100 kyr), varying from elliptical to nearly circular
2- the *obliquity* of the Earth's axis (~ 41 kyr) respect to the plane of the ecliptic cycles[4]
3- the *precession of the equinoxes* in the Earth's orbit (21.7 ky)[5]

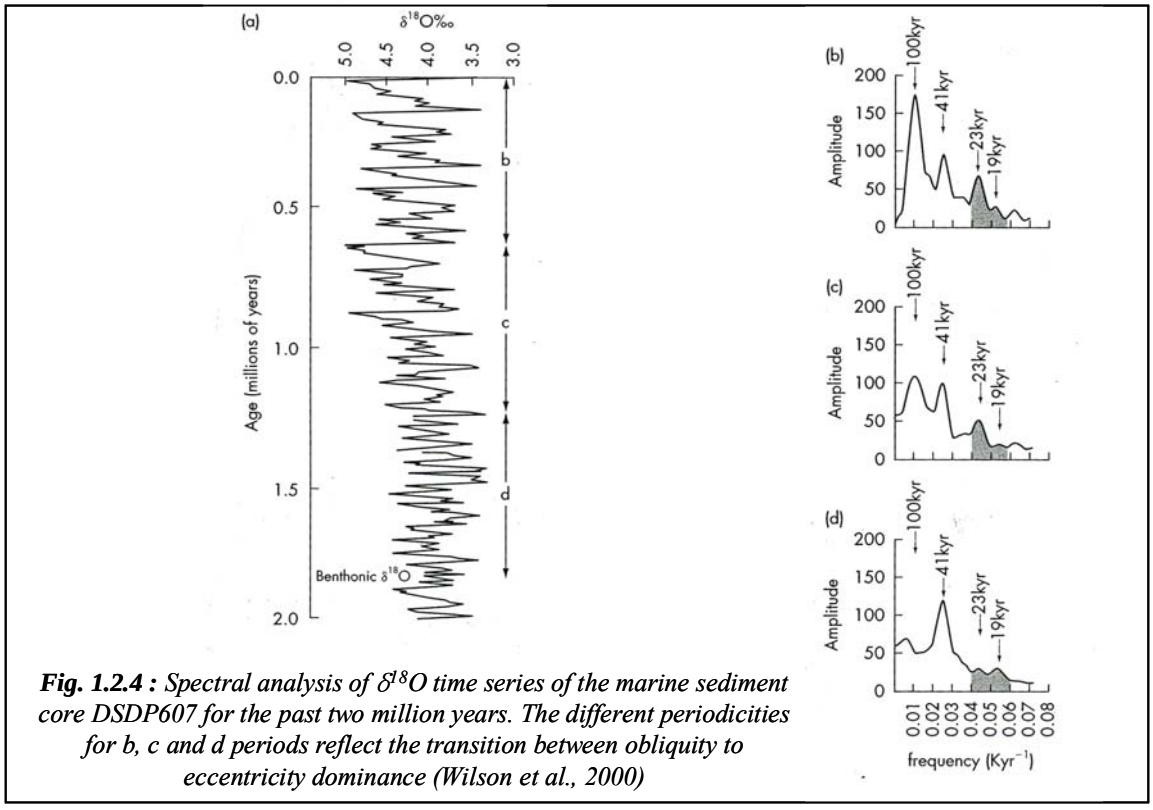

Fig. 1.2.4 : *Spectral analysis of $\delta^{18}O$ time series of the marine sediment core DSDP607 for the past two million years. The different periodicities for b, c and d periods reflect the transition between obliquity to eccentricity dominance (Wilson et al., 2000)*

[3] James Croll, a British scientist, first pointed out in 1867 that the major ice ages of the past might be linked with these regular variations. His ideas were developed in 1920 by Milutin Milankovitch, a climatologist from Yugoslavia, whose name is usually linked with the theory. This theory however was not widely accepted until the 1970's.

[4] The 41 kyr periodical changes in the axial tilt span the range from 21.8° to 24.4° and influence the radiation at high latitudes.

[5] It must be noted that the periods mentioned correspond to the average of the principal periodic terms. In particular, for the precessional parameter the most important terms in the series correspond to periods of ~23.7, ~22.4 and ~19 kyr. The 21.7 kyr periodicity is an average of the main periods (~23.7, ~22.4 and ~19 kyr) but some climatic records are capable to resolve separately these periods.

However, **Figure 1.2.4** indicates a clear shift between the dominance of the obliquity effects, before about 600 ky BP, to the eccentricity regime, in the last eight climatic cycles.

Nevertheless, the late Quaternary is known to have been highly unstable and prone to rapid climatic changes of millennial scale duration. The Dansgaard-Oeshger events[6], the Heinrich events[7] and the Bond's cycles[8] are an example.

The potential mechanisms driving, amplifying and correlating variability on centennial and millennial timescales include internal ocean-atmosphere systems (Sarnthein et al., 2002). The variability in the global thermohaline circulation (THC) and its effect on the atmospheric system is one of the potential elements of climate forcing and feedback mechanisms (Broecker and Denton, 1989; Duplessy et al., 1991). The THC variability, in turn, may have direct or indirect climate responses, and each of these can show a given phasing at regional scale (Sarnthein et al., 2002).

1.3 Paleo-environmental evidences of Quaternary environmental changes

Reconstructing past climates and a timetable of climatic changes is akin to detective work. It requires a painstaking search for clues and the ability to piece them together in a logical and consistent way. Fortunately the Earth's climate system in the past did not commit the perfect crime, for it left many clues behind which are described below.

[6] Dansgaard-Oeschger (D-O) events: Large amplitude and repetitive millennial-scale changes in air temperature occurring during the last glacial period (from ~11 to 74 kyr B.P.) and recorded for the first time by Willi Dangsgaard and Hans Oeschger in the Camp Century Greenland ice core (Dansgaard et al., 1984). An average fundamental pacing period of ~1470 years seems to control the timing of the onset of the D-O events.

[7] Heinrich events: succession of layers rich in Ice Rafted Detritus (IRD) observed for the first time by H.Heinrich (1988) in a sediment core from NE Atlantic.

[8] Bond's events : events of abrupt climate shifts registered in North Atlantic deep sea cores in glacial and interglacial climates. During such events, cold and ice-carrying waters from North Iceland are advected to the South. These episodes correspond to abrupt changes in the atmospheric circulation above Greenland. The periodicity of such events is 1374 ± 502 yrs for the Holocene, and 1536 ± 563 years for the glacial periods. On average, the pacing of the so called Bond's events is 1470±532 years (Bond et al., 1997).

Process	
<u>Cryosphere</u>: glaciers, sea ice and polar ice sheets	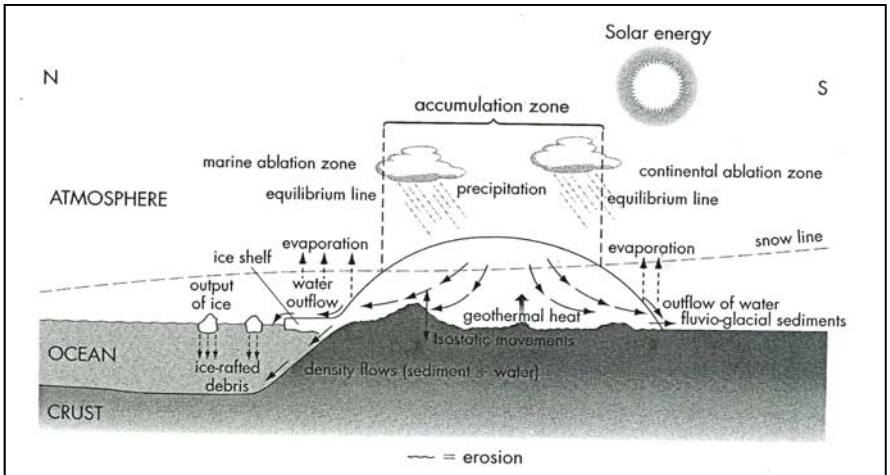 ***Fig. 1.3.1:*** *A sketch showing the features of ice caps and the principal linkages between them and other components of the Earth system (Wilson et al., 2000)* - **Northern Hemisphere**: During LGM: extension of the Northern Hemisphere ice sheet, with the North American Laurentide Ice Sheet extending up to the northern Great Plains and New England, and in Europe the Fennoscandinavian Ice Sheet, including all Scandinavia, the British Island up to northern Germany (Clark and Mix, 2002; Dyke et al., 2002; Svendsen et al., 2004). - **Southern Hemisphere**: Antarctic ice sheet: main changes probably affected the West Antarctica, while the East area did not change so much in term of extension and height (Ritz et al., 1992; 2001; Peyaud et al., 2007) : higher sea ice formation during cold regimes (Crosta et al., 1998a; 1998b; Gersonde et al., 2005) - **Temperate glaciers**: extensively wider during LGM: the Andes, Southern New Zealand mountains ranges were covered by perennial ice (Hulton et al., 2002; McGlone et al., 1993) - **Alpine glaciers**: between the end of 16th century and the middle

	of the 19th century alpine glaciers were generally 0.8 to 1.6 km longer than now and that the major retreat took place during the 20th century (Haeberli et al., 2002; Vincent et al., 2004).
Sea level changes	As a consequence of ice sheets growth, global sea level at LGM was about 120m lower than present day 0 level (Siddall et al., 2003).
Desert and arid areas	The coldest Quaternary periods have been associated to an enhancement of aridity. Most part of Africa and Australia (except for the Equatorial Western Africa and coastal Australia) consisted of semi-arid, arid or desert landscapes. Sand dunes were periodically active well beyond their present-day limits and widespread loess deposits formed. 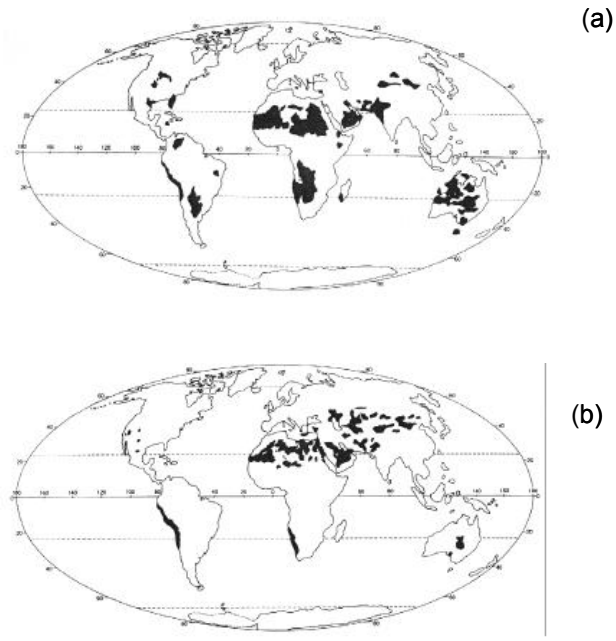 ***Fig. 1.3.2:*** *Earth's distribution of sand dunes at LGM (a) and at present day (b) (adapted from Samthein, 1987; Goudie, 1983)*
Lake levels	The reconstruction of past lake levels permit to study paleo-changes of the hydrological cycle. For example, Markgraf et al. (2000) reports results of paleo-climate reconstruction from paleo-lake levels estimation along the Pole-Equator-Pole transect of the Americas

Terrestrial fauna and flora changes	- changes between the glacials and interglacials: fossil remains of pollen, plants, beetles and vertebrates in sediments - the current distribution of species may indicate the existence of refugia in the past, especially in tropical forests - **low latitudes**: during glacials: tropical forest was invaded and dissected by grassland (Wilson et al., 2000) - **higher latitudes**: during glacials: glacial tundra expands at the expense of boreal and deciduous broad-leaved forest. The longer lived trees (and perhaps large mammals) may have been killed during cooling phases (Wilson et al., 2000)
Atmospheric circulation	The position of the Intertropical Convergence Zone (ITCZ), the Westerlies belt, and the major oceanic and continental anticyclones varied during the Quaternary, in association with changes of wind strength . The past atmospheric circulation can be reconstructed through multiproxy indicators for the different regions of the globe. Regional syntheses for the Southern Hemisphere can be found in Bowler (1976), Clapperton (1993), McGlone et al. (1993), Wright et al. (1993) and Partridge (1993).

1.4 Climatic tales from EPICA/Dome C ice core

Since few decades, it has become obvious that the two large ice sheets in Antarctica and Greenland contain paleoclimatic information. There is a bidding war going on in Antarctica. This bidding started with 80,000 for the Byrd ice core. Vostok raised the bid to 160,000 and then 420,000. Now a new ice core, the European Project for Ice Coring in Antarctica (EPICA) Dome C core, has raised a record of the longest time period possible, ~ 800,000 years ago, which corresponds to the Marine Isotopic Stage (MIS) 20.2 (Jouzel et al., 2007).

The ice contains information related to a host of environmental factors: temperature, wind speed and transport paths, sea ice extent, volcanism, oxidation capacity of the atmosphere, greenhouse gas concentration, marine biological activity, etc.

Water isotopes and Temperature

Most water is $H_2{}^{16}O$, but the main reservoir (the oceans) contains a small proportion of $HD^{16}O$ and $H_2{}^{18}O$. In nature, fractionation occurs during transfer between the condensed and vapour phases. In successive cycles of evaporation and condensation, the heavy molecules evaporate less easily and condense more easily. This reduces the amount of heavy isotopes (^{18}O and D are depleted), so that δ values of precipitation are always negative. As an air mass containing water vapour from the oceans moves towards the poles, it is cooled and loses water vapour (condensation leading to precipitation). It therefore becomes more and more depleted in the heavy isotopes (δ becomes more negative).

Dansgaard et al. (1969) concluded that the most important factor governing δ values in precipitation is the temperature difference between the ocean source and the sampling site. Since sea surface temperatures are relatively stable compared to air temperatures at high latitudes, δ is most dependent on T at the time and place of deposition. Increasing δ's upward in the core indicate warming climate, and decreasing δ's indicate cooling climate in the course of time.

The deep-sea benthic oxygen-18 record (Lisiecki and Raymo, 2005) and the δD_{ice} Dome C record are in excellent overall agreement back to ~ 800,000 years BP (**Figure 1.4.1**). Such an agreement justifies the use of the marine sediment nomenclature for Marine Isotopic Stages (MIS).

From new experiments performed with an atmospheric General Circulation Model including water isotopes (Jouzel et al., 2007), it derives that Antarctic surface temperatures were up to ~ 4.5°C warmer compared to the late Holocene during MIS 5.5 and 9.3, and down to ~ 10°C colder for the coldest period (MIS 2). A strong and persistent obliquity component is identified in this record, and Jouzel et al. (2007) suggest that the interplay between obliquity and precession accounts for the variable intensity of interglacial periods.

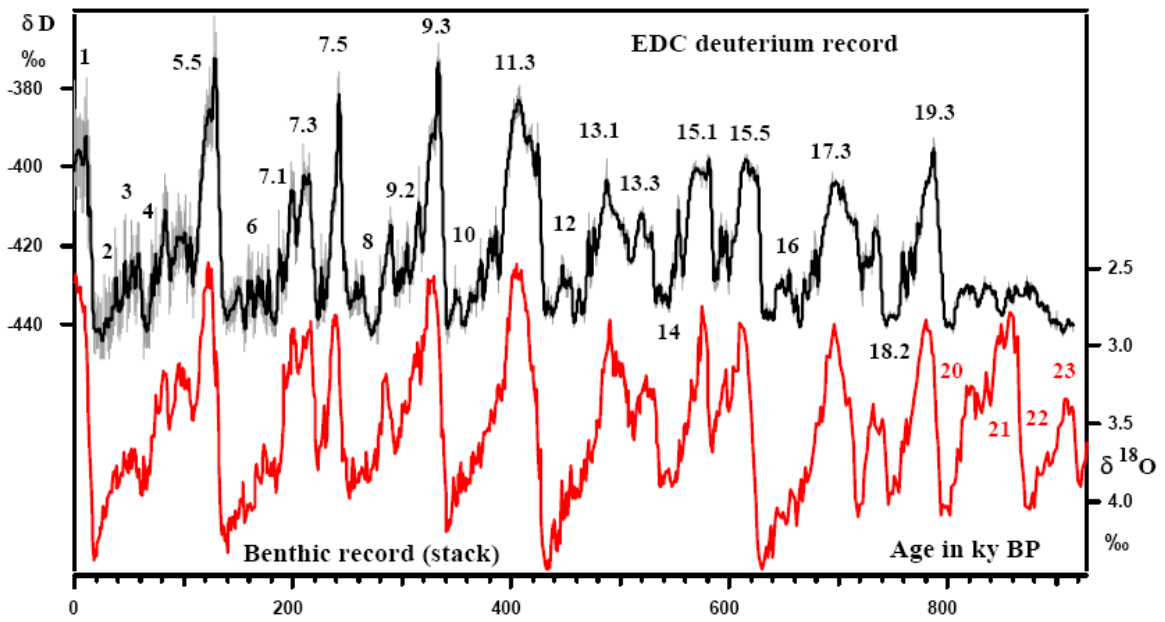

Fig. 1.4.1: *Comparison of the δD Dome C record on the EDC3 timescale (Parrenin et al.,2007) (with all data points in light grey and a smoothed curve in black) with the benthic oxygen-18 record on its own timescale (Lisiecki and Raymo, 2005) (from Jouzel et al., 2007)*

Greenhouse gases

CO_2, CH_4 and N_2O are called greenhouses gases because they absorb the infrared radiation emitted by the surface of the Earth and the atmosphere (**Figure 1.4.2**) and so, participate to the greenhouse effect. If the atmosphere would not be present, the effective temperature at the Earth's surface would be -18°C.

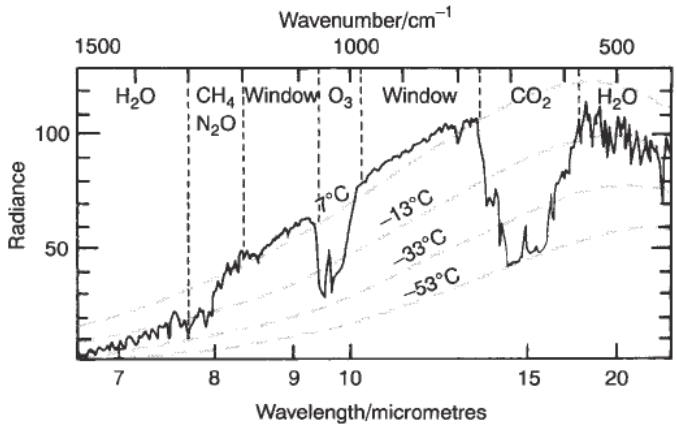

***Fig. 1.4.2*:** Thermal radiation in the infrared (the visible part of the spectrum is between about 0.4 and 0.7μm) emitted from the Earth's surface and atmosphere as observed over the Mediterranean Sea from a satellite instrument orbiting above the atmosphere, showing the parts of the spectrum where different gases contribute to the radiation (Hanel et al.,1971). Between wavelengths of about 8 and 14 μm,apart from the ozone band, the atmosphere, in the absence of clouds, is substantially transparent; this part of the spectrum is called a 'window' region. Superimposed on the spectrum are curves of radiation from a black body at 7°C, −13°C, −33°C and −53°C. The units of radiance are Wm^{-2} per steradian per wavenumber (from Houghton et al., 2005).

Present-day observations show that the surface emits 390 Wm^{-2} and 237 Wm^{-2} must be given back to space, there is trapping of 153 Wm^{-2}. More greenhouse gases means more trapping. The radiative equilibrium at the top of the atmosphere is temporally broken, but finally restored by a global increase of temperature[9]. This response includes the feedbacks and leads, in particular, to a warming at the surface.

The EPICA Dome C ice core shows a remarkable correlation between temperature and greenhouse gas concentrations on glacial-interglacial scales (**Figure 1.4.3**). A combined record of CH_4 measured along the Dome C and the Vostok ice cores demonstrates that preindustrial concentrations over Antarctica have not exceeded 773 ±15 ppbv (parts per billion by volume) during the past 650,000 years (Spahni et al., 2005).

Before 420,000 years ago, when interglacials were cooler, maximum CH_4 concentrations were only about 600 ppbv, similar to lower Holocene values. In contrast to CH_4 record, before 420,000 years ago, the N_2O record shows maximum concentrations of 278 ± 7 ppbv, slightly higher than early Holocene values (Spahni et al., 2005). The differing response to climate change of CH_4 and N_2O suggests that the main source regions and/or strengths may strongly differ during interglacials and intermediate warm periods. High levels are sustained longer for N_2O than for CH_4, either due to the release of oceanic N_2O or because N_2O soil sources are also productive under semiarid conditions (Spahni et al., 2005).

[9] The so-called response of the atmosphere through the Stefan-Boltzmann law.

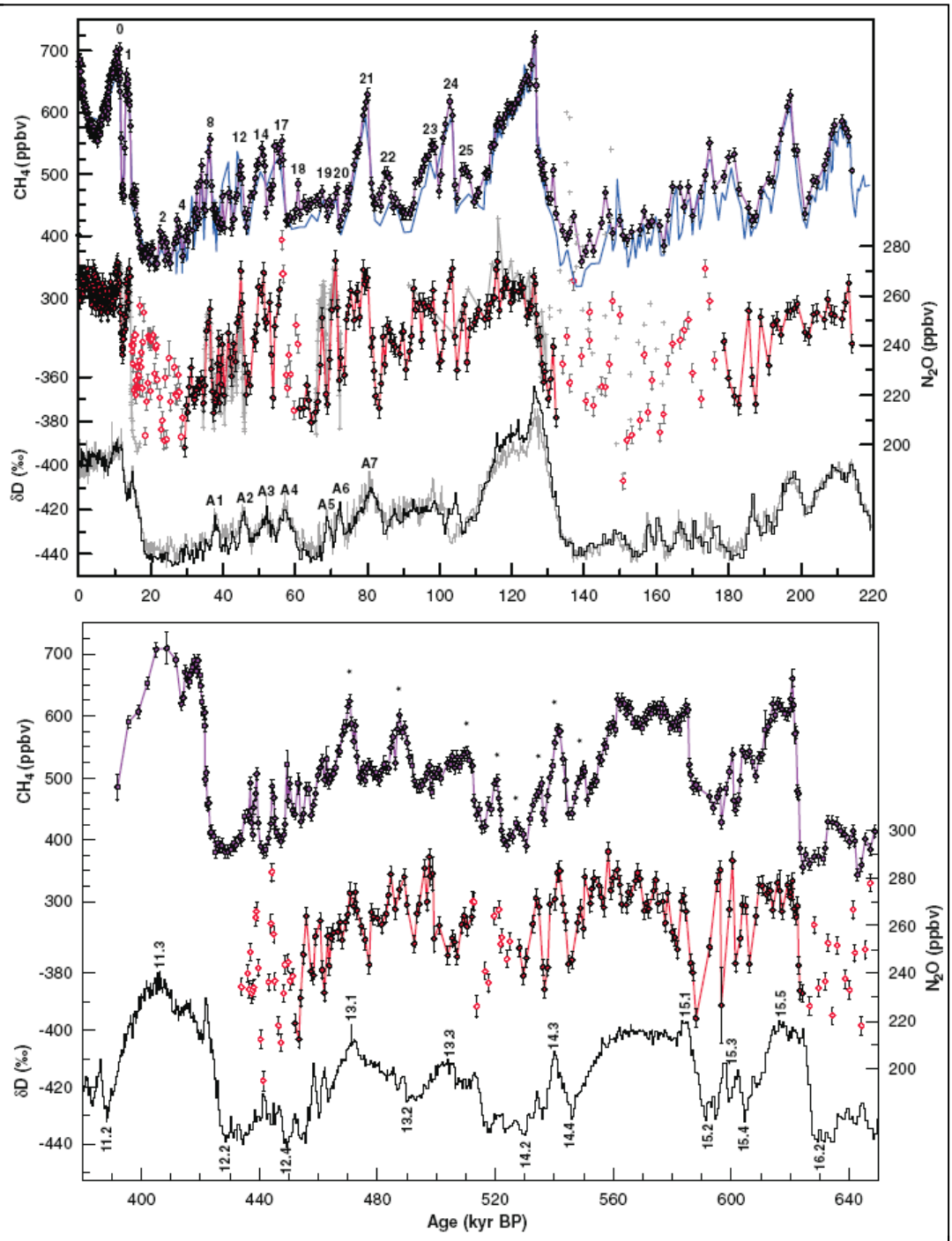

Fig. 1.4.3: *Dome C CH_4 (purple line) and N_2O (red line) records over the period from MIS 1 to MIS 16, together with high-resolution δD data from Dome C (black line). Also shown are Vostok CH4 (blue line)* and *δD data (grey line) over the past 220 ky BP (from Spahni et al., 2005)*

Marine and terrestrial aerosols

Marine aerosol and terrestrial material can be measured in ice. Marine aerosol comes from sea spray, and possibly from the sea ice surface. It is evaluated thanks to the measure of Na^+ and Cl^-. Terrestrial material, which comes from soil and desert dusts, can be investigated through measurements of particle numbers and volume and through markers such as Ca, Al, REE and dust.

In the EPICA/Dome C ice core, the first-order variability of the marine and terrestrial aerosols is anti-correlated with the temperature record over 740,000 years (**Figure 1.4.4**). The input of marine Na, Fe and dust is higher in glacial periods, lower in interstadials and minimum in interglacials.

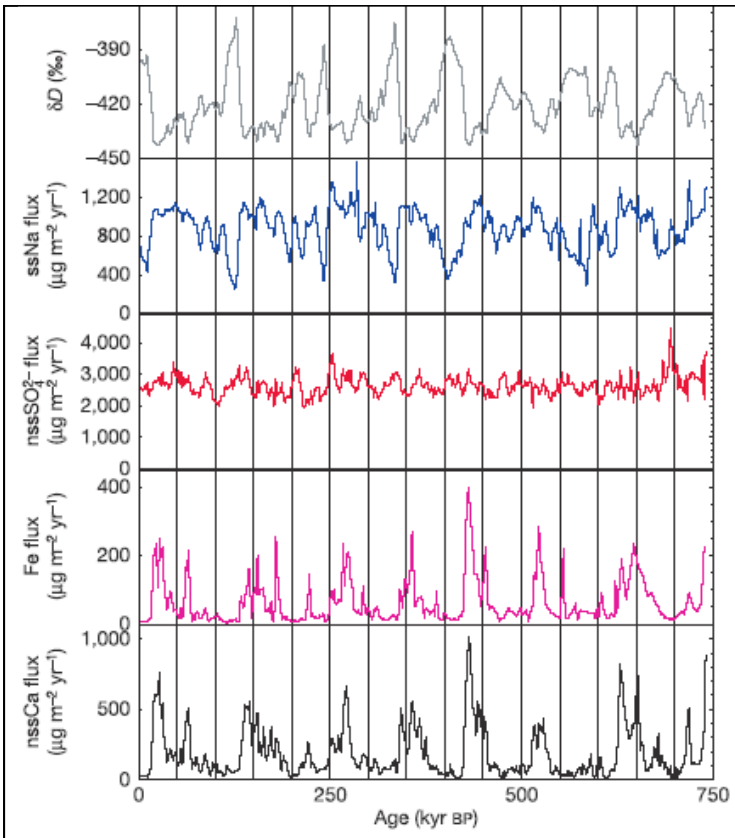

Fig. 1.4.4: *Chemical measurements from the EPICA Dome C ice core , on the EDC2 age scale (EPICA Community members, 2004). (from Wolff et al., 2006)*

The enhanced dust input during cold periods was primarily associated to the widespread aridity on the continents, the high wind speeds and the reduced hydrological cycle. In such cold periods the mineral particles reaching the East Antarctic plateau likely had a southern South American provenance (Basile et al., 1997; Delmonte et al., 2004).

The maximum values of sea-salt Na[10] (representing sea salt) are about double the present-day value, while the minimum observed is about half the present value. It is observed a very close relationship between Na flux[11] and temperature throughout the 740-kyr period, with cold temperatures leading to higher Na flux.

Previously, the increased cold period sea-salt Na flux has been attributed to greater cyclonic activity at the (assumed open water) source, and to greater meridional transport of sea salt into the continent (Petit et al., 1999). However, the modelled flux of sea salt arriving in central Antarctica from an open water source was found to be much lower in the last glacial maximum compared to the present, when the data show the opposite (Reader and McFarlane, 2003). Wolff et al. (2006) conclude that the sea-ice surface (including frost flowers, brine and brine-soaked snow) is probably the main source of sea salt to central Antarctica for recent cold conditions. This would imply that the sea salt flux at East Antarctica (Vostok and Dome C) is related to new sea-ice production in the Indian Ocean sector of Antarctica[12].

[10] calculated ssNa and nssCa assuming a Ca/Na weight ratio of 0.038 for marine aerosols and 1.78 for the average crust (Bowen, 1979).
[11] The flux of a chemical to the ice can be calculated as : $J = C_{SNOW} \times ACC$
where C_{SNOW} is the concentration in ice, ACC is the snow accumulation rata, and the J is the flux.
[12] Indian Ocean sector: relevant region for sea-ice production, based on model estimated for Vostok, with the largest influence between 55° and 60°S (Cosme et al., 2005).

REFERENCES

Alverson K, Bradley R, Pederson T (2001) *Environmental variability and climate change*. IGBP Science volume 3, Eliott S editor, IGBP secretariat, Stockholm

Basile I, Grousset FE, Revel M, Petit JR, Biscaye PE, Barkov NI (1997) Patagonian origin of glacial dust deposited in East Antarctica (Vostok and Dome C) during glacial stages 2, 4 and 6. *Earth and Planetary Science Letters* **146**, 573-589

Berger AL (1978) Long term variations of daily insolation and Quaternary climatic changes. *Journal of Atmospheric Sciences* **35**, 2362-2367

Bond G, Showers W, Cheseby M, Lotti R, Almasi P, DeMenocal P, Priore P, Cullen H, Hajadas I, Bonani G (1997) A pervasive millennial scale cycle in the North Atlantic Holocene and glacial climates. *Science* **278**, 1257-1266

Bowen HJM (1979) *Environmental Chemistry of the Elements*. Academic Press, London

Bowler JM (1976) Aridity in Australia: Age, origins and expression in aeolian landforms and sediments. *Earth Science Reviews* **12**, 279-310

Broeker WS, Denton GH (1989) The role of ocean-atmosphere reorganizations in glacial cycles. *Geochimica et Cosmochimica Acta* **53**, 2465-2501

Clapperton CM (1993) *Quaternary Geology and Geomorphology of South America*. Elsevier, Amsterdam

Clark PU, Mix AC (2002) Ice sheets and sea level of the Last Glacial Maximum. *Quaternary Science Reviews* **21**, 1–7

Cosme E, Hourdin F, Genthon C, Martinerie P (2005) Origin of dimethylsulfide, non-sea-salt sulfate, and methanesulfonic acid in eastern Antarctica. *Journal of Geophysical Research* **110**, D03302, doi:10.1029/2004JD004881

Crosta X, Pichon JJ, Burckle LH (1998a) Application of the modern analog technique to marine Antarctic diatoms: reconstruction of maximum sea-ice extent at the Last Glacial Maximum. *Paleoceanography* **13 (3)**, 284-297

Crosta X, Pichon JJ, Burckle LH (1998b) Reappraisal of Antarctic seasonal sea ice at the Last Glacial Maximum. *Geophysical Research Letters* **25 (14)**, 2703-2706

Crutzen PJ (2002) Geology of mankind. *Nature* **415**, 23

Dansgaard W, Johnsen SJ, Moller J, Langway CC Jr (1969) One thousand centuries of climatic record from Camp

Century on the Greenland ice sheet. *Science* **166**, 377-381

Dansgaard W, Johnsen SJ, Clausen HB, Dahl-Jensen D, Gundestrup NS, Hammer CU, Oeschger H (1984) North Atlantic climate oscillations revealed by deep Greenland ice cores. In: Hansen, J.E. and Takahashi, T. (Eds) *Climate Processes and Climate Sensitivity volume 29*. AGU Geophysical Monograph, pp. 288-298

Delmonte B, Basile-Doelsch I, Petit JR, Maggi V, Revel-Rolland M, Michard A, Jagoutz E, Grousset F (2004) Comparing the EPICA and Vostok dust records during the last 220,000 years: stratigraphical correlation and provenance in glacial periods. *Earth Science Reviews* **66**,573-589

Duplessy JC, Labeyrie L, Julliet–Lerclerc A, Duprat J, Sarnthein M (1991) Surface salinity reconstruction of the North Atlantic ocean during the last glacial maximum. *Oceanology Acta* **14**, 311–324

Dyke AS, Andrews JT, Clark PU, England JH, Miller GH, Shaw J,Veillette JJ (2002) The Laurentide and Innuitian ice sheets during the Last Glacial Maximum. *Quaternary Science Reviews* **21**, 9–31

EPICA community members (2004) Eight glacial cycles from an Antarctic ice core. *Nature* **429**, 623-628.

Gersonde R, Costa X, Abelmann A, Armand L (2005) Sea-surface temperature and sea ice distribution of the Southern Ocean at the EPILOG Last Glacial Maximum- a circum-Antarctic view based on siliceous microfossil records. *Quaternary Science Reviews* **24**, 869-896

Goudie A (1983) *Environmental change*. Second Edition. Clarendon Press, Oxford

Haeberli W, Maisch M, Paul F (2002), Mountain glaciers in global climate-related observation networks. *World Meteorological Organisation Bulletin* **51**, 1–8

Hanel RA, Schlachman B, Rogers D, Vanous D (1971) Nimbus 4 Michelson interferometer. *Applied Optics* **10**, 1376-1382

Heinrich H (1988) Origin and consequences of cyclic ice rafting in the northeast Atlantic Ocean during the past 130,000 years. *Quaternary Research* **29**, 142-152

Houghton J (2005) Global warming. *Reports on Progress in Physics* **68**, 1343-1403

Hulton NRJ, Purves RS, McCulloch RD, Sugden DE, Bentley MJ (2002) The last glacial maximum and deglaciation in southern South America. *Quaternary Science Reviews* **21**, 233-241

Imbrie J, Boyle EA, Clemens SC, Duffy A, Howard WR, Kukla G, Kutzbach J,

Martinson DG, McIntyre A, Mix AC, Molfino B, Morley JJ, Peterson LC, Pisias NG, Prell WL, Raymo ME, Shackleton NJ, Toggweiller JR (1992) On the structure and origin of major glaciation cycles. 1. Linear responses to Milankovitch forcing. *Paleoceanography* **7**, 701-738

Jansen E, Overpeck J, Briffa KR, Duplessy JC, Joos F, Masson-Delmotte V, Olago D, Otto-Bliesner B, Peltier WR, Rahmstorf S, Ramesh R, Raynaud D, Rind D, Solomina O, Villalba R Zhang D (2007) Palaeoclimate. In: Solomon S, Qin D, Manning M, Chen Z, Marquis M, Averyt KB, Tignor M, Miller HL (Eds) *Climate Change 2007: The Physical Science Basis. Contribution of Working Group I to the Fourth Assessment Report of the Intergovernmental Panel on Climate Change*. Cambridge University Press, Cambridge, United Kingdom and New York, NY, USA, pp. 433-499

Jouzel J, Masson-Delmotte V, Cattani O, Dreyfus G, Falourd S, Hoffmann G, Minster B, Nouet J, Barnola JM, Chappellaz J, Fisher H, Gallet JC, Johnsen S, Leuenberger M, Loulergue L, Luethi D, Oerter H, Parrenin F, Raisbeck G, Raynaud D, Schwander J, Spahni R, Souchez R, Selmo E, Schilt A, Steffenson JP, Stenni B, Stauffer B, Stocker TF, Tison JL, Werner M, Wolff EW (2007) Orbital and millennial Antarctic climate variability over the last 800,000 years. *Science* **317**, 793-796

Khiel JT, Trenberth KE (1997) Earth's annual global mean energy budget. *Bulletin of the American Meteorological Society* **78**, 197-208

Lisiecki LE, Raymo ME (2005) A Plio-Pleistocene Stack of 57 globally distributed benthic $\delta^{18}O$ records. *Paleoceanography* **20,** doi:10.1029/2004PA001071

Markgraf V, Baumgartner TR, Bradbury JP, Diaz HF, Dunbar RB, Luckman BH, Seltzer GO, Swetnam TW, Villalba R (2000) Paleocliamte reconstruction along the Pole-Equator-Pole transect of the Americas (PEP 1) *Quaternary Science Reviews* **19** , 125-140

McGlone MS, Salinger MJ, Moar NT (1993) Paleovegetation studies of New Zealand's climate since the Last Glacial Maximum. In: Wright HE, Kutzbach JE, Webb III T, Ruddiman WF, Street-Perrott FA, Bartlein PJ (Ed) *Global Climates since the Last Glacial Maximum*. Minnesota Press, Minneapolis, p 294-317

Meybeck M, Green P, Vörösmarty C (2001) A new typology for mountains and other

relief classes. *Mountain Research and Development* **21**, 34-45

Parrenin F, Barnola JM, Beer J, Blunier T, Castellano E, Chappellaz J, Dreyfus G, Fisher H, Fujita S, Jouzel J, Kawamura K, Lemieux-Dudon B, Loulergue L, Masson-Delmotte V, Narcisi B, Petit JR, Raisbeck G, Raynaud D, Ruth U, Schwander J, Severi M, Spahni R, Steffensen JP, Svensson A, Udisti R, Waelbroeck C, Wolff E (2007) The EDC3 chronology for the EPICA Dome C ice core. *Climate of the Past Discussions* **3**, 575-606

Partridge TC (1993) Warming phases in southern Africa during the last 150 000 years: an overview. *Palaeogeography, Palaeoclimatology, Palaeoecology* **101**, 237-244

Petit JR, Jouzel J, Raynaud D, Barkov NI, Barnola JM, Basile I, Bender M, Chappellaz J, Davis M, Delaygue G, Delmotte M, Kotlyakov VM, Legrand M, Lipenkov VY, Lorius C, Pepin L, Ritz C, Saltzman E, Stievenard M (1999) Climate and atmospheric history of the past 420,000 years from the Vostok ice core, Antarctica. *Nature* **399**, 429-436

Peyaud V, Ritz C, Krinner G (2007) Modelling the early Weishselian Eurasian ice sheets: role of ice shelves and influence of ice-dammed lakes. *Climate of the past discussions* **3**, 221-247

Reader MC, McFarlane N (2003) Sea-salt aerosol distribution during the Last Glacial Maximum and its implications for mineral dust. *Journal of Geophysical Research* **108**, 4253, doi:10.1029/2002JD002063

Ritz C (1992) Un modèle thermo-mécanique d'évolution pour le bassin glaciaire antarctique Vostok glacier Byrd: sensibilité aux valeurs de paramètres mal connus, PhD thesis, Université Joseph Fourier Grenoble I, Grenoble.

Ritz C, Rommelaere V, Dumas C (2001) Modeling the evolution of Antarctic ice sheet over the last 420,000 years: Implications for altitude changes in the Vostok region. *Journal of Geophysical Research* **106 (D23), 31**, 941-964.

Sarnthein M, Kennett JP, Allen J, Beer J, Grootes P, Laj C, McManus J, Ramesh R (2002) Decadal-to-millennial-scale climate variability - chronology and mechanisms: Summary and recommendations. *Quaternary Science Reviews* **21**, 1121-1128

Siddall M, Rohling EJ, Almogi-Labin A, Hemleben Ch, Meishner D, Schmelzer I, Smeed DA (2003) Sea-level fluctuations during the last glacial cycle. *Nature* **423**, 853-858

Spahni R, Chappellaz J, Stocker TF, Loulergue L, Hausammann G, Kawamura K, Flückiger J, Schwander J, Raynaud D, Masson-Delmotte V, Jouzel J (2005) Atmospheric methane and nitrous oxide of the late Pleistocene from Antarctic ice cores. *Science* **310**, 1317-1321

Svendsen JI, Alexanderson H, Astakhov VI, Demidov I, Dowdeswell JA, Funder S, Gataullin V, Henriksen M, Hjort C, Houmark-Nielsen M, Hubberten HW, Ingolfsson O, Jakobsson M, Kjaer KH, Larsen E, Lokrantz H, Lunkka JP, Lysa A, Mangerud J, Matiouchkov A, Murray A, Moller P, Niessen F, Nikolskaya O, Polyak L, Saarnisto M, Siegert C, Siegert MJ, Spielhagen RF, Stein R (2004) Late quaternary ice sheet history of northern Eurasia. *Quaternary Science Reviews* **23**, 1229–1271

Tzedakis PC, Andrieu V, Beaulieu JL, Crowhurst S, Follieri M, Hooghiemstra H, Magri D, Reille M, Sadori L, Shackleton NJ, Wijmstra TA (1997) Comparison of terrestrial and marine records of changing climate of the last 500,000 years. *Earth and Planetary Science Letters* **150**,171-17

Vincent C, Kappenberger G, Valla F, Bauder A, Funk M, Le Meur E (2004) Ice ablation as evidence of climate change in the Alps over the 20th century. *Journal of Geophysical Research* **109**, doi: 10.1029/2003JD003857

Vitousek PM, Mooney HA, Lubchenco J, Melillo JM (1997) Human domination of Earth's ecosystems. *Science* **277**, 494-499

Wilson RCL, Drury SA, Chapman JL (2000) *The Great Ice Age: climate change and life*. Taylor and Francis Group, London

Wolff EW, Fischer H, Fundel F, Ruth U, Twarloh B, Littot GC, Mulvaney R, Röthlisberger R, De Angelis M, Boutron CF, Hansson M, Jonsell U, Hutterli MA, Lambert F, Kaufmann P, Stauffer B, Stocker TF, Steffensen, JP, Bigler M, Siggaard-Andersen ML, Udisti R, Becagli S, Castellano E, Severi M, Wagenbach D, Barbante C, Gabrielli P, Gaspari V (2006) Southern Ocean sea-ice extent, productivity and iron flux over the past eight glacial cycles. *Nature* **440**, 491-496.

Wright HE, Kutzbach JE, III TW, Ruddiman WF, Street-Perrott FA, Bartlein PJ (1993) *Global climates since the Last Glacial Maximum.* Wright HE Jr, Kutzbach JE, Webb III T, Ruddiman WF, Street-Perrott FA, Bartlein PJ (Eds), University of Minnesota, Minneapolis

Chapter 2- TRACE ELEMENTS, TODAY AND IN THE PAST

2.1 History of trace elements production and their use

As the third millennium opens, it is clear that human beings are having a discernible impact on the environment and profound changes are underway. The population growth increases economic activity, with all their implications in terms of higher demands on energy, water and a wide range of resources, both renewable and non-renewable.

Discernible widespread impacts of human activities on atmospheric chemistry began with the early days of extensive metal smelting (Healey, 1978). Although there are indications of these impacts from the Bronze Age onwards, they become much stronger during the time of the antique Greece and Roman Empire for which there are clear signs of enhanced atmospheric concentrations of lead, copper and other trace metals detected in ice core from Greenland (Settle and Patterson, 1980; Hong et al., 1994; 1996; Boutron, 1995; Candelone et al., 1995) and in European lake sediments (Renberg et al., 1994) and peats (Shotyk et al., 1996; 1998; Martinez-Cortizas et al., 1999) (**Figure 2.1.1**).

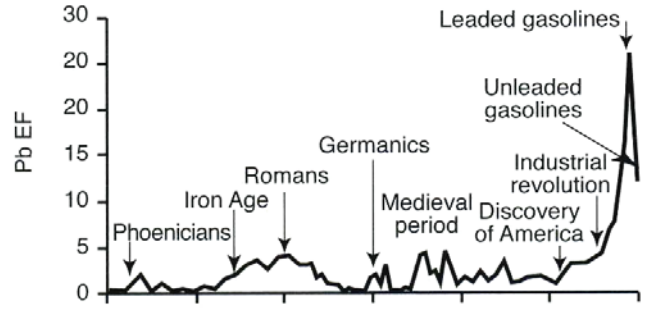

Fig. 2.1.1 : *The lead Enrichment Factor (EF) record from Penido Vello, a peat profile in N Spain (Martinez-Cortizas et al., 1999) set against a series of historical events and cultural stages from 3000 BP onwards (Oldfield and Dearing, 2003)*

The possibility also exists of using natural variations in the abundances of lead isotopes to trace the source of this pollution (Rosman et al., 1997; Renberg et al., 2001). Thanks to lead isotopes measurements, it was demonstrated that atmospheric concentrations of "pollution" lead peak in Greenland and throughout Europe between 100BC and AD200 (**Figure 2.1.2**).

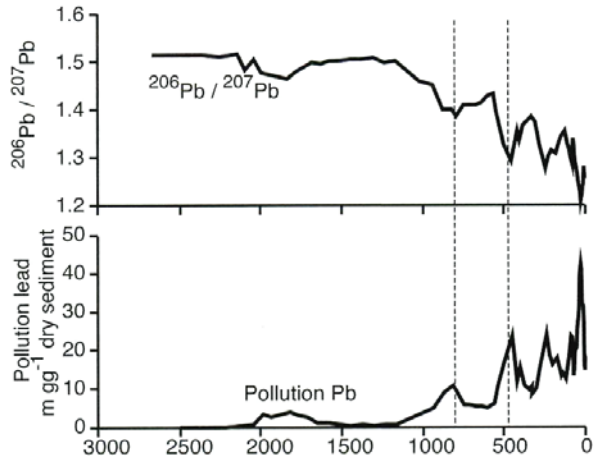

Fig. 2.1.2 : *Pollution lead concentrations and $^{206}Pb/^{207}Pb$ ratios as recorded in Koltjärn, a small lake in S Sweden (Renberg et al., 1994; 2001)*

From early Medieval times onwards, metal burdens increase. Enhanced loadings to remote areas prior to the mid-19th century are recorded, but it is generally only close to industrial or urban sources that evidence for strong contamination is apparent (Brimblecombe, 1987).

Within the period of widespread industrial and urban development over the last century and a half, evidence for atmospheric contamination became ubiquitous. Spatial patterns have changed, mirroring not only the process of industrial expansion but also trends in resource. Evidence for these changes comes from both documentary sources (Brimblecombe, 1987) and paleo-archives such as lake sediments (Edgington and Robins, 1976; Galloway and Likens, 1979; Rippey et al., 1982; Kober et al., 1999), ice cores (Murozumi et al., 1969; Rosman et al., 2000; Barbante et al., 2001; Schwikowski et al., 2004) and ombrotrophic peatlands (Aaby et al., 1979; Norton 1985; Clymo et al., 1990; Shotyk et al., 1996) all of which contain historical records of contamination by a wide range of compounds.

In developed economies, recent turning points detectable in the paleo-records are the rapid increase in power generation beginning in the late 1950's, the increased generation of often environmentally persistent organic compounds, for example polyaromatic hydrocarbons (PAHs) (Hites, 1981; Goodarzi and Mukhopadhyay, 2000; Jiun-Horng et al., 2007) and organochlorine products (Wania and Mackay 1993), and the post 1970s trend towards reduced discharge limits, greater control and improved treatment.

Following the first clear evidence for damage to ecosystems (Oden, 1968), many contaminant emissions peaked in the 1970s and 1980s. The record in environmental archives has confirmed the trend towards an amelioration of air quality in many parts of the world (Nriagu, 1990a; Boutron et al., 1991; Candelone et al., 1995; Schwikowski et al., 1999; Schwikowski et al., 2004) (**Figure 2.1.3)**.

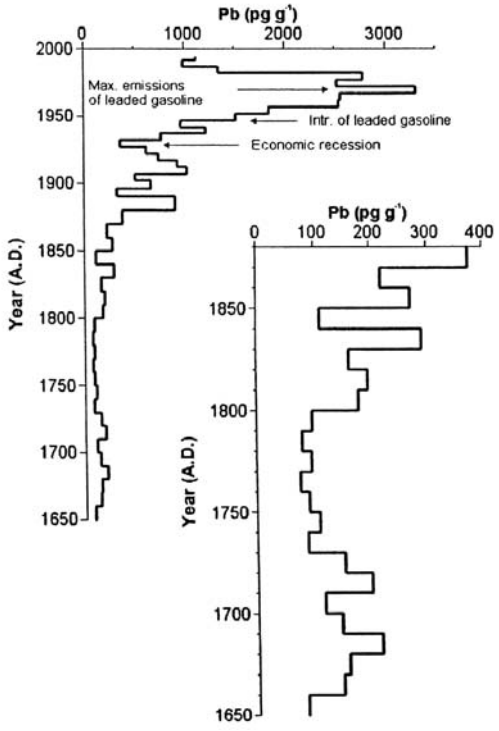

Fig. 2.1.3 : *Combined lead paleo concentration record from the Colle Gnifetti cores as 5-year (period 1890-1995) and 10-year averages (period 1650-1890). The period from 1650 to 1880 is additionally shown with a magnified horizontal axis, to take into account the lower lead concentrations (Schwikowski et al., 2004)*

Nevertheless, even in the richer developed countries, air quality problems persist (Blais 1998). Elsewhere, factors such as the legacy of previous political regimes, continuing on fossil fuel as the main energy source, proliferation of vehicles, population growth and ongoing industrial development often combine and lead to a continued build-up in atmospheric pollution to the level where concern is increasing at both regional and global level.

2.2 Aerosols

The interactions between the atmosphere and the various geochemical reservoirs of the biosphere are numerous and lead to the formation of many types of aerosols[13] containing trace elements. Aerosols have two principal origins: natural (dust, sea salt spray, volcanism etc.) or anthropogenic. Aerosols may be divided into two classes, primary and secondary aerosols, arising from two different basic processes:

- Primary aerosols derive from the dispersal of fine materials from the earth's surface. There are two major categories of natural primary aerosols: sea salts and dust.
- Secondary aerosols are formed by chemical reactions and condensation of atmospheric gases and vapours. The sulphur cycle dominates the tropospheric secondary aerosol budget. In pre-industrial conditions, it is mainly linked to marine biogenic activity which produces large amounts of gaseous dimethylsulfide (DMS).

Primary and secondary particles may interact strongly in the atmosphere, turning atmospheric aerosols into a very complex mixture (Raynaud et al., 2003; Chen and Griffin, 2005). They are removed from the air by both dry and wet deposition (see section 2.5).

Atmospheric aerosols influence climate in two ways: directly through reflection and absorption of solar radiation, and indirectly by modifying the optical properties and lifetimes of clouds. For example, in addition to ash, large explosive volcanic eruptions sporadically inject (a few times per century) huge amounts of SO_2 into the stratosphere. The sulphuric acid veil formed after such eruptions may persist for several years at an elevation of about 20 km, markedly cooling the global climate.

Large amounts of trace elements are transported as aerosols from low and mid latitudes to the polar areas by wind, generally in the troposphere, through sometimes by stratospheric pathways (see section 2.5). In some cases, these substances can act as nutrients, enhancing marine biogenic activity and the rate of atmospheric CO_2 sequestration in the ocean (Ridgwell, 2003).

[13] An aerosol is a suspended liquid or solid particle in a gas. Aerosols constitute a minor (~ one ppb by mass) but important component of the atmosphere. Indeed, aerosols play an active role in atmospheric chemistry.

Aerosol particles are incorporated in snowflakes by nucleation scavenging at cloud level, by below-cloud scavenging[14] and by dry deposition. In Polar Regions, it is generally accepted that wet deposition is dominant when the snow accumulation rate is high (> 20 g cm^{-2} yr^{-1}). On the other hand, at low accumulation sites, such as Dome C and Vostok stations in central Antarctica, dry deposition dominates.

Anthropogenic activities increase the amount of secondary particles in the atmosphere, as well as soot. The majority of anthropogenic aerosols exist in the form of sulphate and carbon, but also of nitrogen compounds. Presently, anthropogenic activity contribute approximately 20% to the global aerosol mass burden, but up to 50% to the global mean aerosol optical depth (Raynaud et al., 2003). It is generally accepted that the net global radiative forcing due to the anthropogenic aerosols is significant and negative[15] (Sato et al., 1993; Jacobson, 2001). However, quantification of their climate effects remains difficult, in particular due to large uncertainties associated with the indirect impact of aerosols on clouds.

Atmospheric aerosol particles have sizes which range from clusters of a few molecules to 100 μm and larger (Pruppacher and Klett, 1998). Studies of the atmospheric aerosol have shown that there are generally three modes of particle size. Aerosol particles with diameters r <0.1 μm belong to the nuclei (Aitken) mode, particles with 0.1 ≤ r ≤ 1.0 μm belong to the accumulation mode, and particles with r > 1.0 μm belong to the coarse mode (Whitby, 1976; 1978; Pruppacher and Klett, 1998; Seinfeld and Pandis, 1998) (**Figure 2.2.1**

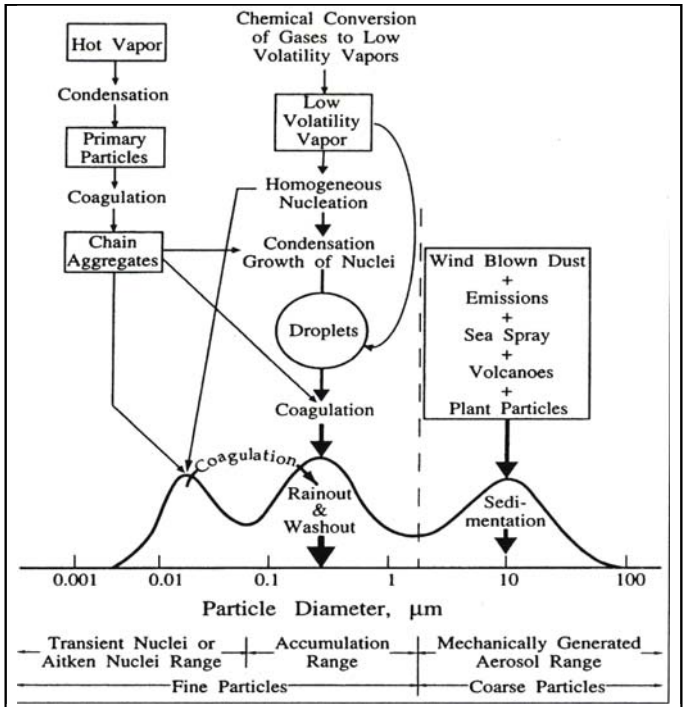

Fig. 2.2.1 : *Schematic representation of the aerosols size distribution depending of their source and major mechanisms taking place during their stay in the atmosphere (from Whitby, 1976)*

[14] This process is however rather unimportant in clean air conditions
[15] tend to cool the average global temperature

and **Table 2.2.1**). The nucleation and coarse particle modes are prevalent near the sources of particles. As an aerosol evolves with time away from sources, the dominant mode is the accumulation mode around 0.1 µm diameter (Singh, 1995).

	Fine particle (0.005- 1 µm)	**Coarse particle (1-100 µm)**
Formation process	Chemical reaction Nucleation Condensation Coagulation	Deflation Bubble bursting Eruptive volcanism
Chemical composition	Sulphate, nitrate, ammonium, carbon, organic compounds, metallic elements such as Pb, Cd, V, Cu, Zn, Mn, Ba, U, Cr, Bi, U…	Mineral dust, sea salt spray, ash, tephra, crustal elements (Si, Al, Fe, Ti, Sc, Ba, Mn…) and metalloids $CaC0_3$, NaCl, pollen, vegetal fragment
Solubility	Very soluble, hygroscopic	Slightly soluble for mineral particles Sea salt spray very hygroscopic
Mean Residence time	Few days to week	Few minutes to few days
Transport distance (km)	Hundreds to thousands	About ten to hundreds

Table 2.1.1: *usual characteristics of aerosols in function of the equivalent diameter (Seinfeld and Pandis, 1998)*

2.3 Natural emissions of trace elements into the atmosphere

2.3.1 Mineral aerosols

Mineral dust particles are mostly generated by winds in arid continental regions and, sporadically, by explosive volcanic eruptions which emit huge amounts of ash particles and by a negligible input of extraterrestrial materials.

Minerals entrapped in East Antarctic ice are mainly clays (about 40% of the total number of particles), followed by about 15% of crystalline silica and a comparable amount of feldspars, and other minor components like pyroxenes and amphiboles, metallic oxides, volcanic glasses (Gaudichet, 1986; 1988). Among clays, illite is the most abundant (>60%) in Vostok and South Pole ice (Gaudichet et al., 1992).

Table 2.3.1.1 give the composition of the mean upper continental crust (UCC) (Wedepohl, 1995), of Argentinean loess (Gallet et al., 1998), Damascus topsoils in Syria (Möller et al., 2005) as well as range concentrations coming across American soils (Nriagu, 1989). This table shows that trace elements concerned in this study (V, Cr, Mn, Fe, Co, Cu, Zn, As, Rb, Cd, Ba, Pb, Bi and U) are present in the earth crust in variable content with concentrations ranging from 0.08 µg/g for Bi up to 30 890 µg/g for Fe.

	Concentration (µg/g)													
	V	**Cr**	**Mn**	**Fe**	**Co**	**Cu**	**Zn**	**As**	**Rb**	**Cd**	**Ba**	**Pb**	**Bi**	**U**
UCC (Wedepohl, 1995)	53	35	527	30 890	11.6	15	52	2.0	110	0.1	668	17	0.08	2
Argentinean Loess (Gallet et al., 1998)	105	35	770	-	-	19	60	-	-	-	-	16	-	2.3
Damascus topsoils, Syria (Möller et al., 2005)	-	57	-	-	13	34	103	-	-	-	-	17	-	-
American soils (Nriagu, 1989)	20-60	60-100	700-800	-	-	15-30	50-80	-	-	0.2-0.8	-	5-15	-	-

Table 2.3.1.1: *Concentrations of trace elements in the UCC, Argentinean loess, Damascus topsoils and American soils*

Concentration of trace elements in American soils, Damascus topsoils and Argentinean loess are noticeably similar to the concentration that we can find in the upper continental crust (**Table 2.3.1.1**).

Estimation of the crustal contribution to trace elements concentration in the EPICA/Dome C ice core

In order to assess the importance of the rock and soil dust contribution for the trace elements studied in the various sections of the EPICA/Dome C ice core, I use the Crustal Enrichment Factor (EF_c). EF_c is defined as the concentration ratio of a given element to that of Ba (which is a

good proxy of continental dust) in the ice, normalized to the same concentration ratio characteristic of the upper continental crust (UCC). For example, the EF_c for V is thus:

$$EF_c\,(V) \quad = \quad \frac{[V]_{ice} / [Ba]_{ice}}{[V]_{UCC} / [Ba]_{UCC}}$$

For our study of the rock and soil dust contribution for the trace elements studied in our work, we have used the data of the upper continental crust given by Wedepohl (1995). It should however be mentioned that the use of other crustal compositions data (American soils, Damascus topsoils or Argentinean loess) not make any significant difference to the interpretation (see **Table 2.3.1.1**).

Despite the fact that the composition of rock and soil dust reaching Dome C might significantly differ from the composition of the mean upper continental crust, EF_c values close to unity (up to ~ 5) will indicate that the corresponding element mainly originated from the continental dust. Conversely, EF_c values much larger than unity will suggest a significant contribution from other natural sources.

2.3.2 Sea salt spray

The main possible natural sources other than continental dust are sea salt spray, volcanic emissions and marine biogenic activity (Nriagu, 1989). Most sea salt particles are produced by evaporation of spray breaking waves at the ocean surface (Raynaud et al., 2003).

Because of the multiple sources and pathways, the baseline (natural) concentrations of trace metals in a given environmental medium often show a wide spatial variation (**Table 2.3.2.1**). These elements can be grouped as a function of their "oceanic behaviour". This behaviour governs the repartition in the water column and the concentration in sea surface, where the sea salt spray is formed.

	Concentration (pg/g)			
	Mean (North Pacific) Yoshiyuki (1999)	Surface (North Pacific and North Atlantic) Donat and Bruland (1995)	Surface (Austral ocean and Atlantic sector)	Behaviour oceanic
V	2000	1100-1700	-	R
Cr	210	150	-	R
Mn	20	25-160	-	S
Fe	30	1.1-28	-	R+S
Co	1.2	0.2-2.9	1.8[a]	S
Cu	150	30-80	120[a]	R+S
Zn	350	6-12	260[a]	R
As	1200	1500	-	S
Rb	120	-	-	C
Cd	70	0.1-1	100[a, c]	R
Ba	15,000	-	-	R
Pb	2.7	2.8-3.0	2.0[a, b]	S
Bi	0.03	0.05	-	S
U	3200	-	-	C

[a] Westerlund et Öhman (1991)
[b] Flegal et al (1993)
[c] Capodaglio et al. (2001)

Table 2.3.2.1: *Mean concentration of trace elements in sea water (North Pacific, North Atlantic, Austral ocean) and oceanic behaviour in the water column (C: Conservative; R= Recycled, S: Scavenged)*

Thus **"conservative"** elements have a uniform vertical profile with identical concentrations in surface and deep waters. They are assumed to have no interaction with the particle cycle, and necessarily have long residence times (>105 yr) ensuring that they are thoroughly mixed within the ocean.

"Recycled" elements are intimately involved in the biologically driven particle cycle. They are removed into particulate material in the surface ocean and regenerated at depth in a simple first order process, resulting in the exponential shape of their vertical profile. Elements with this form of vertical profile necessarily have intermediate residence times (103 – 105 yr). If the residence times were longer than this, the total concentration would be higher in the ocean and although the shape of the profile would be similar, the extent of surface depletion would be much less.

"Scavenged" elements are rapidly removed by adsorption onto particle surfaces. The particles then sink through the water column, and even though the elements are released at mid-depth through recycling processes, they are rapidly removed again onto those particles that remain. As a result of this rapid removal, these elements typically have short residence times (<103 yr). The shape of the profile is dominated by the surface input processes (*i.e.* from eolian dust or from ocean margins) and the concentrations reduce to very low levels in the deep oceans.

Amongst trace elements studied in the **Table 2.3.2.1** only U and Rb show a conservative behaviour, probably due to their ionic form and their constant concentration whatever the depth (Chen et al., 1986). V, Cr, Fe, Cu, Zn, Cd and Ba follow the recycled behaviour. Biological activity tends to reduce concentrations in surface layers and to enrich deep water by mineralization of the organic material (Donat and Bruland, 1995). Mn, Fe, Co, Cu, As, Pb and Bi follow the scavenged behaviour and so have high concentrations in the surface layer and low concentrations for the rest of the water column. Their great affinity for the particulate matter drags them very fast through the water column (Donat and Bruland, 1995). Fe and Cu have hybrid behaviour. They are both influenced by biology and phenomena of adsorption.

Estimation of the sea-salt contribution to trace elements concentration in the EPICA/Dome C ice core

The contribution from sea-salt spray was estimated from Na concentrations measured in the ice (Wolff et al., 2006), after subtracting Na contributed from crustal dust, and metal/Na concentration ratios in bulk ocean water (Yoshiyuki, 1999). These ratios were not combined with possible enrichments in ocean derived aerosols relative to bulk ocean water, when marine aerosol is formed by bubble bursting through the surface micro-layer, since recent studies have put doubt on such possible enrichments (Hunter, 1997).

The study of Hong et al.(1998) in the ice of Law Dome (Antarctic coastal site) shows that 10 to 40% of Pb, 60% of Cd, 10 to 80% of Cu could be explained by the oceanic contribution. So, Ocean may be a significant source of trace elements in coastal snow and ice of the Antarctic continent. However, the oceans were not a significant source of trace elements in the East Antarctic plateau (Boutron et al., 1987; 1990; 1993; Gabrielli et al., 2005b).

2.3.3 Volcanic aerosols

Volcanoes are an important source of gases and aerosol to the atmosphere. A significant amount of aerosol reaches the stratosphere and circle the globe within several weeks, affected the global climate for a few years (Rampino and Self, 1992). Small, passively degassing volcanoes also contribute significant amounts of volatile elements as gases and aerosols to the troposphere (Zreda-Gostynska et al., 1997).

Table 2.3.3.1 compare the variability of metal/S ratios of 14 trace elements for different volcanoes, which is given by various authors (Buat-Menard and Arnold, 1978; Olmez et al., 1986; Patterson and Settle, 1987; Buat-Menard, 1988; Nriagu, 1989; Hinkley et al., 1999).

		Metal / S ($\times 10^{-4}$)													
		V	**Cr**	**Mn**	**Fe**	**Co**	**Cu**	**Zn**	**As**	**Rb**	**Cd**	**Ba**	**Pb**	**Bi**	**U**
Buat-Menard and Arnold, 1978 *Mount Etna*	min	0.6	0.5	9	-	0.1	-	-	-	-	0.6	-	-	-	-
	max	3	0.8	-	-	0.8	-	-	-	-	-	-	-	-	-
Olmez et al., 1986 *Kilauea*	min	0.02	0.15	0.1	-	-	0.6	0.08	-	-	0.02	0.2	-	-	-
	max	0.15	-	0.4	-	-	-	0.4	-	-	0.4	0.05	-	-	-
Patterson and Settle, 1987 *Worldwide volcano emissions*	min	-	-	-	-	-	-	-	-	-	-	-	0.02	0.5	-
	max	-	-	-	-	-	-	-	-	-	-	-	1.9	3.4	-
Buat-Menard, 1988 *Worldwide volcano emissions*	min	-	-	-	-	-	-	0.3	-	-	0.03	-	-	-	-
	max	-	-	-	-	-	-	15	-	-	2.7	-	-	-	-
Nriagu, 1989 *Worldwide volcano emissions*	min	0.1	0.5	2.8	-	0.01	0.6	0.2	-	-	0.09	-	0.4	-	-
	max	2.1	5.8	16	-	2.5	3.5	3.8	-	-	0.3	-	1.2	-	-
Hinkley et al., 1999 *Worldwide volcano emissions*	Mean	-	-	-	-	-	1.0	2.2	0.90	-	0.2	-	0.3	0.16	-

Table 2.3.3.1 : *Variability range of Metal/S ratios given by various authors for 14 trace elements*

Nriagu (1989) estimated that volcanic emanations contribute about 40-50% of Cd and Hg, and between 20 and 40% of As, Cr, Cu, Ni, Pb and Sb emitted annually from natural sources.

However, these estimates are based on scant data and it is likely they are low (Zreda-Gostynska et al., 1997).

Estimation of volcano contribution to trace elements concentration in the EPICA/Dome C ice core

A rough estimate of the contribution from volcanoes was made from the concentrations of non sea-salt sulphate ($nssS0_4$) in the ice (Wolff et al., 2006) by assuming that ~ 10-15% of $nssS0_4$ originates from volcanoes (Boutron and Patterson, 1986). They were combined with available data on metal/S ratios in volcanic emissions (Hinkley et al., 1999). It must however be kept in mind that these estimates are very rough especially because of the wide range of published data for metal/S ratios in volcanic emissions (see **Table 2.3.3.1**).

A possible volcanic source within East Antarctica could be the Mount Erebus active volcano (77°33' S, 161°10' E, 3794 m above sea level), which is the southernmost active volcano in the world. It could be a potential source of Cu, Cd, V and As found in Antarctic snow and atmospheric samples (Zreda-Gostynska et al., 1997).

2.3.4 Biogenic sources

It exists two types of biogenic sources: biomass burning and emissions coming from marine and continental activity.

Biomass burning:

Some elements such as V, Cr, Mn, Cu, Zn, Cd and Pb occur in trace amounts in plants. Some of these elements are essential for the growth and development of plants. The concentration ranges in plant tissue are around µg/g for essential elements such as V, Cr, Mn, Cu, Zn and Cd whereas non-essential elements such as Bi, Pb and U are about ng/g.

The major components of biomass burning are forests (tropical, temperate, and boreal); savannas; agricultural lands after the harvest; and wood for cooking, heating, and the production of charcoal. The burning of tropical savannas is estimated to destroy three times as much dry matter

per year as the burning of tropical forests. The immediate effect of burning is the production and release into the atmosphere of gases and particulates such as trace elements that result from the combustion of biomass matter (Kaufman et al., 1992).

Nriagu (1989) indexes emissions of trace elements in relation to carbon. **Table 2.3.4.1** shows the variation of emission factors for every metal from biomass fire and other biogenic sources. At global scale, biomass fire may be an important source of Cd, Cu, Mn and Zn (Nriagu, 1989).

	V	Cr	Mn	Cu	Zn	Cd	Pb
Biomass Fire	0.1-2.4	0-0.15	6.0-30	0.5-50	1.5-10	0-0.15	0.1-2.5
Continental particulate	0.2-3.5	1.0-4.0	20-100	1.0-10	3-10	0-0.6	0.2-5.0
continental and marine volatile	0.3-1.0	0-0.4	1.0-10	0.3-2.5	0.5-20	0-0.3	0.2-1.5

Table 2.3.4.1 : *Emission factor per element for biomass fire and the other biogenic sources (Nriagu, 1989)*

In the South Hemisphere, it exists some sources for the biomass fires such as Australian bush or savannah of the southern Africa and equatorial forest of South America (Planchon, 2002). However, in Antarctic, the influence of biomass fire on trace element concentrations has never been brought to the fore.

Emissions from marine and continental activity:

Vegetal organisms desorb many chemical volatile compounds emitted into the atmosphere. Amongst these numerous compounds, we recognize non-methan hydrocarbons (NMHC) like isoprene and terpenes, particulate carbon, sulphur compounds (DMS), pollens and spores. These compounds can form various complexes containing trace elements, and so favour their emissions into the atmosphere. Nriagu (1989) suggests flux estimates of trace elements associated to biogenic emissions (**Table 2.3.4.1**) and divides biogenic sources into three categories which depend on the type and emission sources.

DMS (Dimethylsulfide) is produced in the ocean by marine biogenic activity. Methanesulfonic acid (MSA) is the most important compound formed as DMS is oxidized in the atmosphere and it is uniquely attributable to marine biogenic activity (Raynaud et al., 2003). The production of MSA in Antarctic documents the marine biogenic activity with known past climate variability (Legrand et al., 1991; 1992; Arimoto et al., 2004).

Moreover, COS (Carbonyl sulphide) which is the major sulfur compound naturally present in the atmosphere at 0.5 (± 0.05) ppb is produced from the oxidation of DMS and CS_2 (disulphide), and is also directly emitted from oceans as a byproduct of biological and photochemical reactions, which account for 13%, 32, and 22% of the global sources, respectively (Watts, 2000).

Biological activity is responsible for the enrichment of trace elements in ocean surface layers (see section 2.3.2). Some of these trace elements can be bio-methylated by marine bacteria. Pongratz and Heumann (1999) brought to the fore biomethylation processes in polar region for Pb and Cd by marine bacteria. The ionic by-product compounds are not very volatile compared to methyl mercury. Consequently, direct emission into the atmosphere is very unlikely. However, it is possible that such compounds are incorporated to sea salt spray and might explain the enrichment of Cd and Pb of surface layer in marine aerosol, compared to the global average sea (Planchon, 2002).

Estimation of biogenic contribution to trace elements concentration in the EPICA/Dome C ice core

Due to the lack of data on the abundances of trace elements in aerosols produced by biogenic activity, and also the absence of total carbon measurements, it is impossible to evaluate the contribution in trace elements in ice cores coming from biogenic sources.

2.4 Anthropogenic emissions of trace elements into the atmosphere

Many studies have been devoted to the estimation of anthropogenic fluxes of trace elements into the atmosphere, at global scale (Nriagu and Pacyna, 1988; Nriagu, 1990a,b,c; Pacyna and Pacyna, 2001, Wilson et al., 2006) or at regional scale (Pacyna et al.,

1984; Pacyna et al., 2007). All these studies confirm that emissions stemming from human activities largely exceed natural fluxes at global scale for numerous trace elements.

Table 2.4.1 introduce estimation of anthropogenic fluxes for trace elements into the atmosphere for the year 1983 and 1995 (Nriagu and Pacyna, 1988; Pacyna and Pacyna, 2001). We can notice that, for most trace elements, anthropogenic flux estimates largely exceed natural fluxes. The only exceptions are Cr and Mn in which case natural sources are still dominant in global scale (**Table 2.4.1**).

	V	Cr	Mn	Cu	Zn	Cd	Pb
Natural emissions[a] (Kt/yr)	28	43	317	28	45	1.4	12
Anthropogenic emissions[b] (Kt/yr) Year 1995	240	15	11	26	57	3.0	119
Interference factor Anth./Nat.Year 1995	8.6	1.0	0.03	1	1.3	2.3	10
Anthropogenic emissions[c] (Kt/yr) Year 1983	86	31	38	35	132	7.6	332
Interference factor Anth./Nat.Year 1983	3.1	0.7	0.1	1.3	2.9	5.4	28

[a] Nriagu, 1989
[b] Pacyna and Pacyna, 2001
[c] Nriagu and Pacyna, 1988

Table 2.4.1 : *Anthropogenic emissions of trace elements into the atmosphere in 1983 and 1995 and comparison with characteristic natural emissions of actual climatic conditions (in Kt/yr)*

During the 20th century, demand for Pb and other metals has continued to increase, with ~ 90% of total mine outputs being during the 20th century (Nriagu, 1996). The discovery of alkyklead additives for gasoline in the 1920's and their subsequent introduction worldwide has caused another increase in demand for Pb in the 20th century, and has also significantly increased the quantity of Pb emitted to the atmosphere (Bollhöfer and Rosman, 2000). Despite the withdrawal of alkyklead additives for gasoline, Pb still appeared significantly disturbed by anthropogenic activities in 1997 (Kakareka et al., 2004). The increase of oil consumption and its by-product significantly increased the quantity of V emitted to the atmosphere in the last decades (Planchon, 2002).

As a result of the stringent regulations governing the emissions of toxic substances, such as carbon monoxide, from transport vehicles, many countries adopted catalytic converters in order to convert these harmful compounds into less harmful compounds. However, Pt, Pd and Rh, so-called Platinum Group Elements (PGE) are usually deposited on the surface of the monolithic ceramic support which is placed at the end of the exhaust stream system (Jacoby, 1999). In spite of the clear benefits obtained with the use of catalytic converters, the ever increasing use of theses devices might lead to PGE becoming widely dispersed in the environment. Many environmental matrices such as soil, road-side dust, atmospheric particulates etc. have been found to be enriched in PGE with respect to their background values (Barbante and Cescon, 2000).

For the other trace elements, estimates given between 1983 and 1995 indicate a decreasing trend of the anthropogenic emissions. This decrease could be due to the recent use of reduction system for particulate dust emissions or the treatment of gaseous effluents (Planchon, 2001).

2.5 Atmospheric transport of aerosols

Trace elements are transported through the air as particulates, and as such transport is dependent upon the size, shape, mass and other physical and chemical properties of the particles.

During long-range transport, the decrease in particle concentration (from the source a to the sink b) can be described as:

$$C_b = C_a \times f \times e^{-t/T}$$

Where t is the transit time between the source a to the sink b, T is the residence time in the atmosphere, governed by wet and dry deposition processes en route, C_a and C_b the atmospheric concentration at the source and the sink respectively, and f a correction factor. Therefore, the longer will be the transport time, the lower will be the concentration of trace elements at the sink.

Particles can be removed from the atmosphere by dry or wet deposition. Dry deposition includes gravitational settling, where the settling velocity depends on the square of particle size, and

turbulent mixing to the surface, while precipitation-related events like sub-cloud scavenging and in-cloud removal determine the wet deposition.

The removal efficiency is size dependent; hence during transport the size distribution changes. For sands and coarse silts the gravitational settling[16] alone (dry deposition) determines the sedimentation velocity, while for clays the lifetime in the atmosphere is mainly controlled by wet deposition and turbulent mixing.

A parameterization of uplift and deposition (using analyzed winds and rainfall statistics) has been performed by Tegen and Fung (1994) and Tegen and Lacis (1996). The authors obtained atmospheric lifetimes spanning a very large interval, from one hour to about ten days, in function of particle size (**Table 2.5.1** and **Figure 2.5.1**)

Particle Diameter (μm)	Atmospheric Lifetime (hours)
0.30	**231**
0.50	**229**
0.80	**225**
1.6	**219**
3	**179**
5	**126**
8	**67**
12	40
16	**28**
36	4
76	1

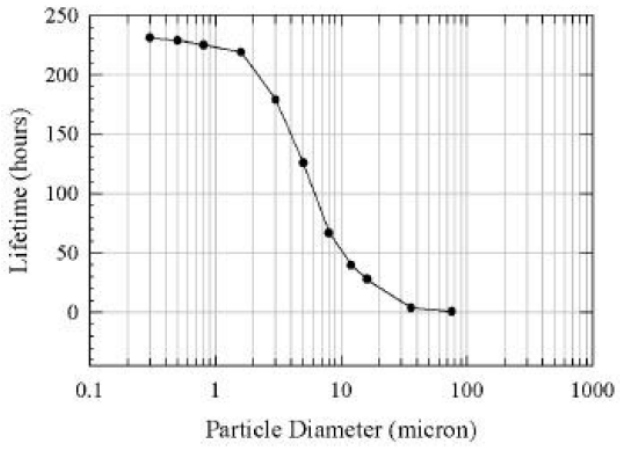

Table 2.5.1 and Figure 2.5.1 : *Atmospheric lifetimes for particles of different diameter(Tegen and Lacis, 1996; Tegen and Fung, 1994)*

[16] In a fluid regime the particle settling velocity is governed by the Stokes law equation which can be expressed:

$$V=[\ \Delta\rho g/18\mu]d^2$$

V= settling velocity ($cm*s^{-1)}$
$\Delta\rho$= particle -fluid density difference ($g*cm^{-3}$)
g= acceleration due to gravity ($cm*s^{-2}$)
μ= viscosity (poise)
and d= particle diameter (cm)

For example, lead is effectively sequestered in the hemisphere in which it is emitted , on account of the ~ 10 days mean atmospheric residence time for anthropogenic Pb aerosols (Patterson and Settle, 1987) and the approximate 1-year period required for significant exchange of aerosols between the Northern and Southern Hemisphere (Levin and Hesshaimer, 1996).

Tegen and Lacis (1996) observed a decrease in particles concentration with increasing atmospheric height, as large particles are removed by gravitational settling before they can reach the higher atmospheric levels. Size distribution is also altitude dependent, since the higher atmospheric levels are depleted of large particles. An interesting issue from Tegen and Fung (1994) is the modelled vertical distribution of dust concentration for individual classes of particles, that exhibits increased concentration of small particles (clays) with respect to larger ones (silts and sands) with height, due to the high sedimentation velocity of these latter. Only clays and small silts therefore are transported within the mid to high troposphere levels and have therefore the potential to reach the interior of the East Antarctic (Delmonte, 2004).

2.6 Literature review

2.6.1 The first reliable evaluation of trace elements concentration in polar snow and ice

During the last five decades, considerable effort has been devoted by various laboratories to decipher the unique atmospheric archives stored in the successive dated snow and ice layers deposited from several hundred thousand years ago to present in the large Antarctic and Greenland ice caps. The earliest measurements of polar ice and snow were invalidated by contamination of the samples, but as it was recognized at the time, these studies concluded that urban areas was as unpolluted as the Earth's most distant and isolated region: the polar ice sheets. In the 1960s, it was demonstrated that reliable results could only be obtained by strict observation and control of sample contamination.

Interest to measure heavy metals was stimulated in the early 1920s by Thomas Midgely (Nriagu, 1990) who discovered the extensive use of the lead additives for gasoline. Unfortunately, the

challenge of demonstrating the threat to environment and health posed by widespread Pb emissions required the distinction of natural Pb levels from typical anthropogenic Pb levels, which was not recognized in the early 1920s. The invention of the atomic absorption spectrometer (AAS) in 1954 by Alan Walsh permitted easily the determination of Pb and other trace elements in various matrices. However, since no one was conscious of contamination issues at the time, the samples collected were entirely contaminated by anthropogenic lead.

The importance of contamination control was first realised in the 1960s by Clair C. Patterson and co-workers at the Department of Earth and Planetary Sciences of the California Institute of Technology (Caltech) (Flegal, 1998). When he became interested in snow and ice, Clair C.Patterson was already a famous scientist and had already given the first accurate determination of the age of the Earth (Patterson, 1956; Patterson et al., 1955). He pioneered the concept of contamination control in handling environmental samples (Patterson and Settle, 1976). However, Patterson's efforts were distinguished not only in regard to the foresight and dedication shown to tackling the many challenges of trace-metal analysis, but also in the effort required to convince an establishment of scientists, governments and corporations that global heavy metal pollution was a real and imminent threat to society and the environment.

While Patterson and co-workers had earlier demonstrated the majority of Pb in urban air and coastal and open ocean waters to be due to the anthropogenic sources, they were yet to establish how Pb levels had changed over time. To do this, they measured trace elements, including lead, in snow and ice deposited in the Greenland and Antarctic ice caps. Extreme conditions were taken to minimize sample contamination (Murozumi et al., 1969). Murozumi et al. (1969) determined that lead concentrations in Greenland had increased significantly since 800 BC and linked these increases with important changes in the industrial and societal uses of Pb. They documented a very spectacular increase of lead concentrations in Greenland snow from the Industrial Revolution onward, up to concentration of ~ 200 ppt in the mid 1960s. A large part of this tremendous increase was observed after the 1930s and was clearly linked with ever-increasing use of lead additives in gasoline. This famous paper played a major role in the phasing out of lead additives.

In 1981, the reliable measurement of Pb in ancient Greenland and Antarctic ice was published, again by Patterson and co-workers (Ng and Patterson, 1981). It was the first time that someone was able to analyse accurately lead and other trace elements in deep ice cores whose outside had been highly contaminated during drilling operations. This was achieved by developing sophisticated procedures which allowed the decontamination of the contaminated core sections by chiselling successive veneer layers of ice in progression from the outside to the center, without transferring contamination present on the outside to the inner core. This major step will allow to obtain the accurate evaluations of concentrations of heavy metals in the 1990s in deep ice cores.

2.6.2 Studies of trace elements in Greenland and Antarctica

Other studies attempted to duplicate the results of Murozumi et al. (1969) from samples of snow and ice obtained from Greenland and Antarctica (Francis Hanappe and Edouard Picciotto at the University of Brussels and Claude Boutron, Martine Echevin and Claude Lorius Cat the Laboratoire de Glaciologie et Géophysique de l'Environnement in Grenoble). These all failed to obtain reliable data for heavy metals. For example, they could not see the steadily-increasing Pb concentrations in the snow since the 18th century (Boutron and Lorius, 1979). Boutron and Lorius (1979) observed fluxes of Pb, Cd, Cu, Zn and Ag which corresponded approximately to emission fluxes from volcanoes, and believed that volcanoes could account for the enrichment of heavy metals observed in the snow. These findings were challenged by results published by Ng and Patterson (1981) however. These studies generally lacked suitable precautions against sample contamination.

During the 1980s and early 1990s a number of important studies were undertaken to resolve the discrepancies of results of Antarctic studies published in the 1970s, largely due to contamination of samples during collection and/or analysis. Boutron, Patterson and co-workers, collaborating closely, published a series of analyses of Pb concentrations in ice cores from several locations in Antarctica (Boutron and Patterson, 1986;1987), confirming the initial results obtained by Patterson and co-workers in 1969 and 1981, and extended the record of lead concentrations in Antarctic ice back to 155,000 years before present.

The heavy metals research undertaken at LGGE, led by Professor Claude Boutron, began with a description of the clean room facilities and analytical capabilities of the laboratory and its graphite furnace atomic absorption spectrometer (GFAAS), and published in *Fresenius Journal of Analytical Chemistry* (Boutron, 1990). The first of several significant publications by Boutron and co-workers regarding heavy metals concentrations in Greenland snow and ice reported decreasing concentrations of anthropogenic Pb, Cd, Cu and Zn in Greenland snows since 1967 (Boutron et al., 1991). The work presented by Boutron et al. (1991) indicated that Pb concentrations in Greenland were closely linked to anthropogenic atmospheric Pb emissions and responded relatively quickly to changes in anthropogenic emissions. They also demonstrated that the Greenland ice sheet was also sensitive to changes in the emissions of other trace metals for which anthropogenic emissions were comparable with natural emissions, such as Cd Cu and Zn.

While the previous studies have made use of snow cores, the drilling and sampling of deep ice cores required a different approach. The deep ice cores penetrated more than three kilometers into the ice sheet, requiring the use of drilling heads, wires and core barrels made of drilling fluid, used to equalize the pressure in the drill hole to that of the surrounding ice. Additionally, techniques had to be developed for cores for which only part of the cross section was available. Candelone et al. (1994) described a technique for decontaminating ice cores, using a special lathe and stainless steel chisels, which provided the solution to these requirements. The technique made use of the approaches adopted by Ng and Patterson (1981) and Boutron and Patterson (1986) for the decontamination of Greenland and Antarctic ice cores but minimized contamination by supporting the core in a custom-built lathe. Candelone et al. (1994) also evaluated the decontamination technique using a number of ice cores sections drilled in Greenland and Antarctica. High concentrations of Cd, Cu, Pb and Zn were observed in all external layers for the ice cores, irrespective of whether or not drilling fluid has been used in the drill hole, or whether the corer was thermal or eletromechanical.

The decontamination procedure described by Candelone et al.(1994) was first employed on the GRIP ice core drilled at Summit, Greenland (Hong et al., 1994). The same technique of decontamination was also used for the Vostok ice core (Hong et al., 2003; 2004; Gabrielli et al., 2005a) and the two first kilometers of the EPICA/Dome C ice core (Gabrielli et al., 2005b;

Vallelonga et al., 2005). Amongst the most spectacular results obtained so far are the evaluation of the natural variations of two platinum group elements (PGEs), Ir and Pt, in Greenland and Antarctic ice cores, during few climatic cycle (Gabrielli et al., 2004a; Gabrielli et al., 2006). A new analytical methodology based on inductively plasma sector field mass spectrometry (ICP-SFMS) coupled with a micro-flow nebulizer and desolvatation has been set up for the quantification of Ir and Pt down to the sub-ppq level in polar ice samples (Gabrielli et al., 2004b).

.

REFERENCES

Aaby B, Jacobsen J, Jacobsen OS (1979) Pb-210 dating and lead deposition in the ombrotrophic peat bog, Draved Mose, Denmark. In: *Denmarks Geologisk Ungersoglse Arbog.* pp. 5-43

Arimoto R, Hogan A, Grube P, Davis D, Webb J, Schloesslin C, Sage S, Raccah F (2004) Major ions and radionuclides in aerosol particles from the South Pole during ISCAT-2000. *Atmospheric Environment* **38**, 5473-7484

Barbante C, Cescon P (2000) Uses and environmental impact of automobile catalytic converters. In: Boutron CF (Ed) *From weather forecasting to exploring the solar system.* EDP Sciences. pp. 125-146

Barbante CA, Veysseyre A, Ferrari C, Van de Velde K, Morel C, Capodaglio G, Cescon P, Scarponi G, Boutron CF (2001) Greenland snow evidence of large scale atmospheric contamination from platinum, palladium and rhodium. *Environmental Science and Technology* **35**, 835-839.

Blais JM (1998) Accumulation of persitent organochlorine compounds in mountains of western Canada. *Nature* **395**, 585-588

Bollhöfer AF, Rosman KJR (2000) Isotopic source signatures for atmospheric lead: The Southern Hemisphere. *Geochimica et Cosmochimica Acta* **64**, 3251-6362

Boutron CF (1990) A clean laboratory for ultralow concentration heavy metals analysis. *Fresenius Journal of Analytical Chemistry* **337,** 482-491

Boutron CF (1995) Historical reconstruction of the earth's past atmospheric environment from Greenland and Antarctic snow and ice cores. *Environmental Reviews* **3**, 1-28

Boutron CF, Lorius C (1979) Trace metals in Antarctic snow since 1914. *Nature* **277,** 551-554

Boutron CF, Patterson CC (1986) Lead concentration changes in Antarctic ice during the Wisconsin/Holocene transition. *Nature* **323**, 222-225.

Boutron CF, Patterson CC (1987) Relative levels of natural and anthropogenic lead in recent Antarctic snow. *Journal of Geophysical Research* **92** (D7), 8454-8464

Boutron CF, Patterson CC, Barkov NI (1990) The occurrence of zinc in Antarctic ancient ice and recent snow. *Earth and Planetary Science Letters* **101,** 248-259

Boutron CF, Görlash U, Candelone JP, Bolshov MA, Delmas RJ (1991) Decrease in anthropogenic lead, cadmium and zinc in Greenland snows since the last 1960s. *Nature* **353**, 153-156

Boutron CF, Rudniev SN, Bolshov MA, Koloshikov VG, Patterson CC and Barkov NI (1993) Changes in cadmium concentrations in Antarctic ice and snow during the past 155,000 years. *Earth and Planetary Science Letters* **117,** 431-441

Brimblecombe P (1987) *The big Smoke.* Methuen, London

Buat-Menard P (1988) Global source strength and long-range transport of trace elements emitted by volcanic activity. In: Knap AH, Kaiser MS (ed) *The long-range transport of natural and contaminant substances,* NATO ASI series, pp. 163-175

Buat-Menard P, Arnold M (1978) The heavy metal chemistry of atmospheric particulate matter emitted by Mount Etna Volcano. *Geophysical Research Letters* **5**, 245-248

Candelone JP, Hong S, Boutron CF (1994) An improved method for decontaminating polar snow and ice cores for heavy metal analysis. *Analytica Chimica Acta* **299**, 9-16

Candelone JP, Hong S, Pellone C, Boutron CF (1995) Post-industrial revolution changes in large-scale atmospheric pollution of the Northern Hemisphere for heavy metals as documented in central Greenland snow and ice. *Journal of Geophysical Research* **100**, 16,605- 16,616

Capodaglio G, Barbante C, Cescon P (2001) Trace metals in Antarctic seawater. In: Caroli S, Cescon P, Walton DWH. (ed) *Environmental contamination in Antarctica, a challenge to analytical chemistry.* Elsevier Science BV

Chen LH, Edwards RL, Wasserburg GJ (1986) 238U, 234U and 232Th in seawater. *Earth and Planetary Science Letters* **80**, 241-256

Chen J, Griffin RJ (2005) Modeling secondary organic aerosol formation from oxidation of -pinene and d-limonene. *Atmospheric Environment* **39**, 7731-7744

Clymo RS, Oldfield F, Appleby PG, Pearson GW, Ratnesar P, Richardson N (1990) The record of atmospheric deposition on a rainwater-dependent peatland. *Philosophical Transactions of the Royal Society of London (B)* **327**, 331-338

Delmonte B, Petit JR, Anderson KK, Basile-Doelsh I, Maggi V, Lipenkov VY (2004) Dust size evidence for opposite regional atmospheric circulation over East Antarctica during the last climatic transition. *Climate Dynamics* **23**, 427-428

Donat JR, Bruland KW (1995) Trace elements in the Oceans. In: Salbu B, Steines E (Ed) *Trace elements in natural waters*, CRC press, Boca Raton, pp. 247-280

Edgington DN, Robbins JA (1976) Records of lead deposition in lake Michigan

sediments since 1800. *Environmental Science and Technology* **10**, 266-274

Flegal AR (1998) Clair Patterson's influence on Environmental Research. *Environmental Research* **78(A)**, 65-70

Flegal AR, Maring H, Niemeyer S (1993) Anthropogenic lead in Antarctic sea water. *Nature* **365**, 242-244

Gabrielli P, Barbante C, Plane JM, Varga A, Hong S, Cozzi G, Gaspari V, Planchon FA, Cairns W, Ferrari C, Crutzen P, Cescon P, Boutron CF (2004a) Meteoric smoke fallout over the Holocene epoch revealed by iridium and platinum in Greenland ice. *Nature* **432**, 1011-1014

Gabrielli P, Varga A, Barbante C, Boutron C, Cozzi G, Gaspari V, Planchon F, Cairns W, Hong S, Ferrari C, Capodaglio G (2004b) Determination of Ir and Pt down to the sub-femtogram per gram level in polar ice by ICP-SFMS using preconcentration and a desolvatation system. *Journal of Analytic Atomic Spectrometry* **19**, 831-837

Gabrielli P, Planchon FAM, Hong S, Lee KH, Hur SD, Barbante C, Ferrari CP, Petit JR, Lipenkov VY, Cescon P, Boutron CF (2005a). Trace elements in Vostok Antarctic ice during the last four climatic cycles. *Earth Planetary and Science Letters* **234**, 249-259.

Gabrielli P, Barbante C, Boutron C, Cozzi G, Gaspari V, Planchon F, Ferrari C, Turetta C, Hong S, Cescon P (2005b) Variations in atmospheric trace elements in Dome C (East Antarctica) ice over the last two climatic cycles. *Atmospheric Environment* **39**, 6420-6429

Gabrielli P, Plane JMC, Boutron CF, Hong S, Cozzi G, Cescon P, Ferrari C , Crutzen PJ, Petit JR, Lipenkov VY, Barbante C (2006) A climatic control on the accretion of meteoric and super-chondritic iridium–platinum to the Antarctic ice cap. *Earth and Planetary Science Letters* **250**, 459-469

Gallet S, Jahn B, Van Vliet L, Dia A, Rosselo E (1998) Loess geochemistry and its implications for particle origin and composition of the upper continental crust. *Earth and Planetary Science Letters* **156**, 157-172

Galloway JN, Likens GE (1979) Atmospheric enhancement of metal deposition in Adirondack lake sediment. *Limnology and Oceanography* **24**, 427-433

Gaudichet A, Petit JR, Lefevre R, Lorius C (1986) An investigation by analytical transmission electron microscopy of individual insoluble microparticles from Antarctic (Dome C) ice core samples. *Tellus*, 250-261

Gaudichet A, Angelis MD, Lefevre R, Petit JR, Korotkevitch YS, Petrov VN (1988) Mineralogy of insoluble particles in the Vostok Antarctic ice core over the last climatic cycle (150 Kyr). *Geophysical Research Letters* **15**, 1471-1474

Gaudichet A, Angelis MD, Jossaume S, Petit JR, Korotkevitch YS, Petrov VN (1992) Comments on the origin of dust in East Antarctica for present and ice age conditions. *Journal of Atmospheric Chemistry* **14**, 129-142

Goodarzi F, Mukhopadhyay (Muki) PK (2000) Metals and polyaromatic hydrocarbons in the drinking water of the Sydney Basin, Nova Scotia, Canada: a preliminary assessment of their source. *International Journal of Coal Geology* **43**, 357–372

Healy JF (1978) *Mining and Metallurgy in Greek and Roman world*. Thames and Hudson editors, London

Hinkley TK, Lamothe PJ, Wilson SA, Finnegan DL, Gerlach TM (1999) Metal emissions from Kilauea, and a suggested revision of the estimated worldwide metal output by quiescent degassing of volcanoes. *Earth and Planetary Science Letters* **170**, 315-325

Hites RA (1981) Sources and fates of polycyclic aromatic hydrocarbons. *American Chemical Society Symposium Series* **167**, 187-196

Hong S, Candelone JP, Patterson CC Boutron CF (1994) Greenland ice evidence of hemispheric lead pollution two millennia ago by Greek and Roman civilizations. *Science* **265**, 1841-1843

Hong S, Candelone JP, Patterson CC Boutron CF (1996) History of ancient copper smelting pollution during roman and medieval times recorded in Greenland ice. *Science* **272**, 246-249

Hong S, Boutron CF, Edwards R, Morgan VI (1998) Heavy metals in Antarctic ice from Law Dome: initial results. *Environmental Research* (A) **78**, 94-103

Hong S, Kim Y, Boutron CF, Ferrari CP, Petit JR, Barbante C, Rosman K, Lipenkov VY (2003) Climate-related variations in lead concentrations and sources in Vostok Antarctic ice from 65,000 to 240, 000 years BP. *Geophysical Research Letters* **22**, 2138, doi: 10.1029/2003GL018411

Hong S, Boutron CF, Gabrielli P, Barbante C, Ferrari CP, Petit JR, Lee K, Lipenkov VY (2004) Past natural changes in Cu, Zn and Cd in Vostok Antarctic ice dated back to the penultimate interglacial period. *Geophysical Research Letters* **31**, L20111, doi: 10.1029/2004GL021075

Hunter KA (1997) Chemistry of the sea-surface microlayer. In: Liss PS, Duce RA (ed) *The sea surface and global change.* Cambridge University Press, pp. 287-319

Jacobson MZ (2001) Global direct radiative forcing due to multicomponent anthropogenic and natural aerosols. *Journal of Geophysical Research* **106 (D2)**, 1551-1568

Jacoby M (1999) Fuel cells heading for sale. *Chemical and Engineering News* **77**, 31-37

Jiun-Horng T, Kuo-Hsiung L, Chih-Yu C, Jian-Yuan D, Ching-Guan C, Hung-Lung C (2007) Chemical constituents in particulate emissions from an integrated iron and steel facility. *Journal of Hazardous Materials* **147**, 111–119

Kakareka S, Gromov S, Pacyna J, Kukharchyk T (2004) Estimation of heavy metal emission fluxes on the territory of the NIS. *Atmospheric Environment* **38 (40)**, 7101-7109

Kaufman YJ, Setzer A, Ward D, Tanre D, Holben BN, Menzel P, Pereira MC, Rasmussen R (1992) Biomass burning airborne and spaceborne experiment in the Amazona. *Journal of Geophysical Research* **97 (D13)**, 14,581- 14,599

Kober B, Wessels M, Bollhöfer A, Mangini A (1999) Pb isotopes in sediments of lake Constance, Central Europe constrain the heavy metals pathways and the pollution history of the cathment, the lake and the regional atmosphere. *Geochimica et Cosmochimica Acta* **63**, 1293-1303

Legrand M, Feniet-Saigne C, Saltzmann ES, Germain C, Barkov NI, Petrov VN (1991) Ice-core record of oceanic emissions of dimethylsulphide during the last climatic cycle. *Nature* **350**, 144-146

Legrand M, Feniet-Saigne C, Saltzmann ES, Germain C (1992) Spatial and temporal variations of methansulfonic acid and non sea salt sulfate in Antarctic ice. *Journal of Atmospheric Chemistry* **14**, 245-260

Levin I, Hesshaimer V (1996) Refining of atmospheric transport model entries by the globally observed passive tracer distributions of ^{85}Krypton and sulphur hexafluoride (SF_6). *Journal of Geophysical Research* **101 (D11)**, 16,745-16,755

Martinez-Cortizas A, Pontevedra-Pombal X, Garcia- Rodeja E, Novoa-Munoz JC, Shotyk W (1999) Mercury in a Spanish peat bog: Archive of climate change and atmospheric metal deposition. *Science* **284**, 939-942

Möller A, Müller HW, Abdullah A, Abdelgawad G, Utermann J (2005) Urban soil pollution in Damascus, Syria: concentrations and patterns of heavy

metals in the soils of the Damascus Ghouta. *Geoderma* **124**, 63-71

Murozumi M, Chow TJ, Patterson CC (1969) Chemical concentrations of pollutant lead aerosols, terrestrial dust and sea salts in Greenland and Antarctic snow strata. *Geochimica et Cosmochimica Acta* **33**, 1247-1294

Ng A, Patterson CC (1981) Natural concentrations of lead in ancient Arctic and Antarctic ice. *Geochimica et Cosmochimica Acta* **45**, 2109-2121

Norton S (1985) Geochemistry of selected Maine peat deposits. *Bulletin of the Maine Geological Survey* **34**, 1-38

Nriagu JO (1989) A global assessment of natural sources of atmospheric trace metals. *Nature* **338**, 47-49

Nriagu JO (1990a) The rise and fall of leaded gasoline. *Science of the Total Environment* **92**, 13-28

Nriagu JO (1990b) Human influence on the global cycling of trace metals. *Paleogeology, Paleoclimatology, Paleoecology* **82**, 113-120

Nriagu JO (1990c) Heavy metals pollution. Poisoning the biosphere? *Environment* **32**, 7-11

Nriagu JO (1996) An history of global metal pollution. *Science* **272**, 223-224

Nriagu JO, Pacyna JM (1988) Quantitative assessment of worldwide contamination of air, water and soils by trace metals. *Nature* **333**, 134-139

Oden S (1968) *The acidification of air precipitation and its consequences in the natural environment*. Energy Commission Bulletin 1, Stockholm, Sweden.Swedish National Science Research Council

Oldfield F, Dearing JA (2003) The role of human activities in past environmental changes. In: Alverson KD, Bradley RS, Pedersen TF (ed) *Paleoclimate, global change and the future*. Springer Verlag, Berlin Heidelberg, pp. 143-163

Olmez I, Finnegan DL, Zoller WH (1986) Iridium emissions from Kilauea volcano. *Journal of Geophysical Research* **91**, 653-663

Pacyna JM, Semb A, Hanssen JE (1984) Emissions and long-range transport of trace elements in Europe. *Tellus* **36(B)**, 163-178

Pacyna JM and Pacyna EG (2001) An assessment of global and regional emissions of trace metals to the atmosphere from anthropogenic source worldwide. *Environmental Reviews* **9**, 269-298

Pacyna EG, Pacyna JM, Fudala J, Strzelecka-Jastrzab E, Hlawiczka S,

Panasiuk D, Nitter S, Pregger T, Pfeiffer H, Friedrich R (2007) Current and future emissions of selected heavy metals to the atmosphere from anthropogenic sources in Europe. *Atmospheric Environment, in press*

Patterson CC (1956) Age of meteorites and the earth. *Geochimica et Cosmochimica Acta* **10**, 230-237

Patterson CC, Tilton G, Inghram M (1955) Age of Earth. *Science* **121**, 69-75

Patterson CC, Settle DM (1976) The reduction of orders of magnitude errors in lead analysis of biological materials and natural waters by evaluating and controlling the extent and sources of industrial lead contamination introduced during sample collection and analysis. *National Bureau of Standards special publication* **422**, 321-351

Patterson CC, Settle DM (1987) Magnitude of lead flux to the atmosphere from volcanoes. *Geochimica et Cosmochimica Acta* **51**, 675-681

Planchon FAM, Boutron CF, Barbante C, Cozzi G, Gaspari V, Wolff E, Ferrari CP, Cescon P (2002) Changes in heavy metals in Antarctic snow from Coats Land since the mid-19th to the late 20th century. *Earth and Planetary Science Letters* **200**, 207-222

Planchon F, Van de Velde K, Rosman K, Wolff EW, Ferrari C, Boutron CF (2003) One hundred fifty year record of lead isotopes in Antarctic snow from Coatsland. *Geochimica et Cosmochimica Acta* **67**, 693-708

Pongratz R, Heumann KG (1999) Production of methylated mercury, lead and cadmium by marine bacteria as a significant natural source for atmospheric heavy metals in polar regions. *Chemosphere* **39,** 89-102

Pruppacher HR, Klett JD (1998) *Microphysics of Clouds and Precipitation*. Kluwer editor, Dordrecht

Rampino MR, Self S (1992) Volcanic winter and accelerated glaciations following the Toba super-eruption. *Nature* **359**, 50-52

Raynaud D, Blunier T, Ono Y, Delmas RJ (2003) The Late Quaternary history of atmospheric trace gases and aerosols: interactions between climate and biogeochemical cycles. In: Alverson KD, Bradley RS, Pedersen TF (Ed) *Paleoclimate, global change and the future*. Springer Verlag, Berlin Heidelberg, pp. 13-33

Renberg I, Persson MW, Emteryd O (1994) Pre-industrial atmospheric lead contaminations detected in Swedish lake sediments. *Nature* **368**, 323-326

Renberg I, Bindler R, Brännvall ML (2001) Using the historical atmospheric lead-deposition record as a chronological marker in sediment deposits in Europe. *The Holocene* **11,** 511-51

Ridgwell, A. J. (2003), Implications of the glacial CO2 ‘‘iron hypothesis’’ for Quaternary climate change. *Geochemistry Geophysics Geosystems* **4(9)**, 1076, doi:10.1029/2003GC000563

Rippey B, Murphy RJ, Kyle SW (1982) Anthropogenically derived changes in the sedimentary flux of Mg, Ni, Cu, Zn, Hg, Pb and P in Louogh Neagh, Northern Ireland. *Environmental Science and Technology* **16**, 23-30

Rosman KJR, Chisholm W, Hong S, Candelone JP, Boutron CF (1997) Lead from Carthagenina and Roman spanish mines isotopically identified in Greenland ice dated from 600 BC to 300 AD. *Environmental Science Technology* **31**, 3413-3416

Rosman KJR, Ly C, Van de Velde K, Boutron CF (2000) A two century record of lead isotopes in high altitude alpine snow and ice. *Earth and Planetary Science Letters* **176**, 413-424

Sato M, Hansen JE, McCornick MP, Pollack JB (1993) Stratospheric aerosol optical depths, 1850-1990. *Journal of Geophysical Research* **98**, 22,987-22,994

Schwikowski M, Brustsch S, Gäggeler HW, Schotterer U (1999) A high-resolution air chemistry record from an Alpine ice-core; Fiescherhorn glacier, Swiss Alps. *Journal of Geophysical Research* **104**, 13,709-13,719

Schwikowski M, Barbante C, Doering T, Gäggeler HW, Boutron C, Schotterer U, Tobler L, Van de Velde K, Ferrari C, Cozzi G, Rosman K, Cescon P (2004) Post-17th- Century changes of European lead emissions recorded in high-altitude Alpine snow and ice. *Environmental Science and Technology* **38 (4)**, 957- 964

Seinfeld JH, Pandis SN (1998) Atmospheric Chemistry and Physics, from air pollution to climate change. In: Wiley J and Sons (ed) New York, pp. 1326

Settle DM, Patterson CC (1980) *Science* **207**, 1167- 1176

Shotyk W, Cheburkin AK, Appleby PG, Frankhauser A, Kramers JD (1996) Two thousand years of atmospheric arsenic, antimony, and lead deposition recorded in an ombrotrophic peat bog profile, Jura Mountains, Switzerland. *Earth and Planetary Science Letters* **145**, 1-7

Shotyk W, Weiss D, Appleby PG, Cheburkin AK, Frei R, Gloor M, Kramers

JD, Reese S, Knaap W (1998) History of atmospheric lead deposition since 12,370 ^{14}C yr BP from a peat bog, Jura Mountains, Switzerland. *Science* **281**, 1635-1640

Singh HB (1995) *Composition, Chemistry, and Climate of the Atmosphere*. Van Nostrand Reinhold editor, New York

Tegen I, Fung I (1994) Modeling of mineral dust in the atmosphere: sources, transport, and optical thickness. *Journal of Geophysical Research* **99**, 22,897-822,914

Tegen I, Lacis AA (1996) Modeling of particle size distribution and its influence on the radiative properties of mineral dust aerosol. *Journal of Geophysical Research* **101**, 19,237-219,244

Vallelonga P, Gabrielli P, Rosman K, Barbante C, Boutron CF (2005) A 220 ky record of Pb isotopes at Dome C Antarctica from analyses of the EPICA ice core. *Geophysical Research Letters* **32**, L01706

Wania F, Mackay D (1993) Global fractionation and cold condensation of low volatility organochlorine compounds in polar region. *Ambio* **22**, 10-18

Watts SF (2000) The mass budgets of carbonyl sulfide, dimethyl sulphide, carbon disulfide and hydrogen disulfide. *Atmospheric Environment* **34**, 761-779

Wedepohl KH (1995) The composition of the continental crust. *Geochimica et Cosmochimica Acta* **59**, 1217-1232

Westerlund S, Öhman P (1991) Cadmium, copper, cobalt, lead and zinc in the water column of the Weddel Sea, Antarctica. *Geochimica et Cosmochimica Acta* **55**, 2127-2146

Whitby K (1976) Physical characterization of aerosols, in methods and standards for environmental measurements. *National Bureau of Standards special publication, Proceeding of 8th IMR Symposium* **464**, 165-173

Whitby KT (1978) The physical characteristics of sulphur aerosols *Atmospheric Environment* **12**, 135-159

Wilson SJ, Steenhuisen F, Pacyna JM, Pacyna EG (2006) Mapping the spatial distribution of global anthropogenic mercury atmospheric emission inventories. *Atmospheric Environment* **40 (24)**, 4621-4632

Wolff EW, Suttie ED (1994) Antarctic snow record of Southern Hemisphere lead pollution. *Geophysical Research Letters* **21,** 781-784

Wolff EW, Fischer H, Fundel F, Ruth U, Twarloh B, Littot GC, Mulvaney R, Röthlisberger R, De Angelis M, Boutron CF, Hansson M, Jonsell U, Hutterli MA,

Lambert F, Kaufmann P, Stauffer B, Stocker TF, Steffensen, JP, Bigler M, Siggaard-Andersen ML, Udisti R, Becagli S, Castellano E, Severi M, Wagenbach D, Barbante C, Gabrielli P, Gaspari V (2006) Southern Ocean sea-ice extent, productivity and iron flux over the past eight glacial cycles. *Nature* **440**, 491-496.

Yoshiyuki N (1999) A fresh look at element distribution in the North Pacific. http://www.agu.org/eos_elec/97025e-refs.html

Zreda-Gostynska G, Kyle PR, Finnegan B, Prestbo KM (1997) Volcanic gas emissions from Mount Erebus and their impact on the Antarctic Environment. *Journal of Geophysical Research* **102**, 15,039-15,055.

Chapter 3- IDENTIFICATION OF CRUSTAL TRACE ELEMENTS ORIGIN THROUGH THE RARE EARTH ELEMENTS (REE). LEAD ISOTOPES SIGNATURE

3.1 Global dust emissions at present time

The wide range of current estimates of the global dust emissions for present climate published in the literature (**Table 3.1.1.1**) highlights the disparity between models and observations, and among models. The uncertainties are linked to the scarcity of global datasets used to determine the model input parameters and to validate model simulations. In fact, observations around the world are very scarce and they are often representative of a limited time period.

Reference	Annual Dust emissions (Mt/yr)
Tegen and Fung, 1994	3000
Tegen and Fung, 1995	1222
Andreae, 1996	1500
Mahowald et al., 1999	3000
Penner et al., 2001	2150
Ginoux et al., 2001	1814
Chin et al., 2002	1650
Werner et al., 2002	1060 ± 194
Tegen et al., 2002	1100
Zender et al., 2003	1490 ± 160
Luo et al., 2003	1654
Mahowald and Luo, 2003	1654
Miller et al., 2004	1018
Tegen et al., 2004	1921

Table 3.1.1 : *model-based present day annual dust budget estimates. Values range between 1000 and 2150 Mt/yr (from Zender et al., 2004)*

However, the IPCC 2007 estimates that the dust emission in the Southern Hemisphere is less than 1/5 the emission estimated for the Northern Hemisphere (about 350 and 1800 Mt/yr respectively).

Commonly, the regions with little or no ground cover, easily wind-erodible soils and associated to seasonal wetness provide the bigger dust fluxes (Mahowald et al., 1999). Chemical weathering is enhanced by the abundance of water, and liquid transport is an efficient mechanism for production of small particles, separated from the soil or from the primary rock and carried to depositional basins or an alluvial plain where, after drying, they become mobilizable by wind (Prospero et al., 2002). Vegetation cover and soil crusting are also two important factors that can sensibly lower or suppress dust emission.

A worldwide geographical mapping of major atmospheric dust sources has been recently provided by Prospero et al. (2002) on the basis of data from TOMS (Total Ozone Mapping Spectrometer) sensor on NIMBUS-7 satellite for a period of 13 years (1980-1992) (**Figure 3.1.1**). The **Figure 3.1.1** is a composite of selected monthly mean TOMS AAI frequency of occurrence distributions[17] for specific regions using those months which best illustrate the configuration of specific dust sources. The distributions were computed using a threshold of 1.0 in the dust belt and 0.7 everywhere else. The authors evidenced that the major sources are located in arid and hyper-arid regions, but also showed association between dust source and water activity. This association is consistent with the consideration that fluvial and chemical weathering processes are extremely efficient in the production of very fine particles (Pye, 1987; Tegen et al., 2002).

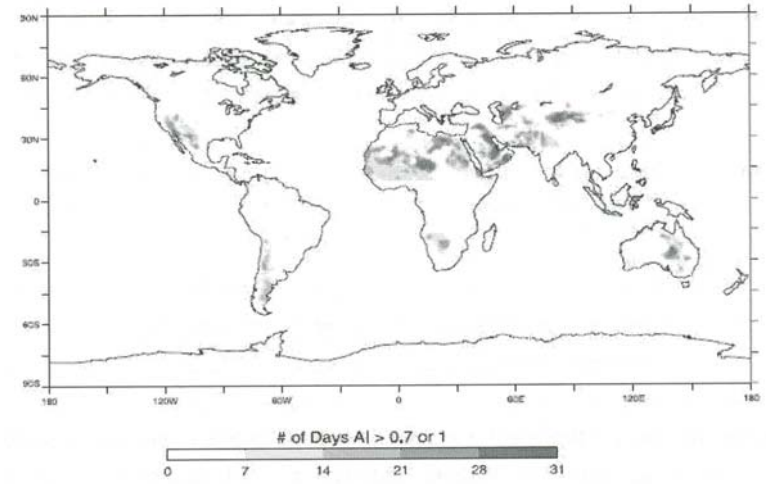

Fig. 3.1.1 : *Global dust sources identified through a Total Ozone Mapping Spectrometer (TOMS) (Prospero et al., 2002)*

.

[17] Total Ozone Mapping Spectrometer (TOMS) Absorbing Aerosol Index (AAI) Frequency of Occurrence (FoO) distribution is expressed as days per month when the AAI equals or exceeds 0.7

The principal sources for dust that can potentially be transported long-distance are located, for the Northern Hemisphere, in North Africa, in the Middle East, in central Asia and in the Indian subcontinent and for the Southern Hemisphere, in Australia, Southern Africa and Southern America.

In the Southern Hemisphere, dust concentrations are very low in comparison to Northern Hemisphere ocean regions (Gao et al., 2001; Heintzenberg et al., 2000). Nonetheless there is evidence that there was considerably more dust activity in the Southern Hemisphere in the past. Antarctic ice cores show that dust concentrations were sporadically much higher, most recently during the Last Glacial Maximum (LGM), ~ 20,000 years ago, when dust concentrations were ~ 30 times greater than today (De Angelis et al., 1992; Gaudichet et al., 1992; Mayewski et al., 1996). The increased dust is broadly attributed to transport from continental sources in Australia, South America, and Africa and from exposed shelf sediments during low sea states (Harrison et al., 2001). The very low dust concentrations in the Holocene portions of the cores are consistent with the present-day dearth of dust sources in TOMS in the Southern Hemisphere and the low dust concentrations measured in field campaigns (Prospero et al., 2002).

3.2 Principal dust "hot spots" in the Southern Hemisphere

According to satellite observation by TOMS AAI FoO on the present day, Australia, Southern Africa and Southern America are the three main regions providing massive amount of dust in the Southern Hemisphere (Prospero et al., 2002). Loess deposits themselves can undergo a massive erosion and so can constitute an important secondary source of mineral dust. Transport of silt and clay by wind is a universal process, occurring under all climates, mainly in desertic and sub-desertic regions. The accumulation of such materials can produce loess (Pye, 1984, 1987). During cold climatic periods the loess accumulation was rapid and soil formation at minimum, while warm phases were associated to weathering of loess mantles and pedogenesis. Therefore, loess sequences can potentially provide a quantitative record of mineral dust deposition under changing climate regimes that is complementary to ice core records.

Australia

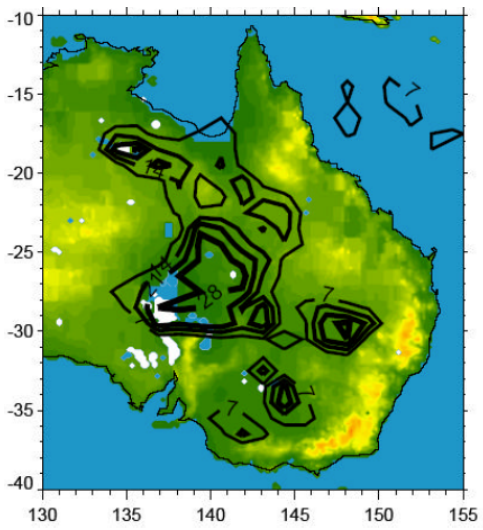

Fig. 3.2.1 : *Australian dust sources expressed as TOMS AAI FoO distribution (Prospero et al., 2002)*

The major dust activity is detected in the Great Artesian Basin feeding the Lake Eyre, which today constitutes a large playa[18]. Ephemeral rivers in this area constitute rich sources of dust during dry phases.

The most active dust area is located in North-East of present-day Lake Eire, corresponding to the pluvial Lake Dieri (ancestral Lake Eire).

The large Simpson Desert only appears as an occasional region for large dust events

Southern Africa

A persistent dust source is located in Botswana, centered over the western end of the Makgadikgadi Depression, occupied during the Pleistocene by a great lake, the Palaeo-Makgadikgadi (Goudie, 1996).

Another smaller but persistent source is located over the Etosha Pan, Northern Namibia, at the extreme northwest of the Kalahari basin. During the Pleistocene also the Etosha Pan basin was occupied by a large lake (Goudie, 1996).

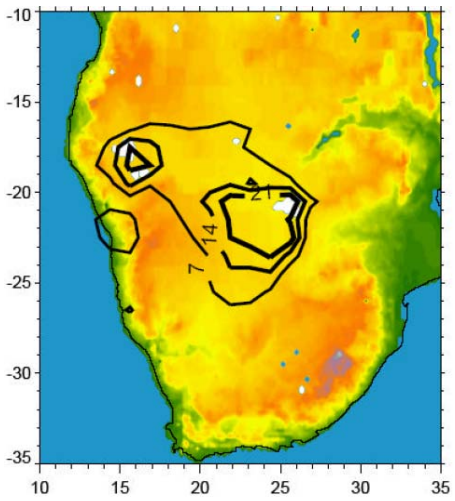

Fig. 3.2.2 : *Southern Africa dust sources expressed as TOMS AAI FoO distribution (Prospero et al., 2002)*

[18] Playas are common features in desert and are among the flattest landforms in the world

Southern America

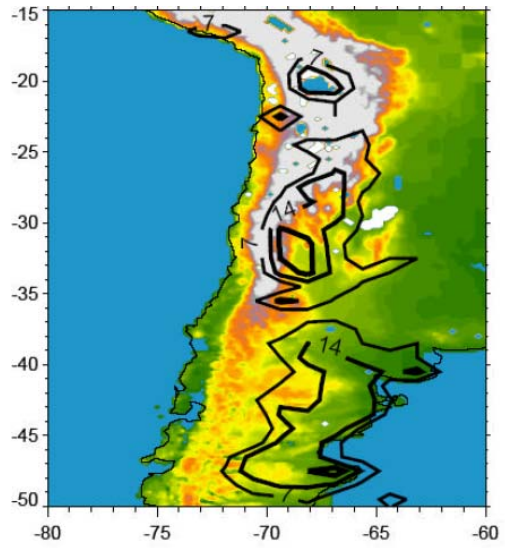

Fig. 3.2.3: *Southern America dust sources expressed as TOMS AAI FoO distribution (Prospero et al., 2002)*

Three persistent dust source regions can be observed:

1- Bolivian Altiplano: in an arid intermountain basin situated at about 3750-4000 m of altitude that includes two of the largest salt flats of the world. A large part of the Altiplano was occupied in the Pleistocene by a lake;

2- Intermountain area between the Andes (West) and the Sierra de San Luis - Sierra de Cordoba (East): most active area lies in the western part of this region which consist of arid and semi-arid sections;

3- 38ºS to 48ºS, includes the Southern Pampas and Northern Patagonia: semi-arid to arid region spanning from the eastern flanks of the Andean Cordillera to the Atlantic coast. A particularly active area is located in the Neuquen Province, extending in the Northern Patagonia and in the Southern Pampas and characterized by great saline areas and sandy deserts.

Loess deposits

Transport of silt and clay by wind is a universal process, occurring under all climates, mainly in desertic and sub-desertic regions. The accumulation of such materials can produce loess[19]. There are three main requirements for the formation of a loess deposits: (1) the presence of a sustained source of dust; (2) an adequate wind energy; (3) a good place where loess can accumulate (Pye, 1995).

During cold climatic periods the alternation of loess accumulation was rapid and soil formation at minimum (intense ice sheets advance), while warm phases were associated to weathering of loess

[19] *Loess* usually defines some silt-rich, wind-produced deposits of material that started to accumulate about 2.6 My ago, originated as Aeolian dust and mainly composed by particles in the range 10-50 μm (Derbyshire, 2003)

mantles and pedogenesis[20]. Consequently, loess sequences can potentially provide a quantitative record of mineral dust deposition under changing climate regimes that is complementary to ice core records, particularly for reconstructions of past variations in the hydrological cycle (Iriondo, 1999).

The most extensive area of loess deposition of the world is located in Northern Hemisphere; it is the Chinese loess plateau (440,000 km^2, 33-40°N , 98-115°E, Kohfeld and Harrison, 2001). Outside China, other wide loess deposits in the Northern Hemisphere are located in North America (Great Plains), in south-central Europe, Ukraine and central Asia. In the Southern Hemisphere, the thicker and more extensive loess and aeolian deposits occur in Argentina (¨Prospero et al., 2002). Thick Pleistocene loess-paleosol deposits are present also in New Zealand (Livingstone and Warren, 1996).

Southwest and south of the Paranà-Rio de la Plata estuary, extensive formations of loess and sand covering an area of ~1000-1100 km^2 constitute the so called Pampean loess formation (Clapperton, 1993). This loess formation covers a wider area than the Pampas, extending over the western Chaco plains (NW Argentina).

Loess differ themselves by composition and so can be significantly different from one to another loess. For example, some loess from Argentina and New Zealand have high content of volcanic glass and feldspar, while other deposits, such as in Central Asia and in the Mississippi Valley, show up to 30% of carbonate minerals. However, the majority of loess deposits are composed for more than a half of silt particles, but the percentages of sand and clays are quite variable in different regions (Gallet et al., 1998).

3.3 The dust provenance during glacial periods in the East Antarctic Plateau

Several works used isotopic ratios of Sr and Nd as indicator of geographical provenance[21] due to their properties which permit to detect the origin of polar dust (Grousset et al., 1992;

[20] formation of soil layers
[21] Dust, soil land sediments have an isotopic signature related to the rocks from where they derive and dependent to the lithology and the geologic age of the geographical area

Basile et al., 1997; Delmonte et al., 2004). It has been pointed out by these three authors that the Sr-Nd isotopic ratios for EPICA/Dome C, Vostok, Dome B and Komsomolskaia[22] glacial samples (Stage 2, 4 and 6) are very similar among the sites and for all the climatic periods investigated; that evidences a common dominant source of dust for all glacial periods and over a large portion of the East Antarctic plateau.

In **Figure 3.3.1a**, Delmonte et al. (2004) notice that South Africa, Australia and the exposed rocks of coastal East Antarctica show the typical signature of old continental crust (low radiogenic $^{143}Nd/^{144}Nd$ commonly expressed in the form ε_{Nd} (0) and highly radiogenic $^{87}Sr/^{86}Sr$) that originally constituted portions of Gondwanaland. On the other hand, the signatures of New Zealand, the Dry Valleys of Antarctica and southern South America partly overlap.

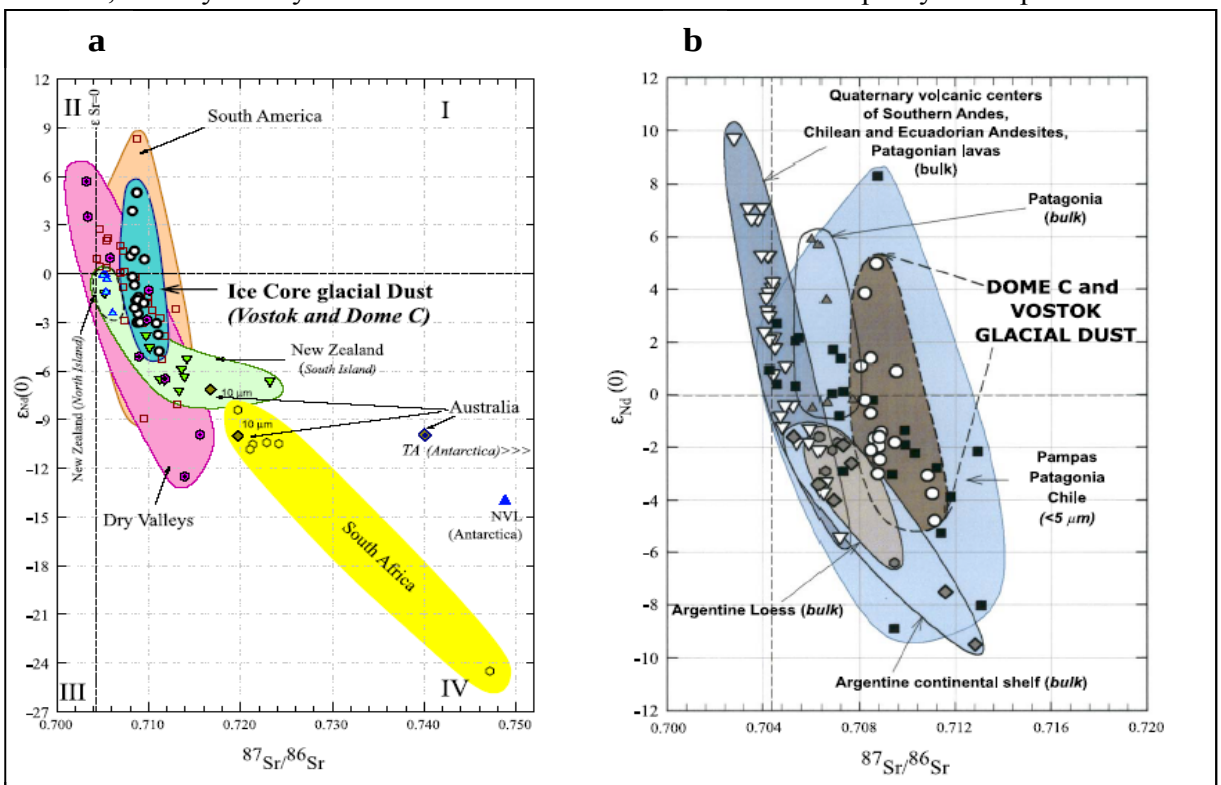

Fig. 3.3.1 : *The four quadrants (I–IV) have been traced to facilitate the interpretation of the data. Comparison between EPICA-Dome C and Vostok glacial dust field (dashed line) and the $^{87}Sr/^{86}Sr$ versus εNd(0) isotopic fields for (a) South America, New Zealand, the Dry Valleys, South Africa and the ice core glacial dust have been arbitrarily defined on the basis of the available points. The Antarctic samples from Terre Adélie overpass the field spanned by the graph; and (b) South America* ***samples (from Delmonte et al., 2004)***

[22] Four ice cores have been studied, EDC (EPICA Dome C), Vostok, Dome B and Komsomolskaia (KMS), in the 94°E–123°E sector of East Antarctica.

In **Figure 3.3.1a**, the Antarctic glacial dust appears very different from South Africa, Australia and coastal East Antarctica and therefore these regions can be excluded as dominant sources in cold periods. On the opposite, the ice core dust signature is situated in the overlap region between New Zealand (South Island), the Dry Valleys and southern South America (**Figure 3.3.1a**). However, complementary arguments excluded New Zealand and the Dry Valleys (see below).

New Zealand

New Zealand has very limited surface extent and seems unlikely a source for the high dust flux in glacial periods to East Antarctica. Actually, studies on volcanic tephras in Vostok ice core (Basile et al., 2001), evidenced a preferential atmospheric pathway for the ashes from the southern part of the Westem Atlantic (South Sandwich Islands, South America, Antarctic Peninsula), and no volcanic events from New Zealand were found in the Vostok core. Therefore, despite the high activity of these regions, such an atmospheric transport path seems very unusual. Moreover, the limited extension of New Zealand makes it difficult for it to be responsible for the big amount of dust carried in glacial times to East Antarctica (Delmonte et al., 2003).

Dry Valleys

In glacial times, the ice-free areas were less extended than today, the glacier's fronts were closer to the coast (Denton et al., 1991) and the transport of dust from coastward to inner plateau was not favoured because of the strong katabic winds which blow off the East Antarctic plateau (**Figure 3.3.2**) (Schwerdtfeger, 1984; King and Turner, 1997).

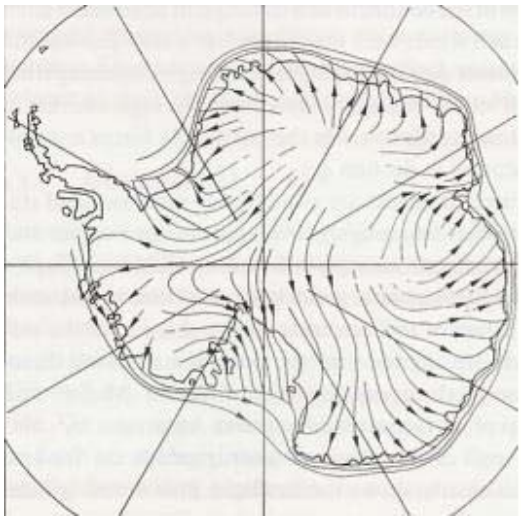

Fig. 3.3.2: *Surface wind streams over Antarctica (King and Turner 1997).*

Finally, a dust advection from the Dry Valleys would carry considerable amounts of salts into the polar Plateau, in particular carbonates and gypsum (Campbell and Claridge, 1987) that have not been found in Antarctic ice (De Angelis et al. 1992; Gaudichet et al., 1992).

Consequently, southern South America can be considered like a dominant source of dust during glacial periods (Stage 2, 4 and 6), as already evidenced by Grousset (1992), Basile (1997) and Delmonte et al. (2004) on the basis of the geochemical signature of dust, and by Gaudichet et al. (1986; 1992) on the basis of mineralogical data. In Figure 3.3.1b, the comparison between the polar dust and southern South America samples indicates that the area that better fits ice core data is Argentina, more precisely Patagonia and Pampas.

During the Last Glacial Maximum (~18,500-30,000 years BP), the geochemical composition of dust (major elements: Si, Al, Fe, Ca, Na, Mg, K and Ti) reaching the East Antarctic plateau shows a signature similar to an exposed continental surface that likely experienced several cycles of chemical weathering. Loess, which corresponds to this definition, shows, in turn, a chemical imprint consistent with LGM polar dust geochemistry; in particular the Pampean loess deposits fit very well in terms of relative abundance of the 8 main crustal elements (Si, Al, Fe, Ca, Na, Mg, K and Ti) (Marino, 2006). Moreover, this correspondence is consistent with the hypothesis that the wind systems responsible for loess formation, could have mobilized and transported part of this aeolian material towards higher latitudes (Delmonte et al., 2002) and this scenario agrees with the proposed mechanism of a northward shift of the Westerlies during LGM (Gersonde et al., 2005). If so, it limits the role of Patagonia as polar dust source areas for the LGM.

However, the latitudinal extent of the Westerlies equatorward shift is still a matter of discussion. A poleward shift of the Westerlies (Wainer et al., 2005) would imply a dominant role of Patagonia, instead of Pampas, as polar dust supplier during LGM, as also suggested by Gaiero et al. (2004).

During Stage 4 (~ 55,000- 67,000 years BP), the composition in term of major elements geochemistry (Si, Al, Fe, Ca, Na, Mg, K and Ti), is different to this found during the LGM (Marino, 2006), whereas isotopic studies draw a common Nd/Sr imprint for polar dust reaching the East Antarctic plateau during all the main Late Quaternary glacial periods (Basile et al., 1997; Delmonte et al., 2004). Opposite values of insolation parameter (precessional cycles; Stuut and Lamy, 2004) during stage 4 would lead to a higher aridity at the Andean Piedmonts area, large Argentinian sand sea formation due to the massive formation of unconsolidated material by

glacial grinding, and a minor impact of chemical weathering due to a lower activity of the fluvial system (Iriondo, 1997; Stuut and Lamy, 2004). For all these reasons, a likely predominance of Patagonia as dust supplier at that time could be considered, accounting for the observed compositional difference between Stage 4 and LGM dust.

During Stage 6 (~ 135,000- 190,000 years BP), the geochemistry of dust compositions seems to be intermediate between these of the LGM and Stage 4. In fact, Stage 6 includes three precessional cycles, likely suggesting an alternance of relative by milder and drier conditions at the dust source regions (Marino, 2006). If so, varying moisture regimes could have promoted the dominance of chemical or physical alteration processes on continental surfaces, leading to the formation of, respectively, more or less weathered secondary materials[23], and hence aeolian mineral dust.

3.4 The dust provenance during interglacials to the East Antarctic Plateau

Between glacial and interglacial stages, the Quaternary climatic and environmental changes modified sensibly the conditions in continental areas; for example, vegetation cover and pedogenesis developed, sea level rose, hydrological conditions changed as well as the atmospheric circulation.

The isotopic signature of interglacial samples of the East Antarctic plateau appears clearly less radiogenic in Nd with respect to glacial dust (**Figure 3.4.1**) (Basile, 1997; Delmonte et al., 2003) The Chemical Index of Alteration (CIA) and the Index of Compositional Variability (ICV) clearly evidence a difference of composition between glacial and interglacial samples (Marino, 2006).

This suggests a possible contribution from an additional source during warm periods. It is due to the fact that the glacial/interglacial isotopic difference, different elements abundance and overall

[23] Continental glaciers favoured the alteration of primary rocks, providing sandy and silty particles. These can be either *primary* sources for long-range dust transport or they can be mobilized and transported (in liquid or aeolian phase) to another site topographically suitable for concentration of sediments. In this latter case they can become *secondary* sources for mineral aerosol.

compositional variability is unlikely due to environmental changes occurring *at* the source through environmental processes like pedogenesis.

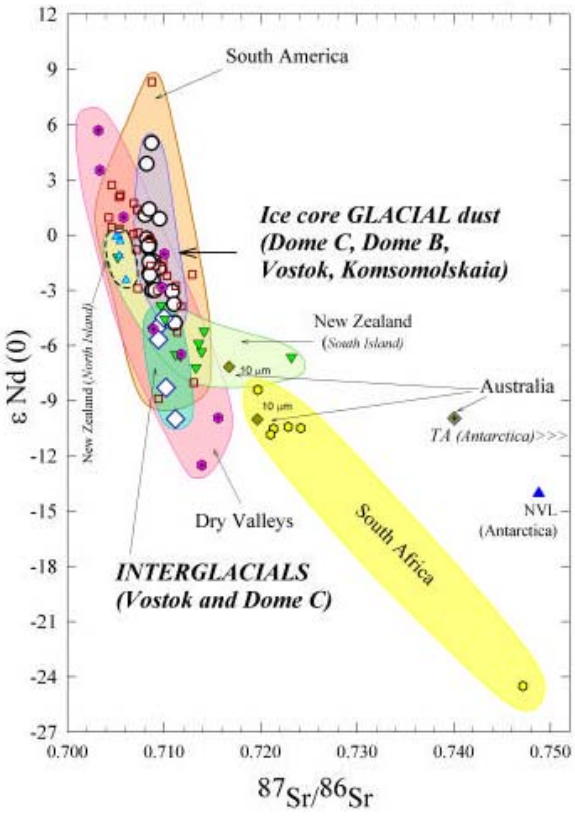

Fig. 3.4.1 : *Isotopic fields for glacial and interglacial ice core dust and all Potential Source Areas (PSAs).(from Delmonte, 2003)*

Similarity arising between the ice core interglacial dust and the Dry Valleys isotopic field suggests a possible contribution from these areas (Delmonte, 2003), but such apparent match could be fictitious and seems not confirmed. Effectively, a direct atmospheric transport of dust from the Dry Valleys to the interior of the high plateau seems not favoured by the strong catabatic winds blowing off the continent towards the sea. However, mesoscale cyclonic activity (in the Ross Sea region) can allow air uplift and advection of mild and moist maritime air towards the ice-sheet interior (Gallée, 1996), but the influence of such vortices is limited to the lower tropospheric levels (below 300 m) (Carrasco et al., 2003).

A contribution from rock outcrops of coastal East Antarctica and from South Africa can reasonably be discarded from isotopic arguments; on the other hand, a mixture of Eastern Australia and South America dust seems quite probable (Delmonte, 2003). Moreover, the $^{87}Sr/^{86}Sr$ and $^{143}Nd/^{144}Nd$ isotopic composition of the fine (<5 µm) fraction of Australian dust samples show that the dust contribution from Australia could have been dominant during interglacials (Holocene and Marine Isotopic Stage 5.5) (**Figure 3.4.2**) (Revel-Rolland et al., 2006), but the Australian dust samples display a shift towards more radiogenic Sr values. Another explanation could be the possibility of a Western Australian and/or South African contribution to Antarctica, but the South African and Western Australian dust isotopic field is still insufficiently documented.

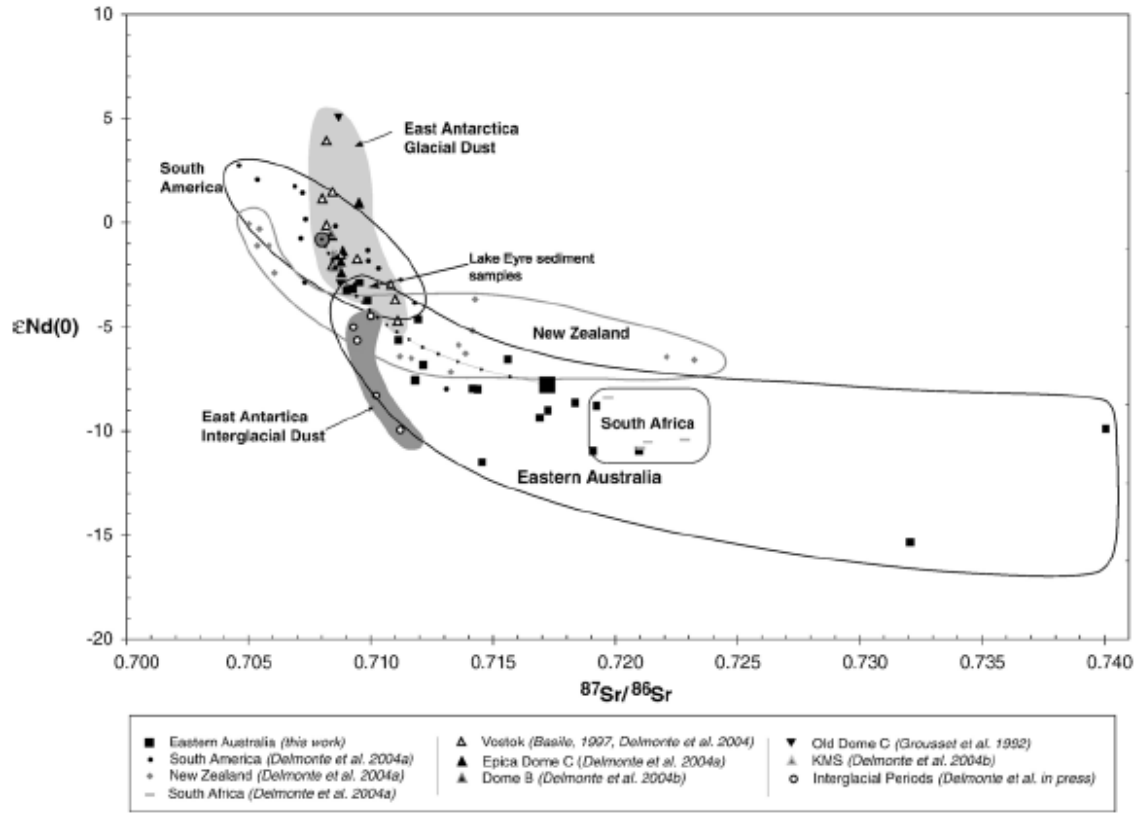

Fig. 3.4.2 : *87Sr/86Sr versus εNd(0) isotopic signature of East Antarctic ice core dust from interglacial (Holocene and isotopic stage 5.5) and from glacial (MIS 2 to MIS 12) and comparison with the samples from Eastern Australia, New Zealand, South America and South Africa (from Revel-Rolland et al., 2006)*

Actually, several proxies clearly show that a climatically stable period as the Holocene is claimed to be, was characterized by pronounced alterations of drier and moister phases (Marino, 2006). Several works concerning South American lakes levels at different latitudes, Holocene soils and sand deposits buried in Argentinean loess stratigraphies point a higher complexity of the Holocene period, and even Marine Isotopic Stage 5.5, characterized in Argentina by cycles of changing levels of humidity (Iriondo, 1999).

If so, the Holocene and Marine Isotopic Stage 5.5 should be considered as periods when the possibility of a certain degree of weathering does exist (at least higher than during the glacial periods, as indicated by CIA and ICV index, Marino, 2006), alternated to drier periods when dust could be uplifted and transported to Antarctica, even if in a lower extent with respect to LGM and the other glacial periods.

3.5 REE in sedimentary rocks: influence of provenance

3.5.1 REE properties

Rare Earth Elements comprise the lanthanide elements, La-Lu, as well as Y (atomic number from 57 up to 71) (Puddephatt, 1972) (**Figure 3.5.1.1**). Rare Earth Elements can be divided in three groups of elements: Light Rare Earth Elements (La to Nd); Middle Rare Earth Elements (MREE; Sm to Tb) and Heavy Rare Earth Elements (HREE; Er to Lu). In terms of geochemical behaviour, Y mirrors the heavy lanthanides Dy-Ho, and is typically included with them for discussions.

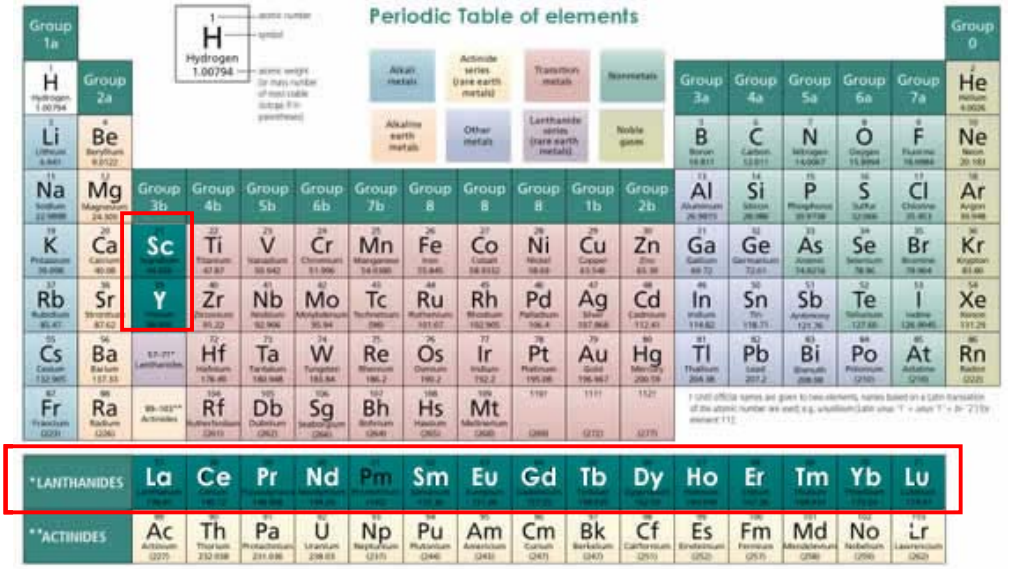

Fig. 3.5.1. : *Periodic table of Mendeleyev showing the Rare Earth Elements (REE) (inside red squares)*

Under the pressure-temperature conditions found within the Earth, the REE mostly exist in a trivalent state. There are two exceptions to this:

1- Under reducing conditions, such as those found within the mantle or lower crust, europium may exist in the divalent state (Eu^{2+}). This results in an increase in ionic radius of about 17% (**Table 3.5.1.1**) making it identical to Sr^{2+}. The consequence of this is that Eu substitutes freely in place of Sr in felspars, notably Ca-palgioclase, leading to distinctive geochemical behaviour compared to the other REE (McLennan, 1989);

2- Under oxidizing conditions, Ce^{3+} may be oxidized to Ce^{4+} leading to a decrease in ionic radius of about 15% (**Table 3.5.1.1**). The only place on Earth where this reaction occurs on a large scale is the marine environment, associated with the formation of manganese nodules. The distinctive Ce depletion found in ocean waters and phases precipitated in equilibrium with seawater is the immediate consequence of this reaction (McLennan, 1989).

Apart from these anomalies, the REE behave as an unusually coherent group of elements. There is a regular decrease in ionic radius from La^{3+} to Lu^{3+} (**Table 3.5.1.1**), which is due to an increase in effective nuclear charge as the shielded, non-valence 4f or 5f electron shell is filled and contracts during the development of the lanthanide series. This property also affects the stability of various complexes of REE cations, which is also of geochemical significance (Woyski and Harris, 1963).

		Z	Trivalent Ionic Radius (Å)[1]	Atomic weight [2]
La	Lanthanum	57	1.032	138.9055
Ce	Cerium	58	1.01	140.115
Pr	Praseodymium	59	0.99	140.9077
Nd	Neodymium	60	0.983	144.24
Sm	Samarium	62	0.958	150.36
Eu	Europium	63	0.947	151.96
Gd	Gadolinium	64	0.938	157.25
Tb	Terbium	65	0.923	158.9254
Dy	Dysprosium	66	0.912	162.50
Ho	Holmium	67	0.901	164.3033
Er	Erbium	68	0.890	167.26
Tm	Thulium	69	0.880	168.9342
Yb	Ytterbium	70	0.868	173.04
Lu	Lutetium	71	0.861	174.967
Y	Yttrium	39	0.900	88.9059
Eu^{2+}			1.17	
Ce^{4+}			0.87	

[1] *Shannon, 1976*
[2] *De Bievre et al., 1984*

Table 3.5.1.1.: *Some basic REE data*

This slight difference of radius leads to a progressive fractionation of REE between each other. After being chondrite-normalized[24] (values of Taylor and McLennan, 1985), REE profiles show, according to the magma nature, enrichment or depletion[25] in LREE (La/Sm ratio), HREE (Yb/Gd ratio) or LREE/HREE (La/Yb ratio) and variables enrichments in relation to chondrites (Basile, 1997). For example, melting of mantle or crustal rocks tends to cause an enrichment of LREE over the HREE.

The REE pattern of average sediments reflects the average upper continental crust and thus the Eu anomaly found in most sedimentary rocks (**Figure 3.5.1.2**) similarly interpreted to be a feature of the upper continental crust.

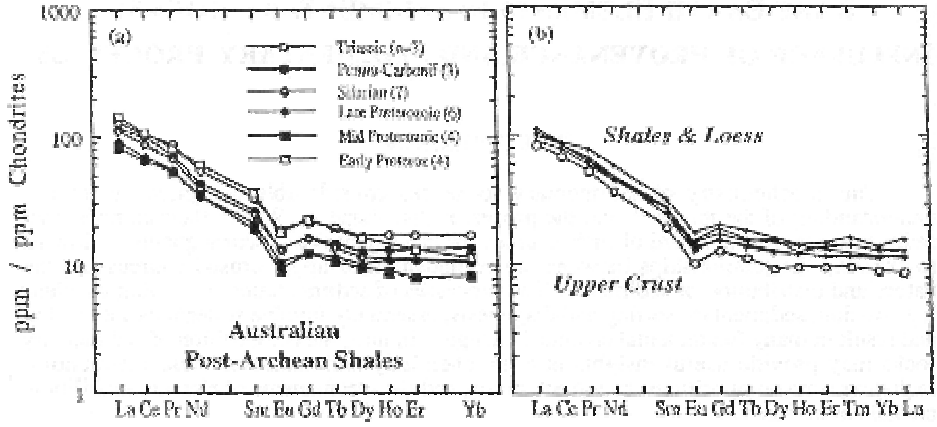

Fig. 3.5.1.2 : *Chondrite-normalized REE diagrmas for sediment and sedimentary rocks of various age (a) Average post-Archean Australian shales of various age (b) Various averages and composites of shales and loess; the average sedimentary REE pattern is taken to be parallel to the average REE pattern of the upper continental crust.*

Note the similarity in the patterns with LREE enrichment, flat HREE distributions and the ubiquitous negative Eu-anomaly (from McLennan, 1989)

In the following discussion, a subscript 'N' denotes chondrite-normalized values, Europium is commonly enriched (positive Eu anomaly) or depleted (negative Eu anomaly) relative to other

[24] Chondritic meteorites have been chosen as normalisation values because they are supposed to be representative of non fractionated samples of the solar system. Moreover, this normalization allows to free REE from abundances differences between atomic numbers even and odd numbers of these elements.

[25] Enrichment or depletion are used to describe increases and decreases, respectively, in abundances of elements. As an example, depleted mantle has LREE/HREE abundances ratios less than chondritic ratios; primitive mantle has chondritic LREE/HREE ratios; and enriched mantle has LREE/MREE ratios greater than chondritic ratios.

REE on chondritic-normalized diagrams and this can be quantified by the term Eu/Eu*, where Eu* is the expected Eu value for a smoothed chondrite-normalized REE pattern, such that:

$$Eu/Eu^* = Eu_N / (Sm_N \times Gd_N)^{0.5}$$

An arithmetic mean ($(Sm_N + Gd_N)/2$) is commonly used to calculate Eu*, however, this is incorrect and may lead to serious errors, especially for steep chondritic-normalized REE patterns (McLennan, 1989).

3.5.2 REE and provenance studies

The REE have been extensively used to understand the formation of the major Earth reservoirs (crust-mantle), the origin of volcanic rocks, the sedimentary system, and processes in oceanography (Hanson, 1980; Elderfield and Greaves, 1982; Hofmann et al., 1984; Taylor and McLennan, 1985; Kay and Mahlburg-Kay, 1991). Measurement of precise Sm, Nd and Lu concentrations also underpins two important isotopic systems (Sm-Nd, Lu-Hf) that are used to date geological samples.

A fundamental conclusion that may be drawn from previous studies is that for terrigenous sedimentary rocks, the REE patterns generally reflect the average compositions of the provenance. However, when we normalize with chondritic ratios, whatever the loess deposits of the world (Gallet et al. 1996; 1998; Jahn et al., 2001; Ding et al., 2001; Smith et al., 2003), generally all samples are characterized by light REE (LREE) enriched patterns, relatively flat heavy REE (HREE) trends and negative europium anomalies (**Figure 3.5.2.1**).

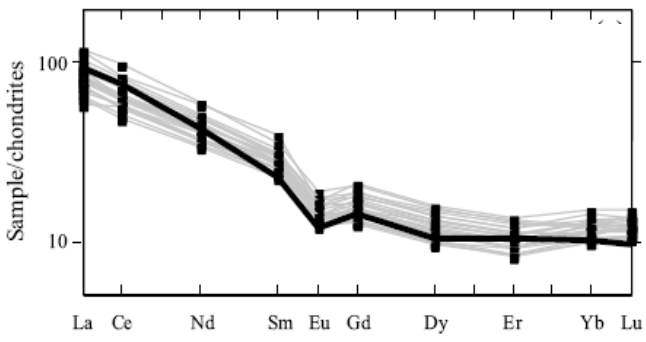

Fig. 3.5.2.1 : *Chondrite-normalized REE plots for Argentinean loess (black squares and grey lines).Also plotted for comparison (thick black line) are the UCC values of Taylor and McLennan (1985) (Smith et al., 2003).*

Furthermore, loess deposits are very similar to the average upper continental crust (UCC) (**Figure 3.5.2.1**). In detail, however, there are subtle differences when loess REE concentrations are normalized to the UCC values (values from Wedepohl, 1995 for our study). For exemple, Smith et al. (2003), observed small differences both between five sites sampled span a wide geographical area. This geographical area extends from Tucuman (El lambedero) through Cordoba (Lozada) and northern Buenos Aires province (Baradero, Gorina) to southern Buenos Aires province (Hipodromo) and other continental loess deposits (UCC) (**Figure 3.5.2.2**). These small differences between the samples and continental loess deposits presumably reflect the greater influence of young volcanic source regions (Andes/Patagonia/Parana) on South American loess, while the subtle differences between sites reflect the varying importance of this provenance relative to contributions from old continental crustal material (Smith et al., 2003).

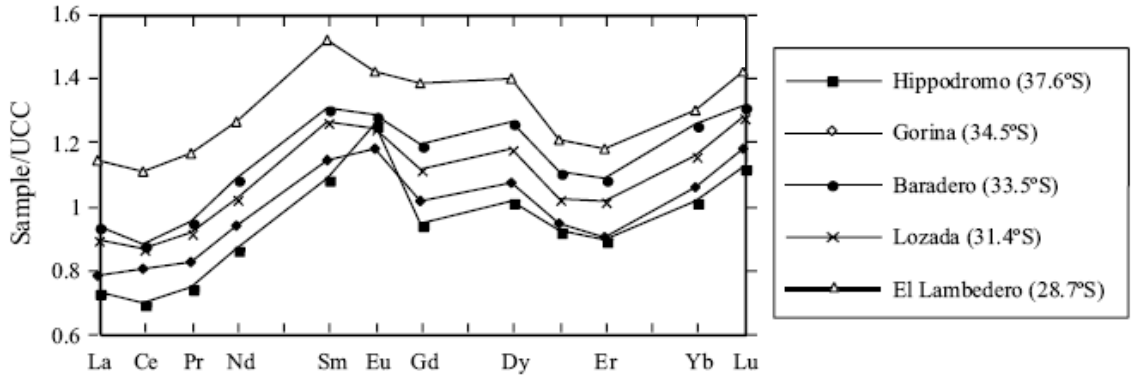

Fig. 3.5.2.2 : *Loess REE concentrations from Argentinean loess (28-38°S) normalized to the UCC values of Taylor and McLennan (1985) (from Smith et al., 2003)*

Several works (Basile et al., 1997; Smith et al., 2003; Gaiero et al., 2004) have investigated the source of dust to Antarctica during glacial periods. The REE profiles of both the Dome C and Vostok dusts normalized to the UCC display rather flat patterns (**Figure 3.5.2.3**) (Basile et al., 1997). Such flat patterns are the same as the flat REE patterns characterizing samples from the PSAs[26] (Patagonia, Australia, Africa…). However, the volcanic patterns are very different from

[26] A PSA sample may consist in of a primary source of rnineral aerosol, directly derived from mechanical and/or chemical alteration of parent material, or in a secondary source, i. e. in a mixture of particles that have already undergone a first phase of transport (aeolian and/or liquid), or in a mixture of both.

dust REE patterns. The hypothesis of a major volcanic source contribution for dust in East Antarctica can be then ruled out.

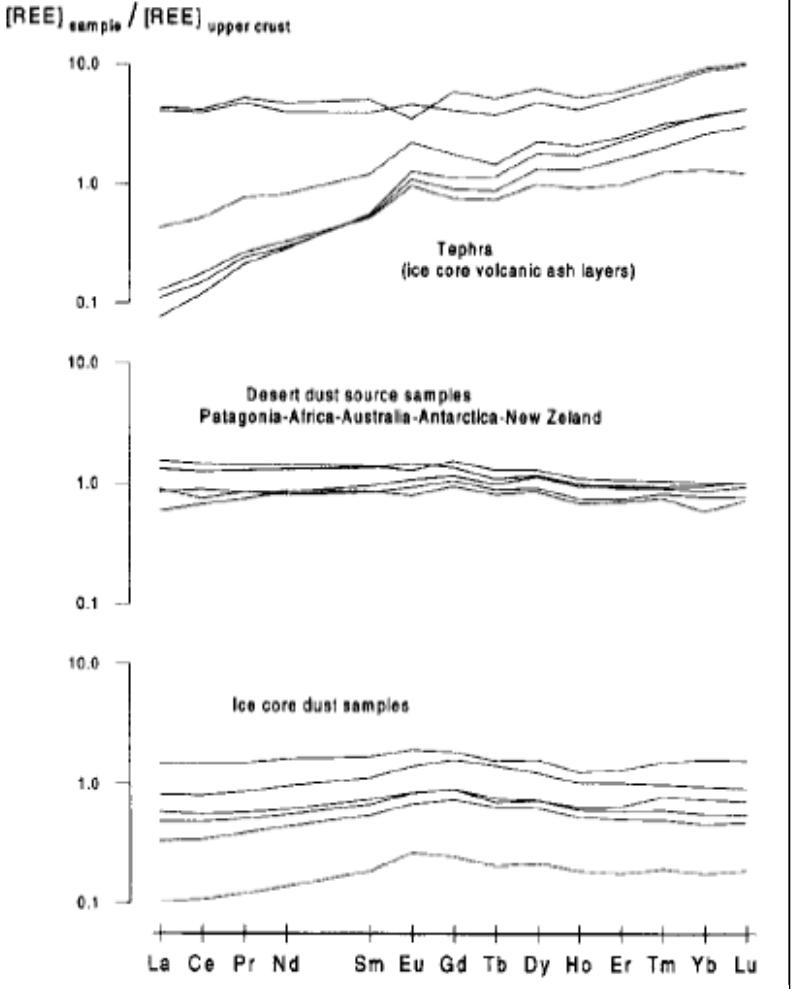

Fig. 3.5.2.3 : *REE patterns for volcanic ash layers, desert dust from continental sources, and ice cores dust (Vostok and Dome C). REE concentrations are normalized to REE concentrations of the mean upper crust (Taylor and McLennan, 1995) (from Basile et al. 1997)*

Regardless of differing concentrations, the pattern of REE_{UCC} composition of most ice cores (Vostok and Dome C) (Grousset et al., 1992; Basile et al., 1997) matches reasonably well with the shadowed area representing the mean REE_{UCC} composition of Patagonian eolian dust and the Buenos Aires loess (Gaiero et al., 2004).

The most remarkable feature of ice core dust samples during the Holocene, stages 2, 4 and 6 is the low mean Eu* anomaly (1.09), when compared to mean Patagonian dust (Eu* anomaly = 1.21) and mean Buenos Aires loess (Eu* anomaly = 1.18). However, Gaiero et al. (2004) have already demonstrated that a high proportion of smectite in Patagonian riverine suspended matter and topsoils promote a low Eu* anomaly in sediments. Thus, a higher proportion of smectite in a dominant clay size fraction could lower the Eu* anomaly and thus locate Antarctic dust composition in the field characterizing sediments from the Cordoba Province. Another hypothesis could be a mixture provided by combining different source areas. The ice-core dust sources during the Holocene, stages 2, 4 and 6 could be explained by a mixture

of Patagonian dust in dominant proportions, combined with Australian, Dry Valleys and Southern Africa dust (Basile et al., 1997; Delmonte, 2003; Revel-Rolland et al., 2006), the relative proportions of each one depending on climatic periods (glacial times or interglacials).

3.6 An introduction to the lead isotopic system

3.6.1 Lead properties

Lead is a very soft, low-melting metal, solid at room temperature and recognized for its blue-grey colour, malleability and fairly high density. Lead melts at 327°C and boils at 1751°C. Lead is a trace element in the Earth's crust, with a mean abundance of ~ 13 ppm, but it can be present in large quantities as Galena (PbS) and co-mineralized with copper, silver, gold, zinc, tin, arsenic, and antimony (Greenwood and Earnshaw, 1984).

Lead has four naturally occurring stable isotopes, ^{204}Pb, ^{206}Pb, ^{207}Pb and ^{208}Pb, which are produced by stellar nucleosynthesis and by terrestrial radiogenic decay of Uranium and Thorium. ^{206}Pb, ^{207}Pb and ^{208}Pb are end products of the radioactive decay chains of ^{238}U, ^{235}U and ^{232}Th, respectively (Faure, 1986). In addition to nucleosynthesis, ^{204}Pb is produced radiogenically by the double β^-decay of ^{204}Hg; however due to the low probability of this type of radiative decay, the terrestrial abundance of ^{204}Pb essentially remains constant.

Representative atomic abundances of each of the stable Pb isotopes, ^{204}Pb, ^{206}Pb, ^{207}Pb and ^{208}Pb are 1.4%, 24.1%, 22.1% and 52.4%, respectively (Rosman and Taylor, 1998). These isotopes vary in terrestrial samples due to the different rate of radiogenic production for each isotope, with the isotopic composition of Pb in the Earth's crust steadily changing. However, the isotopic composition of Pb in an ore body does not change and remains identical to that at the time of formation of the ore body, because the Pb is separated geochemically from the parent U and Th (Faure, 1986).

The heterogeneity between Pb isotopic compositions in different ore bodies is important in geological and environmental research, as the Pb isotopic compositions of ores from different regions with different geological histories can be distinguished (Rosman, 2001)(**Table 3.6.1.1**).

Source of Ore	$^{206}Pb/^{207}Pb$	$^{208}Pb/^{207}Pb$	$^{204}Pb/^{206}Pb$
Recently mined			
Broken Hill, Australia	1.0399	2.3165	0.06248
British Columbia, Canada	1.064	2.3349	0.05995
New Brunswick, Canada	1.160	2.4319	0.05441
Idaho, USA	1.052	2.3249	0.06078
Missouri, USA	1.385	2.5927	0.04591
Taxco & Durango, Mexico	1.195	2.4917	0.05311
Shuikoushan, China	1.1779	2.4709	0.05422
Cerro de Pasco, Peru	1.200	2.4917	0.05302
Rammeisberg, Germany	1.1678	2.4444	0.05868
Altay, Kazakhstan	1.131	2.465	0.05868
Ancient workings			
Rio Tinto, Spain	1.1637	2.4482	0.05494
Mazarron region, Spain	1.1955	2.4865	0.05341
Laurion, Greece	1.2027	2.4771	0.05296
Mendips & Bristol, Britain	1.1803	2.4567	0.05415

Table 3.6.1.1 : *The isotopic compositions of some selected ores used for industrial purposes (Rosman, 2001)*

Environmental scientists employ Pb isotopes to identify sources of Pb pollution, at regional and hemispheric scales.

Region	General trend
South America and South Africa	slight increase from $^{206}Pb/^{207}Pb$ ratios of 1.07 from 1994 to 1995 to 1.08 from 1997 to 1999 (Bollhöfer and Rosman, 2000) for both continent. This indicates a common supplier for alkyllead, as leaded petrol was in use almost exclusively in both regions in 1993. However, the increase could also be because of a relative increase from industrial sources due to a slow phasing out of leaded petrol in both regions.
Austalia	Melbourne and Perth: slightly more radiogenic during the Southern Hemisphere summer and lower during winter. Probably due to an enhancement of crustal lead during the dry, dustier months as compared to wetter months (Bollhöfer and Rosman, 2002).

Europe	- Low isotopic ratios typical for alkyllead used in France and the U.K. (Monna et al., 1997) are accompanied by higher airborne Pb levels, indicating a significant contribution from the burning of leaded petrol with low radiogenic isotopic ratios. In UK, despite the introduction of unleaded petrol, the relative contribution of alkyllead to airborne Pb still accounts for approximately one third of atmospheric Pb pollution. Assuming that the Pb isotopic signature of leaded petrol in France has not changed significantly over the past 20 yr, the increase in isotopic ratios indicates an increasing relative contribution from industrial sources; - In northern Italy, the Pb isotopic composition of leaded petrol is higher with $^{206}Pb/^{207}Pb$ ($^{208}Pb/^{207}Pb$) ratios of 1.156 (2.428) (Bollhöfer and Rosman, 2001), which is probably responsible for the higher ratios measured in Venice; - The highest ratios were measured in Germany, where airborne Pb concentrations were lowest. It is most probably from (Eastern) European and Russian Pb ores with relatively radiogenic signatures (Hopper et al., 1991), there is no leaded petrol available, and the Pb isotopic ratios reflect the composition of other sources
United States and Canada	- West Coast of U.S. aerosols were less radiogenic than those from the East Coast of U.S. and tended towards higher $^{208}Pb/^{207}Pb$ ratios. Generally, $^{206}Pb/^{207}Pb$ ratios measured in Canada are lower than U.S.; - The decrease in isotopic composition of the westerlies coincides with a drastic decrease of vehicle Pb emissions in the United States from 62189 tonnes per year in 1980 to 1690 tonnes per year in 1990 (Bollhöfer and Rosman, 2002) - Emissions and the transport of pollution from China with the westerlies might account for the lower $^{206}Pb/^{207}Pb$ and relatively enriched $^{208}Pb/^{207}Pb$ ratios observed on the West Coast (Bollhöfer and Rosman, 2001).

Differences in the isotopic compositions of Pb emitted by natural and anthropogenic processes are essential for the identification and evaluation of pollution in natural archives using isotopic analyses. The predominant natural sources of Pb emission to the atmosphere are wind-blown rock

and soil dust and volcanoes (Nriagu, 1989). The relative importance of each of these sources depends upon the geographical location being considered. Volcanoes are recognized as a source of Pb emissions through quiescent degassing or from explosive or effusive eruptions. Pb is enriched in volcanic plumes relative to crustal levels (Hinkley et al., 1994), and volcanoes have been attributed as a significant source of local Pb emissions (Zreda-Gostynka et al., 1997; Monna et al., 1999).

The various proportions and quantities of natural Pb emissions linked to the dust emissions have varied greatly over the history of the Earth, particularly as a result of past glacial periods. Conversely, there is no evidence to indicate that the quantity of Pb emitted due to volcanism has significantly changed over the period of natural history recorded by ice core records (~ 220 ky) (Vallelonga et al., 2005).

3.6.2 Lead concentration and $^{206}Pb/^{207}Pb$ ratios

Nriagu (1989) has evaluated fluxes of Pb to the atmosphere from natural sources such as crust and soil, volcanoes, sea-salt spray, marine biogenic activity and wild forest fires. Thanks to Patterson and co-workers, accurate and precise measurements of Pb in polar snow and ice can now be made and demonstrate the significant increase in atmospheric lead concentrations over the past 3000 years in Greenland studies. Pb fluxes are reasonably known in Greenland (Boutron et al., 1991; Hong et al., 1994) and in Antarctica in recent times (Wolff and Suttie, 1994; Barbante et al., 1997; Planchon et al., 2003; Vallelonga et al., 2002a; Van de Velde et al., 2005) and for ancient ice (Ng and Patterson, 1981; Boutron and Patterson, 1986; Vallelonga et al., 2005).

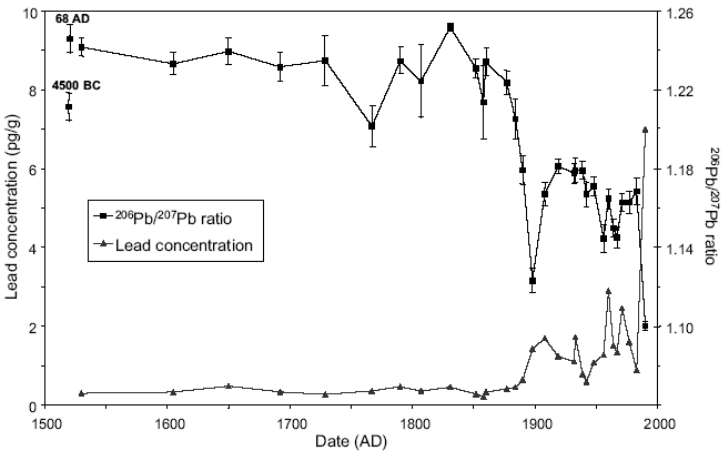

Fig. 3.6.2.1 : *The $^{206}Pb/^{207}Pb$ ratio and Pb concentration at Law Dome over the past 65OO years (Vallelonga et al., 2002a)*

'Natural' lead concentrations to Antarctica display little variation between 4500 BC and 1884 AD, with Pb concentrations averaging 0.36 pg/g and varying within the range 0.21-0.48 pg/g (Rosman et al., 1998; Vallelonga, 2002a). Moreover, Vallelonga et al. (2002a) showed that at local scale, Pb concentrations in Antarctic snow and ice are independent of variations in the snow accumulation rate. These 'natural' samples show a very low lead concentration combined with a high $^{206}Pb/^{207}Pb$ ratio (average ~ 1.23, range between 1.20 and 1.25) (**Figure 3.6.2.1**). The trend of Ba concentrations is similar to Pb, with relatively low values until late in the 19th century. Natural Ba concentrations average 1.34 pg/g and range between 0.67 to 3.21 pg/g. Natural Pb/Ba ratios average 0.31 and vary from 0.09 to 0.62 at Law Dome (**Figure 3.6.2.2**), whereas Coats Land samples are somewhat lower (Pb/Ba ~ 0.1). These Pb/Ba ratios are much higher than average Pb/Ba ratios found in crustal material (~ 0.03, based on compilations of crustal values reported (Vallelonga et al. 2002a)). Consequently, Pb/Ba ratios are indicative of additional inputs of Pb relative to Ba (volcanoes, sea-salt spray and marine biogenic activity) and suggest that a greater proportion of crustal Pb is deposited at Coats Land relative to other natural sources.

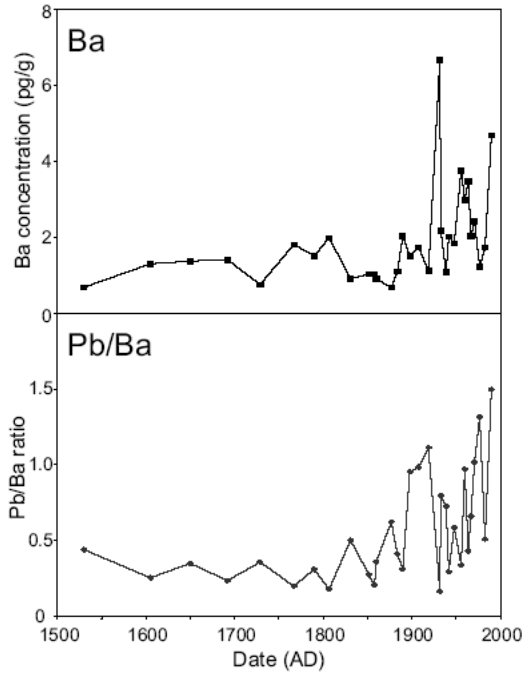

Fig. 3.6.2.2 : *Ba concentrations and Pb/Ba ratios at Law Dome from 1530 to 1989 AD (Vallelonga et al. 2002a)*

Recent times

From 1890 to 1983 AD, Pb concentrations at Law Dome are elevated and clearly have been influenced by anthropogenic lead. Lead concentrations vary in the range 0.6-2.9 pg/g, with an average of 1.4 pg/g, with higher concentrations from 1898 to 1919 and from 1960 to 1977 (Rosman et al., 1998; Vallelonga et al., 2002a). These most recent samples show a very high lead concentration combined with a low $^{206}Pb/^{207}Pb$ ratio (average ~ 1.12) (**Figure 3.6.2.1**). Similar

behaviour has been found at Victoria Land and Coats Land (**Figure 3.6.2.3**)(Van de Velde et al., 2005; Planchon et al., 2003).

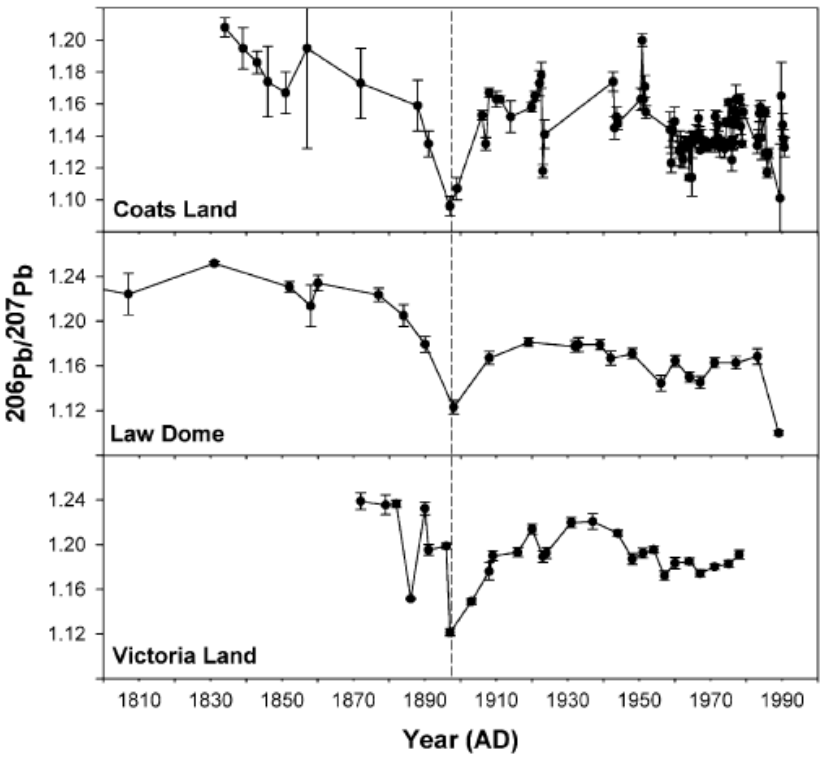

Fig. 3.6.2.3: *A comparison of $^{206}Pb/^{207}Pb$ ratios at Coats Land (Planchon et al., 2003), Law Dome (Vallelonga et al., 2002a), and Victoria Land over the past 200 years (Van de Velde et al., 2005) (from Van de Velde et al., 2005).*

A significant fraction of lead in pre-1880s samples at Coats Land and Victoria Land had a natural origin (time period 1 in **Figure 3.6.2.4**). It must indeed be kept in mind that anthropogenic emissions of Pb to the atmosphere were already significant in the Southern Hemisphere, especially because of mining activities and coal burning in South America.

Three distinct periods of Pb pollution can be identified: 1890-1930 (coal combustion and non-ferrous metal production) (time period 2), 1930-1950 (coal burning and mining) (time period 3) and 1956-1989 (alkyl-Pb additives in gasoline) (time period 4) (**Figure 3.6.2.4**). Moreover, the smoothed curve of time period 2 suggests that there might have been two successive maxima. One maximum during the early 1900s can be linked to whaling activities, coal combustion and non-ferrous metal production from Australia. The other one during the 1920s is linked to whaling activities and significant input from South America mines. There was a decline in the Pb

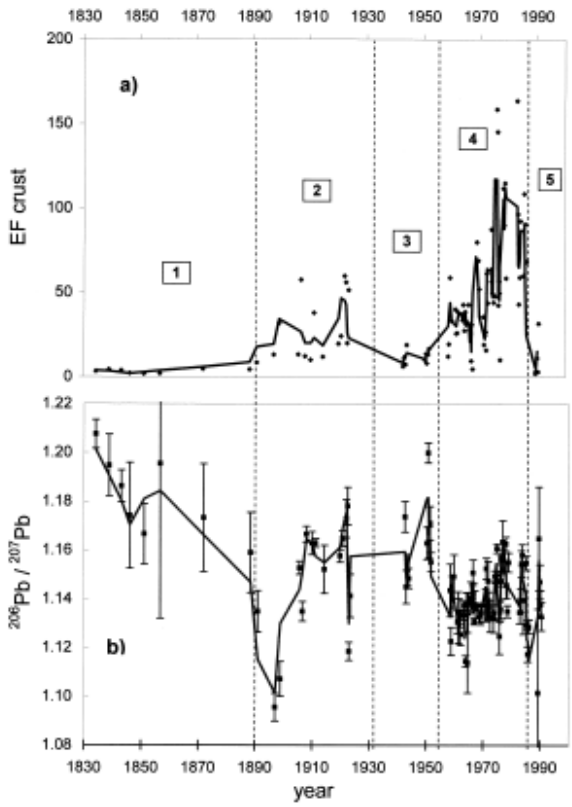

Fig. 3.6.2.4: *Coats Land, Antarctica, observed changes in (a) Pb crustal enrichment factor and (b) $^{206}Pb/^{207}Pb$ ratio in snow from the 1830s to the 1990s. The curves that are shown are four-point running averages (from Planchon et al., 2003)*

emissions from 1930s to 1950s compared with the previous period because of the economic recession and World War II (time period 3 in **Figure 3.6.2.4**). For the time period 4, there is no doubt that this pronounced increase is a consequence of the very large rise in the use of leaded gasoline in the Southern Hemisphere continents during that period (Barbante et al., 1997) combined with the continuous increase in nonferrous metal production in South America, South Africa, and Australia (Barbante et al., 1997). Finally, the data for the most recent samples (time period 5 in **Figure 3.6.2.4)** shows that there has been a ~10-fold decrease in Pb concentration, reaching values similar to those observed during the 1940s. One cause for this decrease certainly lies with the fall in the use of Pb additives at that time.

Ancient ice

Pb and Ba concentrations and $^{206}Pb/^{207}Pb$ ratios are reported in EPICA Dome C core samples dating to 220 ky BP (Vallelonga et al., 2005). Low Pb (~ 0.4pg/g for Pb) was found during the Holocene and the last interglacial (Marine Isotopic Stage 5.5) while higher Pb concentrations (~ 12 pg/g for Pb) were found during cold climatic periods (Marine Isotopic Stage 2, 4 and 6). These variations of concentrations of Pb can be linked to enhanced aerosol production by such mechanisms as lowered sea levels, stronger winds and reduced hydrological washout of aerosols, favouring the long-distance transport of dust from continents of the Southern Hemisphere to Antarctica (Delmonte et al., 2004). $^{206}Pb/^{207}Pb$ ratios decrease during glacial periods (~ 1.20),

with the lowest values occurring during colder climatic periods (~ 1.19) and the Holocene (~ 1.20) and the highest during the transition (~1.26) (**Figure 3.6.2.5**).

Increases in $^{206}Pb/^{207}Pb$ ratios occur at glacial-interglacial transitions, most clearly seen in climate stage 2, indicating an increasing proportion of volcanic Pb in Antarctic aerosols. Just prior to and during the Antarctic Cold Reversal (ACR), $^{206}Pb/^{207}Pb$ ratios were substantially higher (1.22-1.23) than those during the LGM and Holocene. $^{206}Pb/^{207}Pb$ ratios were also observed near the end of stage 2, the coldest part of the ACR, the end of climate stage 6. These variations appear to be climate related but the relationship between the $^{206}Pb/^{207}Pb$ ratios and the temperature (δD) is not a simple linear one.

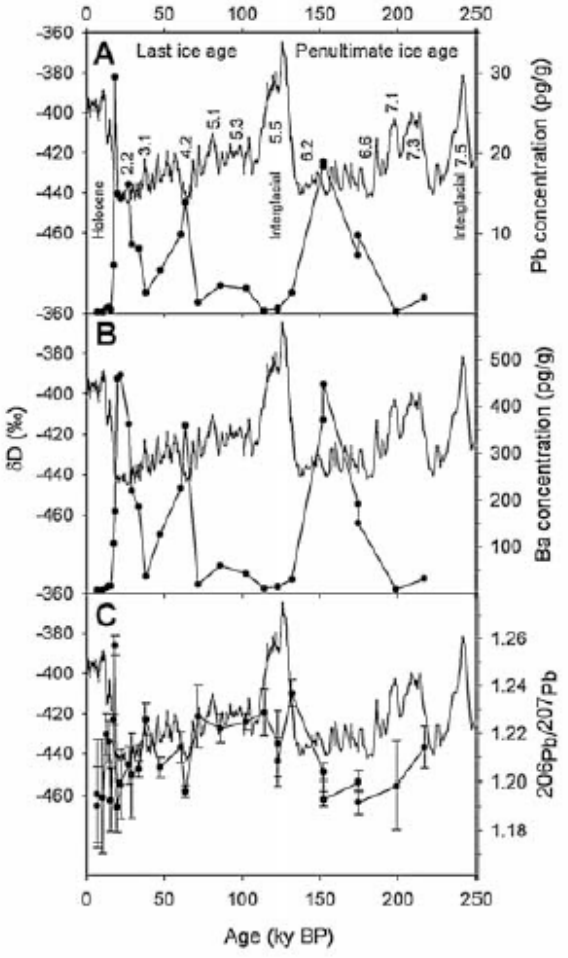

Fig. 3.6.2.5 : *220 kyr record of δ deuterium [EPICA Community Members, 2004] and Pb concentration (a), Ba concentration (b) and $^{206}Pb/^{207}Pb$ (c) from the EPICA Dome C ice core. Marine isotope stage numbers [Delmonte et al., 2004] are also shown in Figure 2a (from Vallelonga et al., 2005).*

The average Pb/Ba ratio observed at Dome C (~ 0.05) indicates that mineral dust contributes ~70% of Pb in ice. Higher Pb/ Ba ratios indicate that Pb from other sources, most likely volcanic emissions, occasionally contributed up to 65% of Pb at Dome C. More-radiogenic Pb isotopic compositions occur in samples with higher Pb/Ba ratios, suggesting that these samples contain greater proportions of volcanic Pb. The clearest sign of volcanic Pb in Dome C ice is an LGM sample (471.4 m, 18.2 kyr BP) with exceptionally high $^{206}Pb/^{207}Pb$ and Pb/Ba ratios, indicating a dust Pb proportion of ~20%.

3.6.3 The $^{206}Pb/^{207}Pb$ versus $^{208}Pb/^{207}Pb$ isotopic ratios

The $^{206}Pb/^{207}Pb$ ratio of natural Pb deposited at Law Dome between 4500 BC and 1884 AD ranges between 1.20 and 1.25, with an average ~1.23, while $^{208}Pb/^{207}Pb$ ratios range between 2.47 and 2.50 with an average of 2.48. This differs greatly from the Northern Hemisphere, where natural $^{206}Pb/^{207}Pb$ ratios were only maintained until ~680 BC (Rosman et al., 1997). In Antarctica (Law Dome, Taylor Dome, Coats Land and Victoria Land), the proportion of dust Pb in ice is consistently less than 30%. Closer examination of the data on a three-isotope plot (of $^{206}Pb/^{207}Pb$ vs. $^{208}Pb/^{207}Pb$; **Figure 3.6.3.1**) shows that they are grouped along a line. This usually indicates that the Pb in the samples is a binary mixture, the sources being the end-points of the line. We can identify at least three possible sources, Australian Pb ores being the anthropogenic end-member, Mount Erebus volcanic rock being the radiogenic end-member, and South Atlantic Ocean pelagic sediments or South Sandwich volcanic rocks lying also close to the line amidst the samples (**Figure 3.6.3.1**).

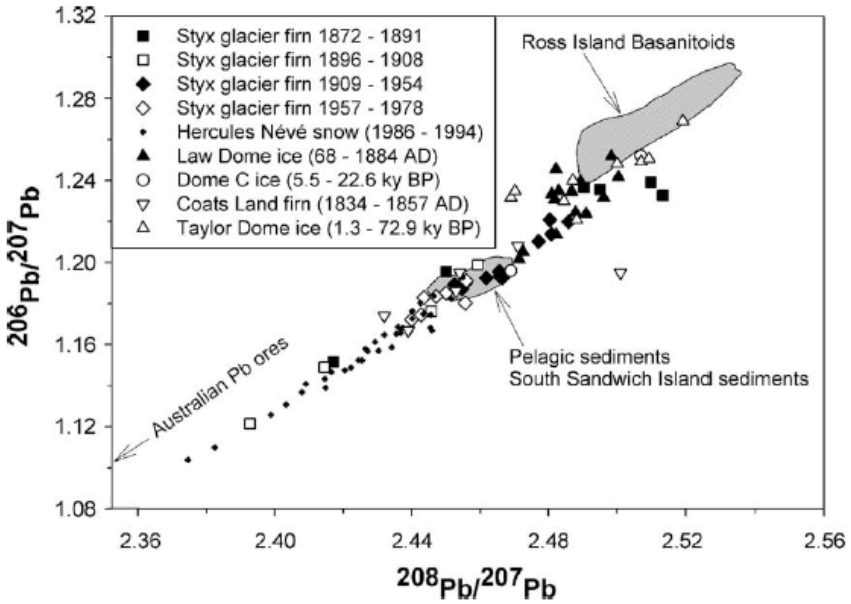

Fig. 3.6.3.1 : *Lead isotopic compositions at Victoria Land from 1872 AD to 1994 AD (Van de Velde et al., 2005). Also included are Pb isotopic compositions of Law Dome ice (Vallelonga et al., 2002a), Dome C ice (Rosman et al., 1994; Planchon et al., 2002), Coats Land firn (Planchon et al., 2003), Taylor Dome ice (Matsumoto and Hinkley, 2001), Australian Pb ores, South Atlantic Ocean pelagic sediments, South Sandwich Island sediments, and Ross Island basanitoids (from Van de Velde et al., 2005).*

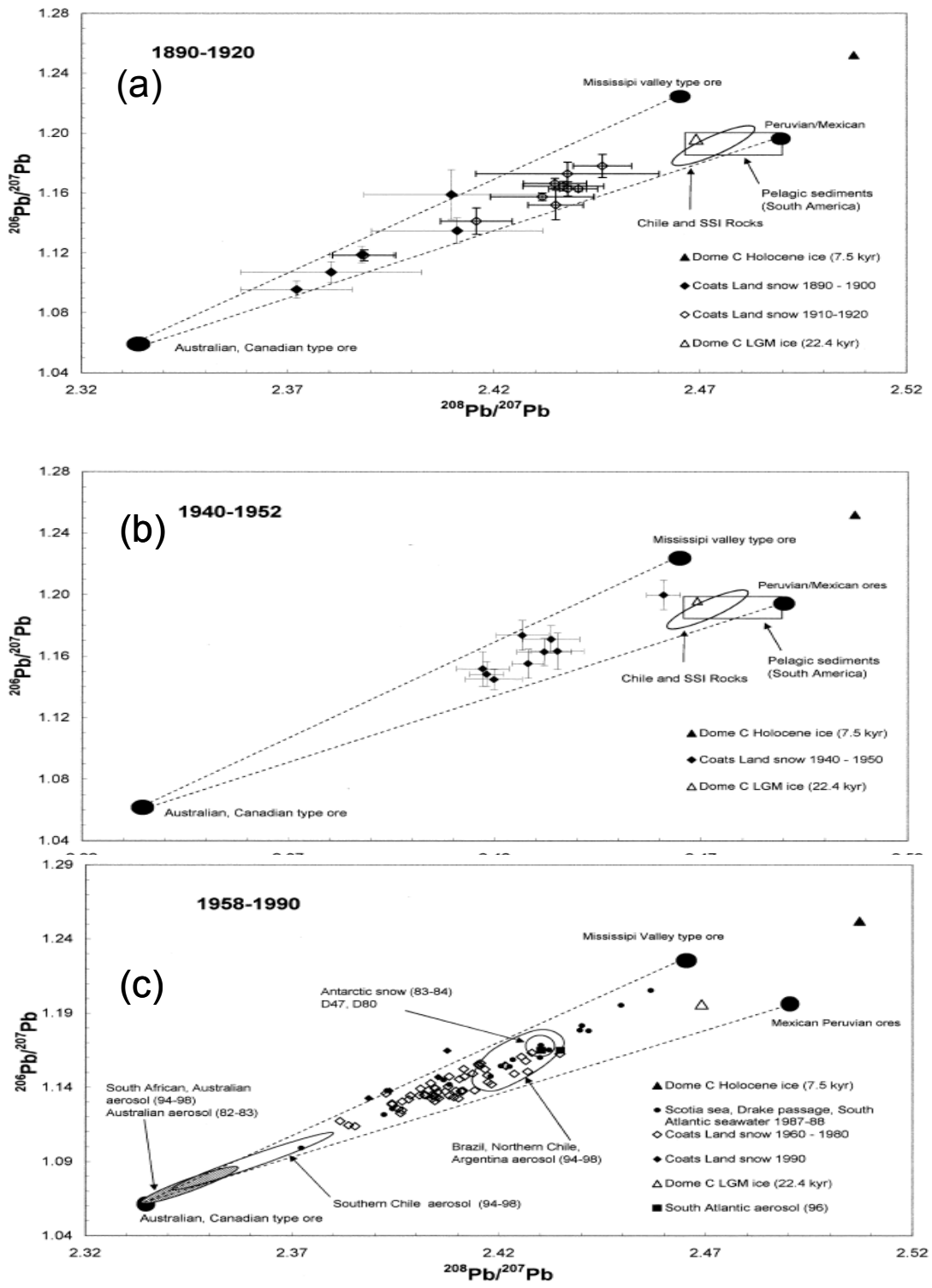

Fig. 3.6.3.2: *Coats Land, Antarctica, three-isotope plot for snow dated a) from 1890 to 1920; b) from 1940-1952; c) from 1958 to 1990. Also included are data for South Sandwich Islands (SSI) rocks, Chile rocks and pelagic sediments, Dome C Antarctic Holocene and LGM ice, typical ores and Antarctic seawater from Scotia Sea and Drake Passage (from Planchon et al., 2003)*

From 1890 to 1920, Pb isotopic signatures in Antarctica (Coats Land firn and Law Dome ice) are similar to Pb signatures in coal, South American Pb ores and pelagic sediments ores bodies (**Figure 3.6.3.2a**). Moreover, the isotopic signature of anthropogenic Pb found at Law Dome is consistent with ores from the Broken Hill Ag/Pb/Zn ore body ($^{206}Pb/^{207}Pb$: 1.0407±0.0006; $^{208}Pb/^{207}Pb$: 2.3153±0.0013), which was discovered in 1883 (Vallonga et al., 2002a).

From 1940 to 1962, Southern Hemisphere base metal production increased steadily, while the influence of automobiles and gasoline Pb additives was still relatively small. For exemple, in Coats Land, the corresponding three-isotope plot (**Figure 3.6.3.2b**) shows that, on the whole, the observed isotopic ratios are rather similar to those previously observed from 1890 to 1920 (**Figure 3.6.3.2a**) despite the fact that the main sources involved had varied considerably. Pb found in Coats Land snow during that period is probably a mixture of South American and Australian Pb.

From 1958 to 1990, it is clear that Pb found in Coats Land snow originated from different geographical areas, especially South America and Australia. It is, however, likely that the relative geographical contributions have varied during these three decades. At Law Dome, for example, low $^{206}Pb/^{207}Pb$ ratios are observed between 1950 and 1970, while higher ratios are observed in the late 1970s and 1980s. During this period, anthropogenic Pb emissions in the Southern Hemisphere were dominated by combustion of petrol containing alkyl-Pb additives (Wolff and Suttie, 1994; Bollhöfer and Rosman, 2000; Vallelonga et al., 2002a). The lower $^{206}Pb/^{207}Pb$ ratios observed between 1950 and 1970 are compatible with inputs of alkyl-Pb from Australia and New Zealand, while higher Pb isotopic ratios observed in the late 1970s and 1980s suggest increased influence of gasoline Pb emissions from countries in the northern part of South America, such as Brazil.

REFERENCES

Barbante C, Turetta C, Capodaglio G, Scarponi G (1997) Recent decrease in the lead concentration of Antarctic snow. *International Journal of Environmental Analytical Chemistry* **68**, 457-477.

Basile I (1997) Origine des aerosols volcaniques et continentaux de la carotte de glace de Vostok (Antarctique), PhD thesis, Université Joseph Fourier Grenoble I, Grenoble, France

Basile I, Grousset FE, Revel M, Petit JR, Biscaye PE, Barkov NI (1997) Patagonian origin of glacial dust deposited in East Antarctica (Vostok and Dome C) during glacial stages 2, 4 and 6. *Earth and Planetary Science Letters* **146**,573-589

Basile I, Petit JR, Touron S, Grousset FE, Barkov NI (2001) Volcanic tephra in Antarctic (Vostok) ice-cores: source identification and atmospheric implications. *Journal of Geophysical Research* **106**, 31915- 31931

Bay RC, Bramall N, Price PB (2004) Bipolar correlation of volcanism with millennial climate change. *Proceedings of the National Academy of Sciences USA* **101**, 6341-6345

Bollhöfer AF, Rosman KJR (2000) Isotopic source signatures for atmospheric lead: The Southern Hemisphere. *Geochimica et Cosmochimica Acta* **64**, 3251-3262

Bollhöfer A, Rosman KJR (2001) Isotopic source signatures for atmospheric lead: The Northern Hemisphere. *Geochimica et Cosmochimica Acta* **65,** 1727–1740

Bollhohöfer AF, Rosman KJR (2002) The temporal stability in lead isotopic signatures at selected sites in the Southern and Northern Hemispheres. *Geochimica et Cosmochimica Acta* **68**, 1375-1386

Boutron, C.F. and Patterson, C.C., 1986. Lead concentration changes in Antarctic ice during the Wisconsin/Holocene transition. *Nature* **323**, 222-225

Boutron C, Görlach U, Candelone JP , Bolshov MA, Delmas RJ (1991) Decrease in anthropogenic lead, cadmium and zinc in Greenland snows since the late 1960's. *Nature* **353**, 153-156

Campbell IB, Claridge GGC (1987) *Antarctica: soils, weathering processes and environment*, Vol 16. Elsevier

Carrasco JF, Bromwich DH, Monaghan AJ (2003) Distribution and characteristics of mesoscale cyclones in the Antarctic: Ross sea eastward to the Weddel sea. *Monthly Weather Review* **131**, 289-301

Clapperton CM (1993) *Quaternary Geology and Geomorphology of South America*, Elsevier, Amsterdam, pp. 779

De Angelis M, Barkov NI, Petrov VN (1992) Sources of continental dust over Antarctica during the last glacial cycle. *Journal of Atmospheric Chemistry* **14**, 233-244

De Bièvre P, Gallet M, Holden NE, Barnes IL (1984) Isotopic abundances and atomic weight of the elements. *Journal of Geophysical Chemistry Reference Data* **13**, 809-891

Delmonte B, Petit JR, Maggi V (2002) Glacial to Holocene implications of the new 27,000-year dust record from the EPICA Dome C (East Antarctica) ice core. *Climate Dynamics* **18**, 647-660

Delmonte B, Basile-Doelsch I, Petit JR, Michard A, Revel-Rolland M, Gemmiti B (2003) Refining the isotopic (Sr-Nd) signature of potential source areas for glacial dust in East Antarctica.

Delmonte B, Basile-Doelsch I, Petit JR, Maggi V, Revel-Rolland M, Michard A, Jagoutz E, Grousset F (2004) Comparing the EPICA and Vostok dust records during the last 220,000 years: stratigraphical correlation and provenance in glacial periods. *Earth Science Reviews* **66**,573-589

Denton GH, Prentice ML, Burckle LH (1991) Cainozoic history of the Antarctic ice sheet. In: Tingey RJ (ed) *The Geology of Antarctica*, Vol 17. Oxford Monogr. Geology Geophys., pp. 365-433

Derbyshire E (2001) Loess and the dust indicators and records of terrestrial and marine paleoenvironments (DIRTMAP) database. *Quaternary Science Review* **22**, 1813-2052

Ding ZL, Sun JM, Yang SL, Liu TS (2001) Geochemistry of the Pliocene red clay formation in the chinese loess plateau and implications for its origin, source provenance and paleoclimate change. *Geochimica et Cosmochimica Acta* **65**, 901-913

Elderfield H and Greaves MJ (1982) The rare earth elements in seawater. *Nature* **296**, 214-219

EPICA community members (2004) Eight glacial cycles from an Antarctic ice core. *Nature* **429**, 623-628.

Faure G (1986) *Principles of isotope geology*. Wiley, New York

Gaiero DM, Depetris PJ, Probst JL, Bidart SM, Leleyter L (2004) The signature of river- and wind-borne materials exported from Patagonia to the southern latitudes: a view from REEs and implications for

paleoclimatic interpretations. *Earth and Planetary Science Letters* **219**, 357-376

Gallée H (1996) Mesoscale atmospheric circulations over the southwestern Ross Sea sector, Antarctica. *Journal of Applied Meterology* **35**, 1142-1152

Gallet S, Jahn BM, Torii M (1996) Geochemical characterization of the Luochuan loess-paleosol sequence, China, and paleoclimatic implications. *Chemical Geology* **133**, 67-88

Gallet S, Jahn BM, Lanoe BVV, Dia A, Rossello E (1998) Loess geochemistry and its implications for particle origin and composition of the upper continental crust. *Earth and Planetary Science Letters* **156**,157-172

Gao Y, Kaufman YJ, Tanre D, Kolber D, Falkowski PG (2001) Seasonal distributions of aeolian iron fluxes to the global ocean. *Geophysical Research Letters* **28**, 29–32

Gaudichet A, Petit JR, Lefevre R, Lorius C (1986) An investigation by analytical transmission electron microscopy of individual insoluble microparticles from Antarctic (Dome C) ice core samples. *Tellus*, 250-261

Gaudichet A, De Angelis M, Joussaume S, Petit JR, Korotkevitch YW, Petrov VN (1992) Comments on the origin of dust in East Antarctica for present and ice age conditions. *Journal of Atmospheric Chemistry* **14**, 129–142

Gersonde R, Crosta X, Abelmann A, Armand L (2005) Sea-surface temperature and sea ice distribution of the Southern Ocean at the EPILOG Last Glacial Maximum- a circum-Antarctic view based on siliceous microfossil records. *Quaternary Science Reviews* **24,** 869-896

Goudie AS (1996) Climate, past and present. In: Adams WM, Goudie AR, Orme AR (ed) *The physical geography of Africa*. Oxford University Press, New York, pp. 44-59

Gow AJ, Williamson T (1971) Volcanic ash in the Antarctic ice sheet and its possible climatic implications. *Earth Planetary and Science Letters* **13**, 210-218

Greenwood NN, Earnshaw A (1984) *Chemistry of the elements*. Pergamon, Oxford

Grousset FE, Biscaye PE, Revel M, Petit JR, Pye K, Joussaume S, Jouzel J (1992) Antarctic (Dome C) ice-core dust at 18 k.y. B.P.: isotopic constraints and origins. *Earth and Planetary Science Letters* **111**, 175– 182

Hanson GN (1980) Rare earth elements in petrogenetic studies of igneous systems.

*Annals Review of Earth and Planetary Sciences 8***,** 371-406

Heintzenberg J, Covert DC, Van Dingenen R (2000) Size distribution and chemical composition of marine aerosols: A compilation and review. *Tellus* **52**, 1104–1122

Hinkley TK, Le Cloarec MF, Lambert G (1994) Fractionation of families of major, minor, and trace metals across the melt-vapor interface in volcanic exhalations. *Geochimica et Cosmochimica Acta* **58(15)**, 3255-3263

Hofmann AW, Feigneson MD, Raczek I (1984) Case studies on the origin of basalt: III. Petrogenesis of the Mauna Ulu eruption, Kilauea, 1969-1971. *Contribution of Mineralogy and Petrology* **88**, 24-35

Hong S, Candelone JP, Patterson CC Boutron CF (1994) Greenland ice evidence of hemispheric lead pollution two millennia ago by Greek and Roman civilizations. *Science* **265**, 1841-1843

Hopper JF, Ross HB, Sturges WT, Barrie LA (1991) Regional source discrimination of atmospheric aerosols in Europe using the isotopic composition of lead. *Tellus* **43,** 45–60

Iriondo M (1997) Models of loess and loessoids in the upper Quaternary South America. *Journal of South America Earth Sciences* **10**, 71-79

Iriondo M (1999) Climatic changes in the South American plains: Records of a continent-scale oscillation. *Quaternary Research* **57/58**, 93-112

Jahn BM, Gallet S, Han JM (2001) Geochemistry of the Xining, Xifeng and Jixian sections, Loess plateau of China: eolian dust provenance and paleosol evolution during the last 140 ka. *Chemical Geology* **178**, 71-94

Kay RW, Mahlburg-Kay S (1991) Creation and destruction of lower continental crust. *International Journal of Earth Sciences* 80, 259-278

King JC, Turner J (1997) *Antarctic Meteorology and Climatology*. Cambridge University Press

Kohfeld K, Harrison SP (2001) DIRTMAP: the geological record of dust. *Earth Science Reviews* **54**, 81-114

Livingstone I, Warren A (1996) *Aeolian geomorphology: an introduction*. Longman (ed) England

Mahowald N, Kohfeld K, Hansson M, Balkanski Y, Harrison SP, Prentice IC, Schulz M, Rodhe H (1999) Dust sources and deposition during the Last Glacial Maximum and current climate: a comparison model results with paleodata

from ice cores and marine sediments. *Journal of Geophysical Research* **104**, 15895-15916

Marino F (2006) Geochemical characterization of the EPICA Dome C ice core dust by major elements PIXE analysis and its paleoclimatic implications, PhD thesis, Università degli studi di Siena, Siena

Matsumoto A, Hinkley TK (2001) Trace metal suites in Antarctic pre-industrial ice are consistent with emissions from quiescent degassing of volcanoes worldwide. *Earth and Planetary Science Letters* **186**, 33-43

Mayewski PA (1996) Climate change during the last glaciation in Antarctica. *Science* **272**, 1636–1638

McLennan SM (1989) Rare Earth Elements in sedimentary rocks: influence of provenance and sedimentary processes. In: Lipin BR, McKay GA (Eds) *Geochemistry and Mineralogy of Rare Earth Elements*. Reviews in Mineralogy, vol.21, the Mineralogical Society of America, Washington DC, pp. 169-196

Monna F, Lancelot J, Coiudace IW, Cundy AB, Lewis JT (1997) Pb isotopic of airborne particulate material from France and the Southern United Kingdom: Implications for Pb pollution sources in urban areas. *Environmental Science Technology* **31,** 2277–2286

Monna F, Aiuppa A, Varrica D, Dongarra G (1999) Pb isotope composition in lichens and aerosols from Eastern Sicily: insights into the regional impact of volcanoes on the environment. *Environmental Science and Technology* **33**, 2517-2523

Ng A, Patterson CC (1981) Natural concentrations of lead in ancient Arctic and Antarctic ice. *Geochimica et Cosmochimica Acta* **45**, 2109-2121

Nriagu JO (1989) A global assessment of natural sources of atmospheric trace metals. *Nature* **338**, 47-49

Planchon FAM, Boutron CF, Barbante C, Cozzi G, Gaspari V, Wolff EW, Ferrari CP, Cescon P (2002) Short-term variations in the occurrence of heavy metals in Antarctic snow from Coats Land since the 1920s. *Science of the Total Environment* **300**, 129– 142

Planchon FAM, Van de Velde K, Rosman KJR, Wolff EW, Ferrari CP, Boutron CF (2003) One hundred fifty-year record of lead isotopes in Antarctic snow from Coats Land. *Geochimica et Cosmochimica Acta* **67**, 693–708

Prospero JM, Ginoux P, Torres O, Nicholson SE (2002) Environmental characteristics of global sources of

atmospheric soil dust derived from the NIMBUS-7 TOMS absorbing aerosol product. *Review of Geophysics* **40**, 1002, doi: 1010.1029/2000RG000095

Puddephatt RJ (1972) *The periodic table of the elements*. Oxford University Press, Oxford, pp. 84

Pye K (1984) Loess. *Progress in Physical Geography* **8**, 176–217

Pye K (1987) *Aeolian dust and dust deposits*. Academic Press, San Diego, California

Pye K (1995) The nature, origin and accumulation of loess. *Quaternary Science Review* **14**, 653-667

Revel-Rolland M, De Deckker P, Delmonte B, Hesse PP, Magee JW, Basile-Doesch I, Grousset F, Bosh D (2006) Eastern Australia: A possible source of dust in East Antarctica interglacial ice. *Earth and Planetary Science Letters* **249**, 1– 13

Rosman KJR, Chisholm W, Boutron CF, Candelone JP, Patterson CC (1994) Anthropogenic lead isotopes in Antarctica. *Geophysical Research Letters* **21**, 2669–2672

Rosman KJR, Chisholm W, Hong S, Candelone JP, Boutron CF (1997) Lead from Carthaginian and Roman Spanish mines isotopically identified in Greenland ice dated from 600 BC to 300 AD. *Environmental Science and Technology* **31**, 3413-3416

Rosman KJR, Taylor PDP (1998) Isotopic compositions of the elements 1997. *Journal of Physical and Chemical Reference Data* **27(6)**, 413-424

Rosman KJR, Chisholm W, Boutron CF, Hong S, Edwards R, Morgan V, Sedwick PN (1998) Lead isotopes and selected metals in ice from Law Dome, Antarctica. *Annals of Glaciology* **27**, 349-354

Rosman KJR (2001) Natural isotopic variations in lead in polar snow and ice as indicators of source regions. In: Caroli S, Cescon P, Walton DWH (Eds) *Environmental Contamination in Antarctica: A challenge to Analytical chemistry*. Elsevier Science, pp 87-106

Shannon RD (1976) Revised effective ionic radii and systematic studies of interatomic distances in halides and chalcogenides. *Acta Crystallographica* **A32**, 751-767

Schwerdtfeger W (1984) *Weather and Climate in the Antarctic*, Vol 15, Elsevier Science, Amsterdam, pp. 261

Smith J, Vance D, Kemp RA, Archer C, Toms P, King M, Zarate M (2003) Isotopic constraints on the source of Argentinian loess-with implications for atmospheric circulation and the provenance of Antarctic dust during recent glacial maxima. *Earth*

and Planetary Science Letters **212**, 181-196

Stuut JBW, Lamy F (2004) Climate variability at the southern boundaries of the Namib (southwestern Africa) and Atacama (northern Chile) coastal deserts during the last 120,000 year. *Quaternary Research* **62**, 301-309

Taylor SR, McLennan SM (1985) *The continental crust: its composition and evolution. An examination of the geochemical preserved in sedimentary rocks*. Blackwell.

Tegen I, Harrison SP, Kohfeld K, Prentice IC, Coe M (2002) The impact of vegetation and preferential source areas on global dust aerosol: results from a model study. *Journal of Geophysical* Research **107**, doi: 10.1029/2001JD000963

Vallelonga P, Van de Velde K, Candelone JP, Morgan VI, Boutron CF, Rosman KJR (2002a), The lead pollution history of Law Dome, Antarctica, from isotopic measurements on ice cores: 1500AD to 1989 AD. *Earth and Planetary Science Letters* **204**, 291–306

Vallelonga P, Van de Velde K, Candelone JP, Ly C, Rosman KJR, Boutron CF, Morgan VI, Mackey DJ(2002b), Recent advances in measurement of Pb isotopes in polar ice and snow at sub-picogram per gram concentrations using thermal ionisation mass spectrometry, *Analytica Chimica Acta* **453**, 1 – 12

Vallelonga P, Candelone JP, Van de Velde K, Curran MAJ, Morgan VI, Rosman KJR (2003) Lead, Ba and Bi in Antarctic Law Dome ice corresponding to the 1815 AD Tombora eruption: an assessment of emission sources using Pb isotopes. *Earth and Planetary Science Letters* **211**, 329-341

Vallelonga P, Gabrielli P, Rosman KJR, Barbante C, Boutron CF (2005) A 220 kyr record of lead isotopes at Dome C Antarctica from analyses of the EPICA Dome C ice core. *Geophysical Research Letters* **32**, L01706, doi: 10.1029/ 2004GL021449

Van de Velde K, Vallelonga P, Candelone JP, Rosman KJR, Gaspari V, Cozzi G, Barbante C, Udisti R, Cescon P, Boutron CF (2005) Pb isotope record over one century in snow from Victoria Land, Antarctica. *Earth and Planetary Science Letters* **232**, 95-108

Wainer I, Clauzet G, Ledru MP, Brady E, Otto-Bliesner B (2005) Last Glacial Maximum in South America: paleoclimate proxies and model results. *Geophysical Research Letters* **32**, L08702, doi: 10.1029/2004GL021244

Wedepohl KH (1995) The composition of the continental crust. *Geochimica et Cosmochimica Acta* **59**, 1217-1232

Wolff EW, Suttie ED (1994) Antarctic snow record of Southern Hemisphere lead pollution. *Geophysical Research Letters* **21,** 781-784

Woyski MM, Harris RE (1963) The rare earth and rare-earth compounds. In: Kolthoff IM, Elving PJ (ed) *Tritise on Analytical chemistry. Part II-Analytical chemistry of the elements*, vol.8, Interscience, New York, pp. 1-14

Zender CS, Miller RL, Tegen I (2004) Quantifying mineral dust mass budgets: systematic terminology constraints, and current estimates. *EOS* **85** (48) 509-529

Zreda-Gostynska G, Kyle PR, Finnegan B, Prestbo KM (1997) Volcanic gas emissions from Mount Erebus and their impact on the Antarctic Environment. *Journal of Geophysical Research* **102**, 15,039-15,055.

Chapter 4- MERCURY, TODAY AND IN THE PAST

4.1 Mercury properties

Mercury, also called quicksilver, is a chemical element in the periodic table that has the symbol Hg (Latinized Greek: *hydrargyrum*, meaning *watery* or *liquid silver*) and atomic number 80 (atomic weight 200.59 g/mol). A heavy, silvery transition metal, mercury is one of the five elements that are liquid at or near room temperature and pressure (Senese, 2007). The others are the metals cesium, francium, and gallium and the non-metal bromine. Mercury is a transition element that belongs to the group IIB (column 12), and is situated below zinc and cadmium in the periodic table of the elements (see **Figure 3.5.1**, section 3.5.1). In its pure form, mercury is recognized for its grey-white colour and high density (13.58 g/cm^3). There are seven stable isotopes of mercury (^{196}Hg, ^{198}Hg, ^{199}Hg, ^{200}Hg, ^{201}Hg, ^{202}Hg and ^{204}Hg) with ^{202}Hg being the most abundant (29.86%) and four unstable isotopes (^{194}Hg, ^{195}Hg, ^{197}Hg and ^{203}Hg). The longest-lived radioisotopes are ^{194}Hg with a half-life of 444 years, and ^{203}Hg with a half-life of 46.6 days. Most of the remaining radioisotopes have half-lives that are less than a day. ^{199}Hg and ^{201}Hg are the most commonly studied NMR-active nuclei, having spins of ½ and 3/2 respectively. Its high vapour pressure (14 mg/m^3) largely exceeds average concentrations of mercury vapour allowed during an occasional (0.05 mg/m^3) or permanent (0.015 mg/m^3) human exposure to this pollutant (WHO, 1976). Stabilized mercury has other unique properties such as a low electrical resistivity, a high thermal expansion and the ability to combine with the so-called precious metals (gold, silver, platinum and palladium) in order to form amalgams. For all these reasons, mercury is a compound largely used for its industrial, technological and medical applications.

Hg is the modern chemical symbol of mercury. The element was named after the Roman god Mercury, known for speed and mobility. It is associated with the planet Mercury. The astrological symbol for the planet is also one of the alchemical symbols for the metal. Mercury is the only metal for which the alchemical planetary name became the common name.

In soils, mercury is usually associated with sulphur in order to form HgS, which constitutes the most abundant mercury species in the Earth's crust (60ng/g; Wedepohl, 1995). With a

$[Xe]4f^{14}5d^{10}6s^2$ electronic configuration, mercury naturally occurs in three different oxidation states: 0 (metallic, Hg^0), + I (mercurous, Hg_2^{2+}) and + II (mercuric, Hg^{2+}). Among the ionic forms, Hg^{2+} is the most stable in the environment. Redox reactions allow oxidation state conversions between inorganic species. Moreover, biotic processes are able to transform inorganic compounds into organic by-products (**Figure 4.1.1**) (e.g. chemical and abiotic methylation and demethylation).

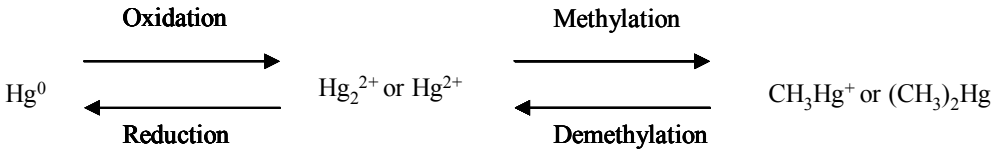

Fig. 4.1.1: *Common mercury transformation in the environment (Poissant et al., 2002)*

Properties and chemical reactivity of mercury strongly depend on its oxidation state. For example, elemental mercury is less water soluble than divalent species such as $HgCl_2$.

Among heavy metals, and particularly in comparison with tin and lead, mercury is one of the most studied environmental pollutants. This is largely due to its extreme toxicity, particularly in the methylated form and its high mobility in the environment. Mercury can be transported thousands of kilometers through the troposphere, which makes it a global pollutant.

The toxicity of mercury strongly depends on its redox state and is primarily associated with the divalent oxidation state. Liquid mercury (Hg^0) appears to have no adverse effects in contact with the skin, but its vapours can be readily absorbed by humans via the respiratory tract. Inhalation of Hg^0 vapour is, in general, associated with acute, corrosive bronchitis and pneumonitis (Craig, 1986) and the toxicity is primarily the result of its oxidation to Hg^{2+} inside the human body. The symptoms of low-level chronic mercury exposure and toxicity can be very difficult to diagnose on the basis of the symptoms alone, because most of them overlap with other health disorder symptoms. An attempt to classify the chronic symptoms of mercury poisoning is given in **Table 4.1.1** (Jitaru, 2004).

Erethism (nervousness, irritability)	Uremia (urine products in the blood)
Personality change	Tremor
Suicidal tendency	Gingivitis (inflammation of mouth and gums)
Paraesthesia	Renal damage
Impaired hearing	Insomnia
Speech disorders	Infertility
Abnormal reflexes	Pneumonitis (lung disease)
Visual disturbance	Immune system dysfunction

Table 4.1.1: *Major symptoms of low-dose chronic poisoning with mercury compounds*

The most consistent and pronounced effects of chronic exposure to mercury (inhalation of Hg^0 or ingestion of Hg^{2+} compounds, including organometallic species) are neurological and psychological. Hence, the main result of mercury poisoning is damage to the central nervous system. This is primarily the consequence mercury reacting with sulfur atoms in brain proteins, enzymes, and other macromolecules, which results in perturbation of their function (Craig, 1986). Some other effects of mercury poisoning include kidney damage and dysfunction of the immune system.

4.2 History of mercury production and its use

Mercury was known to the ancient Chinese and Hindus, and was found in Egyptian tombs that date from 1500 BC. In China, India and Tibet, mercury use was thought to extend life, heal fractures, and maintain generally good health. China's first emperor, Qin Shi Huang Di - said to have been buried in a tomb that contained rivers of flowing mercury, representative of the rivers of China - was driven insane and killed by mercury pills intended to give him eternal life. The ancient Greeks used mercury in ointments and the Romans used it in cosmetics. By 500 BC, mercury was used to make amalgams with other metals. The Indian word for alchemy is *Rasavātam* which means 'the way of mercury'. Alchemists often thought of mercury as the First Matter from which all metals were formed. Different metals could be produced by varying the quality and quantity of sulphur contained within the mercury. An ability to transform mercury into any metal resulted from the essentially mercurial quality of all metals. The purest of these was gold, and mercury was required for the transmutation of base (or impure) metals into gold as was the goal of many alchemists (Hylander and Meili, 2003). Since many centuries, mercury has played an important role in medicine and chemistry.

From the mid-18th to mid 19th centuries, a process called "carroting" was used in the making of felt hats. Animal skins were rinsed in an orange solution of the mercury compound mercuric nitrate, $Hg(NO_3)_2.2H_20$ (Lee, 1998). This process separated the fur from the pelt and matted it together. This solution and the vapours it produced were highly toxic. Its use resulted in widespread cases of mercury poisoning among hatters. Symptoms included tremors, emotional lability, insomnia, dementia and hallucinations. The United States Public Health Service banned the use of mercury in the felt industry in December 1941.

In the beginning of 20th century, chlorine is produced from sodium chloride (common salt, NaCl) using electrolysis to separate the metallic sodium from the chlorine gas. By-products of any such chloralkali process are caustic soda (sodium hydroxide (NaOH) and hydrogen (H_2)). By far the largest use of mercury (Barry, 2002) in the late 1900s was in the mercury cell process (also called the Castner-Kellner process) where metallic sodium is formed as an amalgam at a cathode made from mercury; this sodium is then reacted with water to produce sodium hydroxide). Many of the industrial mercury releases of the 1900s came from this process, although modern plants claimed to be safe in this regard (Barry, 2002). After about 1985, all new chloralkali production facilities that were built in the United States used either membrane cell or diaphragm cell technologies to produce chlorine.

Elemental mercury is also the main ingredient in dental amalgams. Controversy about the health effects from the use of mercury amalgams began shortly after its introduction into the western world, nearly 200 years ago. However, the risk of this amalgam is known; in particular, on the effects of mercury-laden fillings on children and the foetuses of pregnant women with fillings, and the release of mercury vapour on insertion and removal of mercury fillings.

Today, the use of mercury in medicine has greatly declined in all respects, especially in developed countries. Thermometers containing mercury were invented in the early 18th and late 19th centuries, respectively. In the early 21st century, their use is declining and has been banned in some countries and medical institutions. Mercury compounds are found in some over-the-counter drugs, including topical antiseptics, stimulant laxatives, diaper-rash ointment, eye drops, and nasal sprays. Mercury is still used in some diuretics, although substitutes now exist for most

therapeutic uses. So, because of the extreme and pronounced toxicity of mercury, environmental contamination due to increased industrial use of the metal has resulted in many episodes of human poisoning. One of the earliest and best-known examples of environmental mercury poisoning occurred in Japan in 1953 with the first reported cases of "Minamata desease" (Imura et al., 1971). Despite the recognition of the toxicity of mercury and mercury vapour in the 17th century in the Almadén (Spain) mercury mines (Nriagu, 1994) (**Figure 4.2.1**), Minamata was the first identified example of the *in situ* methylation and bioaccumulation of mercury in fish.

Fig. 4.2.1: *Mercury losses from the refining of silver in colonial South America. The consumption and discharge of mercury year is derived from the mercury output by the Hunacavelica mines, 85% of the output by the Almaden, and any imports from the Idrija mines (from Nriagu et al., 1994)*

Table 4.2.1 shows the annual emission of Hg in different regions of the world during the 1990s (Pirrone et al., 1996). The inventories of global anthropogenic emissions of mercury for years from 1979/1980 to 1995 suggest a substantial reduction in the 1980s and almost constant emissions afterwards (Pirrone et al., 1996; Slemr et al., 2003). However, it's not completely true. There is no stabilization of these emissions after the 1980s according to other literature sources reviewed for the AMAP program. There is an increase of Hg emissions on global scale, particularly in Asia and Africa. In contrast to emission inventories, measurements of atmospheric mercury suggest a concentration increase in the 1980s and a decrease in a 1990s. This discrepancy suggest that either the temporal change of anthropogenic emissions is substantially larger than estimated or that the approximate ratio of man-made to natural emissions of about 1:1 is substantially underestimated.

Region	Source category	1983	1984	1985	1986	1987	1988	1989	1990	1991	1992
North America	Coal combustion	68.4	73.7	75	73.7	76.5	80.6	81.4	81.4	80.6	81.3
	Solid waste incineration	91.1	92.7	94.4	96.2	105	117.1	122.1	127.2	128.6	129.4
	Oil combustion	24.6	25.5	25.6	26.3	27	28.2	28.3	27.9	27.5	28.2
	Pyrometallurgical processes										
	_Zn production	27.5	29.3	30	29.2	28.3	38.5	41.1	42	40.9	39.6
	_Pb production	4.4	4.4	4.8	4.4	4.6	5.9	5.9	6.3	5.9	6.2
	Wood combustion	4.4	4.6	4.9	5.1	5.3	5.6	5.6	4.4	4.4	4.4
	Miscellaneous	33.1	34.5	35.2	35.2	37	41.4	42.7	43.4	43.2	43.4
	Total	254	265	270	270	284	317	327	333	331	332
Central and South America	Coal combustion	4.2	4.7	5	5.2	5.3	4.8	6	5.6	6.2	6.2
	Solid waste incineration	21.3	21.7	22.1	22.5	23	23.4	23.8	24.2	24.7	24.8
	Oil combustion	10.5	10.6	10.5	11.1	11.6	11.7	11.8	11.8	12	12.1
	Pyrometallurgical processes										
	_Zn production	7.1	7.1	7.9	7.9	7.8	9.9	9.9	11.1	11	11
	_Pb production	0.51	0.59	0.56	0.6	0.59	0.68	0.78	0.74	0.8	0.79
	Wood combustion	9.7	9.6	9.5	9.4	9.3	9.1	9.4	8.7	8.2	8.2
	Miscellaneous	8	8.1	8.3	8.5	8.6	9	9.2	9.3	9.4	9.5
	Total	61	62	64	65	66	69	71	71	72	73
Western Europe	Coal combustion	95.1	88.4	101.2	101.4	96	95.5	94.5	95.4	95.6	94.6
	Solid waste incineration	76.6	77	75.6	78.2	83.7	91.4	94.2	97.1	97.6	99
	Oil combustion	33.8	33.9	33.8	34.9	35.1	35.8	36	36.2	37.3	37.6
	Pyrometallurgical processes										
	_Zn production	44.4	46.4	48.3	48.3	49.7	62.2	65	67.7	67.7	68.5
	_Pb production	3.6	3.9	3.8	3.8	3.8	4.9	5.1	5	5	5
	Wood combustion	1.4	1.5	1.5	1.6	1.6	1.7	1.6	1.6	1.6	1.6
	Miscellaneous	38.3	37.7	39.6	40.2	40.5	43.7	44.5	45.5	45.7	46
	Total	293	289	304	308	310	335	341	348	351	352
Eastern Europe and former U.S.S.R	Coal combustion	247.2	246.7	251	259.6	264	267	262.8	166.6	130.4	114.4
	Solid waste incineration	37.9	38.4	39	39.3	38.5	39.7	40	40.4	40.7	41
	Oil combustion	41.1	40.9	41.1	41.1	41.2	40.7	40	38.2	37	29.9
	Pyrometallurgical processes										
	_Zn production	34.5	35.5	35.5	35.7	36.6	48.3	49.7	49.6	49.9	51.3
	_Pb production	3.5	3.6	3.7	3.7	3.6	4.7	4.8	4.9	4.9	4.8
	Wood combustion	3.9	4	4	4.1	4.1	4.2	3.9	3.6	3.6	3.6
	Miscellaneous	55.2	55.4	56.1	57.5	58.4	60.7	60.2	45.5	40	36.8
	Total	423	424	430	441	447	465	461	349	307	282
Africa	Coal combustion	22	23.1	23.9	24.3	25.2	25.9	25.2	24.6	29.7	28.7
	Solid waste incineration	25.8	27	28.2	29.4	30.3	31.2	32.2	34.2	34	35
	Oil combustion	6.1	6.3	6.5	6.5	6.6	6.8	7.1	7.5	7.7	8
	Pyrometallurgical processes										
	_Zn production	5.4	5.5	5.4	5.1	5.4	7.6	7.6	7.6	7.1	7.6
	_Pb production	0.4	0.4	0.4	0.5	0.5	0.6	0.5	0.6	0.6	0.6
	Wood combustion	13.9	14.6	15.4	16.1	16.9	17.6	18	18.5	18.5	18.5
	Miscellaneous	11	11.5	12	12.3	12.7	13.4	13.6	14	14.6	14.8
	Total	85	88	92	94	98	103	104	107	112	113
Asia	Coal combustion	282	301	331.4	348.4	369.6	379.2	410.4	412	417.6	420
	Solid waste incineration	239.8	246.6	253.2	260.5	264.5	275.5	282.3	288.9	296.8	300.5
	Oil combustion	46.6	48	48.6	50.3	52	55.3	59	61.5	63.8	68.4
	Pyrometallurgical processes										
	_Zn production	29.4	28.7	36.7	37.5	39.8	41.2	40.2	51.3	52.4	55.7
	_Pb production	2	2.2	2.4	2.6	2.6	2.7	3	3.1	3.5	3.5
	Wood combustion	26.8	27.6	28.4	29.3	30.1	30.9	31.5	31.8	32	32
	Miscellaneous	94	98.1	105.1	109.3	113.9	117.7	124	127.3	129.9	132
	Total	721	752	806	838	872	903	950	976	996	1012
Oceania	Coal combustion	6.3	5.1	5.3	6.1	6.9	7.4	8.1	8.1	7	8.6
	Solid waste incineration	5.1	5.2	5.2	5.3	5.8	6.5	6.7	7	7.2	7.3
	Oil combustion	1.1	1.2	1.2	1.2	1.2	1.3	1.3	1.4	1.4	1.4
	Pyrometallurgical processes										
	_Zn production	7.4	7.6	7.2	7.7	7.8	10.4	10.6	10.1	10.7	10.9
	_Pb production	1.2	1.2	1.2	1.1	1.2	1.6	1.6	1.6	1.4	1.7
	Wood combustion	0.3	0.31	0.32	0.33	0.34	0.35	0.35	0.35	0.35	0.35
	Miscellaneous	3.2	3.1	3.1	3.3	3.5	4.1	4.3	4.3	4.2	4.5
	Total	25	24	24	25	27	32	33	33	32	35
World total		1861	1905	1989	2042	2104	2224	2288	2217	2201	2199

Table 4.2.1 : *Worldwide mercury emissions to the atmosphere by region and by source category (t yr^{-1})(from Pirrone et al., 1996)*

4.3 Natural release of mercury in the environment

Mercury occurs naturally in the atmosphere, soils and water. Natural sources include volcanoes, evaporation from soil and water surfaces, degradation of minerals and forest fires (UNEP). Volcanoes are largely recognized as the most significant natural source of mercury in the atmosphere (Nriagu and Becker, 2003). On the Earth, naturally occurring mercury deposits are generally found as cinnabar[27] but mercury can be found in most geological media in various concentrations. However, the natural sources of atmospheric mercury are in general concentrated within a number of 'belts" associated to plate tectonic boundaries (Gustin, 2003). These include areas of fossil and current geothermal activity, recent volcanic activity spots and organic rich sedimentary rocks (Gustin, 2003). Nriagu (1998) provides an inventory of global mercury estimation from natural sources (see **Table 4.3.1**)

Source Category	Range	Geometric mean
Windblown soil particles	0-100	10
Natural rock degassing	500-2500	1120
Volcanoes	100-2000	447
Wild forest fires	0-100	10
Biogenic processes	300-2700	900
Sea salt spray		
Global Total	800-7400	2487

Table 4.3.1 : *Worldwide emissions of mercury (tons per year) from natural sources (from Nriagu, 1998)*

The natural mercury emissions must be considered part of our local and global living environment. It is necessary to keep these sources in mind, however, as it does contribute to the environmental mercury levels. In some areas of the world, the mercury concentrations in the Earth's crust are naturally elevated, and contribute to elevated local and regional mercury concentrations in those areas (Vasiliev et al., 1998).

It should be emphasized that mercury defies the attempt to neatly categorize its sources into "natural" and "anthropogenic". Pollutant mercury deposited in many ecosystems is readily re-

[27] HgS, the most important mercury ore

emitted to the atmosphere by a number of the "natural" processes (Shroeder et al., 1989; 1992). The ease with which Hg is recycled through the atmosphere thus obscures its anthropogenic past and industrial mercury probably accounts for a significant fraction of the estimated "natural flux" of 2500 t/yr. Mason et al. (1994) have concluded that about two-thirds of the Hg currently being released into the global atmosphere has had an industrial origin. This makes it very difficult to determine the actual natural mercury emissions (UNEP Global assessment of mercury, 2003).

4.4 Biogeochemical cycle of mercury

Given the unique properties among all metals, mercury can 'travel' easily from one environmental compartment to another. Hence, once mercury enters into the ecosystem, it can cycle indefinitely. Moreover, its biogeochemical cycle is complex and still not completely understood.

The important reactions or processes controlling the distribution of mercury species in the environment (concentration, mobility and toxicity) are oxidation/reduction, methylation/demethylation, precipitation/dissolution and sorption/desorption. A simplified representation of the biogeochemical cycle of mercury is shown in **Figure 4.4.1**.

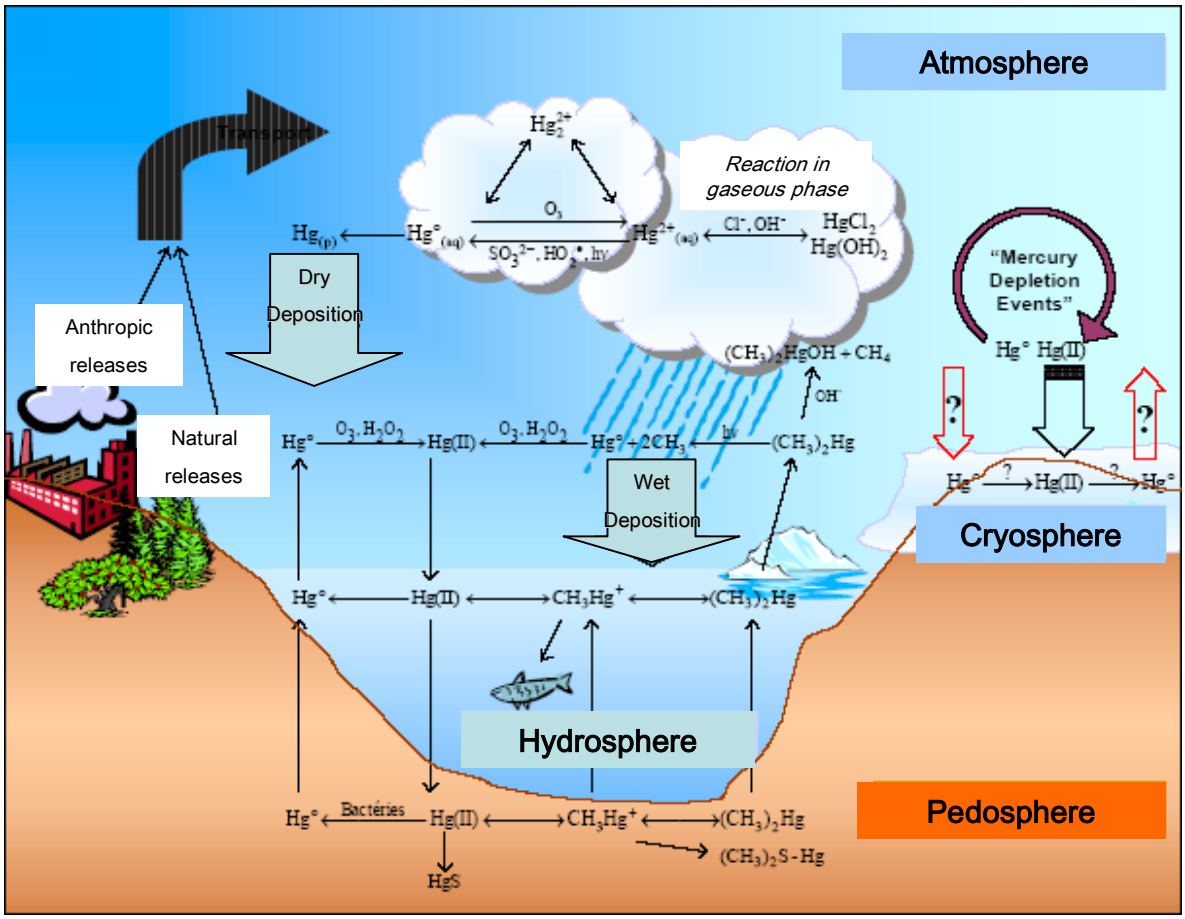

Fig. 4.4.1: *Representation of the mercury global cycle (from Stein et al., 1996; Temme, 2003)*

4.4.1 Atmospheric cycle

After its emission by way of anthropogenic or natural release, mercury can be transported in the atmosphere, according to its oxidation state, over both long and short distances. In the atmosphere, mercury consists predominantly of elemental gaseous form (Hg^0) since it is not very water soluble and is relatively unreactive (Hedgecock and Pirrrone, 2001).

However, the atmosphere is not only a medium for transport but also for chemical transformations (Sommar et al., 2001). In the atmosphere, mercury exists in two oxidation states (0 and +II) and chemical forms, but also in different physical forms with different behaviours in terms of transport and environmental impact (Munthe et al., 2001). It is generally accepted that the main forms of mercury in the atmosphere are *gaseous elemental mercury* (GEM), *reactive*

gaseous mercury (RGM) and *total particulate mercury* (TPM) (Slemr et al., 1985; Braman and Johnson, 1974; Lindberg and Stratton, 1998).

Gaseous elemental mercury is operationally defined as comprising the species that pass through a 0.45 μm pore size filter (or some other simple filtration device such as wool plugs) and which are collected on gold or other collection material. GEM is mainly composed of elemental mercury vapor (Hg^0) with minor fractions of other volatile species such as Me_2Hg, MeHg and to a lesser extent $HgCl_2$. At remote locations, GEM constitutes the dominant form (>99%) of the total mercury concentration in air.

RGM is defined as water-soluble mercury with sufficiently high vapor pressure to exist in the gas phase. The most likely candidate for RGM is in the form of HgX_2. RGM is mainly collected using denuders coated with KCl.

Finally, the TPM fraction consists of mercury bound or adsorbed on atmospheric particulate matter. The mercury species ($Hg^0$and/or RGM, including MeHg) can be chemically bound and/or adsorbed to the particle surface or integrated in the particulate matter itself.

When mercury becomes oxidized in a gaseous divalent state or adsorbed on particles, it is removed from the air by both dry and wet deposition on land and water bodies.

Wet deposition of atmospheric mercury refers to removal processes associated with precipitation. Because of its higher solubility, RGM has an atmospheric lifetime of days or at maximum weeks (Munthe et al., 2001).

Such physical deposition processes (wet and dry deposition) account mostly for GEM and include gravitational settling, impaction with objects on the ground and adsorption on liquid water or solid surfaces such as vegetation or soil. It should be emphasized that GEM has the longest environmental life, ranging between 0.5-2 years due to the low water solubility and reactivity and consequently slow removal efficiency from the atmosphere (Mason et al., 1994).

Reactivity of GEM in the atmosphere is weak except under special conditions in which GEM can be rapidly oxidized. These fast atmospheric processes known as Atmospheric Mercury Depletion

Events (AMDEs) have been observed in various places in Arctic regions in Canada (Schroeder et al.,1998 ; Poissant et al.,2002), USA (Alaska) (Lindberg et al.,2001),Norway (Berg et al.,2003), Greenland (Skov et al.,2004)and in Antarctica (Ebinghaus et al.,2002 ; Sprovieri et al., 2002; Temme et al.,2003).

It is now thought that the chemistry that causes the well known ozone depletion events (ODs) (Barrie et al., 1988) is similar to what drives AMDEs (Goodsite et al., 2004). The depletion of GEM in the polar atmosphere is thought to be caused by the oxidation of GEM by reactive halogens; namely Br atoms or BrO radicals (Goodsite et al.,2004; Skov et al., 2004a). The reactive halogen species oxidizing Hg are assumed to be generated from open water regions such as leads or polynyas from refreezing sea ice forming on open waters and UV radiation (Lindberg et al., 2002; Sprovieri et al., 2005).

4.4.2 Mercury in water and biota

It is estimated that in most cases over 90% of the mercury loading the watersheds results from atmospheric deposition (USEPA, 2000). Background concentrations of (total) mercury in unpolluted waters range from subnanogram to more than 1 nanogram per litre in open ocean waters (North Atlantic Ocean: Mason et al., 1998; Arctic Russian estuaries: Coquery et al., 1995; high Arctic watershed: Semkin et al., 2005) and 2.0 to 15 pg/g in coastal estuaries and rainwater (Stein et al., 1996; St. Louis et al., 2005). An overview of mercury concentration measured in various aquatic environments is shown in **Table 4.4.2.1**.

	Ground-water	Rain-water	Rivers/ lakes	Urban lakes	Remote lakes	Coastal ocean	Open ocean	Contamina--ted lakes [b]
Hg_T [a]	2.0-4.0	2.0-10	1.0-5.0	~2.0	0.2-5.5	2.0-15	0.5-3.0	5.0-80

[a] total mercury, pg g^{-1} ; [b] by chlor-alkali factories

Table 4.4.2.1: *Overview of mercury concentrations in aquatic environments (Stein et al., 1996)*

Similarly with the case of the atmosphere, the behavior, mobility and fate of mercury in the aquatic environment is controlled by its speciation. Hg^0 deposited from the atmosphere has a low

water solubility (~ 5 x 10^{-5}g l^{-1}), but in aerobic conditions it is easily oxidized to its highly soluble form, Hg^{2+} (Schroder et al., 1991). The half-life of mercury in water ranges from minutes to years, depending on its speciation (Sorensen et al. 1990). As summarized by Stein et al. (1996), the main processes that Hg^{2+} undergoes in the aquatic environment are as follows:

• Microbial methylation and biomagnification by biota;
• Microbial and/or photochemical reducing to Hg^0 and volatilization to atmosphere;
• Conversion to insoluble HgS and precipitation in sediments.
• Conversion to MeHg, mainly under anaerobic conditions, via methylation[28].

Moreover, as discussed above (see section 4.4.1), it is assumed that sea ice is a necessary ingredient in the recipe for producing AMDEs as sea ice is a source of the reactive halogens required to facilitate AMDEs reactions (Lindberg et al., 2002). Douglas et al. (2005) collected ice crystals formed near leads that yielded the highest Hg concentrations ever reported in snow or ice to date (up to 820 ng L^{-1}). Further evidence has been reported linking sea ice with elevated Hg concentrations in nearby ecosystems is provided by a recent study in Antarctica where soils, lichens and mosses down wind of an open water polynya in Antarctica have yielded higher Hg concentrations than were at control sites far from the polynya (Bargagli et al., 2005). These results suggest that the processes driving elevated Hg deposition near open water regions of sea ice may affect nearby ecosystems.

A greater understanding of: 1) the role sea ice plays in Hg scavenging; 2) the connection between halogens on sea ice and Hg and 3) the relationship between snow and ice crystal formation processes and Hg scavenging must be achieved.

4.4.3 Mercury species in soil and sediments

Soils

Soils characteristics (pH, temperature, content of humic material) are generally favourable to the formation of divalent inorganic compounds ($HgCl_2$, $Hg(OH)_2$) or partially organic compounds (Schuster, 1991). In soils, conversion of Hg^{2+} by various biotic processes forms methylmercury

[28] Formation of covalent bonds between methyl groups and mercury alters the physical properties, mainly the water solubility and volatility (Compeau and Bartha, 1985). Moreover, the methylation drastically increases the toxicity of mercury (Schroeder and Munthe, 1998).

(USEPA, 1997). Incorporated Hg^{2+} can be reduced easily in Hg^0 with the presence of some humic substances or light (Carpi and Lindberg, 1997) after which Hg^0 can be diffused in soils and released back to the atmosphere. However, mercury accumulation in soils is possible by reaction producing bonds between organic matter and mercury (Stein et al., 1996).

Sediments

In many lakes, sedimentation of particles containing mercury is the main sink of mercury in the water column (Sorensen et al., 1990). In open ocean, sedimentation rates are much lower than those found in lakes owing to the long water mixing cycles. In anoxic sediments, mercury exists predominantly as HgS, a very stable compound extremely insoluble that remains unreactive in anoxic conditions (Stein et al., 1996). The other divalent mercury species can be reduced to Hg^0 then either released back to the water column or can be involved in the methylation-demethylation cycle.

4.4.4 Mercury in the cryosphere

Mercury can be deposited onto snow surfaces through both wet and dry deposition. Dry deposition in Polar Regions mainly corresponds to the deposition of RGM formed during AMDEs (Lu et al., 2001; Lindberg et al., 2002; Ariya et al., 2004). Mercury in snow is mainly found in its oxidised form (e.g. Hg (II)) with concentrations that can range from a few up to hundreds of ng L^{-1} (Lalonde et al., 2002; Lindberg et al., 2002; Ferrari et al., 2005; Lahoutifard et al., 2006). AMDEs can lead to an increase of Hg concentrations in the surface snow (up to 500 ng L^{-1} (Lu et al., 2001; Lindberg et al., 2002; Brooks et al., 2006)), however, it has also been observed that within 24 hours after deposition of Hg from the atmosphere, a fraction is re-emitted as GEM back to the atmosphere (Lalonde et al., 2002; Dommergue et al., 2003). Polar snow packs themselves have been investigated for their role as a chemical reactor that leads to the formation of active oxidants/reductants (Dominé and Shepson, 2002). Hence it appears that snow packs can act both as a sink and a source of Hg to the atmosphere depending on the environmental conditions (e.g. temperature, irradiation, presence of water layers around snow grains) and the chemical composition of the snow (e.g. presence of halogens, organic substances)

(Lalonde et al., 2002; Dommergue et al., 2003; Lalonde et al., 2003; Ferrari et al., 2005; Fain et al., 2006).

4.5 Mercury as a global pollutant in remote areas

Polar ecosystems are generally considered to be the last pristine environments on the earth. The Arctic, for example, is populated by few people and has little industrial activity (except select areas in the Russian Arctic (Bard, 1999)) and is therefore perceived to be relatively unaffected by human activity. As well, Antarctica is considered to be even less affected than the Arctic by anthropogenic influences because of its isolated location far from industrial activities which are predominantly in the northern hemisphere. However, long distance atmospheric transport brings anthropogenic contaminants from mid- and low latitude sources to both Polar Regions (Fitzgerald et al., 1998; Bard, 1999). So, Polar Regions encompass fragile ecosystems and unique conditions that make the impact of external pollutants a larger threat than in other regions (Macdonald et al., 2005).

In the future the rising human population is likely to generate more waste and use more fuels and therefore environmental concentrations might increase, despite great efforts from international conventions (Madison Conference Declaration 2006). As a consequence of the current human-health and environmental concerns associated with elevated levels of mercury (especially methylmercury) in freshwater and marine fish-eating fish, there has been focused attention on mercury as a global pollutant as well as an expansion in mercury research.

4.5.1 Studies of mercury in the Arctic: recent studies

Over the past 10 years, the Arctic Monitoring and Assessment Programme (AMAP) has conducted three major assessments of the pollution status of the Arctic (AMAP). These have documented the sources, levels and trends, and effects of a wide range of contaminants, including mercury. The main conclusions of these assessments are that: “In comparison with most other areas of the world, the Arctic remains a clean environment. However, for some

pollutants, combinations of different factors give rise to concern in certain ecosystems and for some human populations. These circumstances sometimes occur on a local scale, but in some cases may be regional or circumpolar in extent." In response to the AMAP findings, the Arctic Council Action Plan to Eliminate Pollution of the Arctic (ACAP) was initiated. Mercury is one of the priority pollutants that have been selected for action under ACAP, and in 2001 the project "Reduction of Atmospheric Mercury Releases from Arctic States" was launched.

High levels of mercury

In the Arctic, Hg levels are shown to be higher in the upper layers of the marine sediment indicating that Hg input to the Arctic is post-industrially driven (Hermanson, 1998). Further evidence from ice core samples confirms these results. Ice core studies from Greenland (Boutron et al., 1998; Mann et al., 2005) observed lower Hg concentrations in snow between the late 1940s to the mid 1960s than in more recent snow when industrial activities producing Hg were high. As well, this trend has been observed in other media such as peat from Southern Greenland (Shotyk et al., 2003).

Effects for living populations

Reports have found that some marine mammals in the Canadian Arctic exceed human consumption guidelines and that Hg has been recorded above acceptable levels in cord blood of mothers (Arnold et al., 2003; Lockhart et al., 2005). Perhaps most striking is that Hg levels recorded in some northerners living in the Arctic are higher than those recorded in people from more temperate, industrialized regions where most of the Hg originates (Arnold et al., 2003). Mercury readily bioaccumulates in freshwater ecosystems and in marine wildlife and the pathways by which Hg is introduced to these environments are not well understood (**Figure 4.5.1)**. The unpredictability in the spatial and temporal trends of Hg levels in marine wildlife throughout the Arctic indicate that the high concentrations of Hg found in some species are likely driven by local and regional influences (Riget et al., 2007). The traditional way of life for northerners relies heavily on the consumption of country food (the wildlife) and this is of concern because much of these foods contain elevated Hg levels.

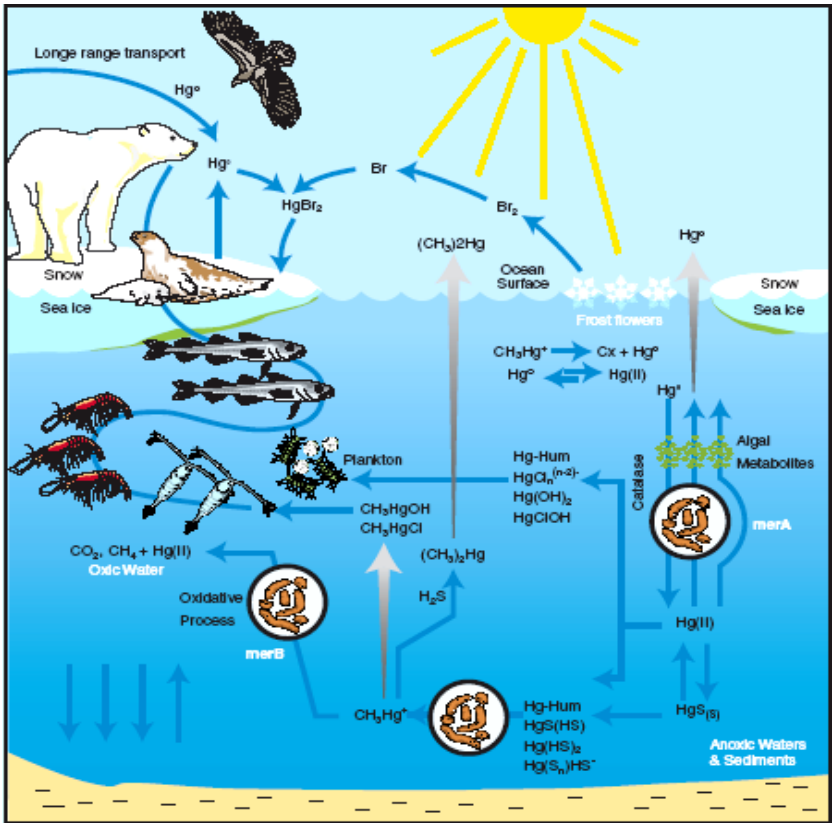

Fig. 4.5.1.1 : *Fate of mercury in the Arctic (Skov et al., 2004b)*

Atmospheric Mercury Depletion Events (AMDEs)

Recently, it has been shown that during the polar sunrise a significant increase in mercury deposition occurs (Shroeder et al., 1998). Further measurements at Alert in 1996 (to present times) corroborated the distinctive behaviour of GEM after polar sunrise and revealed a strong correlation between GEM and ground level ozone concentrations as shown in **Figure 4.5.1.2** (Schroeder et al., 1998). During and after polar sunrise, GEM and ozone concentrations were found to deplete at the same time with excellent correlations during the period between late March and mid-June (correlation coefficient [r_2] between GEM and O_3 is ~0.8). This relationship between ozone and GEM appears endemic to other locations in Arctic Regions (Lindberg et al., 2001; Berg et al., 2003; Skov et al., 2006) and the sub-arctic (Poissant and Pilote, 2003).

Lu and Shroeder (2004) suggested that GEM was being converted to total particulate and reactive gas phase mercury (RGM) when AMDEs occurred. This hypothesis that RGM is produced during AMDEs was confirmed in 2000 through direct measurements by Lindberg et al. (2001) at Barrow, Alaska, USA. Steffen et al. (2002) also demonstrated that, during depletion events, on average only 50% of the converted GEM remains in the air during AMDEs. It was proposed that the remainder of the converted Hg is deposited onto the nearby snow and ice surfaces. **Figure 4.5.1.3** shows a summary schematic of the cycling of Hg resulting from AMDEs around Polar Regions.

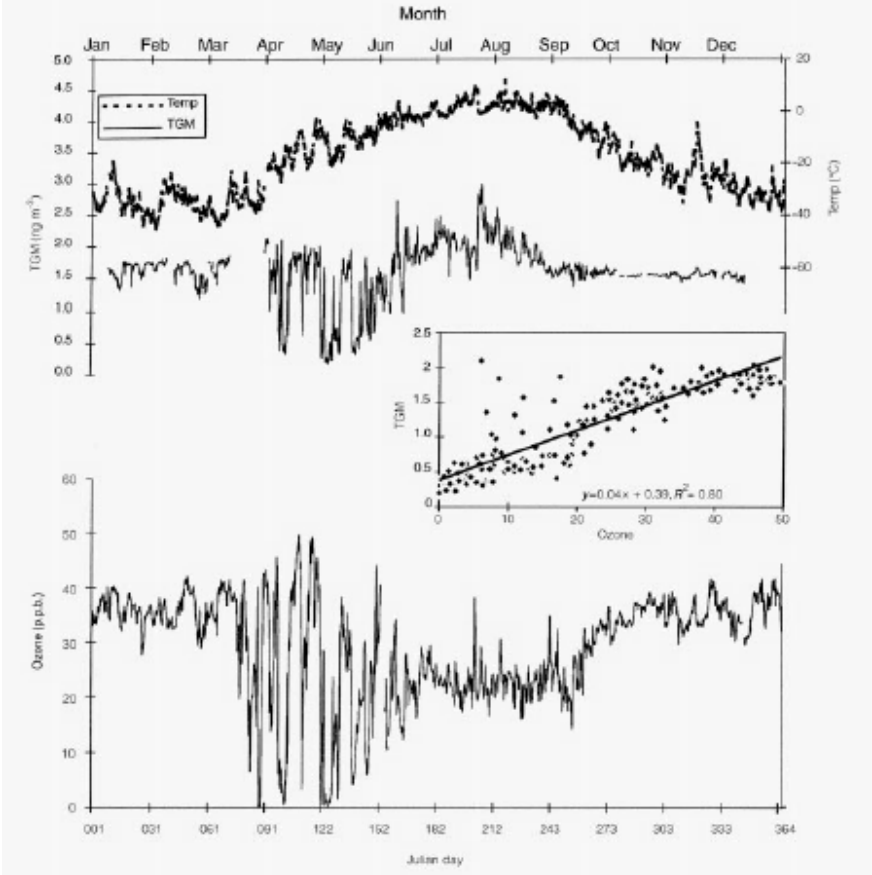

Fig. 4.5.1.2: *Time series of six-hour average values for air temperature and for total gaseous mercury (TGM) and ozone concentrations at Alert, Canada, in 1995. The inset shows concentrations of TGM versus ozone at Alert for the period from 9 April 1995 to 29 May 1995. (Shroeder et al., 1998)*

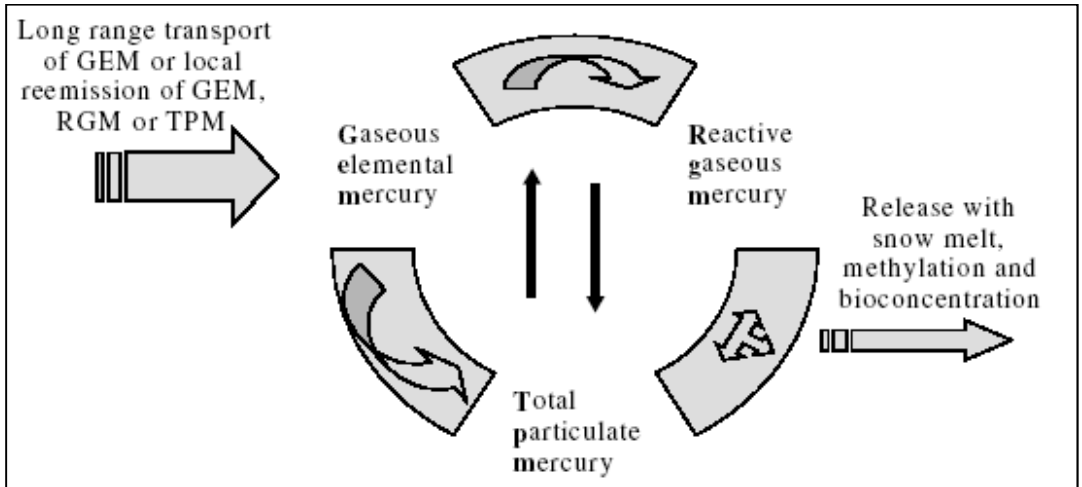

Fig. 4.5.1.3: *A simple scheme of the processe of atmospheric mercury in Polar regions during AMDE (Skov et al., 2004b)*

4.5.2 Studies of mercury in Antarctica

Although in the last years a number of studies focused on the determination of various metallic pollutants (Al, Sc, Sr, V, Cr, Mn, Fe, Co, Cu, Ag, Ba, Cd, Zn, Pb, Bi, Ir, Pt, Pd, Rh and U) in snow and/or ice from Antarctica (Planchon et al., 2002; Gabrielli et al., 2005a; Gabrielli et al., 2005b; Gabrielli et al., 2006), reliable information concerning the mercury levels in Antarctic snow and ice and especially the speciation of mercury is still lacking. Apart from the difficulties such as contamination (Murozumi et al., 1978), stability during storage etc., this is mainly because of difficulties in the analytical techniques. The concentration of Hg reported earlier in Antarctic ice (Murozumi et al., 1978; Dick et al., 1990; Vandal et al., 1993; Planchon et al., 2004) and snow (Dick et al., 1990; Sheppard et al., 1991; Vandal et al., 1995; Temme et al., 2003) is generally below 2.5 pg g^{-1} and 0.5 pg g^{-1}, respectively. Highly sensitive analytical methods are thus required for the quantification of individual mercury species in Antarctic Regions.

Paleo studies
To date, Antarctic ice cores provided depositional records for the past 34 kyr BP. These indicated three major climatic regimes. These stages included: (1) The Holocene (0-12 kyr BP), (2) The Last Glacial Maximum (LGM: 18-28 kyr BP) and (3) early Last Ice Age (28-34 kyr BP) (Vandal et al., 1993). The concentrations were rather low during the Holocene (Vandal et al., 1993; Planchon et al., 2004) and up to 4 times higher during the LGM. Such a pronounced difference cannot be explained by a variation in the snow accumulation rate, which varied in DC by only a factor of 2 between glacial and interglacial periods. Hence, changes in the source, transport and deposition processes of mercury need to be considered.

Vandal et al. (1993) noticed that mercury concentrations were strikingly elevated during the last glacial maximum (18,000 years ago), when oceanic productivity may have been higher than it is today (see **Table 4.5.2.1**). As oceanic mercury emission is correlated with productivity (see **Figure 4.5.2.1**), Vandal et al. (1993) suggested that this was the principal pre-industrial source of mercury to Antarctica; mercury concentrations in Antarctic ice might therefore serve as a paleoproductivity indicator for the most distant past.

Location	Depth (m)	Age (years)	Time period	Hg conc (pg/g)	
				Range	Mean
Mizuho plateau[a]	4-10.1	-	20th century	8.9-21.9	14.6
Windless Bight[b]	-	1987 AD	1987 AD	-	<1.0
Coats Land[c]	Surface	1982-1984 AD	80s	3.0-8.3	-
	0-16.3	1834-1986 AD	Pre- and Industrial period	0.2-16.1	-
Dome C[d]	172.8-373.9	3,850-9,800 BP	Holocene	0.19-0.49	0.33
	602.2-704.2	20,600-27,600 BP	Last Glacial Maximum	2.14-2.21	2.16
	796.9	33,700 BP	Early Last Ice Age	-	1.08
Dome C/EPICA[c]	152-594	3500-18,000 BP	Holocene-Early LGM	0.7-3.2	-

[a] Murozumi et al., 1978
[b] Dick et al., 1990
[c] Planchon et al., 2004
[d] Vandal et al., 1993

Table 4.5.2.1 : *Measured Hg concentrations in various ice samples from Antarctica at different time period*

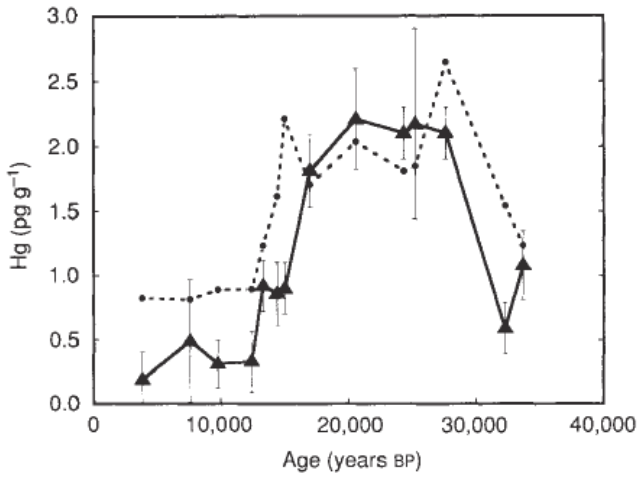

Fig. 4.5.2.1: *(▲) Mercury distribution as a function of age in the Dome C ice core.(-.-) The predicted distribution of Hg in the Dome C ice core based on the marine derived non sea-salt S04 concentrations and the estimated Hg/S ratio for gaseous evasion. The Hg/S ratio used is representative of a productive ocean region and the ratio of their emissions during the Holocene may be lower (from Vandal et al., 1993)*

The concentrations obtained in recent period (Dick et al., 1990; Vandal et al., 1995) are similar to Holocene age whilst Coats Land measurements for the period 1982–1984 are significantly higher than data from other sites. Planchon et al. (2004) have hypothesised that the differences in the analytical determination of Hg as can be made because the few previously published results (Dick et al., 1990; Vandal et al., 1995) were obtained using a CV-AFS and a photoacoustic Hg

analyser. Moreover, in the latter study, analytical blanks represented more than 80% of the measured concentrations. The significantly higher concentrations found in Coats Land snow can also be due to different sampling site characteristics (accumulation rate, source contributions, distance from the sea).

Atmospheric Mercury Depletion Events (AMDEs)

American and Canadian researchers recently found very high levels of RGM and TPM species in the Arctic environment. Dramatically increased levels of TPM and RGM were measured during atmospheric mercury depletion events (AMDEs) in the time during and after polar sunrise (see section 4.5.1). Depletions of tropospheric mercury during and after polar sunrise, were strongly correlated with ground-level ozone concentrations (see section 4.5.1). Later, AMDEs have also been observed in the Antarctic (Ebinghaus et al., 2002) and, photochemically mediated reactions involving sea salt on snow/icepack or aerosols lead to chemical oxidation of elemental mercury in the troposphere.

Vandal et al. (1995) reported a mean Hg concentration from 0.50 pg/g at the coastal site to 0.13 pg/g at D80, an inland site (**Table 5.4.2.2**). Deposition at the three inland sites (D47, D80 and South Pole) was between 5.2 and 2.1 pg cm^{-2} yr^{-1} whilst mercury deposition at D40, a coastal site, was much higher, 32 pg cm^{-2} yr^{-1}. Vandal et al. (1995) suppose at this date that the highest result in coastal site could be linked to an enhanced of scavenging at this coastal site where the precipitation rate is much higher. In fact, the high concentration at the coastal site was directly link to AMDEs. Calvert and Lindberg (2004) concluded that depletions of Hg can be enhanced by the presence of photochemically active iodine compounds. Thus sea ice is a necessary ingredient in the recipe for producing AMDEs as sea ice is a source of the reactive halogens required to facilitate AMDE reactions (Ariya et al., 2004).

Dick et al. (1990) have shown a general decrease in the amount of Hg determined as the season progressed at Windless Bight. They supposed that the decreasing concentrations could be that the deposited snow was continually losing Hg. In fact, it appears that snow packs can act both as a sink and a source of Hg to the atmosphere depending on the environmental conditions (e.g. temperature, irradiation, presence of water layers around snow grains) and the chemical

composition of the snow (e.g. presence of halogens, organic substances) (Ferrari et al., 2005; Fain et al., 2006). The reduction and subsequent re-emission of a fraction of Hg from the snow pack is largely believed to occur through photochemical processes (Lalonde et al., 2002).

Location	Time period	Hg conc (pg/g)
Site D40, 33km from the coast[a]	Sept.' 82-Jan.' 83	0.50
Site D47, 103km from the coast[a]	June 82-Jan.' 83	0.20
Site D80, 433km from the coast[a]	June 82-Jan.' 83	0.13
South Pole, 1274km from the coast[a]	Nov.' 82-Jan.' 84	0.25
Windless Bight[b]	13 December 1987	9.25
	15 December 1987	2.9
	16 December 1987	3.1
	18 December 1987	3.3
	19 December 1987	2.1
	20 December 1987	0.8
	21 December 1987	0.6
77°32'S, 159°50'E[c]	Dec.'88	0.9
Neumayer Station[d]	Dec.'2000-Feb.'2001	0.27-2.34

[a] Vandal et al., 1995
[b] Dick et al., 1990
[c] Sheppard et al., 1991
[d] Temme et al., 2003

Table 5.4.2.2 : *Measured Hg concentration in various snow samples in Antarctica*

Antarctic mosses

In line with the data on the metal content of air and snow in southern Victoria Land (Dick et al., 1990; De Mora et al., 1993), a preliminary survey on mercury distribution in ice-free areas along the coast of northern Victoria Land (Bargagli et al., 1993) showed that the average concentration in surface soils was very low (0.012 ± 0.007 µg/g). By contrast, mercury concentrations in lichens roughly corresponded to those in epiphytic lichens from moderately polluted areas in the northern hemisphere (Northern Victoria Land: 0.055-0.156 µg/g; Greenland, Northern Hemisphere: 0.07-0.13 µg/g; Austria, Northern Hemisphere: 0.02-0.05 µg/g) (Bargagli et al., 1998a). The analysis of moss samples (*Bryum pseudotriquetrum, Sarconeurum glaciale, B. argentatum, B. pseudotriquetrum, Ceratodon purpureus and Pottia heimii*) from the same coastal area corroborated this result. It was already demonstrated that mercury concentrations in soil were very low and their distribution pattern was found to be unaffected by the presence of scientific stations and other human activities (Bargagli et al., 1993).

The significance of volcanic emissions as primary sources of Hg is well documented (Varekamp and Buseck, 1986; Kyle et al., 1990; Zreda-Gostynska et al., 1997). Emissions from fumaroles in northern Victoria Land (Bargagli et al., 1996) and those of Mt. Erebus, an active volcano to the south of Edmonson Point, may enhance atmospheric concentrations of Hg in northern Victoria Land. The release of gaseous Hg from the highly productive Ross Sea (Smith and Nelson, 1985) could be another important natural source of this metal (Vandal et al., 1993).

Antarctic biota

Antarctic organisms are especially sensitive to human impact, since they usually have low capacity of larval dispersion, narrow reproductive season, low fecundity, low growth rates during crucial development stages. Moreover, they are subject to natural environmental stresses (Smith and Simpson, 1995; King and Riddle, 2001). Antarctic web chains are generally simple, and studies in such food chains may give a better understanding of transfer rates between trophic levels (Nygard et al., 2001).

Mercury levels in Antarctic biota are considered low - Primary producers and consumers had total Hg concentrations lower than or close to the lower limit of ranges usually reported for related species from other marine areas-, as would be expected in this remote area (Bargagli et al., 1998b). This could be explained by low input of both natural (lithogenic) and anthropogenic sources associated with low bioavailability of metals probably caused by sulphide formation in anoxic sediments (Santos et al., 2005). In fact, atmospheric and seawater mercury concentrations in the Southern Ocean are lower than those reported for Arctic and central Atlantic (Pongratz and Heumann, 1999).

However, the involvement of benthic organisms in the food chain lengthens the chain and causes further biomagnification of Hg (Bargagli et al., 1998b). There was a sharp increase in Hg concentrations between benthic molluscs and muscle of demersal fish, fish-eating seabirds and Weddell seals. Levels of the metal in tissues of this mammal and eggs and feathers of the Antarctic skua were similar to those reported in samples collected in the northern hemisphere (Bargagli et al., 1998b). The global pollutant distribution process can also be a route for mercury deposition in remote environments (Sheppard et al., 1991).

REFERENCES

AMAP. Arctic Monitoring and Assessment Programme. Oslo, Norway. http:// www.amap.no/

Ariya P, Dastoor A, Amyot M, Schroeder W, Barrie L, Anlauf K, Raofie F, Ryzhkov A, Davignon D, Lalonde J, Steffen A (2004) The Arctic: A sink for mercury. *Tellus* **56**, 397-403

Arnold D, Ayotte P, Bondy G, Cha L, Dewailly E, Furgal C, Gill U, Kalhok S, Kuhnlein H, Loring E, Muckle G, Myles E, Receveur O, Stokker Y, Tracy B (2003). In: Oostdam J, Donaldson S, Feeley M, Trembley N (Eds) Canadian Arctic Contaminants Assessment Report II: Human Health, pp. 21-24

Barbante C, Cozzi G, Capodaglio G, Van de Velde K, Ferrari C, Veysseyre A, Boutron CF, Scarponi G, Cescon P (1999) *Analytical Chemistry* **71**, 4125-4133

Bard SM (1999) Global transport of anthropogenic contaminants and the consequences for the Arctic marine ecosystem. *Marine Pollution Bulletin* **38 (5),** 356-379

Bargagli R, Battisti E, Focardi S, Formichi P (1993) Preliminary data on the environmental distribution of mercury in northern Victoria Land, Antarctica. *Antarctic Science* **1**, 3-8

Bargagli R, Broady PA, Walton DWH (1996) Preliminary investigation of the thermal biosystem of Mount Rittmann fumaroles (northern Victoria Land, Antarctica). *Antarctic Science* **8**, 121-126

Bargagli R, Sanchez-Hernandez JC, Martella L, Monaci F (1998a) Mercury, cadmium and lead accumulation in Antarctic mosses growing along nutrient and moisture gradients. *Polar Biology* **19**, 316-322

Bargagli R, Monaci F, Sanchez-Hernandez JC, Cateni D (1998b) Biomagnification of mercury in an Antarctic marine coastal food web. *Marine Ecology Progress Series* **169**, 65-76

Bargagli R, Agnorelli C, Borghini F, Monaci F (2005) Enhanced deposition and bioaccumulation of mercury in antarctic terrestrial ecosystems facing a coastal polynya. *Environmental Science of Technology* **39**, 8150-8155

Barrie LA, Bottenheim JW, Schnell RC, Crutzen PJ, Rasmussen NA (1988) Ozone destruction and photo-chemical reactions at polar sunrise in the lower Arctic atmosphere. *Nature* **334**, 138-141

Barry LR (2002) Chapter 3: Manufacturing Processes involving Mercury. In: *Use and release of mercury in the United States*, National risk management research laboratory, office of research and development, US Environmental Protection Agency, Cincinnati, Ohio. http://www.epa.gov/nrmt/pubs/600r02104/600r02104chap3.pdf

Berg T, Sekkesaeter S, Steinnes E, Valdal AK, Wibetoe G (2003) Springtime depletion of mercury in the European Arctic as observed at Svalbard. *Science of The Total Environment* **304**, 43–51

Boutron CF, Vandal GM, Fitzgerald WF, Ferrari CP (1998) A forty-year record of mercury in central Greenland snow. *Geophysical Research Letters* **25**, 3315-3318

Braman RS, Johnson DL (1974) Selective absorption tubes and emission technique for determination ambient forms of mercury in air. *Environmental Science of Technology* **8**, 996-1003

Brooks SB, Saiz-Lopez A, Skov H, Lindberg SE, Plan JMC, Goodsite MEG (2006) The mass balance of mercury in the springtime arctic environment. *Geophysical Research Letters* **33**, L13812, doi:10.1029/2005GL025525

Calvert JG, Lindberg SE (2004) The potential influences of iodine containing compounds on the chemistry of the troposphere in the polar spring II. *Atmospheric Environment* **38**, 5105-5116

Carpi A, Lindberg SE (1997) Sunlight-Mediated Emission of Elemental Mercury from Soil Amended with Municipal Sewage Sludge. *Environmental Science and Technology* **31**, 2085-2091

Compeau GC, Bartha R (1985) Sulfate reducing bacteria: principal methylators of mercury in anoxic estuarine sediments. *Applied Environmental Microbiology* **50**, 498-502

Coquery M, Cossa D, Martin JM (1995) The distribution of dissolved and particulate mercury in three Siberian estuaries and adjacent Arctic coastal waters. *Water, Air and Soil Pollution* **80**, 653-664

Craig PJ (1986) Organometallic compounds in the environment. Principles and reactions. Craig PJ (ed), Longman Group Limited, Leicester, UK

De Mora SJ, Patterson JE, Bibby DM (1993) Baseline atmospheric mercury studies at Ross Island, Antarctica. *Antarctic Science* **3**, 323-326

Dick AL, Sheppard DS, Patterson JE (1990) Mercury content of Antarctic surface

snow: initial results. *Atmospheric Environmnent* **24A**, 973-978

Dominé F, Shepson PB (2002) Air-Snow Interactions and Atmospheric Chemistry. *Science* **297**, 1506-1510

Dommergue A, Ferrari CP, Gauchard PA, Boutron CF, Poissant L, Pilote M, Jitaru P, Adams F (2003) The fate of mercury species in a sub-arctic snowpack during the snowmelt. *Geophysical Research Letters* **30(12)**, 1621-1624

Douglas TA, Sturm M, Simpson W, Brooks S, Lindberg S, Perovich E (2005) Elevated mercury measured in snow and frost flowers near arctic sea ice leads. *Geophysical Research Letters* **32**, L04502

Ebinghaus R, Kock H, Temme C, Einax J, Löwe A, Richter A, Burrows J, Schroeder, WH (2002) Antarctic springtime depletion of atmospheric mercury. *Environmental Science and Technology* **36**, 1238–12 44

Fain X, Ferrari CP, Gauchard PA, Magand O, Boutron CF (2006) Fast depletion of elemental gaseous mercury in the kongsvegen Glaciersnowpack in Svalbard. *Geophysical Research Letters* **33**, L06826, doi:10.1029/2005GL025223

Ferrari CP, Dommergue A, Boutron CF (2004) Profiles of mercury in the snow pack at Station Nord, Greenland shortly after polar sunrise. *Geophysical Research Letters* **31(3)**, L03401, doi: 10.1029/2003GL18961

Ferrari CP, Gauchard PA, Dommergue A, Magand O, Nagorski S, Boutron CF, Temme C, Bahlmann E, Ebinghaus R, Steffen A, Banic C, Aspmo K, Berg T, Planchon F, Barbante C, Snow to air exchange of mercury in an Arctic seasonal snow pack in Ny-Ålesund, Svalbard. *Atmospheric Environment* **39**, 7633-7645

Fitzgerald WF, Engstrom DR, Mason RP, Nater EA (1998) The case of atmospheric mercury contamination in remote areas. *Environmental Science and Technology* **32**, 1-7

Gabrielli P, Planchon FAM, Hong S, Lee KH, Hur SD, Barbante C, Ferrari CP, Petit JR, Lipenkov VY, Cescon P, Boutron CF (2005a). Trace elements in Vostok Antarctic ice during the last four climatic cycles. *Earth Planetary and Science Letters* **234**, 249-259.

Gabrielli P, Barbante C, Boutron C, Cozzi G, Gaspari V, Planchon F, Ferrari C, Turetta C, Hong S, Cescon P (2005b) Variations in atmospheric trace elements in Dome C (East Antarctica) ice over the last two climatic cycles. *Atmospheric Environment* **39**, 6420-6429

Gabrielli P, Plane JMC, Boutron CF, Hong S, Cozzi G, Cescon P, Ferrari C , Crutzen PJ,

Petit JR, Lipenkov VY, Barbante C (2006) A climatic control on the accretion of meteoric and super-chondritic iridium–platinum to the Antarctic ice cap. *Earth and Planetary Science Letters* **250**, 459-469

Goodsite ME, Plane JMC, Skov H (2004) A theoretical study of the oxidation of Hg^0 to $HgBr_2$ in the troposphere. *Environment Science and Technology* **38 (6)**, 1772-1776

Gustin MS (2003) Are mercury emissions from geologic sources significant?: A stautus report. *Science of the Total Environment* **304**, 153-167

Hedgecock IM, Pirrrone N (2001) Mercury and photochemistry in the marine boundary layer-modelling studies suggest the in situ production of reactive gas phase mercury. *Atmospheric Environment* **35**, 3055–3062

Hermanson MH (1998) Anthropogenic mercury deposition to Arctic lake sediments. *Water, Air and Soil Pollution* **101**, 309-321

Hylander LD, Meili M (2003) 500 years of mercury productions: global annual inventory by region until 2000 and associated emissions. *Science of the Total Environment* **304**, 13-27

Imura N, Sukegawa E, Pan SK, Nagao K, Kim JY, Kwan T, Ukita T (1971) Chemical Methylation of inorganic mercury with methylcobalamin, a vitamin B_{12} analog. *Science* **172**, 1248-1249

Jitaru P (2004) Ultra-trace speciation analyses of mercury in the environment, PhD thesis, Universiteit Antwerpen, Faculteit Wetenschappen, Belgium

King CK, Riddle MJ (2001) Effects of metal contaminants on the embryonic and larval development of the common Antarctic sea urchin Sterechinus neumayeri (Meissner). *Marine Ecology Progress Series* **215**, 143-154

Kyle PR, Meeker K, Finnegan D (1990) Emission rates of sulphur dioxide, trace gases and metals from Mount Erebus, Antarctica. *Geophysical Research Letters* **17**, 2125-2128

Lahoutifard N, Poissant L, Scott SL (2006) Scavenging of gaseous mercury by acidic snow at Kuujjuarapik, Northern Québec. *Science of the Total Environment* **355**, 118-126

Lalonde JD, Poulain AJ, Amyot M (2002) The Role of Mercury Redox Reactions in Snow on Snow-to-Air Mercury Transfer. *Environmental Science and Technology* **36**, 174-178

Lalonde JD, Amyot M, Doyon MR, Auclair JC (2003) Photo-induced Hg(II) reduction in snow from the remote and temperate

Experimental Lakes Area (Ontario, Canada). *Journal of Geophysical Research* **108**, 4200, doi:10.1029/2001JD001534

Lee JD (1998) *Concise inorganic chemistry*. Blackweek Sience ltd, UK

Lindberg SE, Stratton WJ (1998) Atmospheric mercury speciation: concentrations and behaviour of reactive gaseous mercury in ambient air. *Environmental Science of Technology* **32**, 49-57

Lindberg SE, Brooks S, Lin CJ, Scott K, Meyers T, Chambers L, Landis M, Stevens R (2001) Formation of reactive gaseous mercury in the Arctic: evidence of oxidation of Hg^0 to gas-phase Hg-II compounds after Arctic sunrise. *Water,Air and Soil Pollution* **1 (5/6)**, 295–302

Lindberg SE, Brooks S, Lin CJ, Scott KJ, Landis MS, Stevens RK, Goodsite M, Richter A (2002) Dynamic oxidation of gaseous mercury in the Arctic troposphere at polar sunrise. *Environment Science and Technology* **36**, 1245-1256

Lockart WL, Wilkinsom P, Billeck BN, Hunt RV, Wageman R, Brunskill GJ (1995) Current and historical inputs of mercury to high-latitude lakes in Canada and to Hudson Bay. *Water,Air and Soil Pollution* **80**, 603-610

Lockhart L, Stern GA, Low G, Hendzel M, Boila G, Roach P, Evans MS, Billeck BN, DeLaronde J, Friesen S, Kidd K, Atkins S, Muir DCG, Stoddart M, Stephens G, Stephenson S, Harbicht S, Snowshoe N, Grey B, Thompson S, DeGraff N (2005) A history of total mercury in edible muscle of fish from lakes in northern Canada. *Science of the Total Environment* **351**, 427-463

Lu JY, Schroeder WH, Barrie LA, Steffen A, Welch HE, Martin K, Lockhart L, Hunt RV, Boila G, Richter A (2001) Magnification of atmospheric mercury deposition to polar regions in springtime: the link to tropospheric ozone depletion chemistry. *Geophysical Research Letters* **28**, 3219-3222

Lu JY, Schroeder WH (2004) Annual time-series of total filterable atmospheric mercury concentrations in the Arctic. *Tellus* **56B**, 213-222

Macdonald R, Harner T, Fyfe J (2005) Recent climate change in the Arctic and its impact on contaminant pathways and interpretation of temporal trend data. *Science of the Total Environment* **342**, 5-86

Madison Conference Declaration, Eighth International Conference on mercury as a global pollutant, Madison, Wisconsin,

USA, August 6-11 (2006). http:// www.mercury2006.org/

Mann JL, Long SE, Shuman CA, Kelly WR (2005) Determination of Mercury content in a shallowfirn core from Greenland by isotope dilution inductively coupled plasma mass spectrometry. *Water, Air, and Soil Pollution* **163**, 19-32

Mason RP, Fitzgerald WF, Morel FM (1994) The biogeochemical cycling of elemental mercury: anthropogenic influences. *Geochimica et Cosmochimica Acta* **58**, 3191-3198

Mason RP, Rolfhus KR, Fitzgerald WF (1998) Mercury in the North Atlantic. *Marine Chemistry* **61**, 37-53

Munthe J, Wangberg I, Pirrone N, Iverfeldt A, Ferrara R, Ebinghaus R, Feng X, Gardfeldt K, Keeler G, Lanzillotta E, Lindberg SE, Lu J, Mamane Y, Prestbo E, Schmolke S, Schroeder WH, Sommar J, Sprovieri F, Stevens RK, Stratton W, Tuncel G, Urba A (2001) Intercomparison of methods for sampling and analysis of atmospheric mercury species. *Atmospheric Environment* **35**, 3007-3017

Murozumi M, Nakamara S, Yoshida Y (1978) Glaciological studies in Mizuho plateau, East Antarctica, 1969-1975. *National Institute of Polar Research* **7**, 255-263

Nygard T, Lie E, Rov N, Steinnes E (2001) Metal dynamics in an Antarctic food chain. *Marine Pollution Bulletin* **42 (7),** 598-602

Nriagu JO (1989) A global Assessment of natural sources of atmospheric trace metals. *Nature* **338**, 47-49

Nriagu JO (1994) Mercury pollution from the past mining of gold and silver in the Americas. *Science of the Total Environment* **149**, 167-181

Nriagu JO (1998) Global atmospheric metal pollution. In: Boutron CF (Ed) *From urban air pollution to extra-solar planets*. EDP Sciences. pp.205-226

Nriagu J, Becker C (2003). Volcanic emissions of mercury ot the atmosphere : global and regional inventories. *Science of the Total Environment* **304**, 3-12

Pirrone N, Keeler GJ, Nriagu JO (1996) Regional differences in worldwide emissions of mercury to the atmosphere. *Atmospheric Environment* **30**, 2981-2987

Planchon FAM, Boutron CF, Barbante C, Cozzi G, Gaspari V, Wolff E, Ferrari CP, Cescon P (2002) Changes in heavy metals in Antarctic snow from Coats Land since the mid-19th to the late 20th century. *Earth and Planetary Science Letters* **200**, 207-222

Planchon FAM, Gabrielli P, Gauchard PA, Dommergue A, Barbante C, Cairns WRL,

Cozzi G, Nagorski SA, Ferrari CP, Boutron CF, Capodaglio G, Cescon P, Varga A, Wolff EW (2004) Direct determination of mercury at the sub-picogram per gram level in polar snow and ice by ICP-SFMS. *Journal of Analytical Atomic Spectrometry* **19**, 823-830

Poissant L, Dommergue A, Ferrari CP (2002) Mercury as a global pollutant. In: Boutron CF (ed) *From the impact of Human activities on our climate and environment to the mysteries of Titan*. ERCA vol. 5, EDP Sciences, Journal de Physique IV 12, pp. 143-160

Poissant L, Pilote M (2003) Time series analysis of atmospheric mercury in Kuujjuarapik/Whapmagoostui (Quebec). *Journal de Physique IV* **107 (2),** 1079-1082

Pongratz R, Heumann KG (1999) Production of methylated mercury, lead, and cadmium by marine bacteria as a significant natural source for atmospheric heavy metals in polar regions. *Chemosphere* **39 (1),** 89-102

Riget F, Dietz R, Born EW, Sonne C, Hobson KA (2007) Temporal trends of mercury in marine biota of west and northwest Greenland. *Marine Pollution Bulletin* **54**, 72- 80

Santos IR, Silva-Filho EV, Schaefer CE, Albuquerque-Filho MR, Campos LS (2005) Heavy metals contamination in coastal sediments and soils near the Brazilian Antarctic Station, King George Island. *Marine Pollution Bulletin* **50**, 185-194

Schroeder WH, Munthe J, Lindqvist O (1989) Cycling of mercury between water, air and soil compartments of the environment. *Water, Air and Soil Pollution* **48**, 337-347

Schroeder WH, Yarwook G, Niki H (1991) Transformation processes involving mercury species in the atmosphere : results from a literature survey. *Water Air Soil Pollution* **56**, 653-666

Schroeder WH, Lindqvist O, Munthe J, Xiao Z (1992) Volatilization of mercury from lake surfaces. *Science of the Total Environment* **125**, 47-66

Schroeder WH, Anlauf KG, Barrie LA, Lu JY, Steffen A, Schneeberger DR, Berg T (1998) Arctic springtime depletion of mercury. *Nature* **394**,331–332

Schroeder WH, Munthe J (1998) Atmospheric mercury – An overview. *Atmospheric Environment* **32**, 809-822

Schuster G (1991) The behaviour of mercury in soils with special emphasis on complexation and adsorption processes –

A review of the literature. *Water Air and Soil Pollution* **56**, 667-680

Semkin RG, Mierle G, Neureuther RJ (2005) Hydrochemistry and mercury cycling in a High Arctic watershed. *Science of the Total Environment* **342**, 199-221

Senese F (2007) *Why is mercury a liquid at STP?*http://www.intox.org/databank/documents/chemical/mercuy/ukpid27.htm

Sheppard DS, Patterson JE, McAdam MK (1991) Mercury content of Antarctic ice and snow: Further results. *Atmospheric Environment, Part A: General Topics* **25 (8),** 1657-1660

Shotyk W, Goodsite ME, Roos-Barraclough F, Heinemeier J, Frei R, Asmund G, Lohse C, Stroyer TH (2003) Anthropogenic contributions to atmospheric Hg, Pb, and As deposition recorded by peat cores from Greenland and Denmark dated using the 14C ams "bomb pulse curve". *Geochimica et Cosmochimica Acta* **67**, 3991-4011

Skov H, Christensen J, Goodsite ME, Heidam NZ, Jensen B,Wahlin P, Geernaert G (2004a) Fate of elemental mercury in the Arctic during atmospheric mercury depletion episodes and the load of atmospheric mercury to the Arctic. *Environmental Science and Technology* **38**, 2373–2382

Skov H, Christensen J, Asmund G, Rysgaard S, Nielsen TG, Dietz R, Riget F (2004b) *Fate of the mercury in the Artcic (FOMA).* NERI technical report No. 511. National Environmental Research Institute, Denmark

Skov H, Goodsite ME, Lindberg SE, Meyers TP, Landis M, Larsen MRB, and McConville G (2006) The fluxes of Reactive Gaseous mercury measured with a newly developed method using relaxed eddy accumulation. *Atmospheric Environment* **40**, 5452-5463

Slemr F, Seiler W, Schuster GJ (1985) Distribution, speciation and budget of atmospheric mercury. *Atmospheric Chemistry* **3**, 407-434

Slemr F, Brunke EG, Ebinghaus R, Temme C, Munthe J, Wängberg I, Shroeder W, Steffen A, Berg T (2003) Worldwide trend of atmospheric mercury since 1977. *Geophysical Research Letters* **30**, doi: 10.1029/2003GL016954

Smith WO, Nelson DM (1985) Phytoplankton bloom produced by a receding ice edge in the Ross Sea: spatial coherence with the density field. *Science* **227**, 163-166

Smith SDA, Simpson RD (1995) Effects of the Nella Dam oil spill on the fauna of

Durvillaea antarctica holdfasts. *Marine Ecology Progress Series* **121**, 73-89

Sommar J, Gardfeldt K, Stromberg D, Feng X (2001) A kinetic study of the gas-phase reaction between the hydroxyl radical and atomic mercury. *Atmospheric Environment* **35**, 3049-3054

Sorensen JA, Glass GE, Schmidt KW, Huber JK, Rapp GR Jr (1990) Airborne mercury deposition and watersheds characteristics in relation to mercury concentrations in water, sediments, plankton, and fish of eighty northern Minnesota lakes. *Environmental Science and Technology* **24(11)**, 1716-1727

Sprovieri F, Pirrone N, Hedgecock IM, Landis MS, Stevens R (2002) Intensive atmospheric mercury measurements at Terra Nova Bay in Antarctica during November and December 2000. *Journal of Geophysical Research* **107** (Art. No. 4722)

Sprovieri F, Pirrone N, Landis M, Stevens RK (2005) Oxidation of gaseous elemental mercury to gaseous divalent mercury during 2003 polar sunrise at Ny-Ålesund. *Environmental Science and Technology* **39**, 9156-9165

St. Louis VL, Sharp MJ, Steffen A, May A, Barker J, Kirk JL, Kelly DJA, Arnott SE, Keatley B, Smol JP (2005) Some Sources and Sinks of Monomethyl and Inorganic Mercury on Ellesmere Island in the Canadian High Arctic. *Environmental Science and Technology* **39**, 2686-2701

Stein ED, Cohen Y, Winer AM (1996) Environmental distribution and transformation of mercury compounds. *Critical reviews in Environmental Science and Technology* **26**, 1- 43

Steffen A, Schroeder WH, Bottenheim J, Narayan J, Fuentes JD (2002) Atmospheric mercury concentrations: measurements and profiles near snow and ice surfaces in the Canadian Arctic during Alert 2000. *Atmospheric Environment* **36**, 2653-2661

Temme C (2003) Reaktionen des Quecksilbers und seiner Spezies in bodennahen Luftschichten der Antarktis, PhD thesis, Friederich-Schiller-Universität Jena, Jena, Germany

Temme C, Einax JW, Ebinghaus R, Schroeder WH (2003) Measurements of Atmospheric Mercury Species at a Coastal Site in the Antarctic and over the South Atlantic Ocean during Polar Summer. *Environmental Science and Technology* **37,** 22-31

UNEP Global Assessment of Mercury (2003) *Geneva: United Nations Environment Programme*. http://www.chem.unep.ch/mercury/Report/Key-findings.htm

United Nations Environment Program (UNEP) *Mercury Program*. http:// www.chem.unep.ch/mercury/Report/Chapter6.htm.

USEPA (1997) Mercury study report to congress. *Office of air Quality Planning and Standards, Office of Research and Development, US Government Printing Office,* Washington, DC

USEPA (2000) *Total maximum daily load development for total mercury and fish consumption guidelines*. http:// www.epa.gov/owow/tmdl/examples/mercury/ ga_savfinal.pdf

Vallelonga P, Van de Velde K, Candelone JP, Ly C, Rosman KJR, Boutron CF, Morgan VI, Mackey DJ(2002b), Recent advances in measurement of Pb isotopes in polar ice and snow at sub-picogram per gram concentrations using thermal ionisation mass spectrometry. *Analytica Chimica Acta* **453**, 1 – 12

Vandal GM, Fitzgerald WF, Boutron CF, Candelone JP (1993) Variations in mercury deposition to Antarctica over the past 34,000 years. *Nature* **362**, 621-623

Vandal GM, Fitzgerald WF, Boutron CF, Candelone JP (1995) Mercury in ancient ice and recent snow from the Antarctic. *NATO ASI series* **130**, 401-415

Varekamp JC, Buseck PR (1986) Global mercury flux from volcanic and geothermal sources. *Applied Geochemistry* **1**, 65-73

Vasiliev OF, Obolensky AA, Yagolnitser MA (1998) Mercury as a pollutant in Siberia: sources, fluxes and a regional budget. *Science of the Total Environment* **213**, 73-84

Wedepohl KH (1995) The composition of the continental crust. *Geochimica et Cosmochimica Acta* **59**, 1217-1232

WHO (1976) Environmental Health Criteria I. Mercury. *World Health Organisation*, Geneva

Wilson SJ, Steenhuisen F, Pacyna JM, Pacyna EG (2006) Mapping the spatial distribution of global anthropogenic mercury atmospheric emission inventories. *Atmospheric Environment* **40**, 4621-4632

Zreda-Gostynska G, Kyle PR, Finnegan B, Prestbo KM (1997) Volcanic gas emissions from Mount Erebus and their impact on the Antarctic Environment. *Journal of Geophysical Research* **102**, 15,039-15,055

Chapter 5- ANALYTICAL TECHNIQUES, MATERIALS AND METHODS

5.1 The European Project for Ice Coring in Antarctica (EPICA)

The European Project for Ice Coring in Antarctica (EPICA) is a consortium of laboratories and Antarctic logistics operators from ten nations, with the goal of obtaining two deep ice cores in East Antarctica (EPICA Community members, 2004). This programme has been motivated primarily by the urgent need to predict more accurately how global climate is likely to respond to increased emissions of greenhouse gases as a result of human activities. In order to predict the future, it is necessary to determine how global climate has responded to variations in greenhouse gas concentrations in the past, in combination with other forcing factors such as changes in solar output and in the earth's orbit.

The polar ice sheets are the only archive preserving information about changes both in past climate and in the atmosphere's composition. Valuable information covering at least a full climatic cycle (the last 420,000 years) has already been obtained from deep ice cores drilled through the Greenland and Antarctic ice caps. However, the Antarctic ice sheet spans an area comparable to the size of Europe and it covers a correspondingly wide range of both climatological and glaciological regimes. No single site can deliver a climate record that is representative of the whole continent, nor yield a record that has optimal resolution across the whole time range of interest. New high resolution records from Antarctica are needed to complement the records recently obtained in central Greenland. There is also a need to go back further in time to ascertain whether recent patterns are relatively unique, or typical of other climatic cycles.

EPICA, which was run about eight years, has been developed in collaboration with the European commission to meet these objectives. Fresh technical challenges have to be overcome, mainly due to the much lower temperatures in continental Antarctica compared with Greenland, and the necessity to work in unexplored regions, requiring extensive meteorological and geophysical work to select drill sites. A new drill has been designed, built and tested in North Greenland, drawing on the designs of drills used successfully in the Greenland Ice Core Project (GRIP)

(Dansgaard et al., 1993) and by Japan in central East Antarctica (Watanabe et al., 2003).

EPICA is an ambitious programme to drill deep cores in two different regions of Antarctica. The aim is to achieve optimal resolution at different time scales, and to obtain a broader perspective relating to the Antarctic continent as a whole. The study of one core (named EDML: EPICA Dronning Maud Land), from Kohnen Station in the Dronning Maud Land sector of Antarctica (**Figure 5.1.1**) is aimed at producing a high-resolution record of at least one glacial–interglacial cycle in the sector of Antarctica facing the Atlantic Ocean, for comparison with Greenland records. The second core (named EDC: EPICA Dome C) from Dome C is aimed at producing the longest possible time period (EPICA Community members, 2004).

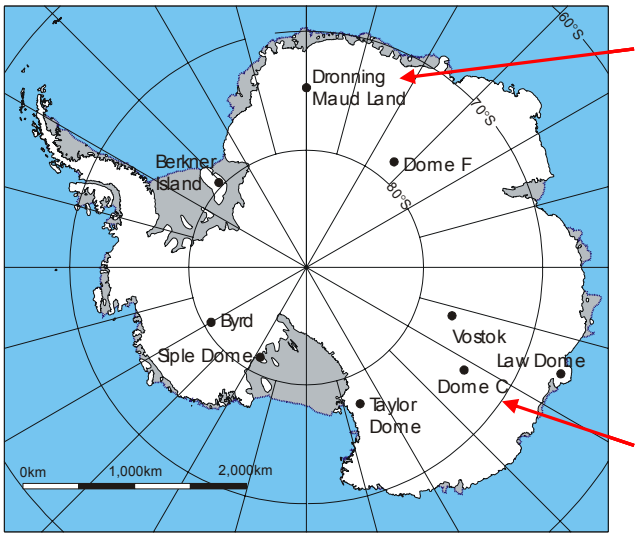

Dronning Maud Land

75°00'S, 00°04'E

Altitude: 2892 m

Mean annual temperature: -44.6°C

Snow accumulation rate: 65.0 kg/m^2/y

Measured ice thickness: 2750 ± 50 m

Dome C

75°06'S, 123°21'E

Altitude: 3233 m

Mean annual temperature: -54.5°C

Snow accumulation rate: 25.0 kg/m^2/y

Measured ice thickness: 3309 ± 22 m

Fig. 5.1.1: *Map of Antarctica showing the EPICA drilling sites: Dronning Maud Land (EDML) and Dome C (EDC)*

The exact drilling site of Dome C was selected with a geodetic and geophysical survey in the austral season 1995-96 to single out the thickest and least disturbed ice sequence, in order to obtain a long and continuous climate record. The drilling of the EPICA ice core (Core EDC96) in Dome Concordia started during the 1996-1997 field season. At the depth of 788 m the drill became unfortunately stuck. The 788m core was named "EDC96". A new drill was built and a new drilling was started in 1999, ~ 10 m apart from the EDC96 core (**Figure 5.1.2**).

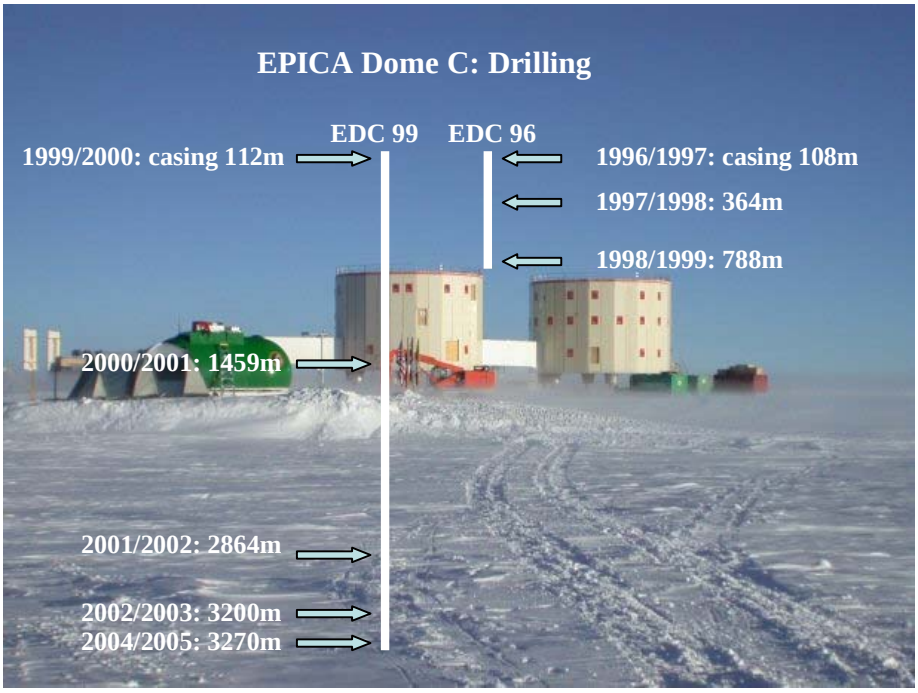

Fig. 5.1.2: *EPICA drilling at Dome C*

On Tuesday 21 December 2004, the drill reached the depth of 3270.2m, which is ~ 5m above the bedrock. The ice is melting at the bedrock and it has been decided to stop at this depth to avoid any danger of direct contamination of the basal water. The drilling operation has therefore been terminated. This 3270m core was named "EDC99".

The new core will extend the record to an age estimated to be more than 800,000 years BP. This is the oldest ice that has been presently recovered.

Each core section (typically 55 cm long, radius ~ 5 cm) was cut in the field according to the EPICA ice core processing scheme reported in **Figure 5.1.3** in order to obtain ice samples available for the analysis of different parameters of interest: dielectric properties (Dielectric Profiling DEP, Electrical Conductivity Method ECM), physical properties (ice crystallography, air bubbles), soluble chemistry (Continuous Flow Analysis CFA), isotopic analysis ($\delta^{18}O$, δD, ^{10}Be), heavy metal and metalloids, crustal trace elements, dust, lead isotopes, rare earth elements, etc. The ice samples analyzed in this work come from the main core cut B and represent ~ 30% of the cross section.

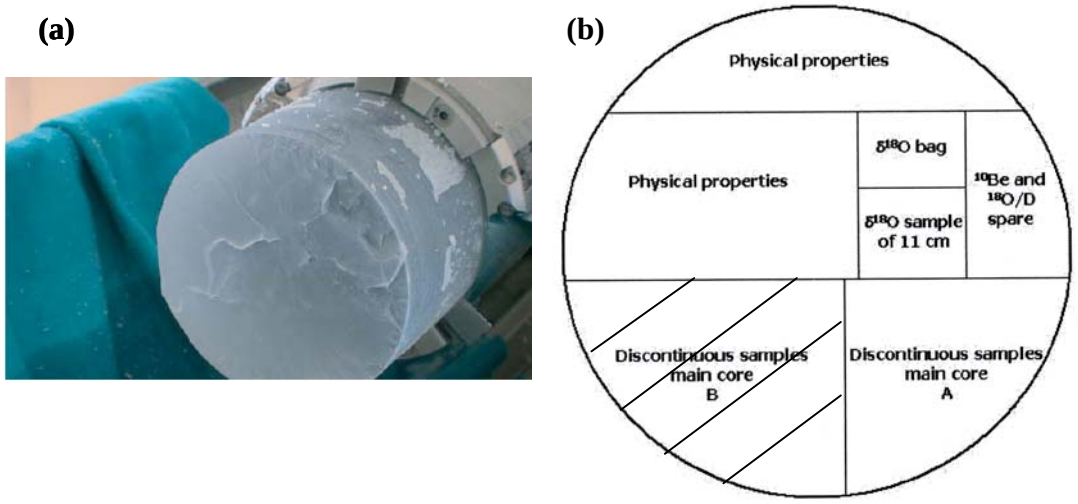

Fig. 5.1.3: *EPICA Dome C 99 (a) an ice core being extracted (b) Ice core processing scheme*

Usually, the inner core from the EDC99 core was cut into three pieces, (1) a 5 cm long part at the bottom of the section for the subsequent determination of Hg; (2) two consecutive 20 cm long parts, which were used for determination of trace elements, rare earth elements and lead isotopes. So, 39 samples have been analyzed for mercury and 78 have been analyzed for trace elements, rare earth elements and lead isotopes concentrations in this thesis work from 2368.6m to 3061.9m, as reported in **Table 5.1.1**. Previously data of trace elements, lead isotopes and mercury have been obtained by Gabrielli et al. (2005a) for the upper 2193 m of the EPICA Dome C ice core (ice dated from 0.5 to 217 ky BP).

Depth (m)	*Section numbers*	*Age (years BP)*	*Climatic period*	*N. of samples*
2368.6 - 2429.4	4308 - 4418	263,565 - 286,413	MIS 8.2	15
2550.1 - 2583.4	4638 - 4698	327,365 - 334,762	MIS 9.3	12
2605.1 -2605.4	4738	343,250-343,403	MIS 10.2	3
2632.6 -2649.4	4788 - 4818	358,780 - 368,303	MIS 10.4	9
2682.1 - 2776.9	4878 - 5048	385,808 - 425,027	MIS 11.3	18
2786.6 -2786.9	5068	432,598 - 432,870	MIS 12.2	3
2803.1 - 2808.9	5098 - 5108	423,598 - 455,550	MIS 12.4	6
2825.1 - 2847.4	5138 - 5178	424,273 - 491,845	MIS 13.1	9
2875,6 - 2902.4	5228 - 5278	511,071 - 528,422	MIS 13.3	6
2907.9 - 2913,4	5288 - 5298	532,841 - 538,194	MIS 14.2	6
2929.6 - 2979.4	5328 - 5418	554,062 - 574,428	MIS 15.1	12
3006.6 - 3028.9	5468 - 5508	591,058 - 616,273	MIS 15.5	9
3040.6 - 3061.9	5528 - 5568	631,304 - 671,706	MIS 16.2	9

Table 5.1.1: *EPICA samples analyzed in this work for Trace elements, REE, lead isotopes and mercury concentration: depth of the samples (m), section numbers, age given by the EDC3Beta6 timescale (Parrenin et al., 2007), relative climatic period and number of samples analyzed in the given depth interval*

5.2 Samples preparation

Antarctica, on the far end of the Southern Hemisphere, senses the effects of the preponderance of oceanic surfaces, small population and limited industrialisation. From a meteorological point of view, this continent is affected by the surrounding zone of cyclonic storms and high precipitation, but also by surface winds flowing radially outwards. This geographical insulation and its peculiar characteristics preserve Antarctica from heavy pollution. So, many chemical compounds in Antarctic snow and ice are present at extremely low levels (below the pg/g level). The use of special sample processing methods and measurements techniques is required to determine the extremely low impurity contents. Progress was hampered in the past (see section 2.6.1) because reported data have suffered from contamination problems.

5.2.1 Clean conditions

Working in ultra-clean conditions is mandatory to limit spurious inputs in trace elements such as heavy metals. Precautions for avoiding contamination concern the whole of the elements that can be in contact with the samples, especially laboratory air, reagents (ultra pure water and acids), equipment (storage bottles, tools for sampling) and also operator (Murphy, 1976; Patterson and Settle, 1976; Moody, 1982; Boutron, 1990).

Clean Room

Both the preparation of the sampling equipment and the analyses took place inside specially designed clean laboratories at the Laboratory of Glaciology and Geophysics of the Environment (LGGE) in Grenoble (Boutron, 1990; Ferrari et al., 2000), the Department of Environmental Sciences (DES) in Venice (Barbante et al., 1997a) and the Curtin University of Technology (CUT) in Perth (Vallelonga et al., 2002) (**Figure 5.2.1.1**).

Clean laboratories have an entrance-room acting also as a dressing-room in which, before entering in the working area, it is necessary to put on special decontaminated garments including shoulder length polyethylene (PE) gloves and special covers for shoes.

Fig. 5.2.1.1: *Class 1000 Clean room with the class 100 laminar flow Teflon clean benches located inside the clean laboratory (containing infrared lamp) (CUT, Perth)*

The working environment where samples are prepared must be at least a class 1000 clean room as classified by Federal Standard 209 (Federal Standard 209, 1988). The floor and the ceiling are made out of sheets of polyvinylchloride (PVC) and the class 100 laminar flow clean benches, storage shelves and cabinets are made with polypropylene. The air inside the clean room is pressurized, preventing outside contaminated air admission. Furthermore the pressurized air must be filtered through high efficiency particulate filters (HEPA filters), able to remove 99.999% of particle greater than 0.5 % μm (Patterson and Settle, 1976; Moody, 1982; Boutron, 1990, Vallelonga et al., 2002). Under such conditions the transfer of airborne particulate to the samples is kept to a minimum (1000 particles/m^3, with only one operator).

This first step of purification, although very efficient, does not allow limiting the contaminant inputs *via* the atmosphere at very low level. For the purest samples, we still need to reduce the particles content in air (100 particles/m^3). We use for doing that laminar flow clean benches, where air of the clean room is filtered again with others high efficiency particulate air (HEPA) filters. Positive air pressures are maintained between laminar flow benches and the clean room to ensure any contamination problems.

Ultra-pure water

It is important to have ultra-pure water for bottle cleaning and for the preparation of standard solutions. This water can be produced by coupling a reversee osmosis system Milli-RO, with

Milli-Q ion-exchange resins (Millipore, Bedford, MA, USA) (DES, Venice), or by passing tap water through a series of activated charcoal and ion-exchange resins (from MAXY, La Garde, France) (LGGE, Grenoble) (Boutron, 1990). **Table 5.2.1.1** reports typical concentration of heavy metals in ultra-pure water produced by these two systems.

	Element concentration (pg/g)				
	Milli-Q		Maxy		Detection limit (in pg/g)
	ICP-MS	ETA-AAS	ICP-MS	Other techniques	
Ag	0.07 (0.01)		0.06 (0.01)		0.03
Bi	0.03 (0.04)		0.02 (0.01)		0.03
Cd	0.8 (0.2)	<0.01	0.6 (0.1)	<0.05	0.3
Co	1.55 (0.04)		1.47 (0.03)		0.09
Cu	0.9 (0.3)	0.3	0.6 (0.2)	<0.1	0.6
Mo	0.32 (0.09)		0.64 (0.07)		0.21
Pb	1.2 (0.2)	0.1	1.04 (0.03)	0.27 , 0.28	0.09
Pd	0.20 (0.02)		0.24 (0.03)		0.09
Pt	0.05 (0.01)		0.043 (0.003)		0.009
Sb	0.15 (0.05)		0.15 (0.02)		0.06
U	0.12 (0.03)		0.06 (0.03)		0.09
Zn	2.1 (0.3)	0.3	1.8 (0.3)	0.3	0.9

Table 5.2.1.1: *Trace element concentration in ultra-pure Milli-Q and Maxy waters (from Barbante et al., 2001)*

Ultra-pure reagents and chemicals

Ultra-pure HNO_3 is extensively used both for cleaning decontamination materials and labware. The high purity HNO_3 acid used for this work was prepared by sub-boiling distillation of analytical reagent grade acid in a quartz still at Curtin University of Technology (CUT), Perth, Australia (Burton et al., 2007).

Chloroform used is a high purity reagent (MERCK "Suprapur"). The range of heavy metals and metalloids content is up to ng/g, or even less for some metal (for example, Hg, Pb). It is used for a first degreasing.

Low Density Polyethylene (LDPE) containers are used to store ice samples after melting. LDPE represents a compromise between chemical resistance during strong cleaning treatments, low content of impurities and a low price. In any case, before use, all the plastic bottles and items

must be extensively cleaned following previous procedures (Boutron, 1990; Barbante et al., 1997a).

Briefly, bottles and other items are cleaned as follows: rough rinse with tap water to remove dust; remove grease with chloroform and rinse with ultra-pure water (three times); immerse in a first 15% HNO_3 acid bath (Merck "Suprapur" HNO_3 in MAXY ultra-pure water, 40°C, 1 week) and rinse three times with MAXY ultra-pure water; immerse in a second 0.1% HNO_3 acid bath (CUT HNO_3 in MAXY ultra-pure water, 40°C, 1 week) and rinse three times with MAXY ultra-pure water; immerse in a third 0.1% HNO_3 acid bath (CUT HNO_3 in MAXY ultra-pure water, 40°C, 1 week) and rinse three times with MAXY ultra-pure water; finally bottles are filled with 0.1% CUT HNO_3 fresh solution in MAXY ultra-pure water and stored inside triple polyethylene acid clean bags, while other tools remain in the last bath until use. Before use, LDPE bottles are rinsed three times and conditioned 12 hours with MAXY ultra-pure water.

5.2.2 Decontamination procedure

The drilling and subsequent storage of ice cores expose them to surface contamination from the drilling fluid, the drilling equipment and urban air containing significant levels of some trace elements like anthropogenic lead. Candelone et al. (1994) described a technique for the removal of contaminated outside layers from ice cores by the sequential chiselling of concentric ice veneer layers from the core while it is suspended in a plastic lathe (**Figure 5.2.21**).

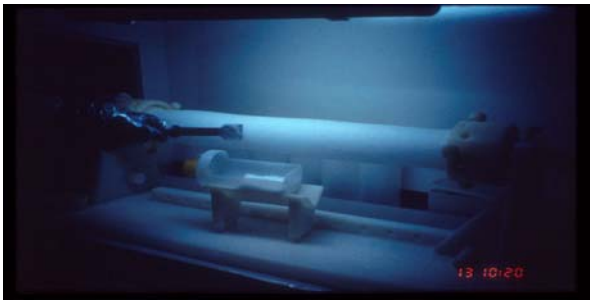

Fig. 5.2.2.1: *The decontamination technique used to remove the ice core veneers, with one operator chiselling the ice core, and the other collecting the chips in a LDPE scoop.*

The EPICA/Dome C ice core sections were decontaminated within a laminar flow bench supplied with HEPA filtered air, located within cold room operated at -15°C, at the Laboratory of Glaciology and Geophysics of the Environment (LGGE) in Grenoble, France. Two core sections

were decontaminated in one day each week, with the apparatus cleaned (two sets of chisels, melting bottles and the rest of the chiselling materials) in sequences of acid baths between 2 decontaminations days.

Tools used in the decontamination procedure were categorized depending upon their role in the procedure, which determined the type of cleaning that was necessary. The different part of the lathe were of low cleaning priority , as they were not intended to contact the core except for the exterior, contaminated, external part of the core. They were cleaned at room temperature in a bath of "Suprapur" HNO_3 in MAXY ultra-pure water 15% for 24 hours, then rinsed three times with MAXY ultra-pure water and stored inside triple polyethylene acid clean bags.

All other equipment (stainless steel chisels, bottles for melting step, collecting scoops, inner core tongs) was of high cleaning priority. They were then cleaned following the procedure of cleaning described above (section 5.2.1) (three successive baths). Two sets of stainless steel chisels, melting bottles, collecting scoops and inner core tongs were used: one for the decontamination of the morning and the other for the decontamination of the afternoon. On the day prior to the decontamination, stainless steel chisels, melting bottles, collecting scoops and inner core tongs of both sets were rinsed with MAXY ultra-pure water, packed in triple acid-cleaned polyethylene bags which were heat-sealed airtight. The set of the morning was transported to the cold room in the afternoon of the day prior to the decontamination. The set of the afternoon was transported to the cold room in the morning of the decontamination.

The 10 stainless steel chisels (5 per set) were cleaned, stored and transported within 2 polyethylene boxes. The melting bottles, collecting scoops and inner core tongs were packed such that melting bottles and collecting scoops used for each external layer were contained in separate triple acid-cleaned polyethylene bags, while the tongs, melting bottles and scoops used for the inner core were all contained in another bag.

Once within the cold room, shoulder length polyethylene gloves were put on. In the air stream of the laminar flow bench within the cold room, the bags were opened and the lathe pieces, chisels and melting bottles were placed inside the bench. The lathe was then assembled. Scoop for the

first (external) layer was removed from its bag and placed within the bench. The ice core section was taken out of its polyethylene bag in which it was packed in the field and then held in the air stream of the bench, but not within the bench. Using chisel number 1, a layer of ice was scraped from the core and discarded onto the cold room floor. Candelone et al. (1994) have indeed shown that the most external layer of a core is usually highly contaminated which makes it highly preferable to discard it before introducing the core into the lathe. Following removal of this layer, chisel 1 was placed in an unused polyethylene glove and no longer touched for the duration of the decontamination.

The core was then introduced into the lathe by one operator, while the other fixed the core extremities in the lathe holders. Using a series of custom made acid cleaned LDPE screws, with the core secured in the lathe, it was free to be rotated, and the collection of ice cores layers could be started.

The collection of veneer layer was standardized, with the core being chiselled along its length by one operator, and the other operator catching the falling chips and slowly rotating the core. Chiselled chips of ice fell directly into a polyethylene scoop. When the scoop was full, these chips were transferred into a melting bottle (LDPE 1L wide-mouth bottle) by having the chips fall directly into the bottle(see **Figure 5.2.2.1**).

For each layer, a new chisel was used in order to minimize the transfer of contamination from one layer to the next one: chisel number 2 was used for the first layer, chisel number 3 for the second layer, chisel 4 number for the third layer and chisel number 5 for the inner core. However, concerning the first layer, the chiselling was made two times in order to remove a high amount of contamination with this layer.

After the first layer was collected, the corresponding scoop was returned to its polyethylene bags, while the melting bottle was kept within the bench. The bag containing the scoop for the second layer was removed from its bag and placed within the bench and the second layer was collected in a similar manner as for the previous layer. After the second layer was collected, the corresponding scoop was returned to its polyethylene bags, while the melting bottle was kept

within the bench. The bag containing the scoop for the third layer was removed from its bag and placed within the bench and the third layer was collected. The bag containing the LDPE tongs for the inner core was then transferred into the bench. After the third layer was collected, the final chisel was used to score, or cut, grooves of the inner core where it would be broken, as shown in **Figure 5.2.2.2**.

While one operator supported the inner core using the LDPE tongs, the inner core was broken at one extremity by striking it firmly with the chisel at the location where it had been scored. After the inner core was broken, the ice core holder was removed and a wide mouth LDPE 1l bottle was placed around the exposed inner core section, as shown in **Figure 5.2.2.2**. The inner core was broken at the next point at which it has been scored and the core section was caught into the wide mouth LDPE 1l bottle. This was repeated for the next inner core section. For the third one, the inner core section of 5cm was collected in a 125ml wide mouth glass bottle. With the final inner core section collected, the decontamination was completed and everything could be returned to the clean room for cleaning. The 5cm inner core section for mercury was stored at -20°C until analysis. The samples (veneer layers and 20cm inner cores) in the wide mouth LDPE bottles were melted inside the laminar flow bench of the clean room and then poured into ultraclean 125ml LDPE bottles. For each of the inner core sections, separate aliquots were made in 60ml, 30ml or 15ml LDPE bottles frozen and kept frozen until analysis by ICP-SFMS (see section 5.3) or TIMS (see section 5.5).

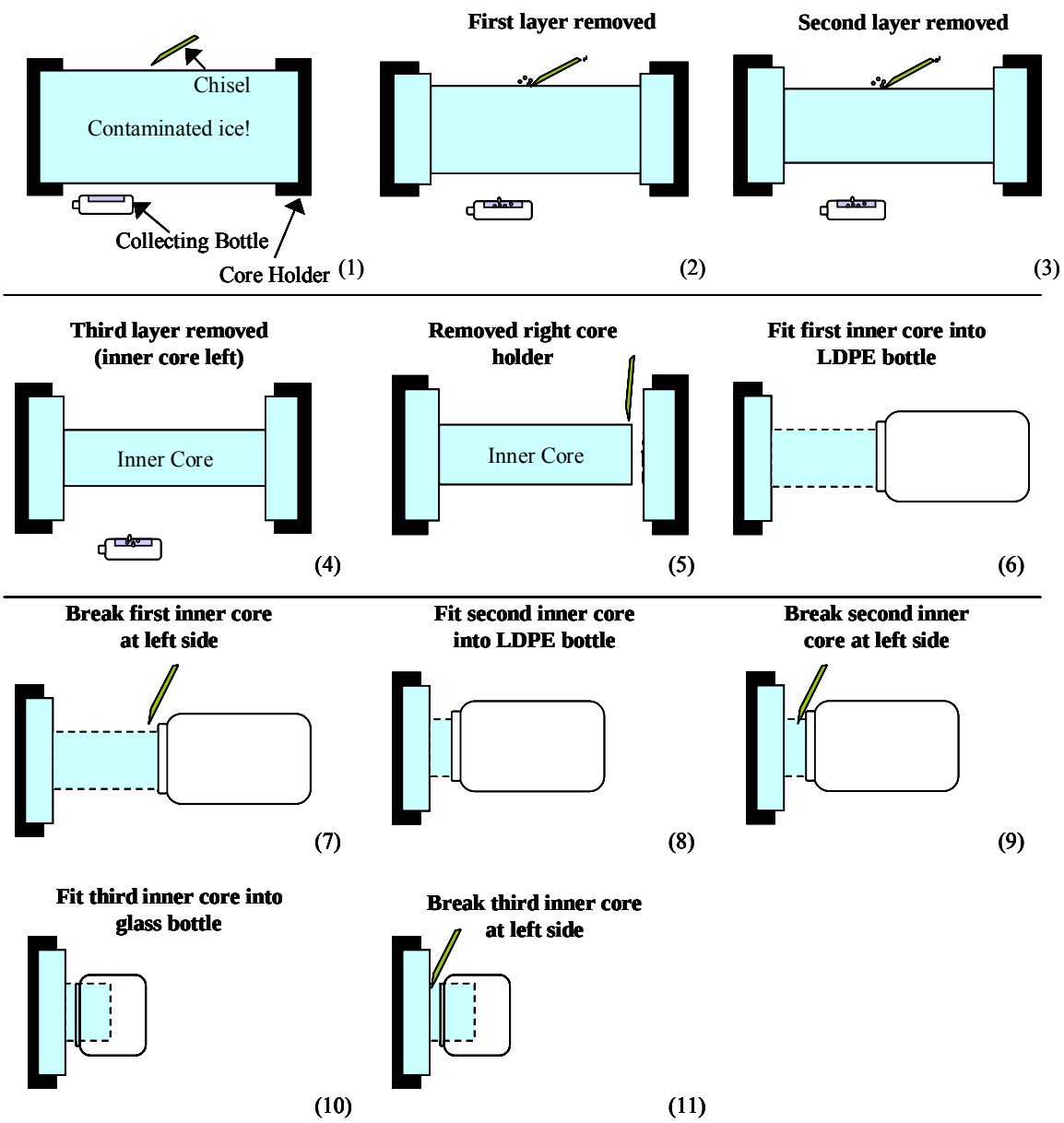

Fig. 5.2.2.2: *The successsive steps of decontamination procedure*

(the removal of the most outside layer outside the clean bench is not shown here)

5.3 The Inductively Coupled Plasma Sector Field Mass Spectrometry (ICP-SFMS)

There are mainly three different kinds of ICP-MS instruments, quadrupole instruments (ICP-QMS), double focusing sector field instruments (ICP-SFMS) and multi-collector instrument (MC-IPC-MS) devices. Of these, ICP-QMS is the oldest being introduced in the early 1980s (Date et al., 1993), followed by ICP-SFMS (in 1988) (Jakubowski et al., 1998; Bradshaw et al., 1989), and more recently MC-IPC-MS (in 1992) (Waldner and Fredman, 1992). The introduction of ICP-SFMS provided the possibility to perform analyses at higher mass resolution, allowing instrumental separation of many species causing spectral interferences in ICP-QMS. ICP-SFMS also provides lower background and higher ion transmission, and consequently better detection limits compared to ICP-QMS (Jakubowski et al., 1998). Another benefit compared to ICP-QMS is a higher precision in isotope ratio determinations due to flat-topped peak in low-resolution mode (Vanhaecke et al., 1996). The multi-collector instruments were developed in order to further enhance the precision of isotope ratio measurements by simultaneous detection of the isotopes, thus primarily reducing the influence of plasma fluctuations on the determination (Jakubowski et al., 1998).

There are different sample introduction systems. The traditional one is a spray-chamber combined with a nebulizer, with different design samples with a high matrix load, samples containing HF and isotope ratio determinations requiring higher stability. There are also more sophisticated introduction systems available based on e.g., ultrasonic nebulisation as well as direct injection and electro-thermal vaporisation (ETV) (Boulyga et al., 2002). Other possibilities involve coupling of chromatographic systems to the nebulizer for on-line separation prior to the analysis (Garcia Alonso et al., 1995; Perna et al., 2003), direct sampling of solid materials using laser-ablation ICP-MS (Becker, 2005) and reduction of isobaric interferences using reaction or collision cells (Koppenaal et al., 2004; Tanner et al., 2004).

The analysis of trace elements, REE and total mercury on which this thesis is based were performed using an ICP-SFMS system (Element 2, Thermo Finnigan, Bremen, Germany) equipped with a micro-flow (<100 µl min^{-1}) PFA nebulisation system (Planchon et al., 2001; Gabrielli et al., 2004; Gabrielli et al., 2006). The instrument is equipped with a class 100 clean bench as a clean sample introduction area (**Figure 5.3.1**).

Fig. 5.3.1: *ICP-SFMS instrument (Element 2, Thermo Finnigan, Bremen, Germany) equipped with a micro-flow (<100 µl min-1) PFA nebulisation system inside a class 100 bench*

For the analysis of REE, a micro-flow nebulisation/desolvatation sample introduction system (Aridus, Cetac technologies, Omaha, NE, USA) was used in order to minimise spectral interferences (Gabrielli et al., 2006). This device is composed of a micro-flow (< 100 µl min^{-1}) PFA nebuliser, a heated PFA spray chamber and a heated microporous PTFE tubular membrane. The sample water vapour passes through the membrane and is removed by an exterior flow of Ar gas (sweep gas). In this way the oxygen based interferences (oxides) caused by the presence of water can be greatly reduced while the sensitivity is increased (Gabrielli et al., 2006).

5.3.1 The ICP-SFMS configuration

In principle, an ICP-SFMS system, such as the Element 2, consists of the following parts: sample inlet system, ICP ion source, interface region, transfer optics and extraction lens, magnetic sector field analyser, electric sector analyser (ESA) and the detection system (Geibmann and Greb, 1994; ThermoFinnigan MAT GmbH, 2001) (**Figure 5.3.1.1**). The sample inlet and argon plasma are maintained under atmospheric pressure, while the pressure is reduced to about 10^{-3} mbar in the interface and transfer optics/extraction lens region and further reduced to about 10^{-7} mbar in the mass analyser and detection regions.

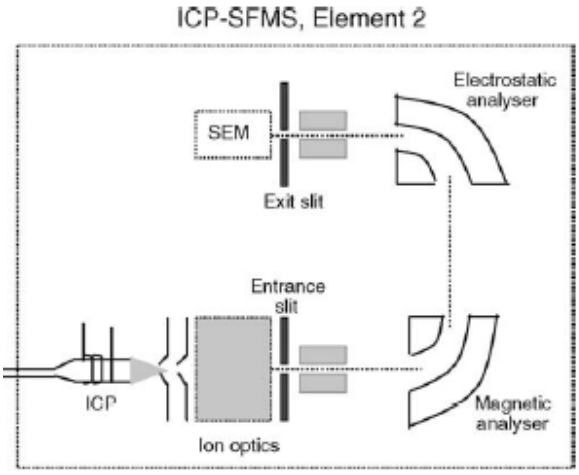

Fig. 5.3.1.1: *Schematic diagram of ICP-SMFS (from Zheng and Yamada, 2006)*

In the inlet system, the sample is transformed into an aerosol of which droplets smaller than 10µm are selected and transferred to the plasma where solvent evaporation, particle vaporisation, atomisation and ionisation occur. The ions are then extracted *via* the sampler and skimmer cones into the entrance slit of the mass analyser, where they are separated according to their mass to charge ion (m/z) in the magnetic field and according to their energy by the ESA. After passing the exit slit, the ions are detected by a conversion dynode coupled to a secondary electron multiplier (SEM). Scanning of the mass to charge range is performed either by altering the acceleration voltage or by changing the magnetic field. Changing the magnetic field allows scanning of the whole m/z range (up to 300) while scanning by changing the acceleration voltage is used for restricted intervals (up to 30% of the start mass set by the magnetic field). Acceleration scanning is substantially faster than magnetic field scanning, and is therefore the preferred mode for isotope ratio determination.

Altering the widths of the entrance and exit slits changes the mass resolution. On the Element 2, three settings are available: low resolution ($m/\Delta m = 400$), medium resolution ($m/\Delta m = 4{,}000$) and high resolution ($m/\Delta m = 10{,}000$). In low resolution, the entrance slit is wider than the exit slit resulting in the flat-topped peaks that are advantageous for measurement stability due to the resultant insensitivity to shifts in mass calibration during the analysis. However, the intensity of the ion-beam decreases with increasing mass-resolution, and so reduces the sensitivity of the

analyses. Hence, low resolution mode is preferred whenever higher mass resolution is not required to separate the analyte peak from any interfering species.

Low resolution mode was used in this work for the determination of Rb, Cd, Ba, Pb, Bi and U, while the medium resolution mode was preferred for V, Cr, Mn, Fe, Co, Cu and Zn and the high resolution mode for As (Barbante et al., 1997b; Planchon et al., 2001; Gabrielli et al., 2005a; 2005b). In order to maximise ion transmission, the low resolution mode (LRM) was used to determine the Rare Earth Elements (Gabrielli et al., 2006) (see **Appendix I**) and total mercury (Planchon et al., 2004).

5.3.2 Spectral interferences

In spite of the relatively high mass resolution achievable with ICP-SFMS, problems with spectral interferences still remain in some cases.

Trace elements

As a rule, in the case of multi-isotopic elements, the strategy for the selection of the isotope was to choose the most abundant and at the same time the least interfered one. The selected isotopes are: low resolution mode: ^{85}Rb, ^{114}Cd, ^{138}Ba, 208Pb, ^{209}Bi and ^{238}U; medium resolution mode: ^{51}V, ^{52}Cr, ^{55}Mn, ^{56}Fe, ^{59}Co, ^{65}Cu and ^{66}Zn; high resolution mode: ^{75}As.

Whenever possible, it is desirable to perform the analyses in low resolution mode because of the higher ion transmission attainable in this way. This is particularly possible for element with high *m/z* values. However, many elements suffer from the overlap from molecular, doubly charged or isobaric ions (V, Cr, Mn, Fe, Co, Cu, Zn and As) (**Table 5.3.2.1**). That is why it was decided to analyse them in the medium resolution mode. Arsenic was analysed in the high resolution mode in order to resolve the interference of ^{40}Ar^{35}Cl on ^{75}As.

The ^{51}V suffers mainly from non-resolved ^{102}Ru^{2+} and ^{102}Pd^{2+} interference. However the possible formation of doubly charged ions is not considered because of the very low concentrations of

these elements in the samples and the really poor formation of doubly charged ions (M^{2+}:M = 0.03). For the same reasons, in the case of ^{52}Cr, ^{56}Fe and ^{59}Co, interferences can be negligible.

The doubly charged $^{110}Cd^{2+}$ partially overlaps with the ^{55}Mn peak also in the medium resolution mode, because the resolution required to separate the peaks completely is 4083 (m/Δm). The Cd concentrations in the same samples are orders of magnitude lower than Mn and hence its influence can be considered negligible.

The ^{65}Cu isotope was selected for the quantification of copper. Careful attention has been paid to the Cu determination since also in medium resolution mode $^{49}Ti^{16}O^{+}$ partially overlaps with the ^{65}Cu peak. Considering that Cu and Ti concentrations in snow and ice samples are of the same order of magnitude and that the typical oxide formation under the instrumental conditions used was about 0.0009-0.0026 (MO^{+}/M^{+}) , then the interference of $^{49}Ti^{16}O^{+}$ can be excluded. Other possible interferences on *m/z* 65 (e.g. $^{33}S^{16}O^{16}O$, $^{36}Ar^{29}Si$, $^{38}Ar^{27}Al$) are so low in abundance that they were not considered.

At *m/z* 66, unresolved interferences may be due to oxide formation ($^{50}Cr^{16}O$ and $^{49}Ti^{17}O$). In both cases the low Cr and Ti concentrations together with the low oxide formation under the adopted plasma conditions do not prevent the quantification of Zn at *m/z* 66.

Analyte		Potential interference		
Isotope	Abundance (%)	Species	Abundance[a] (%)	Required resolution (m/Δm)
^{51}V	99.75	$^{102}Pd^{2+}$	0.80	5763
		$^{102}Ru^{2+}$	31.34	6205
^{52}Cr	83.79	$^{104}Pd^{2+}$	9.30	4516
		$^{104}Ru^{2+}$	18.27	4258
^{55}Mn	100	$^{110}Cd^{2+}$	23.79	4083
		$^{110}Pd^{2+}$	13.50	3780
^{56}Fe	91.72	$^{112}Sn^{2+}$	0.65	3561
		$^{112}Cd^{2+}$	23.79	3403
^{59}Co	100	$^{118}Sn^{2+}$	24.01	3348
^{65}Cu	30.83	$^{49}Ti^{16}O$	5.49	4332
		$^{48}Ti^{17}O$	0.03	3368
		$^{33}S^{16}O^{16}O$	0.75	4127
		$^{36}Ar^{29}Si$	0.02	3997
		$^{38}Ar^{27}Al$	0.06	3940
^{66}Zn	27.90	$^{36}Ar^{30}Si$	0.01	4315
		$^{38}Ar^{28}Si$	0.06	4839
		$^{49}Ti^{17}O$	5.39	4418
		$^{50}Cr^{16}O$	4.33	4111
		$^{32}S^{34}S$	8.00	3905
		$^{40}Ar^{26}Mg$	10.97	3481

[a] *For polyatomic species calculated as the product of the natural abundances of each isotope divided by 100*

Table 5.3.2.1 : *Potential spectral interferences (not resolved in medium resolution mode) that could affect the determination of ultra trace levels of trace elements in the EPICA Dome C ice samples*

Rare Earth Elements (REE)

The selected isotopes are ^{139}La, ^{140}Ce, ^{141}Pr, ^{144}Nd, ^{151}Sm, ^{152}Eu, ^{155}Gd, ^{159}Tb, ^{164}Dy, ^{165}Ho, ^{166}Er, ^{169}Tm, ^{174}Yb and ^{175}Lu. These isotopes chosen for the quantification of REE are the naturally most abundant and/ or less affected by spectroscopic interferences. However, when working in low resolution mode, the separation of the analyte peaks from the interfering species is not feasible. In order to reduce or eliminate spectroscopic interferences, it was necessary to use the desolvatation system described previously (Gabrielli et al., 2006).

However, concerning ^{155}Gd, one or more interfering species affect the accurate determination. The most common interferences for the determination of ^{155}Gd by ICP-SFMS are caused by Ba oxides in the plasma ($^{138}Ba^{16}O^{1}H$). Another possible significant interference for the determination of ^{155}Gd is caused by $^{139}La^{16}O$. Therefore, it was necessary to quantify the possible residual

interference on ^{155}Gd produced by the presence of Ba and La and to apply an appropriate mathematical correction. The correction was calculated with the following equation:

$$I_{Gd} = I_{Gd,s} - (I_{(138)Ba\ s} \times R_{(138)Ba\ (16)O\ (1)H,\ (138)Ba}) - (I_{(139)La\ s} \times R_{(139)La\ (16)O,\ (139)La})$$

where I_{Gd} is the corrected intensity of the element to be determined, $I_{Gd,s}$ the apparent intensity of the interfered element in the sample, $I_{(138)Ba\ s}$ and $I_{(139)La\ s}$ the intensity of the interfering elements in the sample (Ba and La) and $R_{(138)Ba\ (16)O\ (1)H,\ (138)Ba}$ and $R_{(139)La\ (16)O,\ (139)La}$ the ratio between the interfering species ($^{138}Ba^{16}O^{1}H$ and $^{139}La^{16}O$) and the interfering elements (Gabrielli et al., 2006) (see **Appendix I**).

Total mercury

The selected isotope is ^{202}Hg at the low resolution mode was preferred due to its high mass. Polyatomic interferences by compounds such as Ta, Re and W oxides that could affect measurements of Hg can be neglected (Planchon et al., 2004).

5.4 Study of matrix effects using an ICP-SFMS: Trace elements and Rare Earth Elements

Although ancient ice from Antarctica is considered to be high purity water and thus an ideal matrix for the determination of ultra trace elements, the relatively high input of dust to Antarctica that occurred during previous glacial maxima has produced a relatively complex matrix that may possibly interfere with the determination of the analytes (Gabrielli et al., 2004).

Usually, standards are prepared by dilution using ultrapure water, acidified using ultrapure HNO_3 from Curtin University of Technology, Perth, Australia (Burton et al., 2007) to make a 1% solution. Consequently, in order to make sure that the changing amount of dust in the ice could not bias the calibration of the instrument, several different sets of standard solutions were also prepared by dilution using melted Antarctic ice dated from glacial periods (rather high dust content; mix of the third layer of various glacial EPICA/Dome C ice sections) and interglacial periods (low dust content; mix of the third layer of various interglacial EPICA/Dome C ice section).

5.4.1 Trace elements

Firstly some glacial and interglacial EPICA/Dome C ice samples (inner core) were analysed by ICP-SFMS. Trace elements concentrations in these samples are illustrated in **Table 5.4.1.1**.

Element	Average concentration during glacial maxima (pg g^{-1})	Average concentration during interglacials (pg g^{-1})
V	23	2
Cr	13	5
Mn	478	49
Fe[a]	7.4	0.5
Co	10	1.9
Cu	14	4
Zn	100	24
As	11	9
Rb	26	6
Cd	0.8	0.4
Ba	114	17
Pb	10	2
Bi	0.2	0.09
U	0.6	0.12

[a] concentration expressed in ng g^{-1}

Table 5.4.1.1 : *Average concentrations in glacial maxima ice sample (n=34) and interglacial ice samples (n=44) of the EPICA Dome C ice core by ICP-SFMS*

Taking into consideration the trace elements levels in glacial and interglacial EPICA/Dome C ice samples, different sets of multi-element standard solutions were prepared: one set of "synthetic" matrix, one set of "glacial" matrix, one set of "interglacial" matrix. The concentration in the final standard solutions ranged from 0 to 200 pg g^{-1}. The elements of the different matrices standard solution were determined by ICP-SFMS with a nebulisation/desolvatation introduction system (Aridus) and without (**Table 5.4.1.2a**). The slope of the regression line for each trace element, expressed in count per second per pg g^{-1}, was calculated for each matrix, with and without the use of the Aridus during the measurements, as illustrated in **Table 5.4.1.2b**.

(a)

Element	Without Aridus			With Aridus		
	Synthetic matrix	Interglacial matrix	Glacial matrix	Synthetic matrix	Interglacial matrix	Glacial matrix
V	6.3	6.1	6.1	129	152	191
Cr	9.6	9.4	9.4	95	110	138
Mn	14	14	13.5	103	120	169
Fe	11.4	16.2	18.2	84	104	176
Co	12.7	12	12.7	95	114	141
Cu	7.7	7.7	7.65	38	64	51
Zn	2.5	2.5	2.5	30	41	42
As	0.12	0.11	0.11	0.6	0.3	0.5
Rb	321	316	321	1377	1665	2043
Cd	27	26.1	28.3	180	214	273
Ba	275	275	272	1344	1667	2024
Pb	240	254.	246	1305	1864	1965
Bi	417	417	419	2230	2762	3285
U	37	31	39	2211	2845	3456

(b)

Element	Without Aridus		With Aridus	
	((IG-S)/S) × 100	((G-S)/S) × 100	((IG-S)/S) × 100	((G-S)/S) × 100
V	-3.1	-3.9	**17.5**	**47.2**
Cr	-2.5	-1.9	**16.4**	**45.6**
Mn	-1.6	-5.8	**16.6**	**63.8**
Fe	**42.8**	**60.3**	**23.7**	**109.7**
Co	5.8	-0.5	**19.7**	**48.3**
Cu	0.3	-0.7	**66.5**	**32.6**
Zn	2.0	-0.4	**36.7**	**42.7**
As	-5.2	1.7	**-56.4**	**-14.5**
Rb	-1.6	0.3	**20.9**	**48.3**
Cd	-3.5	4.5	**18.9**	**51.7**
Ba	0.1	-1.0	**24.0**	**50.6**
Pb	5.89	2.28	**42.8**	**50.5**
Bi	0.1	0.6	**23.8**	**47.2**
U	**-16.4**	4.5	**28.7**	**56.3**

IG= Interglacial matrix; G = Glacial matrix; S = Synthetic matrix

Table 5.4.1.2: *(a) slope of the regression line for each trace element for various matrices; (b) the effect of matrix on trace elements signals. Negative values represent an under-estimation compared to the real values whilst positive values represent an over-estimation compared to the real values. Bold letters show a high enhancing effect of the matrix on trace element signal.*

Because of a very high enhancing effect of glacial and interglacial matrix on trace elements signals with the use of Aridus (>>5%), it was decided to do the analysis of trace elements on which this thesis is based with a micro-flow (<100 µl min^{-1}) PFA nebulisation system and not with the Aridus system.

The only two elements for which significant effects were observed are Fe (up to 60%) whatever the period and U during interglacial times (up to 16%) (see **Table 5.4.1.2**). It shows that when using standards prepared with laboratory ultra-pure water, U concentrations are under-estimated for interglacial periods while Fe concentration are overestimated whatever the period. A systematic correction was then applied for these two elements.

5.4.2 Rare Earth Elements

Again, the first step was to analyse some glacial and interglacial EPICA/Dome C ice samples (inner core) by ICP-SFMS. The Rare Earth Elements (REE) concentrations in these samples are illustrated in **Table 5.4.2.1**.

Isotope	Average concentration during glacial maxima (pg g^{-1})	Average concentration during interglacials (pg g^{-1})
^{139}La	0.39	22
^{140}Ce	0.9	60
^{141}Pr	0.11	7.1
^{144}Nd	0.5	25
^{151}Sm	0.1	5.7
^{152}Eu	0.01	1.3
^{155}Gd	0.11	5
^{159}Tb	0.01	0.7
^{164}Dy	0.06	3.9
^{165}Ho	0.011	0.74
^{166}Er	0.03	2.0
^{169}Tm	0.004	0.3
^{172}Yb	0.03	1.7
^{175}Lu	0.01	0.23

Table 5.4.2.1 : *Average concentrations in glacial maxima ice sample and interglacial ice samples of the EPICA Dome C ice core by ICP-SFMS (from Gabrielli et al., 2006)*

Taking into consideration the REE levels in glacial and interglacial EPICA/Dome C ice samples, different sets of multi-element standard solutions were prepared: one set of "synthetic" matrix, one set of "glacial" matrix, one set of "interglacial" matrix. The concentration in the final standard solutions ranged from 0 to 20 pg g^{-1}. The elements of the different matrices standard solution were determined by ICP-SFMS with a nebulisation/desolvatation introduction system (Aridus) and without (**Table 5.4.2.2a**). The slope of the regression line for each trace element, expressed in count per seconds per pg g^{-1}, was calculated for each matrix, with and without the use of the Aridus during the measurements, as illustrated in **Table 5.4.2.2b**

(a)

Element	Without Aridus			With Aridus		
	Synthetic matrix	Interglacial matrix	Glacial matrix	Synthetic matrix	Interglacial matrix	Glacial matrix
La	36	37	35	1398	2048	2809
Ce	35	37	30	1282	2005	3154
Pr	70	70.6	63	1515	2270	2757
Nd	32	34	32	404	589	812
Sm	59	61	63	385	559	685
Eu	147	146	154	685	1009	1202
Gd	291	314	356	221	293	351
Tb	192	194	195	1650	2307	2595
Dy	78	83	79	479	2452	746
Ho	197	201	191	1553	799	2452
Er	80	81	82	509	719	799
Tm	242	236	233	1528	2147	2427
Yb	92	95	90	328	455	531
Lu	199	206	202	1392	1941	2214

(b)

Element	Without Aridus		With Aridus	
	((IG-S)/S) × 100	((G-S)/S) × 100	((IG-S)/S) × 100	((G-S)/S) × 100
La	4.3	-1.1	**46.5**	**101.0**
Ce	4.8	-16.1	**56.3**	**146.0**
Pr	0.8	-9.6	**49.8**	**82.0**
Nd	5.7	-1.0	**45.7**	**101.0**
Sm	3.7	5.9	**45.2**	**77.9**
Eu	-0.3	5.2	**47.3**	**75.5**
Gd	**7.9**	**22.6**	**32.8**	**58.9**
Tb	1.1	1.4	**39.8**	**57.2**
Dy	6.3	0.9	**411.9**	**55.7**
Ho	2.1	-3.1	**-48.5**	**57.8**
Er	2.0	2.8	**41.3**	**57.0**
Tm	-2.8	-4.0	**40.5**	**58.8**
Yb	3.0	-2.3	**38.6**	**61.7**
Lu	3.5	1.4	**39.4**	**59.0**

IG= Interglacial matrix; G = Glacial matrix; S = Synthetic matrix

Table 5.4.2.2: *(a) slope of the regression line for each trace element for various matrices; (b) the effect of matrix on trace elements signals. Negative values represent an under-estimation compared to the real values whilst positive values represent an over-estimation compared to the real values. Bold letters show a high enhancing effect of the matrix on trace element signal.*

A high enhancing effect of glacial and interglacial matrix on trace elements signals with the use of Aridus (>>5%) was observed for all REE (**Table 5.4.1.2**). When using a micro-flow (<100 µl min^{-1}) PFA nebulisation system, only one element, Gd, shows significant effects of matrices on its signal (up to 23% for glacial matrix) (**Table 5.4.1.2**). It shows that when using standards prepared with laboratory ultra-pure water, Gd concentrations are overestimated whatever the period.

However, for the analysis of REE, we need to work with a micro-flow nebulisation/desolvatation sample introduction system (Aridus, Cetac technologies, Omaha, NE, USA) in order to minimise spectral interferences. Thus external calibration curves were prepared with glacial matrix for analyses of the glacial EPICA/Dome C ice samples and interglacial matrix for analyses of the interglacial EPICA/Dome C ice samples.

5.5 Thermal Ionisation Mass Spectrometry (TIMS)

The measurement of isotopic abundances began early the last century following the discovery of neon isotopes by J.J.Thompson in 1912. F.W. Aston developed the mass spectrometer into a quantitative instrument for measuring isotopic abundances and by 1935 the isotopic composition of most elements was known. The first International Table of Stable Isotopes was drawn up in 1936, while the latest table of Isotopic Compositions of the Elements appeared recently (Rosman and Taylor, 1998). Lead is an element for which there was early evidence of natural variations in its isotopic composition; these were ultimately used to determine the age of the Earth (Patterson, 1956).

Early applications of mass spectrometry were in the fields of nuclear physics and geochronology. Identification by Nier et al. (1940) of ^{235}U as the fissionable component of natural U led to the construction of isotope separators which were ultimately used to produce enriched isotopes of most elements following World War II. The ready availability of enriched isotopes was particularly important for the development of isotope geology where they are needed for geochronology and isotope geochemistry (Faure, 1986). These enriched materials were used by Patterson during the 1950s to accurately measure Pb and U in terrestrial rocks and meteorites and

resulted in the first accurate age for the Earth. Isotopic techniques developed during the period eventually led to the first reliable measurements of Pb in Greenland ice by Murozumi et al. (1969) and the first determination of Pb isotopes in Greenland snow and ice (Rosman et al., 1993) and Antarctic snow and ice (Rosman et al., 1994).

The analysis of lead isotopes on which this thesis is based was performed using a Thermo-Finnigan Triton thermal ionisation mass spectrometer (**Figure 5.5.1**) equipped with 9 Faraday collectors and an electron multiplier. It is a 90° magnetic sector thermal ionisation mass spectrometer.

Fig. 5.5.1: *ThermoFinnigan Triton TIMS, CUT, Perth, Australia*

5.5.1 Preparation of the samples for Pb isotopes determination

On account of low levels of Pb present in the samples, minimal sample preparation was undertaken. Essentially, sample preparation procedure involved the transfer of Antarctic samples into Teflon PFA (Savillex. Corp.) beakers, weighing, addition of reagents and ionisation enhancers, evaporation and transfer onto a mass spectrometer filament. With the exception of the evaporation stage, all of these procedures were undertaken into a class100 bench (Burton et al., 2007).

Procedure of sample preparation

1- Preconditioning of Teflon beakers

- ultra-pure water + 50 µl HF ultra-pure conc. + 50 µl HNO_3 ultra-pure conc. + 50 µl H_3PO_4 diluted

Beakers were placed within a Teflon chamber, located under an infrared lamp during 2 hours

After 2 hours, beakers were emptied and can be considered as clean

2- The « drop »

- ~ 8ml interglacial sample (or ~2ml glacial sample) + 1 µl spike $^{205}Pb/^{137}Ba$ + 20 µl HF ultra-pure conc. + 10 µl HNO_3 ultra-pure conc. + 6 µl H_3PO_4 diluted

Beakers were placed within a Teflon chamber at sub-boiling temperature located under an infrared lamp during approximately 15 hours

Evaporation of the sample. Obtaining of a drop in each beaker

3- Filament preparation

a) Using an Eppendorf micropipetter, 3 µl of silicagel (dilute or concentrate in function of the nature of the sample) was dispensed into the drop

b) With the same micropipetter, sample (drop) was transferred to degassed, zone-refined Re filaments

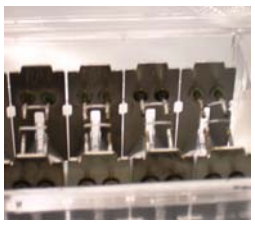

c) The filament is supported in a perspex mount, which includes two electrical contacts which enable a current to be supplied to the central filament, onto which the sample is transferred. A low current is passed through the filament to dry the deposit, then the filament temperature is slowly increased to red heat to evaporate H_3PO_4, leaving a faint white deposit.

The samples are then packed in an airtight box and arranged in the mass spectrometer carousel, ready for loading.

Solid samples are loaded onto filaments, which are then placed into bead holders and assembled on a carousel. The carousel is then loaded into the TIMS source chamber which is pumped down to a pressure suitable for analyses to commence, normally < 5×10^{-8}Torr (<5×10^{-6}Pa).

5.5.2 The TIMS configuration

Through the holders, a current can be passed through the side or central filaments of the Re bead, to degas the samples prior to measurement or to heat the samples until they undergo thermal ionisation. Degassing of the samples removes hydrocarbons and other forms of molecular interference from the bead block and sample surface. During measurement, only the central filament was heated until atoms in the sample begin to evaporate and to be ionised. Moreover, the addition of suspensions of silica gel to Pb samples (Cameron et al., 1969; Gerstenberger and Haase, 1997) increased the ionisation efficiency of Pb heated on a Re filament by several orders of magnitude.

The Triton includes the mass spectrometer instrument, with a sample source chamber, magnetic analyser and collector arrays, and associated vacuum and electronic systems controlled by a computer (**Figure 5.5.2.1**). The process of thermal ionisation results in isotopic fractionation of the ionised sample, which must be corrected if accurate measurements of isotopic compositions are to be accomplished (De Laeter, 2001).

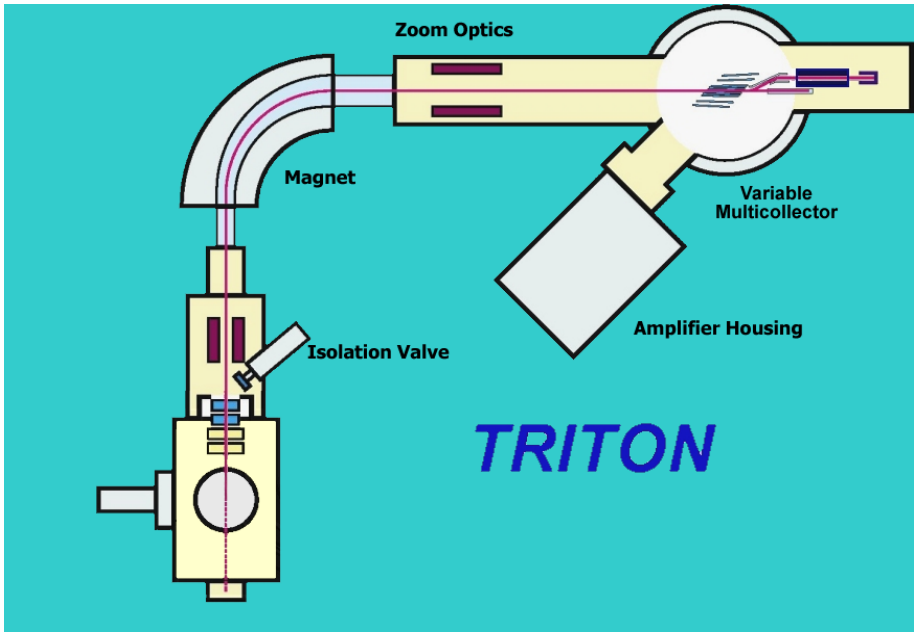

Fig. 5.5.2.1 : *Schematic diagram of the Triton TIMS (ThermoFinnigan)*

Following ionisation, the ions are accelerated through an electric potential and passed through a collimator stack, by which the ion beam could be focussed and directed down the flight path. The various plates and lenses in the collimator stack are used to focus the beam in the vertical (z) and lateral (y) planes. The mass spectrometer separates ions by passing through a magnetic sector field, within which they undergo deflation along circular paths. A particular magnetic field setting is chosen such that the radius of curvature of the Pb ions is equal to the curvature of the flight path, so the Pb ions continue down the centre of the flight path and are collected by the ion detector. Heavier and lighter ions are retarded by collision with the walls of the flight tube. The nine Faraday cups are an all-carbon assembly and combined with the amplifiers, are capable of measuring signal intensities. By means of a relay matrix, each current amplifier can be connected to each Faraday cup. As interblock actions the current amplifier are systematically switched to different cups. Finally, after a complete run all amplifiers have been connected to all Faraday cups and all signals have been measured with same average gain: individual gain uncertainties are cancelled. Thus, this system is able to measure two Ba isotopes (200, 201), five Pb isotopes (204-208), the Bi isotope (209) and three backgrounds (corresponding to masses 203, 203.5 and 204.5) for each sample.

5.5.3 Isotope dilution mass spectrometry

Murozumi et al. (1969) determined the concentration of Pb in Greenland and Antarctic snow and ice by Isotope Dilution Mass Spectrometry (IDMS) (Webster, 1960). They added pure ^{208}Pb tracer to their samples before chemically processing them. Both the mass of tracer and the water sample were measured. After thoroughly mixing the tracer with the sample, Pb was isolated in a chemically pure form and the isotopic ratios were measured in a mass spectrometer. Simple comparison of the ^{208}Pb abundance with the abundance of other isotopes in the mass spectrum allowed the amount of Pb in the sample to be determined. The sensitivity of the technique depends upon the ability of the mass spectrometer ion source to produce a measurable beam of ions from the sample. Then the greatest sensitivity will be achieved when the tracer isotope has the lowest natural abundance.

Chisholm et al. (1995) and Vallelonga et al. (2002) describe most of the current procedures used to measure Pb isotopes in polar ice at pg/g concentrations. Because of the limited quantities of

sample generally available for the analysis and the low Pb concentration involved, the use of a ^{205}Pb tracer, which has a half-life of 1.5×10^7 years, has distinct advantages. The preparation of this isotope has been described by Parrish and Krogh (1987). Because the ^{205}Pb isotope does not occur naturally, a single measurement with the tracer yields both the isotopic compositions and the amount of Pb present. **Table 5.6.3.1** illustrates how the isotopic composition and amount of Pb present are computed from a mixed spectrum of sample and tracer (from Rosman, 2001).

Isotope	(i)	204	205	206	207	208
Measured spectrum	(i/205)	0.1430	1.0000	2.4668	2.2025	5.2108
^{205}Pb spike	(i/205)	0.0005	1.0000	0.0607	0.0079	0.0186
Sample composition	(meas-spike)	0.1425		2.4061	2.1945	5.1922
		$\frac{^{206}Pb}{^{207}Pb}$	$\frac{^{208}Pb}{^{207}Pb}$	$\frac{^{206}Pb}{^{204}Pb}$		
Sample	(i/j)	1.0964	2.3660	16.8869		

$$\text{Sample Pb(pg)} = \frac{\text{Atoms(sample)}}{\text{Atoms(spike)}} * \frac{\text{Atomicweight(sample)}}{\text{Atomicweight(spike)}} * \text{Added spike(pg)}$$

$$= 9.133 * \frac{207.21}{205.10} * 9.89 = 91.3\text{pg}$$

i = isotope

i/j = ratio from meas-spike

Table 5.6.3.1: *Measurement of the amount and isotopic composition of Pb in sample using a ^{205}Pb spike (Chisholm et al., 1995) (from Rosman, 2001)*

Although the IDMS technique is capable of accuracies of better than 0.1% these are not generally achieved in measurements of polar ice. Limitations occur with the calibration of the tracer solution where only a small quantity of tracer can be used for this purpose. In view of problems associated with the measurement of pg amounts of Pb in polar snow and ice, ~ 10-15% is an acceptable accuracy, even using IDMS (Rosman, 2001).

Moreover, accuracy in the isotopic compositions is established through regular measurements of NIST (National Institute of Standards and Technology) Standard Reference Materials which are certified for accuracy. Each batch of samples measured must therefore include the isotopic standard. For example, Chisholm et al. (1995) report a bias of the mass spectrometer they used

(VG354 Isotope Ratio Mass Spectrometer, Fisons Instruments, fitted with a thermal ion source). This bias was obtained by comparing the measured $^{206}Pb/^{207}Pb$ ratio with the certified value (NIST SRM 981) of 0.24 ± 0.06% per amu with an enhancement in the lighter isotopes. After correcting the other ratios by the amount, there is an agreement for the $^{206}Pb/^{204}Pb$ ratio, but the $^{208}Pb/^{207}Pb$ ratio measured is ~ 0.1% lower. Taking account of an 0.04% uncertainty in the certified ratio and a measurement precision, which is typically larger than 0.1%, the difference is generally not significant.

REFERENCES

Barbante C, Turetta A, Capodaglio G, Scarponi G (1997a) Recent decrease in the lead concentration of Antarctic snow. *International Journal of Environmental Analytical Chemistry* **68**, 457-477

Barbante C, Bellomi T, Mezzadri G, Cescon P, Scarponi G, Morel C, Jay S, Van de Velde K, Ferrari C, Boutron CF (1997b) Direct determination of heavy metals at picogram per gram levels in Greenland and Antarctic snow by double focusing inductively coupled plasma mass spectrometry. *Journal of Analytical Atomic Spectrometry* **12**, 925-931

Barbante C, Turetta A, Capodaglio G, Cescon P, Hong S, Candelone JP, Van de Velde K, Boutron CF (2001) Trace elements determination in polar snow and ice. An overview of the analytical procedure process and application in environmental and paleoclimatic studies. In: Caroli S, Cescon P, Walton DWH (eds) *Environmental Contamination in Antarctica*. Elsevier Science B.V.

Becker JS (2005) Inductively coupled plasma mass spectrometry (ICP-MS) and laser ablation ICP-MS for isotope analysis of long-lived radionuclides. *International Journal of Mass Spectrometry* **242**, 183-195

Boulyga SF, Matusevich JL, Mironov VP, Kudrjashov VP, Halicz L, Segal I, McLean JA, Montaser A, Becker JS (2002) Determination of $^{236}U/^{238}U$ isotope ratio in contaminated environmental samples using different ICP-MS instruments. *Journal of Analytical Atomic Spectrometry* **17**, 958-964

Boutron CF (1990) A clean laboratory for ultralow concentration heavy metals analysis. *Fresenius Journal of Analytical Chemistry* **337,** 482-491

Bradshaw N, Hall EFH, Sanderson NE (1989) Inductively coupled plasma as a ion-source for high-resolution mass spectrometry. *Journal of Analytical Atomic Spectrometry* **4**, 801-803

Burton GR, Rosman KJR, Candelone JP, Burn L**,** Boutron CF, Hong S (2007) The impact of climatic conditions on Pb and Sr isotopic ratios found in Greenland ice, 7-150 ky BP. *Earth and Planetary Science Letters* **259**, 557-566

Cameron AE, Smith DH, Walker RL (1969) Mass spectrometry of nanogram-size samples of lead. *Analytical Chemistry* **41(3)**, 525-526

Candelone JP, Hong S, Boutron CF (1994) An improved method for decontaminating

polar snow or ice cores for heavy metals analysis. *Analytica Chimica Acta* **299**, 9-16

Chisholm W, Rosman KJR, Boutron CF, Candelone JP, Hong S (1995) Determination of lead isotopic ratios in Greenland and Antarctic snow and ice at picogram per gram concentrations. *Analytica Chimica Acta* **311**, 141-151

Dansgaard W, Johnson SJ, Clausen HB, Dahl- Jensen D, Gundestrup NS, Hammer CU, Hvidbjerg CS, Steffensen JP, Sveinbjörnsdottir AE, Jouzel J, Bond G (1993) Evidence for general instability of past climate from a 250-kyr ice-core record. *Nature* **364**, 218-220

Date A.R., Gray A.L. (1993) *Application*s *of Inductively Coupled Plasma Mass Spectrometry*. Blackie Academic & Professional, Glasgow, UK

De Laeter JR (2001) *Applications of Inorganic mass spectrometry*. Wiley, Interscience, New York

EPICA Community members (2004) Eight glacial cycles from an Antarctic ice core. *Nature* **429**, 623-628

Faure G (1986) *Principles of Isotope Geology*. Wiley, Interscience, New York

Federal Standard 209 (1988) U.S.

Ferrari CP, Moreau AL, Boutron CF (2000) Clean conditions for the determination of ultra-low levels of mercury in ice and snow samples. *Fresenius Journal of Analytical Chemistry* ***366***, 433

Gabrielli P, Varga A, Barbante C, Boutron C, Cozzi G, Gaspari V, Planchon F, Cairns W, Hong H, Ferrari C, Capodaglio G (2004) Determination of Ir and Pt down to the sub-femtogram per gram level in polar ice by ICP-SFMS using preconcentration and a desolvatation system. *Journal of Analytical Atomic Spectrometry* **19**, 831-837

Gabrielli P, Barbante C, Boutron C, Cozzi G, Gaspari V, Planchon F, Ferrari C, Turetta C, Hong S, Cescon P (2005a) Variations in atmospheric trace elements in Dome C (East Antarctica) ice over the last two climatic cycles. *Atmospheric Environment* **39**, 6420-6429

Gabrielli P, Planchon FAM, Hong S, Lee KH, Hur SD, Barbante C, Ferrari CP, Petit JR, Lipenkov VY, Cescon P, Boutron CF (2005b) Trace elements in Vostok Antarctic ice during the last four climatic cycles. *Earth and Planetary Science Letters* **234**, 249-259

Gabrielli P, Barbante C, Turetta C, Marteel A, Boutron C, Cozzi G, Cairns W, Ferrari C, Cescon P (2006) Direct determination of Rare Earth Elements at the sub-picogram per gram level in Antarctic ice

by ICP-SFMS using a desolvatation system. *Analytical Chemistry* **78**, 1883-1889

Garcia Alonso JI, Sena F, Arboré Ph, Betti M, Koch L (1995) Determination of fission products and actinides in spent nuclear fuels by Inductively Coupled Plasma Mass Spectrometry. *Journal of Analytical Atomic Spectrometry* **10**, 381-393

Geibmann U, Greb U (1994) High resolution ICP-MS – a new concept for elemental mass spectrometry. *Fresenius Journal of Analytical Chemistry* **350,** 186-193

Gerstenberger H, Haase G (1997) A highly effective emitter substance for mass spectrometric Pb isotope ratio determinations. *Chemical Geology* **136**, 309-312

Jakubowski N, Moens L, Vanhaecke F (1998) Sector field mass spectrometers in ICP-MS. *Spectrochimica Acta* **53B**, 1739-1763

Koppenaal DW, Eiden GC, Barinaga CJ (2004) Collision and reaction cells in atomic mass spectrometry: development, status, and applications. *Journal of Analytical Atomic Spectrometry* **19**, 561-570

Moody JR (1982) NBS clean laboratories for trace elements analysis. *Analytical Chemistry* **54**, 1358A- 1376A

Murozumi M, Chow TJ, Patterson CC (1969) Chemical concentrations of pollutant lead aerosols, terrestrial dust and sea salts in Greenland and Antarctic snow strata. *Geochimica et Cosmochimica Acta* **33**, 1247-1294

Murphy TJ (1976) The role of the analytical blank in accurate trace analysis. In: La Fleur P (ed) *Accuracy in Trace analysis*. Nat. Bur. Stand., Washington DC, Spec. Pub. **422**, pp 509-539

Nier AO (1940) A mass spectrometer for routine isotope abundance measurements. *Review of Scientific Instruments* **11**, 212-216

Parrenin F, Barnola JM, Beer JT, Blunier T, Castellano E, Chappellaz J, Dreyfus G, Fisher H, Fujita S, Jouzel J, Kawamura K, Lemieux-Dudon B, Loulergue L, Masson-Delmotte V, Narcisi B, Petit JR, Raisbeck G, Raynaud D, Ruth U, Schwander J, Severi M, Spahni R, Steffensen JP, Svensson A, Udisti R, Waelbroeck C, Wolff E (2007) The EDC3 chronology for the EPICA Dome C ice core. *Climate of the Past* **3**, 575-606

Parrish RR, Krogh TE (1987)Synthesis and purification of ^{205}Pb for U-Pb geochronology. *Chemical Geology* **66**, 103-110

Patterson CC (1956) Age of meteorites and the earth. *Geochimica et Cosmochimica Acta* **10**, 230-237

Patterson CC, Settle DM (1976) The reduction of orders of magnitude errors in lead analysis of biological materials and natural waters by evaluating and controlling the extent and sources of industrial lead contamination introduced during sample collection and analysis. . In: La Fleur P (ed) *Accuracy in Trace analysis*. Nat. Bur. Stand., Washington DC, Spec. Pub. **422**, pp 321-351

Perna L, Jernström J, Aldave de las Heras L, de Pablo J, Betti M (2003) Sample cleanup by on-line chromatography for the determination of Am in sediments and soils by α-spectrometry. *Analytical Chemistry* **75**, 2292-2298

Planchon F, Boutron CF, Barbante C, Wolff EW, Cozzi G, Gaspari V, Ferrari C, Cescon P (2001) Ultra-sensitive determination of heavy metals at the sub-picogram per gram level in ultraclean Antarctic snow samples by inductively coupled plasma sector field mass spectrometry. *Analytica Chimica Acta* **450**, 193-205

Planchon FAM, Gabrielli P, Gauchard PA, Dommergue A, Barbante C, Cairns WRL, Cozzi G, Nagorski SA, Ferrari CP, Boutron CF, Capodaglio G, Cescon P, Varga A, Wolff EW (2004) Direct determination of mercury at the sub-picogram per gram level in polar snow and ice by ICP-SFMS. *Journal of Analytical Atomic Spectrometry* **19**, 823-830

Rosman KJR (2001) Natural isotopic variations in lead in polar snow and ice as indicators of source regions. In: Caroli S, Cescon P, Walton DWH (eds) *Environmental Contamination in Antarctica: a Challenge to Analytical Chemistry*. Elsevier Science B.V, New York, pp 87-106

Rosman KJR, Chisholm W, Boutron CF, Candelone JP, Görlach U (1993) Isotopic evidence for the source of lead in Greenland snows since the late 1960s. *Nature* **362**, 333-334

Rosman KJR, Chisholm W, Boutron CF, Candelone JP, Patterson CC (1994) Anthropogenic lead isotopes in Antarctica. *Geophysical Research Letters* **21**, 2669–2672

Rosman KJR, Taylor PDP (1998) Isotope compositions of the elements. *Pure & Applied Chemistry* **70**, 217-235

Tanner SD, Li C, Vais V, Baranov VI, Bandura DR (2004) Chemical resolution of Pu^+ from U^+ and Am^+ using a band-pass reaction cell inductively coupled plasma

mass spectrompeter. *Analytical Chemistry* **76**, 3042-3048

ThermoFinnigan MAT GmbH (2001) *Element 2 operator manual*. Germany

Vallelonga P, Van de Velde K, Candelone JP, Ly C, Rosman KJR, Boutron CF, Morgan VI, Mackey DJ(2002), Recent advances in measurement of Pb isotopes in polar ice and snow at sub-picogram per gram concentrations using thermal ionisation mass spectrometry, *Analytica Chimica Acta* **453**, 1 – 12

Vanhaecke F, Moens L, Taylor PDP (1996) Precise measurement of isotope ratio with a double-focusing magnetic sector ICP mass spectrometer. *Analytical Chemistry* **68**, 567-569

Waldner AJ, Fredman PA (1992) Isotope ratio measurement using a double focusing magnetic sector mass analyser with an inductively coupled plasma as an ion source. *Journal of Analytical Atomic Spectrometry* **7**, 571-575

Watanabe O, Jouzel J, Johnsen S, Parrenin F, Shoji H, Yoshida N (2003) Homogeneous climate variability across East Antarctica over the past three glacial cycles. *Nature* **422**, 509-512

Webster RK (1960) Mass spectrometric isotope dilution analysis. In: Smales AA, Wager LR (ed) *Methods in Geochemistry*. pp. 202-246

Zheng J, Yamada M (2006) Inductively coupled plasma-sector field mass spectrometry with a high efficiency sample introduction system for the determination of Pu isotopes in settling particles at femtogram levels. *Talanta* **69**, 1246-1253

Chapter 6- RESULTS AND DISCUSSION ABOUT CRUSTRAL TRACE ELEMENTS VARIABILITY IN EAST ANTARCTICA OVER THE LATE QUATERNARY

In this chapter I present the records of 8 crustal trace elements (V, Cr, Mn, Fe, Co, Rb, Ba and U) determined by inductively coupled plasma sector field mass spectrometry (IPC-SFMS) in various sections of the 3270 m deep ice core recently drilled at Dome C on the high East Antarctic plateau as part of the EPICA program. The sections were dated from 263 ky BP (depth of 2368 m) to 671 ky BP (depth of 3062 m). When combined with the data previously obtained by Gabrielli and co-workers (2005a) for the upper 2193 m of the core, it gives a detailed record for these elements during a 671 ky period from the Holocene back to Marine Isotopic Stage (MIS) 16.2.

The development of highly sophisticated ultra-clean and ultra-sensitive procedures to determine various trace elements down to extremely low concentrations levels in these cores (Ng and Patterson, 1981; Boutron and Patterson, 1986; Candelone et al., 1994; Gabrielli et al., 2006) have allowed the analyses of various sections of the 3623m Vostok ice core, which covers the last four climatic cycles (past ~ 420 ky, back to the end of Marine Isotopic Stage (MIS) 11 (Bassinot et al., 1994)). Concentrations of most trace elements are found to be highly variable, with generally low values during interglacial periods and warm interstadials and much higher values during the coldest stages of the last four ice ages (Hong et al., 2003; Hong et al., 2004; Hong et al., 2005; Gabrielli et al., 2005b).

Although the Vostok trace element records are the longest ones presently available, they cover only a rather limited time period. In particular, they do not provide a comprehensive view of the entire MIS 11, which emerges as a key interglacial period from about 390 to 420 ky BP, possibly the best analogue to the present Holocene interglacial (Berger and Loutre, 2003; Droxler et al., 2003). MIS 11 is an unusual and perhaps unique interglacial interval. It exhibited warm interglacial climatic conditions for an interval of at least 30 ky, a duration twice as long as the most recent interglacial stages, with orbital parameters (low eccentricity and consequently weak precessional forcing) similar to those of the present. Moreover, the Vostok trace element record does not provide data for the period between the Mid-Pleistocene Revolution (MPR) (often dated

at about 900 ky BP) (Raymo et al., 1997) and the Mid-Brunhes event (MBE) (which roughly corresponds to the transition between MIS 12 and MIS 11 about 430 ky BP) (Berger and Wefer, 2003). The period between MPR and MBE was characterized by less pronounced warmth in interglacial periods in Antarctica, but a higher proportion of each cycle was spent in the warm mode (EPICA Community members, 2004).

6.1 Concentrations in Antarctic ice back to 670 ky BP

Concentrations measured in the 78 samples are listed in Appendix II, Table I. Changes in concentrations as a function of the depth of the ice are shown in **Figure 6.1.1** together with changes in the deuterium content of the ice (expressed in δD per mil). Pronounced variations in concentrations are observed for all elements from MIS 8.2 to MIS 16.2, with high concentrations values during the coldest climatic stages and low concentrations values during interglacial periods.

For Cr, Mn, Co, Rb and Ba, our data can be combined with the data previously obtained by Gabrielli et al.(2005a) for the upper 2193 m of the EPICA Dome C ice core (ice dated from 0.5 to 217 ky BP), giving comprehensive time series for these five elements over a ~ 671 ky period from the Holocene to MIS 16.2, **Figure 6.1.2** and **Table 6.1.1**. Along this 671 ky period, concentrations of these three elements are found to strongly vary as a function of δD, with high concentrations values during the coldest periods and significantly lower concentrations during warmer periods. However, the earlier period was characterized by less pronounced variations, see **Figure 6.1.2**.

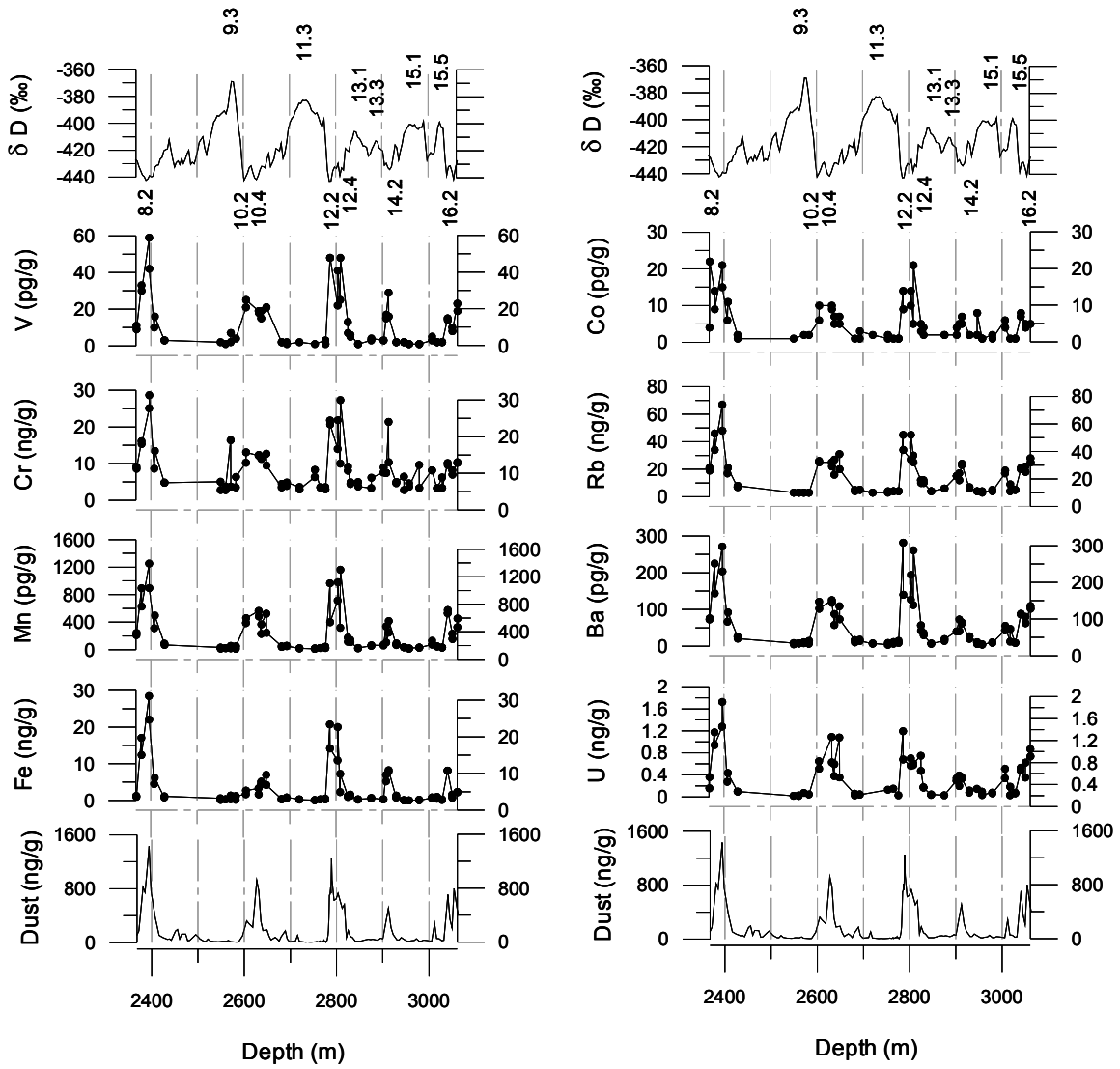

Fig. 6.1.1: *EPICA/Dome C Antarctic ice core: changes in concentrations of V, Cr, Mn, Fe,Co, Rb, Ba and U as a function of depth from 2368.6 m to 3061.9 m (263 to 671 ky BP). Also shown at the top of the figure are the variations in deuterium concentrations (expressed in delta per mil) (EPICA Community members, 2004), Marine Isotopic Stages (MIS) numbers (Bassinot et al., 1994) and at the bottom of the figure changes in dust concentrations (EPICA Community members, 2004).*

			Measured concentration (pg/g)							
Location	Age	Period	V	Cr	Mn	Fe [a]	Co	Rb	Ba	U
Dome C	0.5-220 ky BP	Interglacial	0.6 [c]	7 [b]	5 [b]	0.07 [c]	1.0 [b]	1.2 [b]	2.1 [b]	0.01 [d]
		Glacial	275 [c]	29 [b]	760 [b]	64 [c]	15 [b]	124 [b]	657 [b]	6.6 [d]
Dome C [e]	260-430 kyrBP	Interglacial	0.6	3	12	0.1	0.4	3	4	0.02
		Glacial	59	29	1250	28	21	67	271	1.7
Dome C [e]	430-650 ky BP	Interglacial	1.0	3	14	0.1	0.6	3	4	0.03
		Glacial	48	48	1160	21	21	45	282	1.2
Vostok [f]	4.6-420 ky BP	Interglacial	1.5	2	14	–	0.5	1.5	4.5	0.05
		Glacial	120	53	1300	–	26	115	475	4
Taylor Dome [g]	1,3-13 ky BP	Interglacial	–	–	–	–	–	1.05	8.1	–
	27.2 ky BP	Glacial	–	–	–	–	–	36.3	163	–

[a] concentrations expressed in ng/g
[b] Gabrielli et al, 2005 a
[c] Wolff et al, 2006
[d] V.Gaspari, personal communication
[e] This work
[f] Gabrielli et al, 2005b
[g] Hinkley and Mastsumoto, 2001

Table 6.1.1 : *East Antarctica: concentrations of various crustal trace elements in ice dated from interglacial and glacial maxima periods collected at Dome C, Vostok and Taylor Dome*

It is the first time natural variations have been observed over such a long time period with such high sampling frequency (about 160 depth intervals in total). The only other data covering long periods of time were obtained from the analyses of the Vostok ice core. However, they covered only 420 ky, and only part of MIS 11. Other studies are few and deal with much shorter time periods, **Table 6.1.1**.

Fallout fluxes were calculated for each element by combining concentrations measured in the ice (data from this work for the period from 263 to 671 ky BP; data from Gabrielli et al., 2005a for the period from 0.5 to 217 ky BP) at each depth with the estimated yearly ice accumulation rate at that depth (expressed in g H_2O cm $^{-2}$ y $^{-1}$). The ice accumulation rate at Dome C has varied by a factor ~ 2 between very cold climatic stages (~ 1.3 g H_2O cm $^{-2}$ y $^{-1}$) and interglacial periods (~ 2.7 g H_2O cm $^{-2}$ y $^{-1}$) (EPICA Community members, 2004). Changes in fallout fluxes are found to match very well changes in concentrations. The ratio between the highest and the lowest fluxes is however about half of the corresponding ratio of the concentrations since the accumulation rate is lower during the coldest stages when concentrations are maximum. However, the study of fluxes permit to precise my observation made with the concentrations.

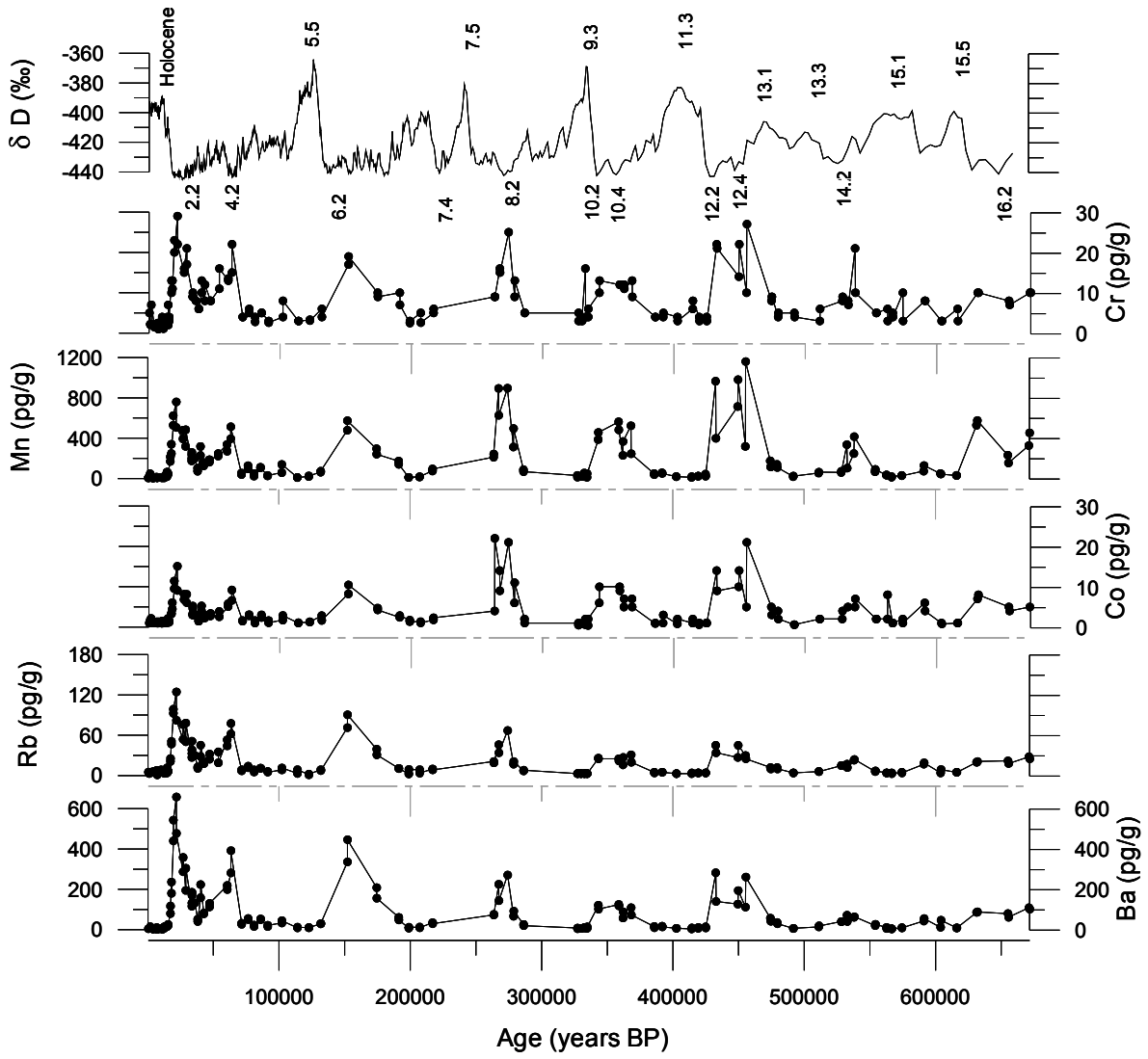

Fig. 6.1.2: *EPICA/Dome C Antarctic ice core: changes in concentrations of Cr, Mn, Co, Rb and Ba during the past 671 ky (EDC3Beta6 timescale from Parrenin et al, 2007). Data for the period from 0.5 to 220 ky BP from Gabrielli et al. (2005b). Also shown at the top of the figure are changes in deuterium concentrations and MIS numbers (EPICA Community members, 2004). All concentrations are expressed in pg/g, except for deuterium (delta per mil)*

6.2 Comparison between Vostok and Dome C for the past 420 ky BP

Present day snow accumulation rates at Dome C (~ 2.7 g H_2O cm^{-2} y^{-1}) and Vostok (~ 3 g H_2O cm^{-2} y^{-1}) are very similar. They have varied by a factor ~ 2 between glacial maxima (Dome C : ~ 1.3 g H_2O cm^{-2} y^{-1}; Vostok : ~ 1.5 g H_2O cm^{-2} y^{-1}) and interglacial periods (Petit et al., 1999 ; EPICA Community members, 2004). It is therefore possible to compare the data obtained at the two locations. For instance, **Figure 6.2.1** compares the Ba concentration profile

previously obtained by Gabrielli et al.(2005b) for Vostok for the past 420 ky with the profile obtained here for the same time interval. It can be seen that the two profiles are in excellent agreement. Especially, high Ba concentration values are observed at both locations for the glacial maxima. The Vostok and Dome C concentration profiles are also in very good agreement for the other metals which have been determined in both cores (V, Cr, Rb, Ba and U).

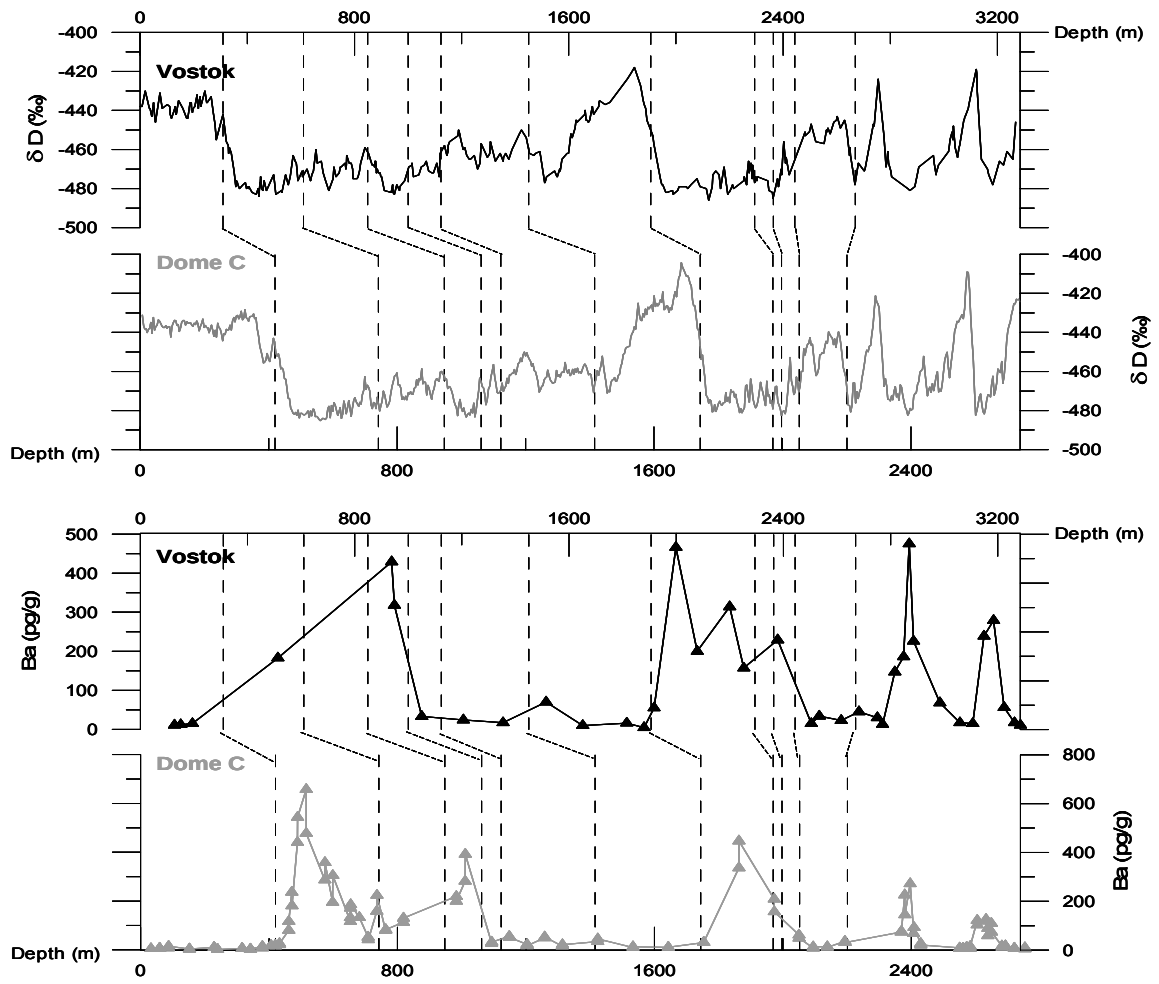

Fig. 6.2.1: *Comparison of the Ba concentration profiles obtained at Dome C (this work and Gabrielli et al, 2005a) and Vostok (Gabrielli et al, 2005b) for the past 420 ky. Also shown are the variations of the deuterium concentrations from EPICA community members, 2004 and Petit et al., 1999. The vertical dotted lines correspond to 10 major dust events observed in both cores by Delmonte et al., 2004*

6.3 Crustal Enrichment Factors (EFc)

In order to assess the importance of the rock and soil dust contribution for the eight elements studied in this work, we have calculated the Crustal Enrichment Factor (EF_c) for each element with depth (Appendix II, Table II). EF_c is defined as the concentration ratio of a given element to that of Mn (which is a good proxy of continental dust) in the ice, normalized to the same concentration ratio characteristic of the upper continental crust (UCC). For example, the EF_c for Rb is thus:

$$EF_c\,(Rb) = \frac{[Rb]_{ice} / [Mn]_{ice}}{[Rb]_{UCC} / [Mn]_{UCC}}$$

We have used here the data for the upper continental crust given by Wedepohl (1995). It should however be mentioned that the use of other crustal compositions data, for instance those given by Rüdnick and Fountain (1995) would not make any significant differences in the interpretation. Despite the fact that the composition of rock and soil dust reaching Dome C might significantly differ from the composition of the mean upper continental crust, EF_c values close to unity (up to ~ 5) will indicate that the corresponding element mainly originated from continental dust. Conversely, EF_c values much larger than unity will suggest a significant contribution from other natural sources.

As shown in Appendix II, Table II, EF_c values for V, Fe, Rb, Ba and U are found to be close to unity, whatever the period, showing that the atmospheric cycle of these elements in the remote areas of the Southern Hemisphere was dominated by crustal dust, both during glacial and interglacial periods. For these elements, the range of maximum to minimum concentrations is up to about 100. Interestingly, this is about the range previously observed for insoluble dust (EPICA Community members, 2004), giving support for these three elements being mainly derived from the continental dust.

The situation appears to be different for Co and Cr. For these elements, EF_c close to unity are observed during the coldest climatic stages, but moderately elevated values are observed during

warmer periods, especially interglacial periods. Moreover, lower maximum/minimum ratios are observed for these two elements (~50). It indicates that the atmospheric cycles of these two elements were dominated by crustal dust during the cold dust climatic stages while contribution from additional sources was probably significant during warmer periods, especially interglacials, as previously suggested by Gabrielli et al (2005a) for the period from 6.9 to 217 kyr BP. This may indicate changes in continental dust source areas or transport processes between glacial and interglacial periods (Röthlisberger et al., 2002; Delmonte et al., 2002; Gabrielli et al., 2005 a, b; Wolff et al., 2006). It might also relate to the high relative contribution of volcanic emissions to the atmosphere during interglacial periods (Vallelonga et al., 2005).

6.4 Crustal trace elements versus climate relationship

As illustrated in **Figure 6.4.1** for Cr, Fe, Ba and dust, concentrations of crustal trace elements in Dome C ice from 263 to 671 ky BP remain very low for δD values between ~ -380 ‰ and ~ - 430 ‰, but shows a sharp increase for δD values below ~ - 430 ‰. It suggests that there is a critical point in the climate mechanism, beyond which the physical and chemical processes of fallout and deposition of crustal elements to the Antarctic Plateau increase enormously. A possibility is that when a critical temperature gradient between low and high latitude was reached, it causes larges changes in wind strength, then allowing larger amounts of crustal trace elements to be transported to the Antarctic ice cap (Gabrielli et al., 2005b). Another possibility could be rapid changes in local conditions in the different source areas such as Patagonia or Australia (Delmonte et al., 2002 ; Revel-Rolland et al., 2006).

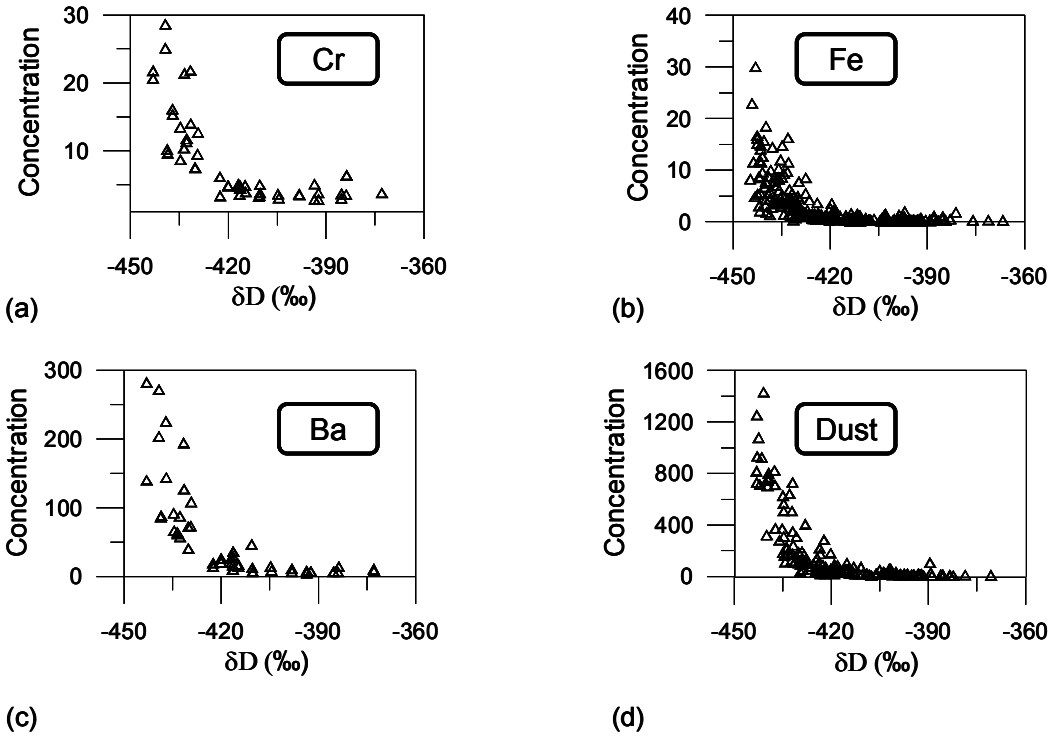

Fig. 6.4.1: *EPICA/Dome C Antarctic ice core: changes in concentrations of Cr (a), Ba (c), Fe (b) and Dust (d) as a function of the deuterium content of the ice from 263 to 671 ky BP. Concentrations in pg/g for Cr and Ba and in ng/g for Fe and Dust. Fe values from this work and Wolff et al.(2006)*

6.5 The mid-Brunhes climate shift

The mid Brunhes event ("MBE") is a phase of global climatic change around 430 ky, which was forced by the orbital eccentricity cycle (EPICA Community members, 2004). Terrestrial and marine geological temperature records indicate that before the MBE, the glacial cycles display smaller amplitudes (McManus, 2004). Even if the coldest periods of the glacial portions of each climatic cycle are roughly similar before and after the MBE, the magnitude of the interglacial periods is clearly less pronounced (Jansen et al, 1986).

The fact that interglacial periods are less warm before the MBE does not seem to result in higher concentrations of the different crust derived elements during these pre-MBE interglacials, compared with those observed during post-MBE interglacials, as illustrated in **Figure 6.1.2**. This

is probably because δD values during these interglacial periods always remain between ~ -380 ‰ and – 405 ‰, when concentrations of crust derived elements do not depend significantly upon δD values (**Figure 6.4.1**).

The situation appears to be different for glacial maxima. High concentrations observed for the various elements during these glacial maxima appear to be lower before the MBE than after the MBE, despite the fact that δD values during these maxima are similar before and after the MBE (**Figure 6.1.2**).

Figure 6.5.1 compares changes in Rb and Ba concentrations as a function of δD before and after the MBE, using a logarithmic scale for concentrations. It can be seen that the relation between concentrations and δD is very similar before and after the MBE.

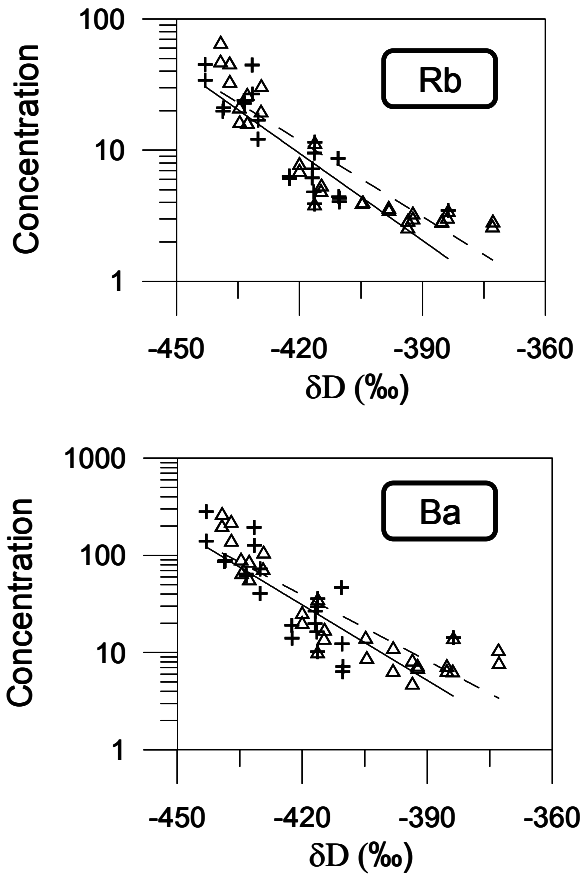

Fig. 6.5.1: *EPICA/Dome C Antarctic ice core: changes in Rb and Ba concentrations (expressed in pg/g) as a function of the deuterium content of the ice before the Mid-Brunhes Event (MBE) (crosses and continuous line) and after the MBE (open triangles and dotted line). A logarithmic scale is used for concentrations*

After normalization using U concentrations, U, Rb and Ba concentrations measured in all our samples both for glacial maxima and interglacials periods are shown in Fig. 7 using ternary diagrams. Different symbols have been used for samples dated from before the MBE (which are shown using crosses) and the samples dated from after the MBE (which are shown using open triangles). It can be seen that during glacial maxima, the data points are very well grouped together both after and before the MBE (Fig. 7a). It points toward a well defined crustal input during glacial maxima both after and before the MBE. The situation appears to be different for interglacial periods, with rather dispersed data points both before and after the MBE (Fig. 7b), suggesting more complex and variable crustal inputs during these periods.

There are various possible explanations for these changes, which could be linked with changes in source areas (Delmonte et al., 2004), atmospheric transport (Krinner and Genthon, 2003) and strength of the Antarctic circumpolar vortex (Berger and Wefer, 2003).

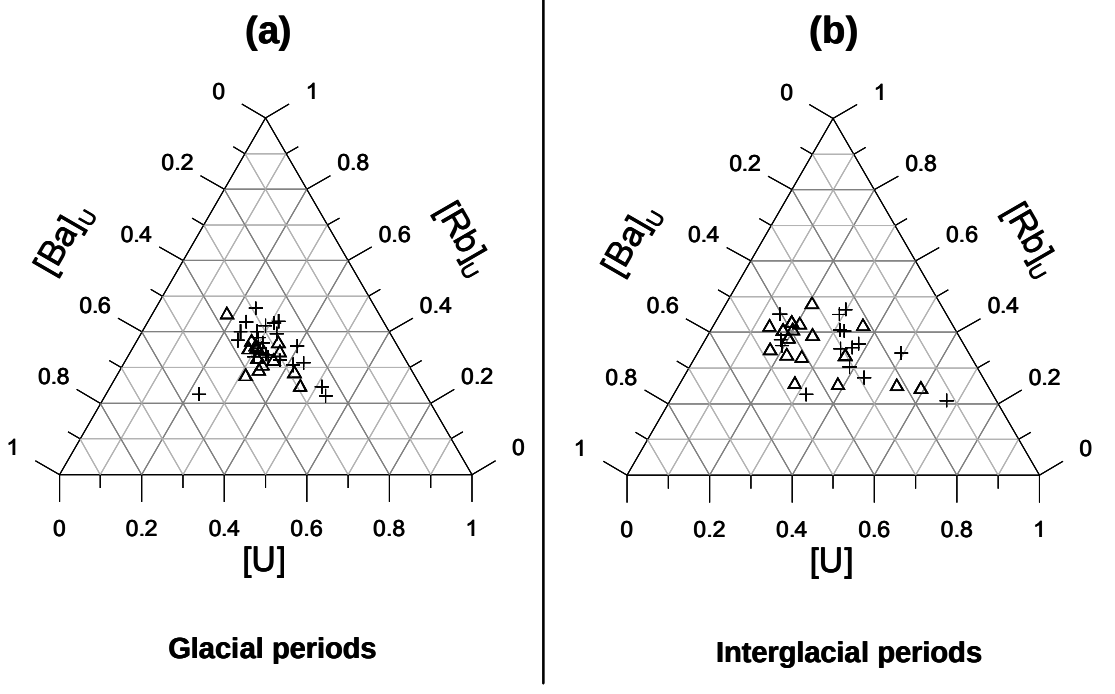

Fig. 6.5.2: *EPICA/Dome C Antarctic ice core: ternary plots for U, Rb, and Ba (Rb and Ba concentrations have been normalized to U concentrations). (a) glacial maxima from MIS 8.2 to MIS 16.2; (b) interglacial periods from MIS 9.3 to MIS 15.5. Crosses are used for ice dated from before the MBE, while open triangles are used for ice dated from after the MBE*

6.6 Observed concentrations during the successive interglacials

As illustrated in **Figure 6.1.2**, the data obtained in this work and in the work of Gabrielli et al. (2005 a) include data for various interglacials from the Holocene (MIS1) to MIS 15.5 (~ 600 ky BP). Amongst these interglacials are MIS 11 which is easily recognized in ice cores and other paleorecords as an exceptionally long interglacial (EPICA Community members, 2004), during which the Earth's orbital parameters were similar to present day ones (Berger and Loutre, 2003). There are indications that every interglacial is probably different, with changing amplitude, duration and shape, as discussed by Wolff et al, 2007.

The only elements for which we have data for each of the seven interglacials considered in this work and the work of Gabrielli et al (2005a) are Cr, Mn, Fe, Co, Rb and Ba. Mean concentration values determined in the successive interglacials are given in **Table 6.6.1**.

MIS Number	MIS 1	MIS 5.5	MIS 7.5	MIS 9.3	MIS 11.3	MIS 13.3	MIS 15.1	MIS 15.5
Time period (ky BP)	0.5-12	121-132	240-244	324-335	395-423	511-528	567-579	608-620
Number of samples	16	4	6	8	8	6	4	2
δ D (‰) [a]	-396.1	-382.5	-388.9	-387.8	-391.2	-418.9	-402.0	-402.2
Cr	4.0	5.0	_	5.6	4.4	6.8	5.5	4.5
Mn	13.1	46.3	33.8	68.6	29.6	63.25	23.3	31.5
Fe	0.2	0. 3	0.6	0.6	0.6	0.5	0.1	0.2
Co	1.2	1.8	1.6	1.5	1.5	2.5	1.2	1.0
Rb	4.7	5.0	_	3.0	3.9	10.5	4.0	5.0
Ba	6.6	20.2	_	29.0	9.9	28.3	7.0	9.0

[a] EPICA Community members, 2004

Table 6.6.1 : *Dome C, East Antarctica: mean concentrations of various crustal trace elements for the successive interglacial periods back to MIS 15.5. Concentrations are expressed in pg/g except for Fe (ng/g). Data for MIS 1 and 5.5 from Gabrielli et al, 2005b. Data for MIS 7.5 from V.Gaspari, personal communication*

Of particular interest is the comparison between concentration values observed during the Holocene, MIS 5.5, MIS 7.5, MIS 9.3 and MIS 11.3, **Table 6.6.1**. These five interglacials are indeed characterized by temperatures above Holocene temperatures. It can be seen that Cr, Co and Rb concentrations are similar during these five interglacials, while Mn, Fe and Ba

concentrations are more variable. For Mn and Ba, higher values are observed for interglacials 5.5, 7.5 and 9.3.

The highest values are observed during MIS 5.5 and 9.3, which are interglacials similar in shape, temperature and amplitude. For each of these two interglacials, there is a warm period followed by a relatively rapid cooling (Petit et al, 1999). This cooling resulted into an enhancement of dust emission in source areas because of an intensification of the wind strength in these areas and an enlargement/displacement of the sources, then resulting into the high concentrations we observe during these two interglacials.

6.7 Observed concentrations during the successive glacial maxima

The data obtained in this work and in the work of Gabrielli et al (2005 b) include data for eight successive glacial maxima from MIS 2.2 (Last Glacial Maximum) to MIS 16.2. As illustrated in **Figure 6.1.2** for Cr, Mn, Co, Rb and Ba, the data show each of these glacial maxima is characterized by high concentration values. However, it appears that the amplitude of these maxima probably shows a decreasing trend from MIS 2.2 to MIS 16.2. This is especially clear for Rb and Ba. For these two elements, the maxima observed for the most recent glacial maxima such as MIS 2.2 and 4.2 are indeed well pronounced, while the maxima are much less pronounced for the oldest glacial maxima such as MIS 14.2 and 16.2.

One possible explanation for these changes in the amplitude of the maxima in concentrations could be linked with changes in the size distribution of dust particles transported from mid-latitude areas such as Patagonia to the Antarctica ice cap, with a decreasing trend in the dust size (as reflected by the fine particle percentage, which is defined as the proportion of particles with a diameter between 1 and 2 μm of the total dust mass, typically between 1 and 5 μm) over the last 500 ky (Lambert et al., 2007). It might be indicative of a strengthening of the subsidence over Antarctica (Lambert et al., 2007). They interpret that as a progressive coupling between low latitudes (up to dust sources in southern South America) and Antarctica climate, leading to a stronger aeolian deflation of Southern South America (Lambert et al., 2007). This phenomenon could be combined with a significantly longer atmospheric particle life-time in the upper

troposphere due to reduced hydrological cycle. Both arguments could explain the increase in the amplitude of the concentration maxima we observe in Dome C ice during the past 671 ky.

This work has allowed to document large natural variations in the occurrence of several crust derived elements in Antarctic ice over the past 670 ky. It will now be interesting to study other elements which mainly derive from crustal dust, especially Rare Earth Elements. It will be also of interest to extend this study to preceding climatic cycles which are covered in the bottom part of the EPICA Dome C ice core back to MIS 20.2, ~ 800 ky BP.

REFERENCES

Bassinot FC, Labeyrie LD, Vincent E, Quidelleur X, Shackleton NJ, Lancelot Y (1994) The astronomical theory of climate and the age of Brunhes-Matuyama magnetic reversal. *Earth and Planetary Science* Letters **126**, 91-108

Berger A, Loutre M F (2003) Climate 400,000 years ago, a key to the Future? In: Droxler AW, Poore RZ, Burckle LH (eds) *Earth's Climate and Orbital Eccentricity: The Marine Isotopic Stage 11 Question*, American Geophysical Union, pp. 17-26, doi: 10.1029/137GM02

Berger WH, Wefer G (2003) On the dynamics of the ice ages: Stage-11 paradox, Mid-Brunhes climate shift, and 100-ky cycle. In: Droxler AW, Poore RZ, Burckle LH (eds) *Earth's Climate and Orbital Eccentricity: The Marine Isotopic Stage 11 Question*, American Geophysical Union, pp. 41-59, doi: 10.1029/137GM04

Boutron CF, Patterson CC (1986) Lead concentration changes in Antarctic ice during the Wisconsin/Holocene transition. *Nature* **323**, 222-225

Candelone JP, Hong S, Boutron CF (1994) An improved method for decontaminating polar snow and ice cores for heavy metal analysis. *Analytica Chimica Acta* **299**, 9-16

Delmonte B, Petit JR, Maggi V (2002) Glacial to Holocene implications of the new 27,000-year dust record from the EPICA Dome C (East Antarctica) ice core, *Climate Dynamics* **18**, 647–660

Delmonte B, Basile-Doelsch I, Petit JR, Maggi V, Revel-Rolland M, Michard A, Jagout E, Grousset F (2004) Comparing the EPICA and Vostok dust records during the last 220,000 years: stratigraphical correlation and provenance in glacial periods. *Earth Science Reviews* **66**, 63–87

Droxler AW, Alley RB, Howard WR, Poore RZ, Burckle LH (2003) Unique and Exceptionally Long Interglacial Marine Isotope Stage 11: Window into Earth Warm Future Climate. In: Droxler AW, Poore RZ, Burckle LH (eds) *Earth's Climate and Orbital Eccentricity: The Marine Isotopic Stage 11 Question*, American Geophysical Union, pp. 1-13, doi: 10.1029/137GM01

EPICA Community members (2004) Eight glacial cycles from an Antarctic ice core. *Nature* **429**, 623-628

Gabrielli P, Barbante C, Boutron C, Cozzi G, Gaspari V, Planchon F, Ferrari C, Turetta C, Hong S, Cescon P (2005a) Variations in atmospheric trace elements in Dome C (East Antarctica) ice over the last

two climatic cycles. *Atmospheric Environment* **39**, 6420-6429

Gabrielli P, Planchon FAM, Hong S, Lee KH, Hur SD, Barbante C, Ferrari CP, Petit JR, Lipenkov VY, Cescon P, Boutron CF (2005b) Trace elements in Vostok Antarctic ice during the last four climatic cycles. *Earth and Planetary Science Letters* **234**, 249-259

Gabrielli P, Barbante C, Turetta C, Marteel A, Boutron C, Cozzi G, Cairns W, Ferrari C, Cescon P (2006) Direct determination of Rare Earth Elements at the sub-picogram per gram level in Antarctic ice by ICP-SFMS using a desolvatation system. *Analytical Chemistry* **78 (6)**, 1883-1889

Hinkley TK, Matsumoto A (2001) Atmospheric regime of dustand salt through 75,000 years of Taylor Dome ice core: Refinement by measurement of major, minor, and trace metals suites. *Journal of Geophysical Research* **106 (16),** 18, 487-18, 493

Hong S, Kim Y, Boutron CF, Ferrari CP, Petit JR, Barbante C, Rosman K, Lipenkov VY (2003) Climate-related variations in lead concentrations and sources in Vostok Antarctic ice from 65,000 to 240, 000 years BP. *Geophysical Research Letters* **22**, 2138, doi: 10.1029/2003GL018411

Hong S, Boutron CF, Gabrielli P, Barbante C, Ferrari CP, Petit JR, Lee K, Lipenkov VY (2004) Past natural changes in Cu, Zn and Cd in Vostok Antarctic ice dated back to the penultimate interglacial period. *Geophysical Research Letters* **31**, L20111, doi: 10.1029/2004GL021075

Hong S, Boutron CF, Barbante C, Hur SD, Lee K, Gabrielli P, Capodaglio G, Ferrari CP, Turetta C, Petit JR, Lipenkov VY (2005) Glacial-interglacial changes in the occurence of Pb, Cd, Cu and Zn in Vostok Antarctic ice from 240 000 to 410 000 years BP. *Journal of Environmental Monitoring* **7**, 1326-1331

Jansen JHF, Kuijpers A, Troelstra SR (1986) A Mid-Brunhes climatic event: Long term changes in global atmospheric and ocean circulation. *Science* **232**, 619-622

Krinner G, Genthon C (2003) Tropospheric transport of continental tracers towards Antarctica under varying climatic conditions. *Tellus* **55B**, 54-70

Lambert F, Delmonte B, Petit JR, Bigler M, Kaufmann PR, Huttterli MA, Stocker TF, Ruth U, Steffensen JP, Maggi V (2007) New constraints on the aeolian dust cycle and climatic implications from an 800 ka ice core record, submitted to *Nature*

McManus JF (2004) A great grand-daddy of ice cores. *Nature* **429**, 611-612

Ng A, Patterson CC (1981) Natural concentrations of lead in ancient Arctic and Antarctic ice. *Geochimica et Cosmochimica Acta* **45**, 2109-2121

Parrenin F, Barnola JM, Beer J, Blunier T, Castellano E, Chappellaz J, Dreyfus G, Fisher H, Fujita S, Jouzel J, Kawamura K, Lemieux-Dudon B, Loulergue L, Masson-Delmotte V, Narcisi B, Petit JR, Raisbeck G, Raynaud D, Ruth U, Schwander J, Severi M, Spahni R, Steffensen JP, Svensson A, Udisti R, Waelbroeck C, Wolff E (2007) The EDC3 chronolgy for the EPICA Dome C ice core. *Climate of the Past Discussions* **3**, 575-606

Petit JR, Jouzel J, Raynaud D, Barkov NI, Barnola JM, Basile I, Bender M, Chappellaz J, Davis M, Delaygue G, Delmotte M, Kotlyakov VM, Legrand M, Lipenkov VY, Lorius C, Pépin L, Ritz C, Saltzman E, Stievenard M (1999) Climate and atmospheric history of the past 420,000 years from the Vostok ice core, Antarctica. *Nature* **399**, 429-436

Raymo ME, Oppo DW, Curry W (1997) The mid-Pleistocene climate transition: A deep-sea carbon isotopic perspective. *Paleoceanography* **12**, 546-559

Revel-Rolland M, De Deckker P, Delmonte B, Hesse PP, Magee JW, Basile-Doelsch I, Grousset F, Bosch D (2006) Eastern Australia: a possible source of dust in East Antarctica interglacial ice. *Earth and Planetary Science Letters* **249**, 1–13

Röthlisberger R, Mulvaney R, Wolff E, Hutterli M, Biegler M, Sommer S, Jouzel J (2002) Dust and sea-salt variability in central East Antarctica (Dome C) over the last 45 kyrs and its implications for southern high latitude climate. *Geophysical Research Letters* **29**, 1963-1966

Rudnick RL, Fountain DM (1995) Nature and composition of continental crust: a lower crustal perspective. *Reviews of Geophysics* **33**, 267-309

Vallelonga P, Gabrielli P, Rosman K, Barbante C, Boutron CF (2005) A 220 ky record of Pb isotopes at Dome C Antarctica from analyses of the EPICA ice core. *Geophysical Research Letters* **32**, L01706

Wedepohl KH (1995) The composition of the continental crust. *Geochimica et Cosmochimica Acta* **59**, 1217-1232

Wolff EW, Fischer H, Fundel F, Ruth U, Twarloh B, Littot GC, Mulvaney R, Röthlisberger R, de Angelis M, Boutron CF, Hansson M, Jonsell U, Hutterli MA, Lambert F, Kaufmann P, Stauffer B, Stocker TF, Steffensen JP, Bigler M, Siggaard-Andersen ML, Udisti R, Becagli S, Castellano E, Severi M, Wagenbach D,

Barbante C, Gabrielli P, Gaspari V (2006) Southern Ocean sea-ice extent, productivity and iron flux over the past eight glacial cycles. *Nature* **440**, 491-496

Wolff E, Fischer H, Lüthi D, Masson-Delmotte V (2007) The occurrence and structure of interglacials in the late Quaternary. 32nd General Assembly of the European Geosciences Union, Vienna, Austria, April 15-20

Chapter 7- CHANGES IN ATMOSPHERIC HEAVY METALS AND METALLOIDS IN DOME C (EAST ANTARCTICA) ICE BACK TO 671 KY BP

For the past decades, considerable attention has been given to the study of various heavy metals such as Pb, Cd, Pt and Hg in the environment. This is because human activities are emitting large amounts of these toxic metals to the atmosphere and other compartments of the environment (see e.g. Nriagu and Pacyna, 1988; Nriagu, 1990; Pacyna and Pacyna, 2001; Von Storch et al., 2003; Wilson et al., 2006). Since the dawn of the Industrial Revolution, the emissions have grown considerably to the extent that today the impacts of the long-term accumulated toxic metals have become global in scope. The most fascinating example is Pb. For this metal, contamination of the Northern Hemisphere started as early as Roman times (Hong et al., 1994; Zheng et al., 2007) while contamination of the Antarctic continent was only significant at the end of nineteenth century (Planchon et al., 2003). The amplitude of the contamination by this metal is extremely pronounced especially because of the huge emissions linked with the widespread use of organolead compounds as anti-knock additives in gasoline from the 1920s onwards (Nriagu, 1990; Von Storch et al., 2003) (see Section 2.1 and 2.6.2).

Any proper assessment of these man induced changes requires a good knowledge of past natural geochemical cycles of these metals and their variations with different climatic conditions, against which recent trends can be evaluated. Such information can only be obtained from archives such as deep Antarctic ice cores (Petit et al. 1999; EPICA Community members, 2004). Deciphering the ice core archives has unfortunately proved to be extremely difficult because heavy metals concentrations in polar ice are extremely low and drilling operations strongly contaminate the outside of deep ice cores. The impetus in the field came from the pioneering work of Patterson, Boutron and co-workers who developed sophisticated methods to decontaminate deep polar ice cores drilled in fluid-filled holes, which allowed for reliable data for heavy metals in these cores to be obtained (Ng and Patterson, 1981; Boutron et al., 1987) (see Section 2.6.1)

Presently available reliable data for heavy metals and metalloids in deep Antarctic ice cores are only for two locations (Dome C and Vostok) and cover limited time periods. For Dome C, available data cover only the past 217 ky, which corresponds to the last two climatic cycles

For Dome C, available data cover only the past 217 ky, which corresponds to the last two climatic cycles (Gabrielli et al., 2005a; Vallelonga et al., 2005). For Vostok, available data cover the past 420 ky, which corresponds to the last four climatic cycles (Hong et al., 2003, 2004, 2005; Gabrielli et al., 2005b). A drawback of the Vostok data is however that they do not allow a comprehensive view of the entire Marine Isotopic Stage (MIS) 11, considered as a key interglacial period from about 390 to 420 ky BP, and probably the best analogue of the present Holocene interglacial (Berger and Loutre, 2003; Droxler et al., 2003). MIS 11 is an unusual and perhaps unique interglacial interval. It exhibited warm interglacial climatic conditions for an interval of at least 30 ky, a duration twice as long as the most recent interglacial periods, with orbital parameters (low eccentricity and consequently weak precessional forcing) similar to those of the present. Moreover, there are no data for the period between the Mid-Pleistocene Revolution (MPR) (often dated at about 900 ky BP) (Raymo et al., 1997) and the Mid-Brunhes event (MBE) (which roughly corresponds to the transition between MIS 12 and MIS 11 about 430 ky BP) (Berger and Wefer, 2003).

I present here comprehensive data on past changes in the occurrence of Cu, Zn, As, Cd, Pb and Bi in Antarctic ice during the period from 263 ky BP (MIS 8.2) to 671 ky BP (MIS 16.2). The data were obtained by analysing various sections of the 3,270 m deep ice core recently obtained at Dome C as part of the European EPICA program, using ultra-clean decontamination procedures and the highly sensitive inductively coupled plasma sector field mass spectrometry (ICP-SFMS) technique. The sections which were analysed include various sections dated from MIS 11, together with sections dated from before and after the Mid-Brunhes Event.

7.1 Changes in concentration during the last eight climatic cycles

Heavy metals and metalloids concentrations measured in the innermost part of the 77 samples are listed in Appendix II, Table III. They range from 0.01 pg/g for Bi in ice dated at 566 ky BP to 186 pg/g for Zn in ice dated at 286 ky BP. They are the first data ever obtained for ice dated back to 671 ky BP.

Figure 7.1.1 shows that concentrations of all metals and metalloids have strongly varied during the ~ 400 ky period covered by our samples. For Cu, Pb and Bi, concentrations appear to be closely linked with climate conditions with high values during the coldest periods such as MIS 8.2, 10.4 and 12.2, and low values during interglacial periods such as MIS 9.3, 11.3 and 15.1 (**Figure 7.1.1**). The situation appears to be less clear for As, Cd and possibly Zn with observed variations which are less clearly linked with deuterium changes. The highest maximum/minimum concentration ratios are observed for Cu, Zn and Pb (~ 40) while lower ratios are observed for As, Cd and Bi (~ 20). These are ratios which are lower than the maximum/minimum ratios observed for dust (~ 100, EPICA Community members, 2004) and for elements such Al, Mn and Ba which mainly derived from crustal dust (see Section 6.3).

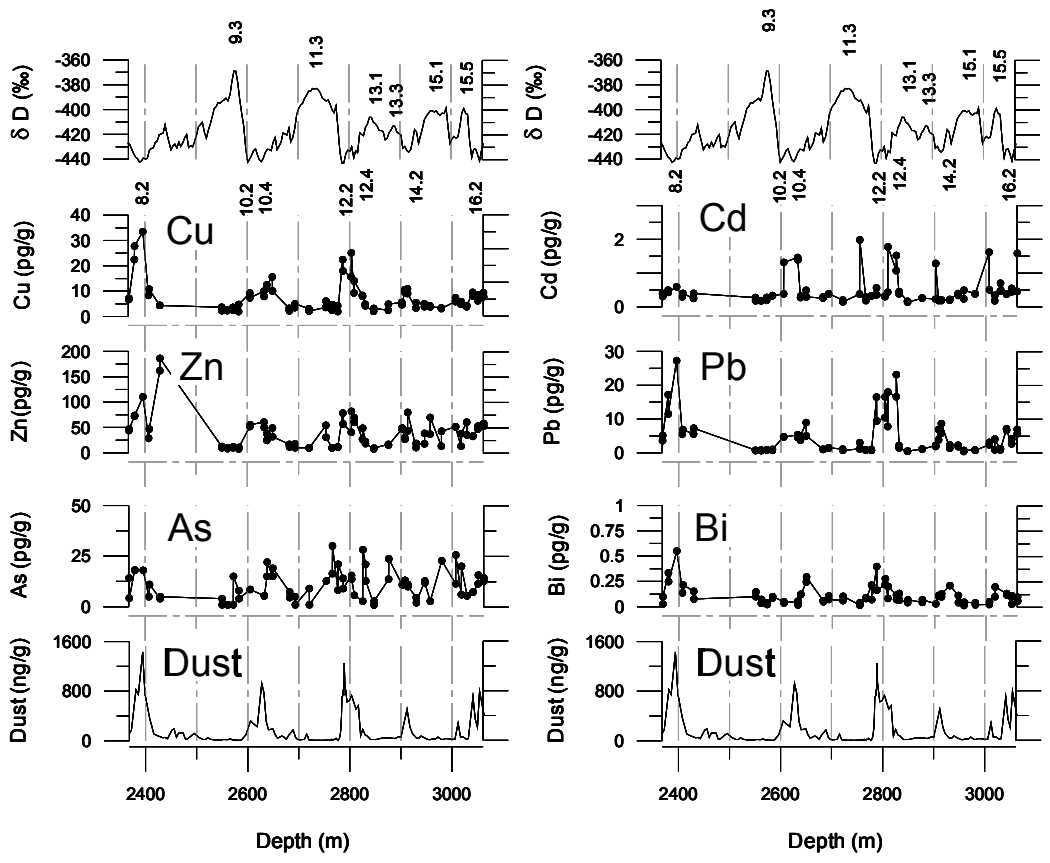

Fig. 7.1.1: *EPICA/Dome C Antarctic ice core: changes in concentrations of Cu, Zn, As, Cd, Pb and Bi as a function of depth from 2368.6 m to 3061.9 m (263 to 671 ky BP). Also shown at the top of the figure are the variations in deuterium concentrations (expressed in delta per mil) (EPICA Community members, 2004), Marine Isotope Stages (MIS) numbers (Bassinot et al., 1994), and at the bottom of the figure changes in dust concentrations (expressed in ng/g) (EPICA Community members, 2004).*

For Cu, As, Cd, Pb and Bi, our data can be combined with the data previously obtained by Gabrielli et al.(2005a) and Vallelonga et al. (2005) for the upper 2193 m of the EPICA Dome C ice core (ice dated from 0.5 to 217 kyr BP), giving comprehensive time series for these five elements over a ~671 ky period from the Holocene to the end of MIS 16.2, **Figure 7.1.2**. It is the first time that past natural variations in heavy metals have been observed during such a long time period with high sampling frequency (about 159 depth intervals in total). During this 671 ky period, variations in concentrations of Cu, Pb and Bi are found to fairly well parallel changes in climate with high concentrations during glacial maxima and a low concentrations during interglacials. The amplitude of the variations appears however to be larger during the most recent climatic cycles than during the oldest ones, especially before the Mid-Brunhes Event (**Figure 7.1.2**). The situation is less clear for As and Cd. For these two metals indeed, elevated concentrations are observed for the most recent glacial maxima (MIS 2.2 and 4.2) but not for earlier maxima such as MIS 12.2.

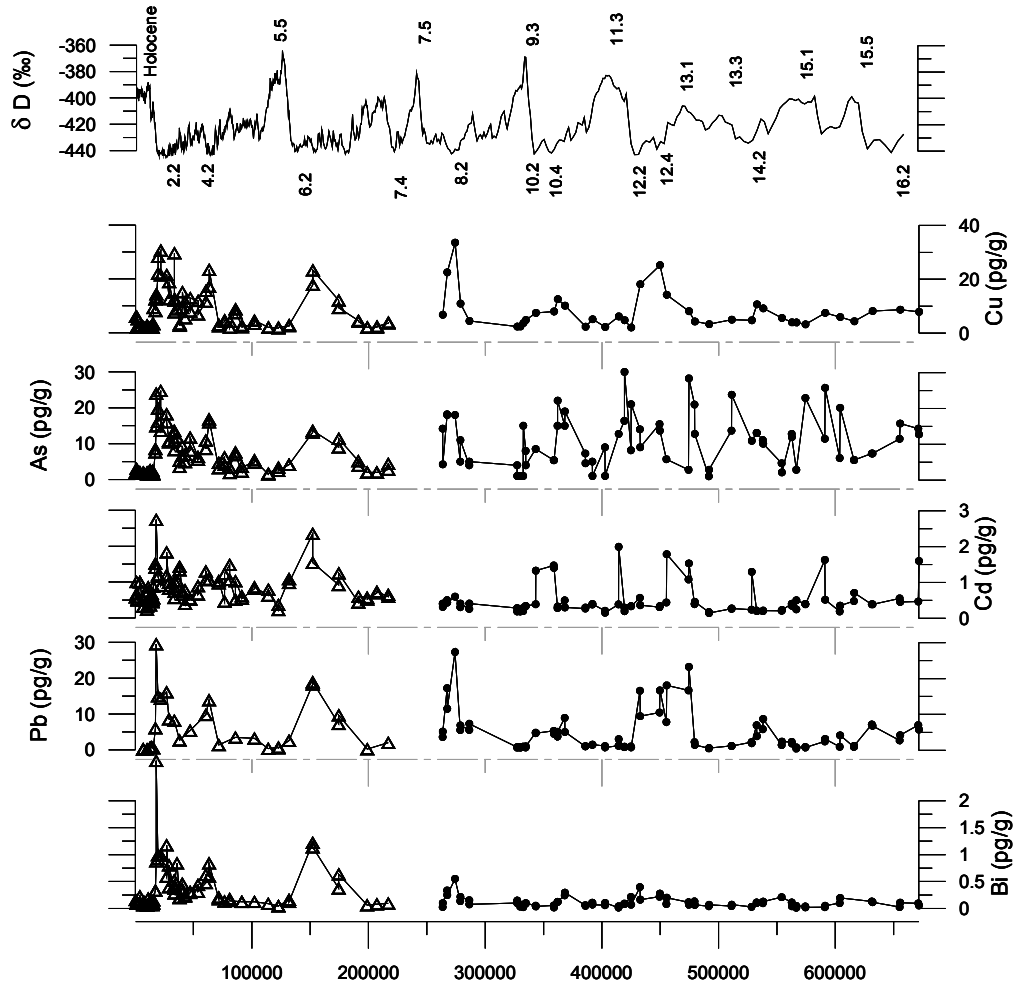

Fig. 7.1.2: *EPICA/Dome C Antarctic ice core: changes in concentrations of Cu, As, Cd, Pb and Bi during the past 671 ky (EDC3Beta6 timescale from Parrenin et al, 2007). Open triangles are used for ice samples dated from 0.5 to 217 ky BP (data from Gabrielli et al., 2005a) while full circles are used for ice samples dated from 263 to 671 ky BP. Also shown at the top of the figure is the deuterium profile and MIS numbers (EPICA Community members, 2004). Concentrations are expressed in pg/g, except for deuterium (delta per mil).*

7.2 Fallout fluxes for heavy metals and metalloids during the past 671 ky

Fallout fluxes were calculated for each metal by combining concentrations measured in the ice for each depth interval with the estimated yearly ice accumulation rate at that depth (expressed in g H_2O cm $^{-2}$ y $^{-1}$). The accumulation rate at Dome C has varied by a factor ~ 2 between glacial maxima (~ 1.3 g H_2O cm $^{-2}$ y $^{-1}$) and interglacial periods (~ 2.7 g H_2O cm $^{-2}$ y $^{-1}$) (F.Parrenin, personal communication).

Changes in fallout fluxes are found to parallel fairly well changes in concentrations during the past 671 ky. The ratio between the highest and the lowest fluxes is however about half of the corresponding ratio for concentrations since the accumulation rate is lower during glacial maxima when concentrations are maximum.

7.3 Heavy metals and metalloids concentration versus deuterium

Concentrations of Cu, Zn, Pb and Bi in Dome C ice during the past 671 ky are found to remain very low for δD values between ~ -380 ‰ and ~ -420 ‰ as illustrated in **Figure 7.3.1** for Cu, Zn, Pb and Bi, but increase strongly when δD values fall below ~ -420 ‰. It suggests that there is a critical point in the climate mechanism, beyond which fallout of heavy metals to the high East Antarctic Plateau increases considerably. A possibility is that when a critical temperature gradient between low and high latitude was reached, it induced changes in wind strength, then allowing larger amounts of heavy metals to be transported to the Antarctic ice cap (Gabrielli et al., 2005b). Another possibility could be rapid changes in local conditions in the different source areas such as Patagonia or Australia from which the crustal contribution to heavy metals originate (Delmonte et al., 2002; Revel-Rolland et al., 2006).

The situation appears to be different for Cd and As. For these two metals indeed, concentrations in the ice does not depend clearly upon δD, as illustrated s illustrated in **Figure 7.3.1 c** for As and **Figure 7.3.1 d** for Cd.. These are metals and metalloids for which crustal dust is not the dominant source, as discussed later.

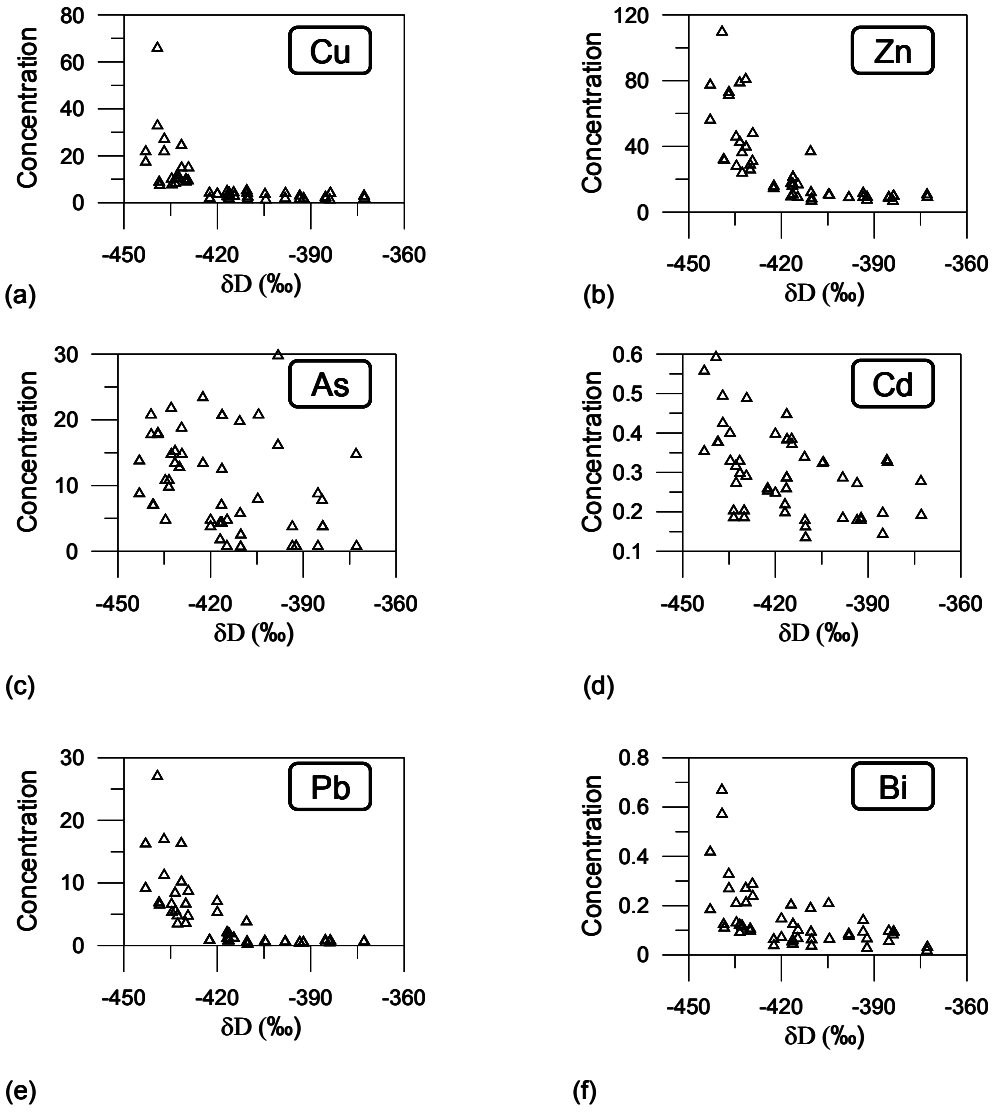

Fig. 7.3.1: *EPICA/Dome C Antarctic ice core: changes in concentrations of Cu (a), Zn (b), As (c), Cd (d), Pb (e) and Bi (f) (expressed in pg/g) as a function of the deuterium content of the ice (expressed in delta per mil) from 263 to 671 ky BP*

7.4 Crustal Enrichment Factors (EFc)

Rock and soil dust is an important source of heavy metals and metalloids in the natural atmosphere (Nriagu, 1989). In order to assess the importance of rock and soil dust contribution in Dome C ice for the metals and metalloids studied in this work, I have calculated Crustal Enrichment Factors (EF_c) for each metal and metalloid and depth. EF_c is defined as the

concentration ratio of a given element to that of Ba (which is also a good proxy of crustal dust, like Mn) (Patterson and Settle, 1976) in the ice, normalized to the same concentration ratio characteristic of the upper continental crust (Wedepohl, 1995). For example, the EF_c for Cu is thus:

$$EF_c\,(Cu) \quad = \quad \frac{[Cu]_{ice} / [Ba]_{ice}}{[Cu]_{crust} / [Ba]_{crust}}$$

Since the composition of rock and soil dust reaching Dome C might significantly differ from the composition of the mean upper continental crust, EF_c values up to ~ 5 will indicate that the corresponding element mainly originated from rock and soil dust. Conversely, EF_c values much larger than unity will indicate a significant contribution from other natural sources such as sea-salt spray and volcanoes.

		Glacial maxima									
		MIS 2.2	MIS 4.2	MIS 6.6	MIS 8.2	MIS 10.2	MIS 10.4	MIS 12.2	MIS 12.4	MIS 14.2	MIS 16.2
Cu	Concentration	34 [a]	20 [a]	21 [a]	28	11	9	20	20	10	8
	EFc	4.7 [a]	2.8 [a]	2.5 [a]	5.6	3.5	3.4	4.9	5.9	7.4	4.8
Zn	Concentration	-	-	-	86	46	55	68	61	62	41
	EFc	-	-	-	6.2	6.3	5.8	4.4	4.8	12.5	6.9
As	Concentration	16 [a]	16 [a]	13 [a]	18	9	5	12	15	11	10
	EFc	14 [a]	17 [a]	12 [a]	34	23	15	19	32	56	45
Cd	Concentration	1.1 [a]	1.1 [a]	1.9 [a]	0.5	0.9	1.4	0.5	0.3	0.2	0.4
	EFc	21 [a]	21 [a]	34 [a]	25	53	77	15	13	21	38
Pb	Concentration	14 [b]	12 [b]	19 [b]	19	5	5	13	14	7	5
	EFc	1.4 [b]	1.6 [b]	1.8 [b]	3.0	1.7	1.6	2.5	3.3	4.5	2.5
Bi	Concentration	0.85 [a]	0.72 [a]	1.18 [a]	0.38	0.10	0.04	0.28	0.25	0.11	0.09
	EFc	12 [a]	12 [a]	17 [a]	9	2.1	1.6	7	9	10	6

[a] Gabrielli et al., 2005a
[b] Vallelonga et al., 2005

Table 7.4.1: *Dome C, East Antarctica: mean concentrations (expressed in pg/g) and mean crustal enrichment factors (EFc) (using Ba as crustal reference element) of various metals and metalloids for the successive glacial maxima back to MIS 16.2*

Table 7.4.1 shows the mean EFc values obtained for the different metals and metalloids during the successive glacial maxima from MIS 2.2 to MIS 16.2, while **Table 7.4.2** shows the mean EFc values calculated for the successive interglacials from the Holocene to MIS 15.5.

		Interglacials							
		MIS 1	MIS 5.5	MIS 9.3	MIS 11.3	MIS 13.1	MIS 13.3	MIS 15.1	MIS 15.5
Cu	Concentration	2.8 [a]	1.7 [a]	2.5	3.8	2.6	6.3	3.6	4.0
	EFc	27 [a]	8.2 [a]	17	22	18	8	29	21
Zn	Concentration	-	-	10	19	8	31	41	48
	EFc	-	-	17	41	16	12	100	69
As	Concentration	2.0 [a]	2.9 [a]	1.0	3.4	1.8	15	13	5.4
	EFc	151 [a]	97 [a]	167	405	87	200	510	203
Cd	Concentration	0.6 [a]	0.3 [a]	0.2	0.3	0.1	0.4	0.4	0.6
	EFc	990 [a]	190 [a]	202	406	150	85	415	426
Pb	Concentration	0.4 [b]	0.5 [b]	0.7	1.3	0.5	2.8	0.7	1.00
	EFc	1.5 [b]	1.5 [b]	3.9	6.5	2.8	2.8	4.1	4.4
Bi	Concentration	0.11 [a]	0.05 [a]	0.06	0.07	0.05	0.06	0.03	-
	EFc	158 [a]	24 [a]	57	44	44	10	27	-

[a] Gabrielli et al., 2005a
[b] Vallelonga et al., 2005

Table 7.4.2: *Dome C, East Antarctica: mean concentrations (expressed in pg/g) and mean crustal enrichment factors (EFc) (using Ba as crustal reference element) of various metals and metalloids for the successive interglacial periods back to MIS 15.5*

When looking at the values listed in **Tables 7.4.1** and **7.4.2**, the metals and metalloids can be separated into two groups. The first group consists of Cu, Zn and Pb. For these three metals, low EFc values are observed during glacial maxima, while moderately elevated values are observed during interglacials (**Tables 7.4.1** and **7.4.2**). This is illustrated for Pb in **Figure 7.4.1 b**, which shows changes in EFc values for this metal during the past 671 ky. It suggests that Cu, Zn and Pb mainly derived from rock and soil dust during glacial maxima, while contributions from other sources were significant during interglacials.

The second group consists of As, Cd and Bi. For As and Cd, elevated EFc values are observed both during glacial maxima and interglacials. The values observed during interglacials are however higher than the values for glacial maxima. This is illustrated for As in **Figure 7.4.1 c**, which shows changes in EFc values for this metal during the past 671 ky. Concerning Bi, moderately low values are observed during glacial maxima, while very high values are observed

during interglacials (**Tables 7.4.1** and **7.4.2**). **Tables 7.4.1**, **7.4.2** and **Figure 7.4.1 c** indicate that rock and soil dust was a minor source of As and Cd during the past 671 ky whatever the period and that they mainly derived from other sources. Bi shows a climatic-dust behaviour but shows also a volcanic contribution, which is most important during interglacials.

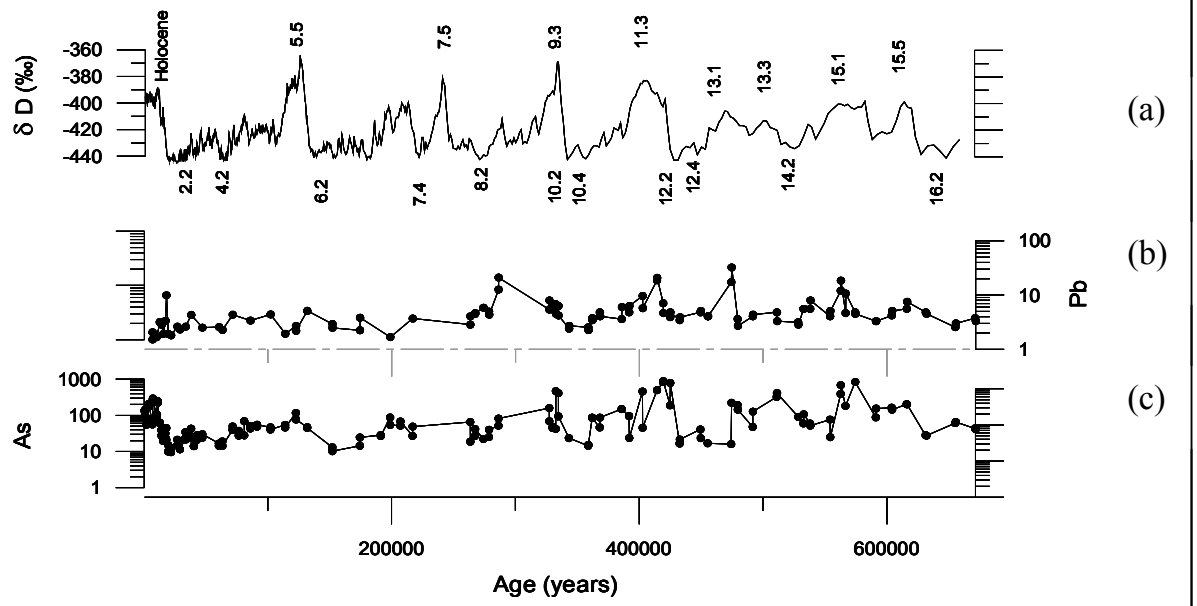

Fig. 7.4.1: *EPICA/Dome C Antarctic ice core: changes in crustal enrichment factors (EFc) for Pb (b) and As (c) during the past 671 ky. A logarithmic scale is used for EFc. Also shown at the top of the figure is the deuterium profile and MIS numbers (EPICA Community members, 2004).*

7.5 Contributions from rock and soil dust, sea salt spray and volcanoes

The main natural sources of atmospheric heavy metals are rock and soil dust, sea-salt spray, volcanic emissions and continental and marine biogenic emissions (Nriagu, 1989).

The contribution from rock and soil dust was evaluated from Ba concentration measured in the ice (see Section 6.3) and the mean metal/Ba concentration ratios in the upper continental crust (Wedepohl, 1995).

The contribution from sea-salt spray was estimated from Na concentrations measured in the ice (Wolff et al., 2006), after subtracting Na contributed from crustal dust, and metal/Na

concentration ratios in bulk ocean water (www.agu.org/eos_elec/97025e-refs.html). These ratios were not combined with possible enrichments in ocean derived aerosols relative to bulk ocean water, when marine aerosol is formed by bubble bursting through the surface micro-layer, since studies have put doubt on such possible enrichments (Hunter, 1997) (see Section 2.3.2).

A rough estimate of the contribution from volcanoes was made from the concentrations of non sea-salt sulphate ($nssS0_4$) in the ice (Wolff et al., 2006) by assuming that ~ 10-15% of $nssS0_4$ originates from volcanoes (Boutron and Patterson, 1986). They were combined with available data on metal/S ratios in volcanic emissions (Hinkley et al., 1999). It must however be kept in mind that these estimates are very rough especially because of the wide range of published data for metal/S ratios in volcanic emissions (see Section 2.3.3).

Available data do not allow evaluating possible contributions from continental and marine biogenic activities although such contributions could be significant (Heumann, 1993, 2001) (see Section 2.3.4).

Table 7.5.1 gives the mean estimated contributions from rock and soil dust, sea-salt spray and volcanoes both during glacial maxima and interglacials. It should be emphasised that the contributions should be considered as rather tentative, especially for the sea-salt spray and volcanoes contributions. This is for instance obvious for the sum of the three different natural contributions does not give 100%, sometimes we get less than 100% and sometimes much more than 100%.

For glacial maxima, it appears clearly that rock and soil dust explains virtually 100% of Cu, Zn and Pb measured in Dome C ice, and part of Bi, while this contribution appears to be rather small for As and Cd. Sea-salt spray contribution is always extremely small. Contribution from volcanoes could explain entirely Bi and Cd in the ice and could be a significant contributor for As (see **Table 7.5.1**).

During interglacials, rock and soil dust remains a major source of Zn and Pb and minor source of Cu and Bi. Sea-salt spray contribution remains negligible. Volcanoes could be the main source of

As, Cd and Bi, and to a lesser extent of Cu (see **Table 7.5.1**). The conclusion that Bi might derived mainly from volcanoes would be in good agreement with the indication by Patterson and Settle (1987) that volcanic emissions of Bi to the atmosphere are by far the predominant source for Bi in the atmosphere during interglacial periods.

	Cu		Zn		As		Cd		Pb		Bi	
	conc	%	conc	%	conc	%	conc	%	conc	%	conc	%
Mean measured concentration in ice during glacial maxima	11		49		11.6		0.6		8		0.16	
Mean natural contribution												
Rock and soil dust[a]	11	99	42	86	1.6	14	0.08	14	8	100	0.1	62
Sea-salt spray[b]	$4x10^{-5}$	<<1[d]	$3x10^{-4}$	<<1[d]	$1x10^{-3}$	<1[d]	$2x10^{-7}$	<<1[d]	$1x10^{-3}$	<1[d]	$4x10^{-5}$	<1[d]
Volcanoes[c]	1	12	3	6	4	32	1.1	>100[e]	0.4	5	0.8	>100[e]
Mean measured concentration in ice during interglacial periods	3.6		22		8.4		0.4		1.1		0.07	
Mean natural contribution												
Rock and soil dust[a]	0.9	23	3.4	60	0.1	1	0.007	2	0.9	87	0.008	11
Sea-salt spray[b]	$1x10^{-6}$	<<1[d]	$2x10^{-5}$	<<1[d]	$1x10^{-4}$	<1[d]	$2x10^{-8}$	<<1[d]	$5x10^{-6}$	<<1[d]	$2x10^{-6}$	<1[d]
Volcanoes[c]	2	40	3.5	16	5	>100[e]	1.4	>100[e]	0.5	48	1	>100[e]

[a] based on metal concentrations in the upper continental crust (Wedepohl, 1995) , see text

[b] contribution calculated from ssNa concentrations in the ice (Wolff et al., 2006) and metal/Na ratio in surface sea water (www.agu.org/eos_elec/97025e-refs.html). We have assumed that there is no enrichment for heavy metals in sea derived aerosols compared with sea water, see text

[c] contribution calculated from nss$S0_4$ concentrations in the ice (Wolff et al., 2006) and metal/S ratio in volcanic emissions (Hinkley et al., 1999), see text

[d] < 1 refers to a percentage which is only slightly lower than 1, <<1 refers to a percentage which is much lower than 1

[e] > 100 refers to a percentage which is higher than 100

Table 7.5.1: *Dome C, East Antarctica: evaluation of the mean contributions from rock and soil dust, sea-salt spray and volcanoes for glacial maxima and interglacial periods, expressed both in concentrations (pg/g) and percentages.*

These changing patterns in the origin of the different metals as a function of climate is further confirmed in **Figure 7.5.1** which shows, as examples, changes in Pb/Ba and As/Ba concentration ratios as a function of Ba concentrations in the ice. The ratios appear to be very different for ice with high Ba concentrations (glacial maxima), and for ice with low Ba concentrations (interglacials). The changes are however less important for Pb/Ba (the rock and soil dust contribution remains important for Pb even during interglacials) than for As/Ba (As appears to derive mainly from volcanic emissions during interglacials, while rock and soil dust contribution is significant for this metal during glacial maxima).

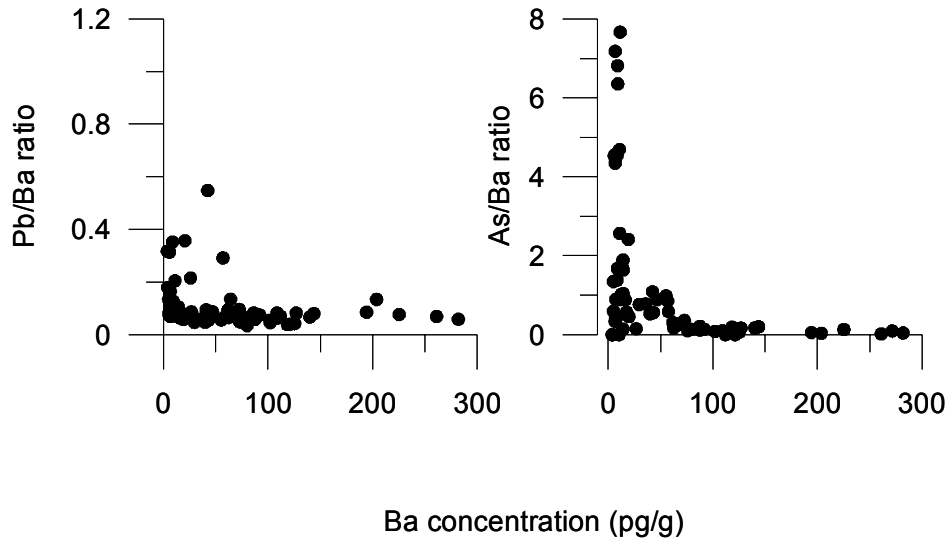

Fig. 7.5.1: *EPICA/Dome C Antarctic ice core: changes in Pb/Ba and As/Ba concentration ratios as a function of Ba concentrations in the ice for the samples dated from 263 to 671 ky BP*

7.6 Principal Components Factor Analyses (PCFA)

Principal components factor analysis (see e.g. Boutron and Martin, 1980 and Toscano et al., 2005) has been performed separately on the data obtained for ice dated from glacial maxima and on the data obtained for ice dated from interglacials. In addition to the six elements considered in our work (Cu, Zn, As, Cd, Pb and Bi), the data sets used for the PCFAs also included Ba, nssSO_4 and ssNa (Wolff et al., 2006). The results are shown in **Figure 7.6.1**, using two dimensional plots with the first two eigen vectors.

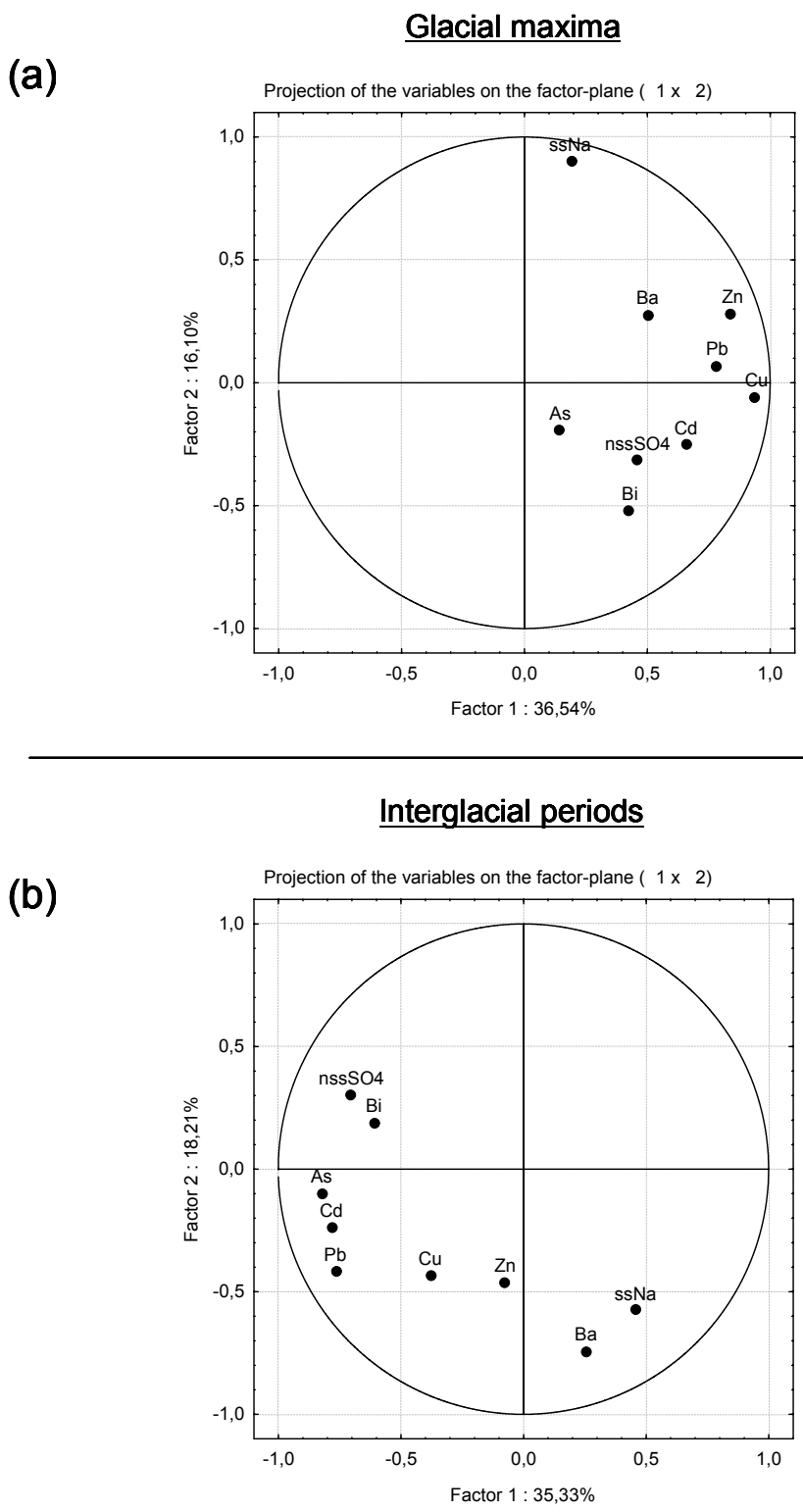

Fig. 7.6.1: *EPICA/Dome C Antarctic core: principal components factor analysis for the samples dated from glacial maxima (a, number of samples: 36) and the samples dated from interglacials (b, number of samples: 36*)

Figure 7.6.1 a shows the results for glacial maxima (total number of samples considered: 36) using the first two eigen vectors (the percentages of variance explained by these two eigen vector are 37 and 16%, respectively). It can be seen that Pb, Zn and Cu fall together with Ba, in good agreement with the conclusion given in Section 7.5 that Pb, Zn and Cu mainly derived from rock and soil dust during glacial maxima. Conversely, As, Cd and Bi are grouped together with $nssS0_4$, suggesting again that volcanic emissions are a possible contributor for these three elements during glacial maxima. ssNa is separated from the other elements, in good agreement with the conclusion that sea-salt spray is not a significant source for heavy metals during glacial maxima.

The situation appears to be different during interglacials, as illustrated in **Figure 7.6.1 b** (total number of samples considered: 36), using the first two eigen vectors (the percentages of variance explained by these two eigen vector are 35 and 18%, respectively). The first eigen vector puts together $nssS0_4$, Bi, As, Cd and Pb, which is in good agreement with the previous suggestions that volcanoes are a significant source of Bi, As, Cd and Pb during interglacials. Cu and Zn are found to be located between $nssS0_4$ and Ba, which is a further indication that these two metals derive both from rock and soil dust and volcanoes.

However, the estimate of the contribution from volcanoes and sea-salt spray was made respectively from the concentrations of non sea-salt sulphate ($nssS0_4$) in the ice and sea-salt sodium (ssNa) measured in different samples where our six elements were determined. It must be kept in mind that variations from one piece of ice to the adjacent one could be very high (especially for ssNa). So, the uncertainty in our proxies could be a major obstacle in the evaluation of the contribution from volcanoes and sea-salt spray.

7.7 Contribution from Antarctic volcanoes

A possible volcanic source within East Antarctica could be the Mount Erebus active volcano (77°33’ S, 161°10’ E, 3794 m above sea level), which is the southernmost active volcano in the world. There have been various studies about emissions of various compound in the persistent volcanic plume which emanates from the summit crater (see e.g. Chuan et al., 1986).

Interest in such measurements came not only from volcanologist wishing to better understand the volcano's behaviour but also from atmospheric scientists trying to establish the sources of natural pollution in the clean Antarctic environment.

Various studies have shown that the Erebus plume is enriched in various heavy metals (see e.g. Kyle et al., 1990 and Zreda-Gostynska et al., 1997). Of special interest are the data obtained by Zreda-Gostynska et al. (1997) for the years 1986 to 1991. They collected plume samples with filters during December 1986, 1988 and 1989 and January 1991. The filters were then analysed by instrumental neutron activation analysis for various trace elements, including several metals considered in our work (Cu, Zn, As and Cd). From their data, they estimated average yearly emission rates for these various elements. The yearly emission rates they found for the four metals considered in our work were 43 metric tons/year (t/y) for Cu, 130 t/y for Zn, 11 t/y for As and 4 t/y for Cd. These values must however be considered with great caution, since the sampling periods were short (for instance, only 5 days in 1986), which makes it very difficult to extrapolate the data over longer time periods.

Zreda-Gostynska et al. (1997) suggested that emissions from Mount Erebus could be transported easily inland over the East Antarctic plateau and could be a major contributor to heavy metals such as Cu, Zn, As and Cd in East Antarctic snow and ice, based on the hypothesis of an homogeneous deposition over the East Antarctic plateau. Their data are however only for very recent periods, and it is impossible to know if such contribution was important during the very long time periods cover by our EPICA/Dome C ice samples. Moreover, it would be necessary to use transport models (see e.g. Cosme et al., 2005) to make quantitative estimates of the deposition patterns over the East Antarctic plateau in order to confirm that emissions from Mount Erebus make a significant contribution to heavy metals in snow and ice in Dome C.

7.8 Ternary diagrams for glacial maxima and interglacials before and after the Mid-Brunhes Event (MBE)

Figure 7.8.1 a, b shows Cu, Zn and Pb concentrations both for glacial maxima (**Figure 7.8.1 a**) and interglacial periods (**Figure 7.8.1 b**) using ternary diagrams (after normalization using Pb concentrations). Different symbols have been used for ice dated before the Mid-Brunhes Event (MBE, about 430 ky BP) and after the MBE.

It can be seen that during glacial maxima the data points are very well grouped together both before and after the MBE, which is consistent with inputs from a single well-defined source for these three elements, namely rock and soil dust (see Section 7.5). For interglacial periods, the situation appears to be different before and after the MBE: the data points are rather dispersed on the ternary plot before the MBE, but are well-grouped together after the MBE. It points towards a more complex input for Cu, Zn and Pb before the MBE.

Figure 7.8.1 c, d show the ternary diagrams for As, Cd and Bi for glacial maxima (**Figure 7.8.1 c**) and interglacials (**Figure 7.8.1 d**), after normalization using Bi concentrations. The data points are found to be strongly dispersed both before and after the MBE, whatever the climatic periods, pointing towards much more complex inputs from several sources.

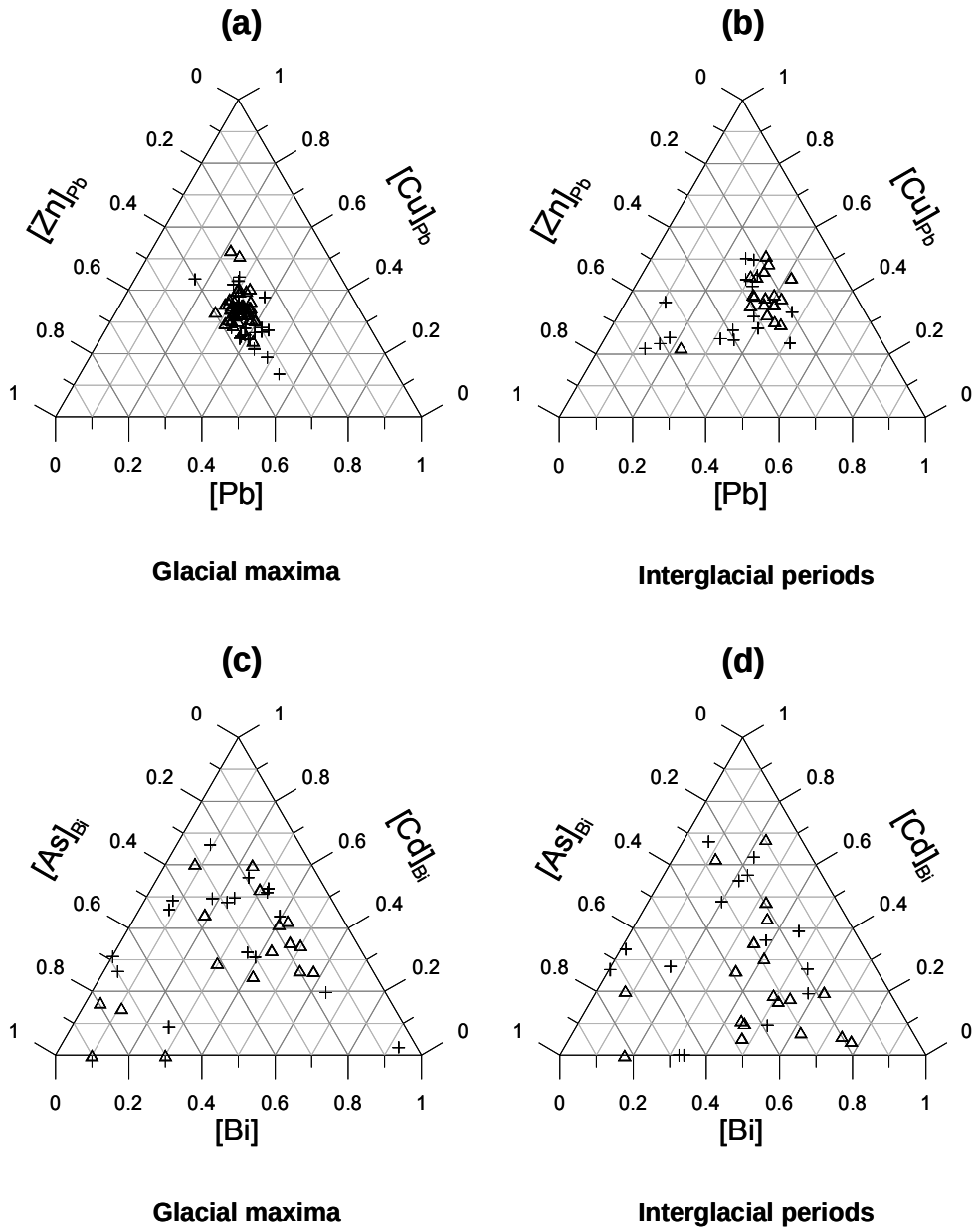

Fig. 7.8.1: *EPICA/Dome C Antarctic ice core: ternary plots for Pb, Cu, and Zn for glacial maxima (a) and interglacials (b) and for Bi, Cd and As for glacial maxima (c) and interglacials (d) Crosses are used for ice samples dated from before the MBE, while open triangles are used for ice dated from after the MBE*

This work has allowed to document large natural variations in heavy metals in Antarctic ice dated back to 671 ky BP (MIS 16.2), with generally elevated concentrations during glacial maxima and much lower values during interglacials. Rock and soil dust appears to be the dominant source for Cu, Zn, Pb and possibly As during glacial maxima, while Cd and Bi appear to derive mainly from volcanoes whatever the period.

It will be interesting in the future to extend this study to the deepest part of the EPICA/Dome C ice core which extends back to MIS 20.2, ~ 800 ky ago. It will also be very interesting to investigate changes in other heavy metals such as Hg and Se (including speciation). Finally, it will be also of high interest to analyse other ice cores which have recently been obtained in other areas in Antarctica, especially in Dronning Maud Land (EPICA Community members, 2006) and at Talos Dome (Stenni et al., 2002).

REFERENCES

Bassinot FC, Labeyrie LD, Vincent E, Quidelleur X, Shackleton NJ, Lancelot Y (1994) The astronomical theory of climate and the age of Brunhes-Matuyama magnetic reversal. *Earth and Planetary Science Letters* **126**, 91-108

Berger A, Loutre M F (2003) Climate 400,000 years ago, a key to the Future? In: Droxler AW, Poore RZ, Burckle LH (eds) *Earth's Climate and Orbital Eccentricity: The Marine Isotopic Stage 11 Question*, American Geophysical Union, pp. 17-26, doi: 10.1029/137GM02

Berger WH, Wefer G (2003) On the dynamics of the ice ages: Stage-11 paradox, Mid-Brunhes climate shift, and 100-ky cycle. In: Droxler AW, Poore RZ, Burckle LH (eds) *Earth's Climate and Orbital Eccentricity: The Marine Isotopic Stage 11 Question*, American Geophysical Union, pp. 41-59, doi: 10.1029/137GM04

Boutron CF, Martin S (1980) Sources of twelve trace metals in Antarctic snows determined by principal component analysis. *Journal of Geophysical Research* **85**, 5631-5638

Boutron CF, Patterson CC (1986) Lead concentration changes in Antarctic ice during the Wisconsin/Holocene transition. *Nature* **323**, 222-225

Boutron CF, Patterson CC, Petrov VN, Barkov NI (1987) Preliminary data on changes of lead concentrations in Antarctic ice from 155,000 to 26,000 years BP. *Atmospheric Environment* **21**, 1197-1202

Chuan RL, Palais J, Rose WI, Kyle PR (1986) Fluxes, sizes, morphology and composition of particles in the Mt. Erebus volcanic plule, december 1983. *Journal of Atmospheric Chemistry* **4**, 467-477

Cosme E, Hourdin F, Genthon C, Martinerie P (2005) Origin of dimethylsulfide, non-sea-salt sulfate, and methanesulfonic acid in eastern Antarctic. *Journal of Geophysical Research* **110**, doi: 10.1029/2004JD004881

Droxler AW, Alley RB, Howard WR, Poore RZ, Burckle LH (2003) Unique and Exceptionally Long Interglacial Marine Isotope Stage 11: Window into Earth Warm Future Climate. In: Droxler AW, Poore RZ, Burckle LH (eds) *Earth's Climate and Orbital Eccentricity: The Marine Isotopic Stage 11 Question*, American Geophysical Union, pp. 1-13, doi: 10.1029/137GM01

EPICA Community members (2004) Eight glacial cycles from an Antarctic ice core. *Nature* **429**, 623-628

Gabrielli P, Barbante C, Boutron C, Cozzi G, Gaspari V, Planchon F, Ferrari C, Turetta C, Hong S, Cescon P (2005a) Variations in atmospheric trace elements in Dome C (East Antarctica) ice over the last two climatic cycles. *Atmospheric Environment* **39**, 6420-6429

Gabrielli P, Planchon FAM, Hong S, Lee KH, Hur SD, Barbante C, Ferrari CP, Petit JR, Lipenkov VY, Cescon P, Boutron CF (2005b) Trace elements in Vostok Antarctic ice during the last four climatic cycles. *Earth and Planetary Science Letters* **234**, 249-259

Heumann KG (1993) Determination of inorganic and organic traces in the clean room compartment of Antarctica. *Analytica Chimica Acta* **283**, 230-245.

Heumann KG (2001) Biomethylation in the Southern Ocean and its contribution to the geochemical cycle of trace elements in Antarctica. In: Caroli S, Cescon P, Walton D (eds) *Environmental Contamination in Antarctica: a challenge to analytical chemistry*. Elsevier, Amsterdam, pp. 181-218

Hinkley TK, Lamothe PJ, Wilson SA, Finnegan DL, Gerlach TM (1999) Metal emissions from Kilauea, and a suggested revision of the estimated worldwide metal output by quiescent degassing of volcanoes. *Earth and Planetary Science Letters* **170**, 315-325

Hong S, Candelone JP, Patterson CC, Boutron CF (1994) Greenland ice evidences of hemispheric pollution for lead two millennia ago by Greek and Roman civilizations. *Science* **265**, 1841-1843

Hong S, Kim Y, Boutron CF, Ferrari CP, Petit JR, Barbante C, Rosman K, Lipenkov VY (2003) Climate-related variations in lead concentrations and sources in Vostok Antarctic ice from 65,000 to 240, 000 years BP. *Geophysical Research Letters* **22**, 2138, doi: 10.1029/2003GL018411

Hong S, Boutron CF, Gabrielli P, Barbante C, Ferrari CP, Petit JR, Lee K, Lipenkov VY (2004) Past natural changes in Cu, Zn and Cd in Vostok Antarctic ice dated back to the penultimate interglacial period. *Geophysical Research Letters* **31**, L20111, doi: 10.1029/2004GL021075

Hong S, Boutron CF, Barbante C, Hur SD, Lee K, Gabrielli P, Capodaglio G, Ferrari CP, Turetta C, Petit JR, Lipenkov VY (2005) Glacial-interglacial changes in the occurence of Pb, Cd, Cu and Zn in Vostok Antarctic ice from 240 000 to 410 000 years BP. *Journal of Environmental Monitoring* **7**, 1326-1331

Hunter KA (1997) Chemistry of the sea-surface microlayer. In: Liss PS, Duce RA

(eds) *The sea surface and global change.* Cambridge University Press, Cambridge, pp. 287-319

Kyle PR, Meeker K, Finnegan D (1990) Emission rates of sulphur dioxide, trace gases and metals from Mount Erebus, Antarctica. *Geophysical Research Letters* **17**, 2125-2128

Ng A, Patterson CC (1981) Natural concentrations of lead in ancient Arctic and Antarctic ice. *Geochimica et Cosmochimica Acta* **45**, 2109-2121

Nriagu JO (1989) A global assessment of natural sources of atmospheric trace metals. *Nature* **338**, 47-49

Nriagu JO (1990) The rise and fall of leaded gasoline. *Science of the Total Environment* **92**, 13-28

Nriagu JO, Pacyna JM (1988) Quantitative assessment of worldwide contamination of air, water and soils by trace metals. *Nature* **333**, 134-139

Pacyna JM, Pacyna EG (2001) An assessment of global and regional emissions of trace metals to the atmosphere from anthropogenic sources worldwide. *Environmental Reviews* **9**, 269-298

Patterson CC, Settle DM (1976) The reduction of orders of magnitude errors in lead analysis of biological materials and natural waters by evaluating and controlling the extent and sources of industrial lead contamination introduced during sample collection and analysis. . In: La Fleur P (ed) *Accuracy in Trace analysis*. Nat. Bur. Stand., Washington DC, Spec. Pub. **422**, pp 321-351

Patterson CC, Settle DM (1987) Magnitude of lead flux to the atmosphere from volcanoes. *Geochimica et Cosmochimica Acta* **51**, 675-681

Petit JR, Jouzel J, Raynaud D, Barkov NI, Barnola JM, Basile I, Bender M, Chappellaz J, Davis M, Delaygue G, Delmotte M, Kotlyakov VM, Legrand M, Lipenkov VY, Lorius C, Pépin L, Ritz C, Saltzman E, Stievenard M (1999) Climate and atmospheric history of the past 420,000 years from the Vostok ice core, Antarctica. *Nature* **399**, 429-436

Planchon F, Van de Velde K, Rosman KJR, Wolff EW, Ferrari CP, Boutron CF (2003) One hundred fifty-year record of lead isotopes in Antarctic snow from Coats Land. *Geochemica et Cosmochemica Acta* **67**, 693-708

Raymo ME, Oppo DW, Curry W (1997) The mid-Pleistocene climate transition: a deep-sea carbon isotopic perspective. *Paleoceanography* **12**, 546-559

Stenni B, Proposito M, Gragnani R, Flora O, Jouzel J, Falourd S, Frezzotti M (2002) Eight centuries of volcanis signal and climate change at Talos Dome (East Antarctica). *Journal of Geophysical Research* **107**, doi: 10.1029/2000JD000317

Toscano G, Gambaro A, Moret I, Capodaglio G, Turetta C, Cescon P (2005) Trace metals in aerosol at Terra Nova Bay, Antarctica. *Journal of Environmental Monitoring* **7**, 1275-1280

Vallelonga P, Gabrielli P, Rosman K, Barbante C, Boutron CF (2005) A 220 ky record of Pb isotopes at Dome C Antarctica from analyses of the EPICA ice core. *Geophysical Research Letters* **32**, L01706

Von Storch H, Costa-Cabral M, Hagner C, Feser F, Pacyna J, Pacyna E, Kolb S (2003) Four decades of gasoline lead emissions and control policies in Europe: a retrospective assessment. *Science of the Total Environment* **311**, 151-176

Wedepohl KH (1995) The composition of the continental crust. *Geochimica et Cosmochimica Acta* **59**, 1217-1232

Wilson SJ, Steenhuisen F, Pacyna JM, Pacyna EG (2006) Mapping the spatial distribution of global anthropogenic mercury atmospheric emission inventories. *Atmospheric Environment* **40**, 4621-4632

Wolff EW, Fischer H, Fundel F, Ruth U, Twarloh B, Littot GC, Mulvaney R, Röthlisberger R, de Angelis M, Boutron CF, Hansson M, Jonsell U, Hutterli MA, Lambert F, Kaufmann P, Stauffer B, Stocker TF, Steffensen JP, Bigler M, Siggaard-Andersen ML, Udisti R, Becagli S, Castellano E, Severi M, Wagenbach D, Barbante C, Gabrielli P, Gaspari V (2006) Southern Ocean sea-ice extent, productivity and iron flux over the past eight glacial cycles. *Nature* **440**, 491-496

Zheng J, Shotyk W, Krachler M, Fisher DA (2007) A 15,800-year record of atmospheric lead deposition on the Devon Island ice cap, Nunavut, Canada: natural and anthropogenic enrichments, isotopic composition, and predominant sources. *Global Biogeochemical Cycles* **21**, GB2027, doi:10.1029/2006GB002897

Zreda-Gostynska G, Kyle PR, Finnegan B, Prestbo KM (1997) Volcanic gas emissions from Mount Erebus and their impact on the Antarctic Environment. *Journal of Geophysical Research* **102**, 15,039-15,055

Chapter 8- CRUSTAL TRACE ELEMENTS PROVENANCE THROUGH THE REE SIGNATURE FROM 263 TO 671 KY BP IN THE EPICA/DOME C ICE CORE

In order to predict the future trend of global climate change, the whole mechanism of natural climate variations must be understood. Natural climate and trace constituents archives such as annual tree rings, corals, sediments or polar ice sheets, serve as an indirect source for information at long time scales. However, the polar ice sheets are the only archive preserving information about changes both in climate and in the atmosphere's composition.

Studies of ice cores place great demands on sampling, sample preparation and the analytical technique owing to the low concentrations level of Rare Earth Elements (REE) and the high risk of contamination. The impetus in the field came from the pioneering work of Patterson, Boutron and co-workers who developed sophisticated methods to decontaminate deep polar ice cores drilled in fluid-filled holes, which allowed for reliable data for trace elements in these cores to be obtained (Ng and Patterson, 1981; Boutron et al., 1987). In recent years a direct method based on inductively coupled plasma sector field mass spectrometry (ICP-SFMS) coupled with a micro-flow nebulizer and a desolvatation system has been successfully applied in the Department of Environmental Sciences, Venice, Italy to determine La, Ce, Pr, Nd, Sm, Eu, Gd, Tb, Dy, Ho, Er, Tm, Yb and Lu down to the sub-pg/g level (1pg/g = 10^{-12} g g^{-1}) in ice core samples (Gabrielli et al., 2006) (see sections 5.3.1 and 5.3.2).

The REE have been widely used to understand the formation of the major Earth reservoirs (crust-mantle), the origin of volcanic rocks, the sedimentary systems and processes in oceanography (e.g., Hanson, 1980; Elderfield and Greaves, 1982; Hofmann et al., 1984; Taylor and McLennan, 1985). Measurement of precise Sm, Nd, Lu and Hf concentrations also underpins two important isotopic systems (Sm-Nd and Lu-Hf) that are used to date geological samples.

The purpose of this chapter is to present the first dataset of REE (La, Ce, Pr, Nd, Sm, Eu, Gd, Tb, Dy, Ho, Er, Tm, Yb and Lu) in the EPICA/Dome C ice core during the period from 263 ky BP to 671 ky BP and to extract characteristic features from them. Until now, the reconstruction of past atmospheric REE changes was restricted to an ombotrophic peat bog profile (Krachler et al.,

2003), Arctic snow samples (Kriews et al., 1995; Kriews and Schrems, 1995), Antarctic snow samples (Ikegawa et al., 1999) and Greenland ice core samples (NGRIP) (Reinhardt et al., 2003). Increasing attention has recently been paid for the chemistry of REE in polar ice core, because the REE content of atmospheric particulate matter will reflect the characteristics of the original site of provenance (Henderson, 1984). During glacial maxima, continental shelves of coastal areas are dry owing to lower ocean levels. As a result of higher erosion more mineral dust is released. During interglacials, the shelves are covered with water and thus sea salt concentration in ice core analysed increases. The analysis of REE patterns (element concentrations and ratios) may give hints about the origin of sources.

8.1 Concentrations in Antarctic ice back from 263 to 671 ky BP

Rare Earth Elements concentrations measured in 77 depth intervals from 2368.6 to 3061.9m are listed in Appendix II, Table IV. RareEarth Elements (REE) can be divided in three groups of elements: Light Rare Earth Elements (La to Nd); Middle Rare Earth Elements (MREE; Sm to Tb) and Heavy Rare Earth Elements (HREE; Er to Lu). **Figure 8.1.1** shows that there is a high variability in concentrations from 263 to 671 ky BP, with generally high values during cold periods and low values during warm periods (see **Table 8.1.1**).

Concentrations are within the sub-pg/g and the pg/g level, ranging between 0.003 and 0.4 pg/g for Tm and up to 0.4 and 65 pg/g for Ce in our samples, which is in good agreement with the previous results found by Gabrielli et al. (2006) for the period from 14 to 207 ky BP in the EPICA/Dome C ice core.

Rare Earth Element	Concentration (pg/g) from 263 to 671 ky (Dome C ice)		Concentration (pg/g) from 14 to 207 ky (Dome C ice)[a]	
	Min	Max	Min	Max
La	0.2	30.5	0.39	22
Ce	0.4	64.9	0.9	60
Pr	0.03	7.5	0.11	7.1
Nd	0.10	26.2	0.5	25
Sm	0.04	6.2	0.1	5.7
Eu	0.01	1.3	0.01	1.3
Gd	0.02	5.8	0.11	5
Tb	0.003	0.8	0.01	0.7
Dy	0.01	4.4	0.06	3.9
Ho	0.003	0.8	0.011	0.74
Er	0.01	2.2	0.03	2.0
Tm	0.002	0.3	0.004	0.3
Yb	0.009	1.8	0.03	1.7
Lu	0.001	0.2	0.01	0.23

[a] Gabrielli et al. (2006)

Table 8.1.1 : *Minimum and maximum of concentrations of REE in the EPICA/Dome C ice core determined in 13 samples from 14 to 207 ky BP and in 77 samples from 263 to 671 ky BP*

For all the REE, five main sharp maxima are observed around ~ 274, 365, 432, 538 and 671 ky BP at the time of particularly cold periods characterized by very low δD values, **Figure 8.1.1**. They correspond to marine isotopic stage 8.2, 10.4, 12.2, 14.2 and 16.2 respectively, **Figure 8.1.1**. Conversely, very low concentrations are observed during warmer periods, characterized by less negative δD values. These variations seem to follow the variations of insoluble dust (EPICA community members, 2004).

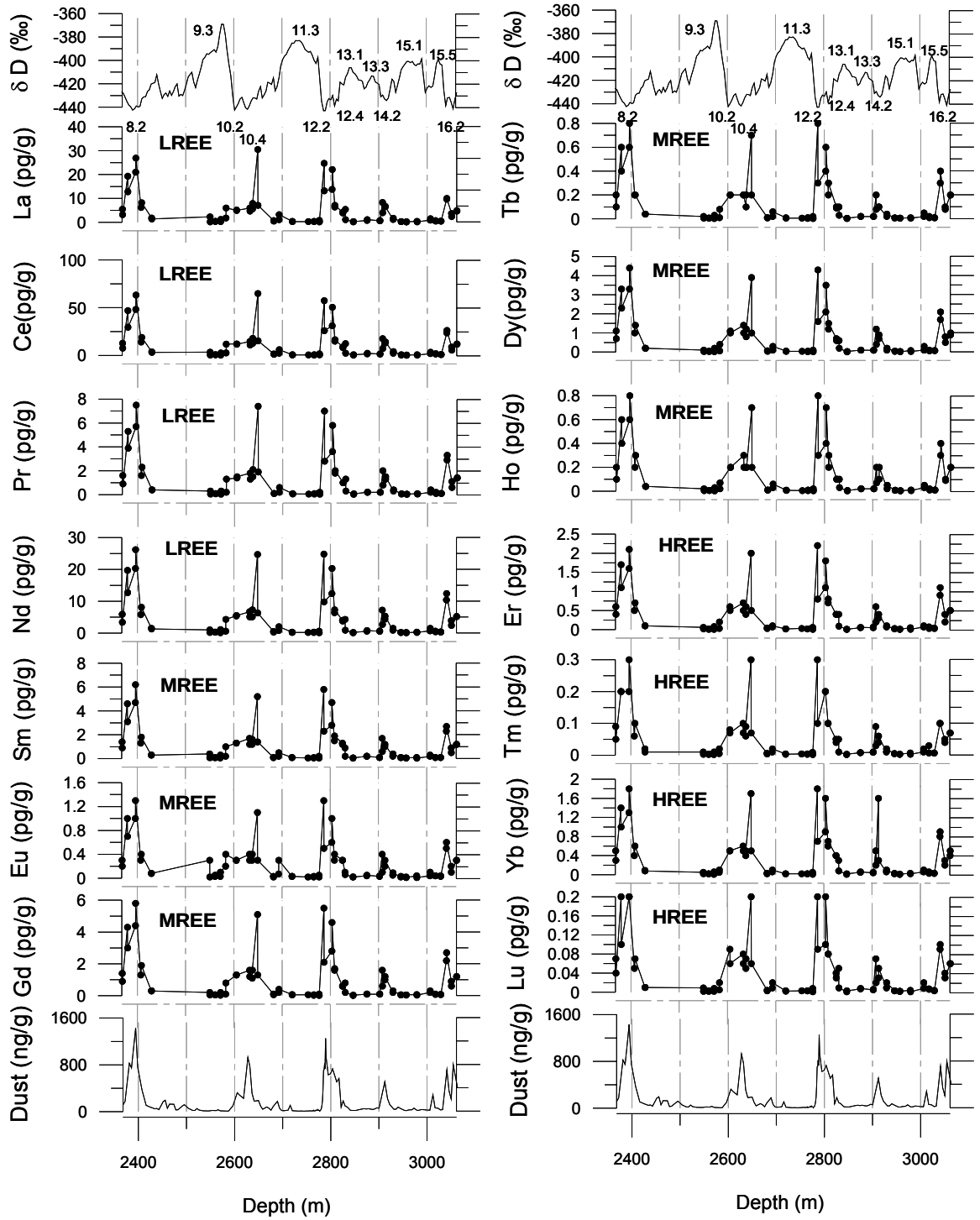

Fig. 8.1.1: *EPICA/Dome C Antarctic ice core: changes in concentrations of LREE, MREE and HREE as a function of depth from 2368.6 m to 3061.9 m (263 to 671 ky BP). Also shown at the top of the figure are the variations in deuterium concentrations (expressed in delta per mil) (EPICA Community members, 2004), Marine Isotope Stages (MIS) numbers (Bassinot et al., 1994), and at the bottom of the figure changes in dust concentrations (expressed in ng/g) (EPICA Community members, 2004).*

8.2 Comparison with dust concentration

Figure 8.2.1 gives a comparison between LREE, MREE and HREE and dust content in the EPICA Dome C ice core from MIS 8.2 to MIS 16.2. Dust data are from by EPICA Community members (2004). The mean rare earth element concentration values are given for each geological time in comparison to the mean values of dust content for the same period (see **Table 8.2.1**). All REE (light, middle and heavy) show a good correlation with the dust content. It is assumed that REE derived from the continental dust.

MIS	8.2	9.3	10.2	10.4	11.3	12.2	12.4	13.1	13.3	14.2	15.1	15.5	16.2
Dust (ng g^{-1})	687.1	16.0	233.5	669.2	20.3	756.1	603.3	23.8	45.8	348.1	22.5	31.7	426.0
Measured isotope													
^{139}La	14	1.5	5	5	0.8	13	18	0.3	3	7	0.3	0.5	6
^{140}Ce	32	3	12	13	1.7	26	41	0.6	5	14	0.5	1.0	16
^{141}Pr	4	0.3	1.5	2	0.2	3	5	0.05	0.6	1	0.05	0.1	2
^{144}Nd	13	1.0	5	6	0.5	10	16	0.2	2.1	5	0.2	0.4	7
^{152}Sm	3	0.3	1.3	1.4	0.2	2	4	0.06	0.5	1.1	0.07	0.1	2
^{151}Eu	0,7	0.1	0.3	0.3	0.06	0.5	0.8	0.02	0.18	0.3	0.02	0.04	0.4
^{155}Gd	5	1.5	2.2	2.4	0.22	4	4	0.3	0.6	1.6	0.08	0.30	2.5
^{159}Tb	0.4	0.02	0.2	0.2	0.02	0.3	0.5	0.004	0.06	0.1	0.007	0.01	0.2
^{164}Dy	2	0.1	1.1	1.2	0.09	2	3	0.02	0.3	0.8	0.04	0.07	1.3
^{165}Ho	0.4	0.02	0.2	0.2	0.02	0.3	0.5	0.005	0.06	0.1	0.006	0.01	0.2
^{166}Er	1.1	0.05	0.6	0.6	0.05	0.8	1.5	0.01	0.2	0.4	0.02	0.04	0.7
^{169}Tm	0.2	0.007	0.08	0.09	0.007	0.1	0.2	0.002	0.03	0.05	0.004	0.007	0.09
^{172}Yb	1.0	0.05	0.5	0.5	0.04	0.7	1.3	0.01	0.2	0,5	0.02	0.03	0.6
^{175}Lu	0.1	0.006	0.07	0.07	0.006	0.09	0.2	0.002	0.02	0.04	0.002	0.004	0.07
^{232}Th	4	0,4	1.06	1.1	0.3	4	6	0.1	0.7	1.8	0.07	0.1	1.8

Table 8.2.1 : *Comparison of REE average values obtained by ICP-SFMS with dust average values given (EPICA community members, 2004) in the respective geological interval.Element concentration given in pg/g*

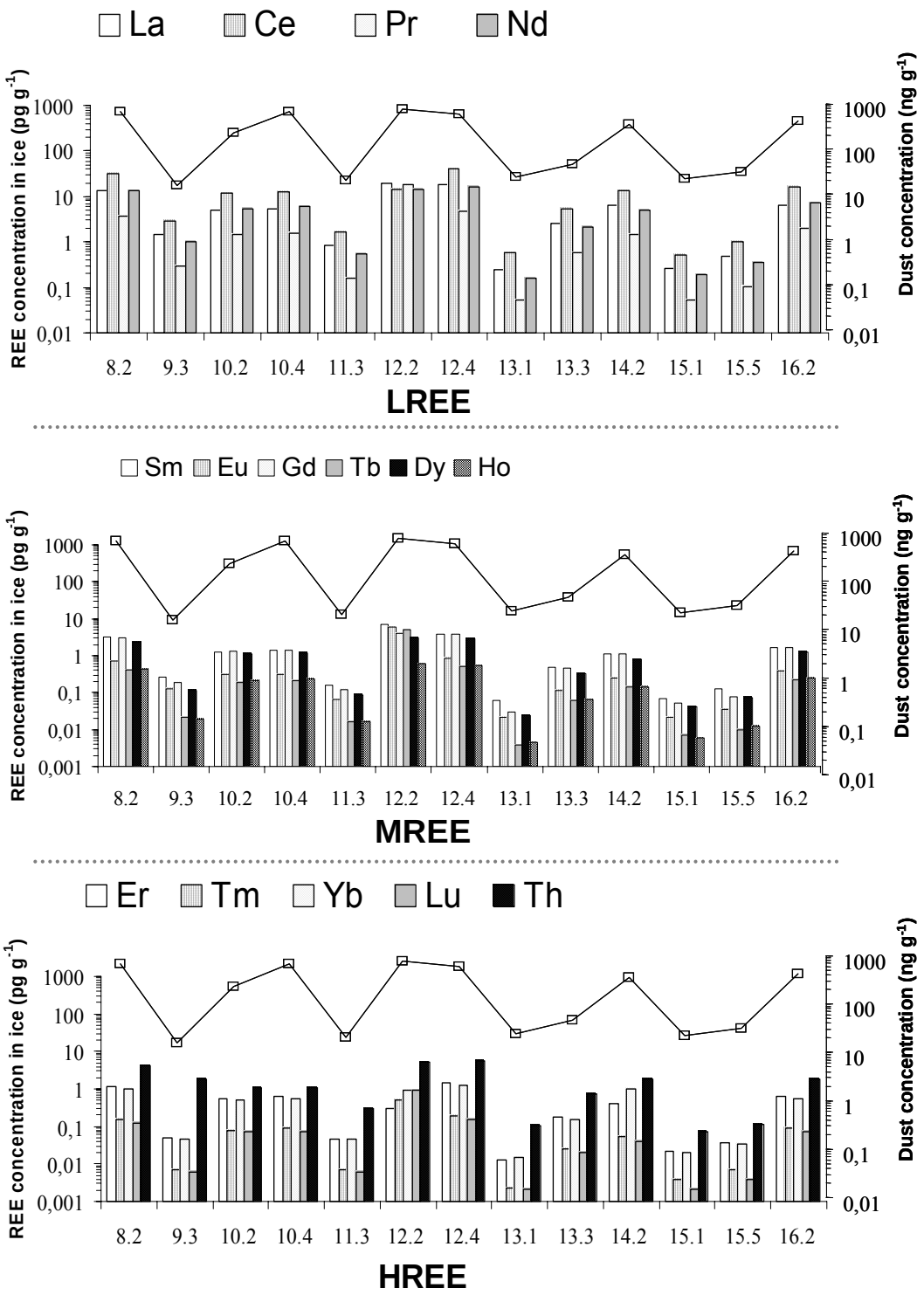

Fig. 8.2.1 : *Comparison of REE average values obtained by ICP-SFMS and dust values (EPICA Community members, 2004) in same geological interval (a) Light Rare Earth Elements (b) middle Rare Earth Elements (c) Heavy Rare Earth Elements. A logarithmic scale is used for the both ordinates. Concentrations are expressed in pg/g for REE and in ng/g for dust. On left side the element concentration is expressed unsing bar plot whilst black open rectangles illustrate the appropriate dust concentration*

Coefficients of correlation (R^2) over 77 samples were obtained by linear regression of element concentration versus Ba concentration, i.e Ba is considered like a good proxy of the continental crust (see section 7.4). Ba concentrations were analysed in the same samples that measurements realized for REE. As listed in **Table 8.2.2**, all REE show R^2 between 0.8 and 1. Interestingly, this is about the range observed for crustal elements such as Rb and U (section 6.3) giving support for Rare Earth Elements being derived from the continental dust. Conversely, Cd shows different behaviour from a geochemical point of view. Like it was already demonstrated (section 7.5), this behaviour could be linked to another origin than the rock and soil dust, like volcanism.

However, I can notice that MREE (except Eu) and HREE show a close link ($R^2 > 0.9$) with dust materials than LREE ($0.8 < R^2 < 0.9$). Smith et al. (2003) have shown that LREE could reflect the influence of volcanic source regions whilst MREE and HREE might reflect the varying importance of the provenance relative to contributions from old continental crustal material.

Element	R^2
Rb	0.9413
U	0.8364
Cd	**0.0593**
La (LREE)	0.8312
Ce (LREE)	0.8585
Pr (LREE)	0.8732
Nd (LREE)	0.8867
Sm (MREE)	0.8800
Eu (MREE)	0.8514
Gd (MREE)	0.9059
Tb (MREE)	0.9193
Dy (MREE)	0.9243
Ho (MREE)	0.9253
Er (HREE)	0.9225
Tm (HREE)	0.9170
Yb (HREE)	0.9172
Lu (HREE)	0.9217
Th (HREE)	0.9017

Table 8.2.2 : *Coefficients of correlation (R^2) obtained by linear regression of REE concentrations versus Ba concentration. Comparison between REE, some typical crustal trace elements (Rb and U) and Cd, which is derived mainly from volcanoes whatever the period*

The idea that REE derived from continental crust was supported by prior measurements of REE and dust in the particulate and soluble phase of Arctic snow samples (Spitzbergen) (Kriews et al., 1995; Kriews and Schrems, 1995), East Antarctic snow samples (Ikegawa et al., 1999) (oversnow traverse along a 2200 km route in East Queen Maud Land in East Antarctica, included the Dome Fuji Station) and Greenland ice core samples (NGRIP) (Reinhardt et al., 2003).

During glacial times, generally cold and dry conditions prevailed on land, with consequent reduction of the total forested area, expansion of grass-dominated vegetation areas (Tegen et al., 2002), and increase of exposed fine-grained lacustrine material due to lake level decrease. In parallel, the hydrological cycle was reduced (Yung et al., 1996) and steeper latitudinal thermal gradients led to generally more vigorous atmospheric circulation (Kohfeld and Harrison, 2001). All these factors contributed to accentuate the global atmospheric dustiness during glacial times. That is why the concentration of atmospheric REE trapped in EPICA/Dome C ice in glacial periods was considerably higher in glacial periods compared to warmer interglacial periods.

8.3 Shale-normalized REE pattern

For this review, two REE normalizing schemes are used: average chondritic meterorites and upper continental crust UCC. The average chondritic REE pattern is likely parallel to primordial abundances in the solar nebula and is also parallel to bulk earth abundances (Mc Lennan, 1989). The values adopted here are from Anders and Grevesse (1989). UCC is convenient for normalizing since the REE pattern of average shale is thought to be parallel to the average UCC. The values adopted here are from Wedephol (1995).

In the following discussion, Eu is commonly enriched (positive Eu anomaly) or depleted (negative Eu anomaly) relative to other REE on chondrite-normalized pattern and UCC-normalized pattern. This can be quantified by the term Eu/Eu*, where Eu* is the expected Eu value for a smooth chondrite-normalized or UCC-normalized REE pattern, such that:

$$Eu/Eu^* = Eu_N / (Sm_N \times Gd_N)^{0.5}$$

Values < 1.0 indicate negative Eu anomalies; values > 1.0 indicate positive Eu anomalies. Because of differing crustal histories, Archean sedimentary rocks usually have positive Eu anomalies, but post-Archean sedimentary rocks typically have negative Eu anomalies. In post-Archean sedimentary rocks, typical Eu/Eu* values range from 0.6 to just under 1.0 (McLennan, 1989).

Figure 8.3.1 shows a chondrite-normalized REE pattern (Anders and Grevesse, 1989) for the 77 samples of the EPICA/Dome C ice core, from 263 to 671 ky BP. Generally, both during glacial maxima and interglacials, all samples are characterized by enriched LREE patterns, negative europium anomalies (range from 0.64 to 0.75 during interglacial periods and from 0.65 to 0.82 during glacial maxima) and relatively flat HREE trends. Smith et al. (2003) have already shown a very similar pattern to the average UCC and some Argentinean loess samples. Furthermore, the patterns are generally consistent with loess deposits from other regions of the world like in China (Gallet et al., 1996; Jahn et al., 2001; Ding et al., 2001; Gallet et al., 1998) (**Figure 3.5.2.1**, section 3.5.2). Consequently, I can argue that EPICA/Dome C ice samples from 263 to 671 ky BP show typical UCC compositions on REE plots (**Figure 8.3.1**).

.

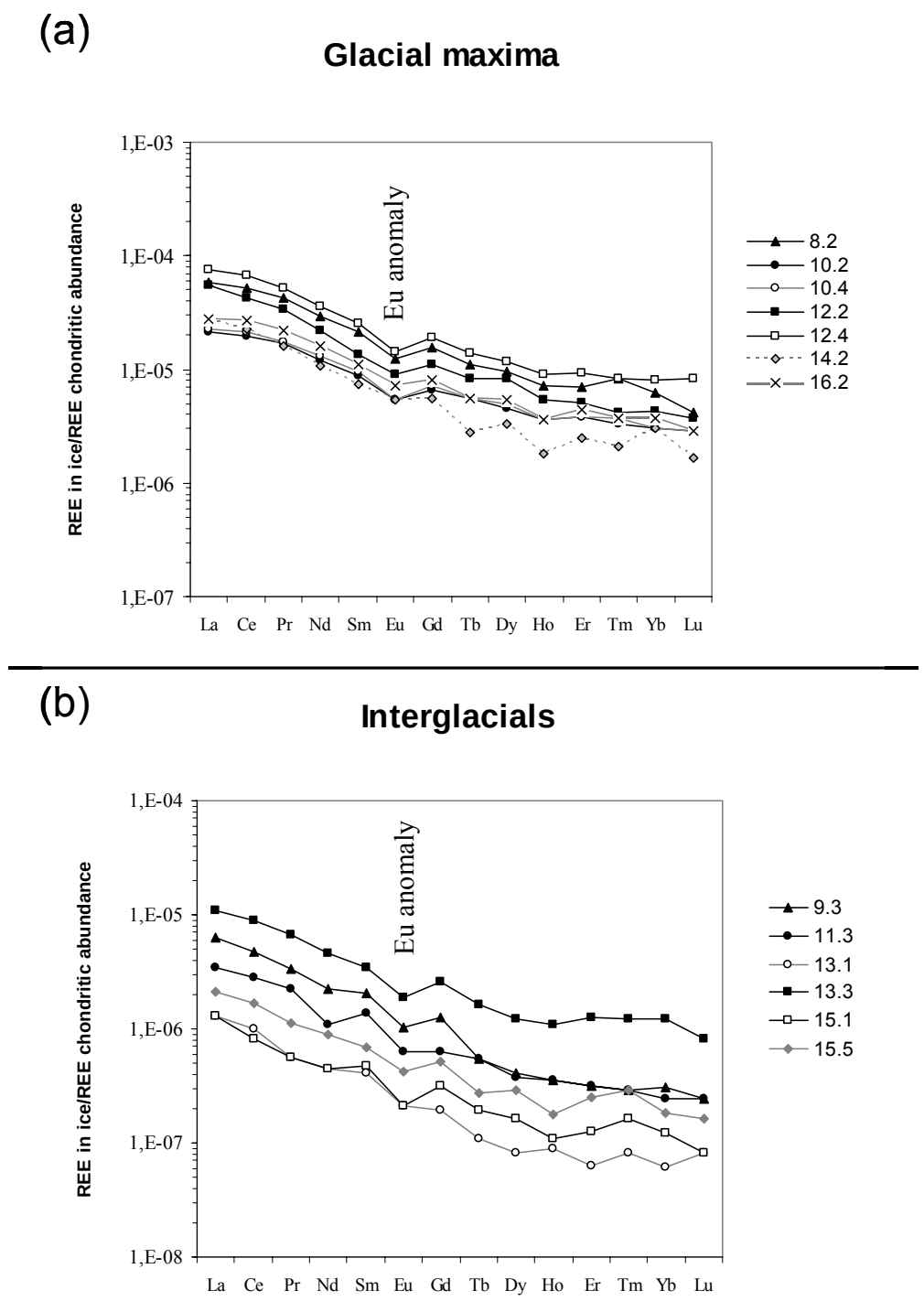

Fig. 8. 3.1 : *Mean REE patterns normalized to the chondritic abundance (Anders and Grevesse, 1989) for various Marine Isotopic stages during glacial maxima (a) and interglacials (b).*

Accordingly to the previous results, REE distributions can be considered as an index to average provenance compositions of the upper continental crust and thus it is important to normalize REE to the upper continental crust with the values given by Wedepohl (1995).

After REE are normalized to UCC, we can notice different UCC-normalized REE patterns between glacial maxima and interglacial periods (see **Figure 8.3.2**).

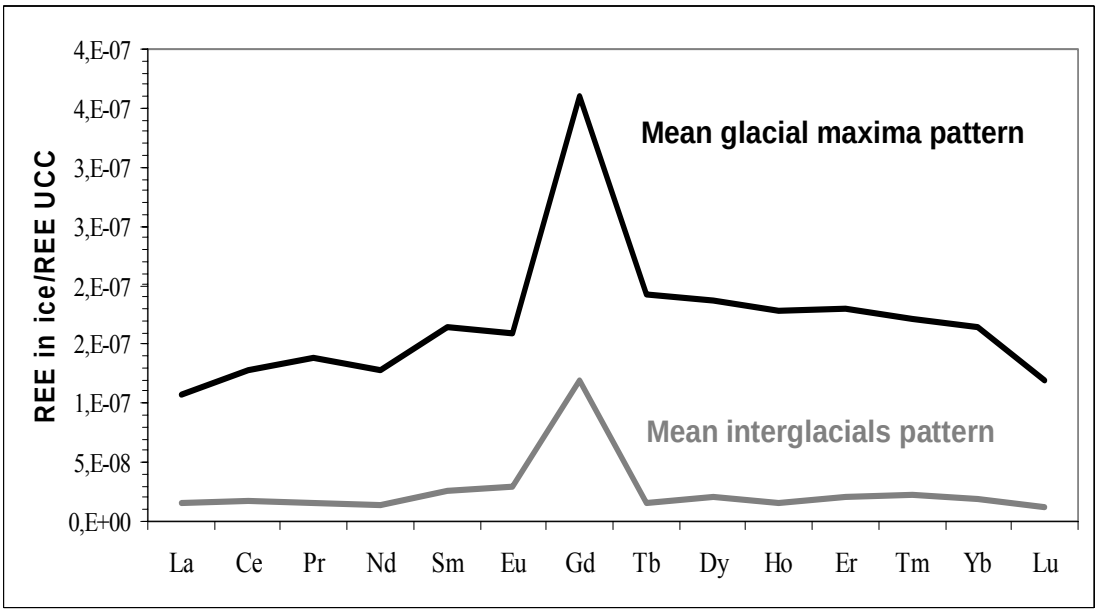

Fig. 8. 3.2 : *Mean REE patterns normalized to the upper continental crust (Wedepohl, 1995) for glacial maxima and interglacials.*

Figure 8.3.3 shows the mean composition of REE normalized to the upper continental crust (REE_{UCC}) (Wedepohl, 1995) during various glacial maxima (**Figure 8.3.3. a**) and interglacials (**Figure 8.2.3 b**).

When using REE in sedimentary geochemistry, it is helpful to reduce the data to certain key elemental ratios that give a quantitative measure of parts of the REE suite. Two measures of REE composition reflect abundances of MREE and HREE. Yb/La_{UCC} is a measure of the overall enrichment of HREE, where $Yb/La_{UCC} > 1$ reflects HREE enrichment (<1 depletion). Sm/La_{UCC}

is a measure of overall enrichment of MREE, where Sm/La_{UCC} >1 indicate enrichment of the MREE (<1 depletion).

Figure 8.3.3. a indicates a similar pattern for all the samples during glacial maxima when REE concentrations are normalized to their crustal abundance. This figure shows that the mean REE for glacial maxima have a minor MREE and HREE enrichment (mean $MREE/LREE_{UCC}$ (Sm/La) = 1.31; mean $HREE/LREE_{UCC}$ (Yb/La) = 1.33). Although REE interglacial results seem to differ slightly from one interglacial to the next one, **Figure 8.3.3 b** shows a trend which can be depicted by a minor enrichment of MREE and a minor depletion of HREE (mean $MREE/LREE_{UCC}$ = 1.29; mean $HREE/LREE_{UCC}$ = 0.90) for all interglacial samples.

These differences of behaviour between REE glacial maxima and REE interglacial results normalized to the upper continental crust could be explained by changes in the characteristics of continental dust arriving at Dome C, such as source area or transport parameters. However, patterns of Rare Earth Elements generally reflect the average compositions of the provenance. Thus, a change in the source mixing between glacial and interglacial times could explain the difference observed between REE glacial maxima and interglacial results.

In the recent past, it was demonstrated that Patagonia and Buenos Aires region can be considered like a possible source of dust during glacial maxima and interglacial periods. Regardless of differing concentrations, the pattern of REE_{UCC} (normalized to the upper continental crust) composition of ice core dust samples from Vostok and Dome C in East Antarctica (Grousset et al., 1992; Basile et al., 1997) matched reasonably well with the mean pattern of REE_{UCC} composition of Patagonian aeolian dust and the Buenos Aires loess (Gaiero et al., 2004) during the Holocene and various glacial stages (2, 4 and 6). Moreover, Gaiero et al. (2004) have analysed REE compositions of the most abundant igneous rock outcropping in Patagonia and link their work with studies from Grousset et al. (1992) and Basile et al. (1997). During glacial maxima and interglacials, it was demonstrated that patterns from Vostok and EPICA/Dome C ice core are strikingly similar to those shown for older (Tryassic) and more evolved (Jurassic) silicic rocks forming the Patagonian upper crust.

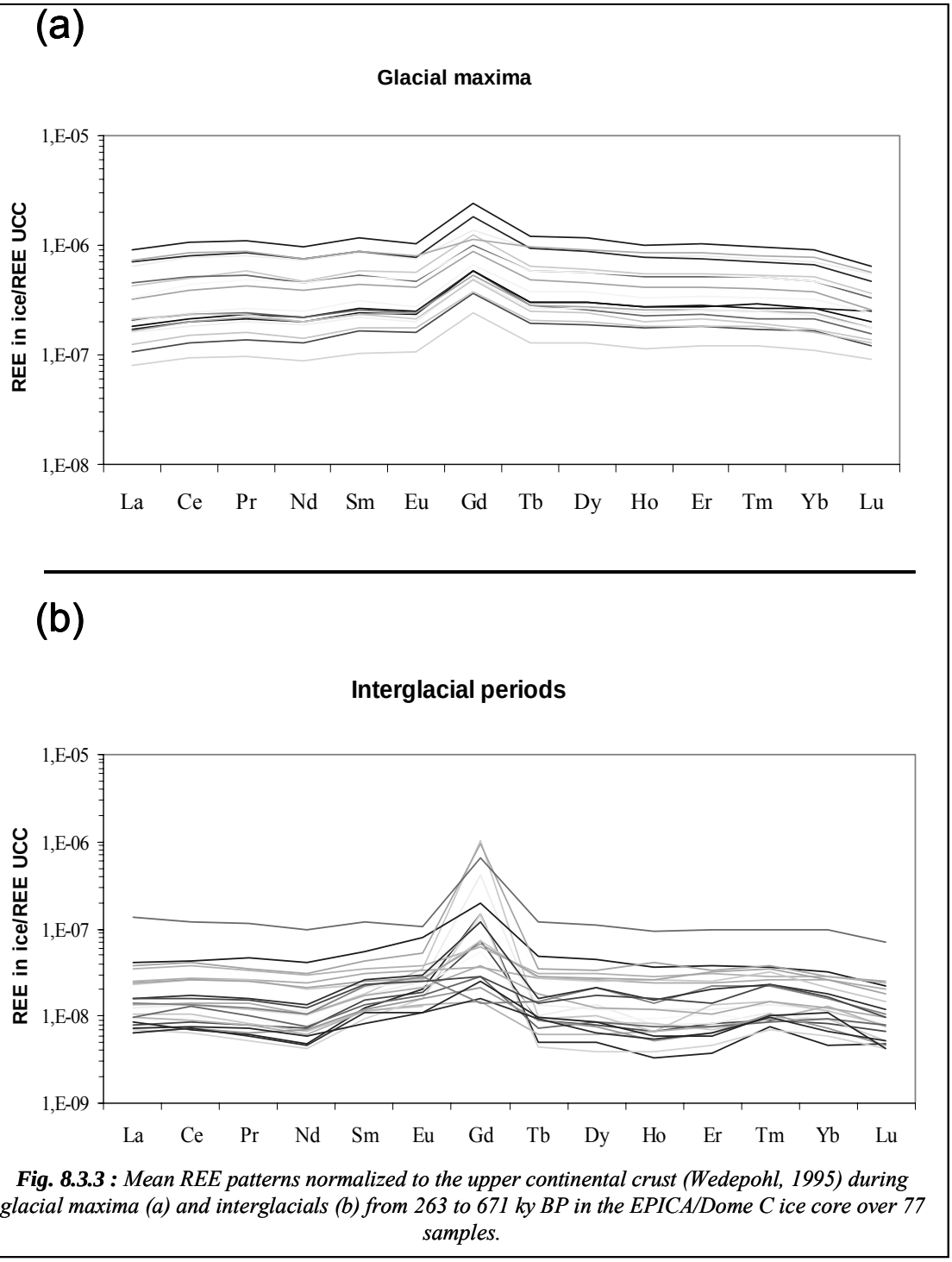

Fig. 8.3.3 : *Mean REE patterns normalized to the upper continental crust (Wedepohl, 1995) during glacial maxima (a) and interglacials (b) from 263 to 671 ky BP in the EPICA/Dome C ice core over 77 samples.*

8.4 Comparison of REE_{UCC} from the EPICA/Dome ice core during glacial maxima with REE_{UCC} from potential source areas (PSAs)

Grousset et al. (1992) and Basile et al. (1997) recognized that during Late Pleistocene glacial events (stages 2, 4 and 6), Patagonia was a source of wind-blown deposits on East Antarctica. For convenience, Basile et al. (1997) used the term Patagonia to refer to the whole southern South America desert/arid/semi-arid continental areas East of the Andes.

In **Figure 8.4.1**, the REE_{UCC} of glacial samples (MIS 8.2 to MIS 16.2) from EPICA/Dome C ice core are plotted within REE_{UCC} of various PSA of the Southern Hemisphere. Areas are drawn following the disposition of plots belong to their respective location (Patagonia, South Argentina, Central Argentina, North Argentina, Transantarctic mountains, Australia, South Africa, glacial maxima and interglacial samples from the EPICA/Dome C ice core). I can notice that areas corresponding to REE_{UCC} of South Africa and Australia show a different area than areas corresponding to REE_{UCC} of the Transantarctic Mountains of Antarctica and South America. I can divide the **Figure 8.4.1** into two parts. Part I show typical signature of old continental crust (low Yb/La normalized to UCC ratios), that is coherent at first approximation with the geological history of these continent which constituted the Gondwanaland. On the other hand, the signatures of the Transantarctic Mountains of Antarctica and South America partly overlap in Part II of the Figure. This could be anticipated by their similar tectonic context, since all are young orogenic environments marked by andesitic volcanic activity.

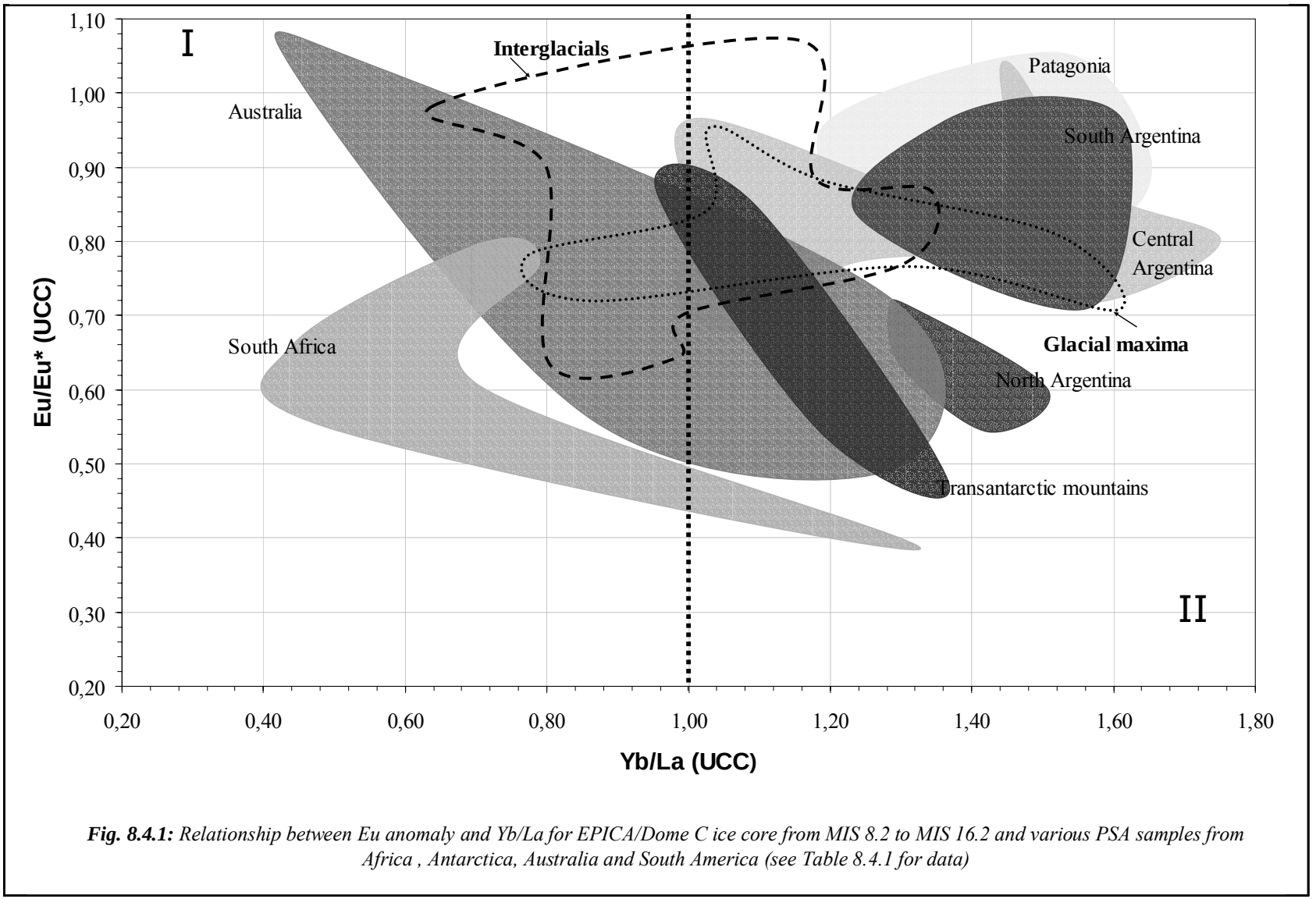

Fig. 8.4.1: *Relationship between Eu anomaly and Yb/La for EPICA/Dome C ice core from MIS 8.2 to MIS 16.2 and various PSA samples from Africa , Antarctica, Australia and South America (see Table 8.4.1 for data)*

Generally, the REE_{UCC} from Antarctic glacial maxima dust have a different pattern than REE_{UCC} from PSA of South Africa and therefore this region can be excluded as dominant source in cold periods. On the opposite, the ice core dust signature from MIS 8.2 to MIS 16.2 is situated on the overlap region between Australia (Lake Eyre, Ceduna and Central Australia), the Transantarctic Mountains and South America (Central Argentina).

The most remarkable feature of glacial maxima EPICA/Dome C ice core samples is the low mean Eu/Eu* (0.74), when compared to mean Patagonian dust (0.94) and mean South Argentina (0.84). Previous studies (Gaiero et al., 2004) have explained the lower Eu/Eu* in dust from Antarctic ice by a higher proportion of smectite in a dominant clay size fraction which is characteristic of sediments from Córdoba Province (Central Argentina). Moreover, it is clear from this figure that the loess from North Argentina (latitudes north of about 30°S) cannot be a significant contributor to Antarctic dust during glacial maxima. Consequently, during glacial periods, Córdoba province could be a source for the glacial dust samples at Dome C, in East Antarctica, from MIS 8.2 to MIS 16.2.

Figure 8.4.1 indicates that most of these glacial maxima samples are plotted within the areas corresponding to various PSA of the Transantarctic Mountains and Australia (Lake Eyre, Ceduna and Central Australia). Furthermore, more pronounced glacial maxima (MIS 8.2, MIS 10.2, 10.4 and 16.2) indicate values tending towards the Argentina dust field whilst less pronounced glacial maxima (12.2, 12.4 and 14.2) indicate values tending towards the Transantarctic Mountains and Australia dust fields (see **Table 8.4.1**).

Although less pronounced glacial maxima (MIS 12.2, 12.4 and 14.2) in the EPICA/Dome C ice core shows a similar REE_{UCC} pattern with the Transantarctic Mountains, several complementary arguments suggest that this region was unlikely to be the principal dust source during glacial maxima (ice-free areas, katabatic winds, atmospheric transport) (see section 3.3). So, I can say that Antarctic dust during glacial maxima consist of a mixture of Córdoba province and Australian materials. Revel-Rolland et al. (2006) reveal a contribution from South America ranging from 90 to 80% and an Australian contribution from 10 to 20%, in Antarctic samples. However, for samples corresponding to the Vostok MIS 12, they estimate a contribution of 50%

for both. Thus, during less pronounced glacial maxima (MIS 12.2, 12.4 and 14.2) at the Dome C in East Antarctica, dust materials come from at 50% to Australia and at 50% to Córdoba province whilst during more pronounced glacial maxima (MIS 8.2, MIS 10.2, 10.4 and 16.2) they come from at 90 to 80% to Córdoba province and at 10 to 20% to Australia. The change in East Antarctic dust origin between less pronounced and more pronounced glacial maxima could reflect either (1) a change in atmospheric circulation patterns and/or (2) a change in atmospheric moisture content and/ or (3) a differential weakening of one source with respect to the other(s).

	Yb/La UCC	Eu/Eu* UCC
SOUTH AMERICA		
Patagonia [a]		
Rio Colorado	1.25	0.85
San Antonio Oeste	1.54	0.91
Peninsula de Valdez 1	1.58	0.93
Peninsula de Valdez 2	1.46	0.99
Garrayalde	1.52	1.03
Fitz Roy	1.63	0.92
San Julian	1.21	0.94
Guer Aike	1.49	0.98
El Calafate	1.44	1.00
Charles Fuhr	1.61	0.88
Central Argentina [a,b]		
Santa Rosa (La Pampa Province)	1.12	0.68
Almafuerte (Cordoba Province)	1.24	0.80
Vic,Mackena (Cordoba Province)	1.02	0.95
Falda del Carmen (Cordoba Province)	1.13	0.84
La Lagunilla (Cordoba Province)	1.31	0.82
Surrounding Cordoba City	1.15	0.83
Surrounding Cordoba City	1.03	0.72
Hudson volcanic ash-1991 (P,San Julian)	1.46	1.02
Gorina	1.20	0.88
Gorina	1.56	0.84
Gorina	1.63	0.76
Gorina	1.70	0.81
Lozada	1.29	0.85
Lozada	1.51	0.75
Lozada	1.46	0.77
Lozada	1.45	0.79
North Argentina [b]		
El lambedero	1.33	0.67
El lambedero	1.26	0.74
El lambedero	1.39	0.71

	Yb/La UCC	Eu/Eu* UCC
SOUTH AMERICA		
South Argentina [b]		
Hippodromo	1.51	0.97
Hippodromo	1.60	0.91
Hippodromo	1.42	0.95
Hippodromo	1.61	0.90
Baradero	1.26	0.84
Baradero	1.53	0.75
Baradero	1.54	0.73
Baradero	1.57	0.75
Baradero	1.53	0.78
AUSTRALIA [c]		
Lake Eyre	0.94	0.80
Ceduna	1.26	0.70
Central Australia	1.21	0.50
Great sandy desert, western Australia	0.52	1.00
SOUTH AFRICA		
Southwestern main Karoo Basin [d]		
Calcite cement	0.72	0.76
from concretions	0.49	0.57
Disseminated calcite in host diamectite	0.48	0.61
Botswana [e]		
Okavango delta sediments	0.92	0.81
Okavango delta sediments	1.25	0.40
Okavango delta sediments	1.14	0.75
Okavango delta sediments	1.20	0.51
Okavango delta sediments	1.20	0.81
Okavango delta sediments	0.89	0.86
Okavango delta sediments	0.72	0.77
ANTARCTICA [f]		
Koettlitz glacier, Transantarctic mountains	1.08	0.80
Koettlitz glacier, Transantarctic mountains	1.32	0.51
Penny Hill Granite	1.18	0.67

	Yb/La UCC	Eu/Eu* UCC
GLACIAL (EDC)		
MIS 8.2	1.46	0.73
MIS 8.2	1.53	0.76
MIS 8.2	1.10	0.79
MIS 8.2	1.20	0.76
MIS 8.2	0.95	0.71
MIS 8.2	1.01	0.71
MIS 8.2	1.03	0.72
MIS 10.2	1.55	0.72
MIS 10.2	1.44	0.78
MIS 10.4	1.59	0.70
MIS 10.4	1.45	0.71
MIS 12.2	0.79	0.49
MIS 12.4	1.03	0.75
MIS 12.4	1.06	0.91
MIS 14.2	0.80	0.74
MIS 16.2	1.18	0.76
MIS 16.2	1.41	0.79
MIS 16.2	1.32	0.79
MIS 16.2	1.39	0.76
INTERGLACIAL (EDC)		
MIS 11.3	0.96	0.73
MIS 11.3	1.12	1.05
MIS 11.3	1.31	0.83
MIS 13.1	0.85	0.87
MIS 13.3	0.94	1.00
MIS 13.3	0.82	0.65
MIS 13.3	0.94	0.66
MIS 13.3	0.93	0.38
MIS 15.1	0.72	0.98
MIS 15.1	1.13	0.85
MIS 15.1	1.18	0.78
MIS 15.5	1.15	0.96

[a] Gaiero et al., 2004
[b] Smith et al., 2003
[c] Gingele et al., 2007
[d] Herbert and Compton, 2007
[e] Huntsman-Mapila et al., 2005
[f] Read et al., 2002

Table 8.3.1 : *Yb/La and Eu/Eu* normalized to UCC (Wedepohl, 1995) for South America, Australia, South Africa, the Transantarctic Mountains and few interglacial/glacial EPICA/Dome C ice core samples from MIS 8.2 to MIS 16.2*

8.5 Comparison of REE_{UCC} from the EPICA/Dome ice core during interglacials with REE_{UCC} from potential source areas (PSAs)

The Quaternary climatic and environmental changes which occurred between glacial and interglacial stages modified sensibly the conditions in continental areas. A basic question arises: was the dust geographic provenance the same during interglacial periods and glacial maxima?

Despite the limited number of samples (43), the interglacial samples have a distinct pattern and depict a higher Eu/Eu* (0.81 ± 0.24) with lower values of $(Yb/La)_{UCC}$ (1.00 ± 0.18), with respect to glacial maxima samples (Eu/Eu*: 0.75 ± 0.08; Yb/La_{UCC} : 1.29 ± 0.20). It is now well-established from ice-core studies from Vostok and Dome C in East Antarctica (Basile et al., 1997; Delmonte et al., 2006) that dust for interglacial 5.5 and the Holocene in East Antarctica is characterized by an isotopic signature less radiogenic in Nd than for glacial maxima. This suggests an additional source during warm periods compared to glacial maxima (Delmonte et al., 2006; Revel-Rolland et al., 2006). An interesting point to underline is that the glacial/interglacial isotopic Nd difference and REE difference of composition are unlikely to be due to environmental changes occurring at the source through environmental processes like pedogenesis.

The REE_{UCC} from Antarctic interglacials (from MIS 9.3 to MIS 15.5) dust have a different pattern than REE_{UCC} from PSA of South Africa (see **Figure 8.4.1**). South Africa seems unlikely a candidate contributor for interglacial dust in Antarctica. On the opposite, the interglacial dust signature from MIS 9.3 to MIS 15.5 is situated on the overlap region between Australia (Lake Eyre, Ceduna and Central Australia), the Transantarctic Mountains and South America (Patagonia, South Argentina and Central Argentina) (see **Figure 8.4.1**).

As observed by Delmonte et al.(2006), the Southern South American (Patagonia and Pampas) dust Sr-Nd isotopic field is definitely outside the interglacial dust values, and this clearly suggests a change in the source mixing between glacial maxima and interglacial times. However, when I compare mean Eu/Eu* of South Argentina (0.84 ± 0.09) and mean Eu/Eu* of Central Argentina

(0.82 ± 0.08) to the mean Eu/Eu* of interglacial samples (0.81 ± 0.24), these data suggest very strongly that South Argentina and Central Argentina can be considered as a source area in interglacial time. Moreover, I observe a difference of values of Eu/Eu* (0.94 ± 0.06) and Sr isotopic composition from PSA of Patagonia compared to interglacial samples of the EPICA/Dome C from MIS 9.3 to MIS 15.5. This difference of values between Patagonia and ice-core dust during interglacial periods can be wholly due to a transport/grain size effect (Smith et al., 2003).

The signature of REE for Koettlitz glacier in the Transantarctic Mountains is similar to the ice core REE signature of interglacial samples (see **Figure 8.4.1**). This suggests a possible contribution from the Transantarctic Mountains region. The Sr/Nd isotopic composition and also the clay mineral composition of dust in Antarctic ice also do not allow to exclude the Transantarctic Mountains as possible source (Gaudichet et al., 1992; Delmonte et al., 2006). However, a direct transport of dust from the Transantarctic Mountains to the inland plateau seems not favoured by the strong katabatic winds blowing off the continent and towards the sea. Mesoscale cyclonic activity can allow air uplift and advection of mild and moist maritime air towards the ice-sheet interior (Gallée, 1996), but the influence of such vortices is limited to the lower tropospheric levels (below 300 km) (Carrasco et al., 2003). The similarity between the signature of interglacial ice core dust and the signature of dust from Koettlitz glacier in the Transantarctic Mountains, therefore, could be misleading and must be considered with caution.

It can be observed also that REE signature for interglacial samples span the same area as the Australian dust samples (see **Figure 8.4.1**), but the latter displays a shift towards less Yb/La (UCC). Revel-Rolland et al. (2006) have also observed a shift towards more radiogenic values (Nd/Sr) for Australia compared to East Antarctic interglacial values. Overall, Australian and East Antarctic interglacial dust isotopic fields are very close, suggesting Australia as a possible dust source to the East Antarctic Plateau during interglacial times. A possible explanation of the shift could be the presence of large amounts of gypsum in the Antarctic interglacial samples with important effect on the Sr isotopic and REE budget.

So, I can say that Antarctic dust during interglacial periods consist of a mixture of South America (South Argentina, Central Argentina and perhaps Patagonia), the Transantarctic Mountains (Koettkitz glacier) and Australian materials.

REFERENCES

Anders E, Grevesse N (1989) Abundances of the elements: meteoritic and solar. *Geochimica et Cosmochimica Acta* **53**, 197-214

Basile I, Grousset FE, Revel M, Petit JR, Biscaye PE, Barkov NI (1997) Patagonian origin of glacial dust deposited in East Antarctica (Vostok and Dome C) during glacial stages 2, 4 and 6. *Earth and Planetary Science Letters* **146**, 573-589

Boutron CF, Patterson CC, Petrov VN, Barkov NI (1987) Preliminary data on changes of lead concentrations in Antarctic ice from 155,000 to 26,000 years BP. *Atmospheric Environment* **21**, 1197-1202

Carrasco JF, Bromwich DH, Monaghan AJ (2003) Distribution and characteristics of mesoscale cyclones in the Antarctic: Ross sea eastward to the Weddel sea. *Monthly Weather Review* **131**, 289-301

Delmonte B, Basile-Doelsch I, Petit JR, Maggi V, Revel-Rolland M, Michard A, Jagout E, Grousset F (2004) Comparing the EPICA and Vostok dust records during the last 220,000 years: stratigraphical correlation and provenance in glacial periods. *Earth Science Reviews* **66**, 63–87

Delmonte B, Petit JR, Basile-Doelsch I, Jagoutz VE, Maggi V (2006) Late Quaternary interglacials in East Antarctica from ice core dust records. In: Franck Sirrocko et al. (Eds) *The Climate of the Past Interglacials.* Elsevier, pp 53-73

Ding ZL, Sun JM, Yang SL, Liu TS (2001) Geochemistry of the Pliocene red clay formation in the chinese loess plateau and implication for its origin, source provenance and paleoclimate change. *Geochimica et Cosmochimica Acta* **65**, 901-913

Elderfield H, Greaves M.J. (1982) The rare earth elements in seawater. *Nature* **296**, 214-219

EPICA community members (2004) Eight glacial cycles from an Antarctic ice core. *Nature* **429**, 623-628

Gabrielli P, Barbante C, Turetta C, Marteel A, Boutron C, Cozzi G, Cairns W, Ferrari C, Cescon P (2006) Direct determination of Rare Earth Elements at the sub-picogram per gram level in Antarctic ice by ICP-SFMS using a desolvatation system. *Analytical Chemistry* **78**, 1883-1889

Gaiero DM, Depetris PJ, Probst JL, Bidart SM, Leleyter L (2004) The signature of river- and wind-borne materials exported from Patagonia to the southern latitudes: a view from REEs and implications for

paleoclimatic interpretations. *Earth and Planetary Science Letters* **219**, 357-376

Gallée H (1996) Mesoscale atmospheric circulations over the southwestern Ross Sea sector, Antarctica. *Journal of Applied Meteorology* **35**, 1142-1152

Gallet S, Jahn BM, Torii M (1996) Geochemical characterization of the Luochan loess-paleosol sequence, China, and paleoclimatic implications. *Chemical Geology* **133**, 67-88

Gallet S, Jahn BM, Lanoe BV, Dia A, Rossello E (1998) Loess geochemistry and its implications for particle origin and composition of the upper continental crust. *Earth and Planetary Science Letters* **156**, 157-172

Gaudichet A, Angelis MD, Joussaume S, Petit JR, Korotkevitch YS, Petrov VN (1992) Comments on the origin of dust in East Antarctica for present and ice age conditions. *J. Atmospheric Chemistry* **14**,129-142

Gingele F, De Deckker P, Norman M (2007) Late Pleistocene and Holocene climate of SE Australia reconstructed from dust and river loads deposited offshore the river Murray Mouth. *Earth and Planetary Science Letters* **255**, 257-272

Grousset FE, Biscaye PE, Revel M, Petit JR, Pye K, Joussaume S, Jouzel J (1992) Antarctic (Dome C) ice-core dust at 18 k.y. B.P.: isotopic constraints on origins. *Earth and Planetary Science Letters* **111**, 175-182

Hanson GN (1980) Rare earth elements in petrogenetic studies of igneous systems. *Review of Earth and Planetary Sciences* **8,** 371-406

Henderson P (1984) General geochemical properties and abundances of the rare earth elements. In *Rare Earth Element Geochemistry* (ed. P. Henderson), pp. 1-32. Elsevier

Herbert T, Compton JS (2007) Depositional environments of the lower Permian Dwyka diamictite and Prince Albert shale inferred from the geochemistry of early diagenetic concretions, southwest Karoo Basin, South Africa. *Sedimentary Geology* **194**, 263-277

Hofmann AW, Feigneson MD, Raczek I (1984) Case studies on the origin of basalt: III. Petrogenesis of the Mauna Ulu eruption, Kilauea, 1969-1971. *Contribution of Mineralogy and Petrology* **88**, 24-35

Huntsman-Mapila P, Kampunzu AB, Vink B, Ringrose S (2005) Cryptic indicators of provenance from the geochemistry of the Okavango Delta sediments, Botswana. *Sedimentary Geology* **174**, 123-148

Ikegawa M, Kimura M, Honda K, Akabane I, Makita K, Motoyama H, Fujii Y, Itokawa Y (1999) Geographical variations of major and trace elements in East Antarctica. *Atmospheric Environment* **33**, 1457-1467

Jahn BM, Gallet S, Han JM (2001) Geochemistry of the Xining, Xifeng and Jixian sections, loess plateau of China: eolian dust provenance and paleosol evolution during the last 140 ka. *Chemical Geology* **178**, 71-94

Kohfeld K, Harrison SP (2001) DIRTMAP: the geological record of dust. *Earth Science Review* **5**, 81–114

Krachler M, Mohl C, Emons H, Shotyk W (2003) Two thousand years of atmospheric Rare Earth Element (REE) deposition as revealed by an ombrotrophic peat bog profile, Jura Mountains, Switzerland *Journal of Environmental Monitoring* **5**, 111-121

Kriews M, Giese H, Schrems O (1996) Bestimmung von Schwermetallen in Schnee und Eis der Arktis, CANAS '95. In: Welz B (ed) *Colloquium Analytische Atomspektroskopie CANAS'95.* Bodenseewerk Perkin-Elmer GmbH, ISSN 0945-2524, pp. 521-529

Kriews M, Schrems O (1995) Pollution analysis in the Arctic: Determination of heavy metals in deposition samples from Spitsbergen.In: Wilken R-D, Förstner U, Knöchel A (eds) *Heavy metals in the environment*. Hamburg, ISBN 0905941543, **1**, pp. 371-374

Ng A, Patterson CC (1981) Natural concentrations of lead in ancient Arctic and Antarctic ice. *Geochimica et Cosmochimica Acta* **45**, 2109-2121

McLennan SM (1989) Rare Earth Elements in sedimentary rocks: influence of provenance and sedimentary processes. In: Lipin BR, McKay GA (Eds) *Geochemistry and Mineralogy of Rare Earth Elements*. Reviews in Mineralogy, vol.21, the Mineralogical Society of America, Washington DC, pp. 169-196

Read SE, Cooper AF, Walker NW (2002) Geochemistry and U-Pb geochronology of the Neoproterozoic-Cambrian Koettlitz Glacier Alkaline Province, Royal Society Range, Transantarctic Mountains, Antarctica. 8th International Symposium on Antarctica Earth Sciences*, The Royal Society of New Zealand Bulletin* **35**

Reinhardt H, Kriews M, Miller H, Lüdke C, Hoffmann E, Skole J (2003) Application of LA-ICP-MS in polar ice core studies. *Analytical and Bioanalytical Chemistry* **375**, 1265-1275

Revel-Rolland M, De Deckker P, Delmonte B, Hesse PP, Magee JW, Basile-Doelsh I, Grousset F, Bosh D (2006) Eastern Australia: A possible source of dust in East Antarctic interglacial ice. *Earth and Planetary Science Letters* **249**, 1-13

Smith J, Vance D, Kemp RA, Archer C, Toms P, King M, Zarate M (2003) Isotopic constraints on the source of Argentinian loess-with implications for atmospheric circulation and the provenance of Antarctic dust during recent glacial maxima. *Earth and Planetary Science Letters* **212**, 181-196

Taylor SR, McLennan SM (1985) *The continental crust: its composition and evolution. An examination of the geochemical preserved in sedimentary rocks*. Blackwell

Tegen I, Harrison SP, Kohfeld K, Prentice IC, Coe M (2002) The impact of vegetation and preferential source areas on global dust aerosol: results from a model study. *Journal of Geophysical Research* **107**, 4576–4603

Wedepohl K H (1995) The composition of the continental crust. *Geochimica et Cosmochimica Acta* **59**, 1217-1232

Yung YL, Lee T, Wang CH, Shieh YT (1996) Dust: a diagnostic of the hydrologic cycle during the Last Glacial Maximum. *Science* **271**, 962–963

Chapter 9- EIGHT GLACIAL CYCLES OF PB ISOTOPIC COMPOSITIONS IN THE EPICA DOME C ICE CORE

Lead is a trace element in the Earth's crust present in polar snow and ice in picogram/gram (10^{-12} g/g) quantities suitable for isotopic analysis by modern mass spectrometers (Rosman, 2001). Lead present in ancient polar ice originates from Aeolian dust sources and volcanic emissions while anthropogenic Pb inputs have been confirmed in Greenland and Antarctic ice from ~700 BC and ~1880 AD, respectively.

Contamination controls necessary for the accurate determination of Pb isotopes in polar snow and ice were pioneered by Patterson and co-workers (Murozumi et al., 1969), and have been subsequently developed (Candelone et al., 1994; Vallelonga et al., 2002a). As levels of analytical blanks for Pb have decreased and instrumental sensitivity has increased, Pb isotopic compositions have been reported in snow and ice from Greenland (Rosman et al., 1997), continental mountain glaciers (Rosman et al., 2000) and Antarctica (Rosman et al., 1998, Matsumoto & Hinkley, 2001, Van de Velde et al., 2005).

When combined with Potential Source Area data, the sensitive techniques developed for the analysis of Pb isotopes in Antarctic ice allow the provenance of continental sources of dust deposited in Antarctica.

Here I present new data extending the existing Pb isotope record at Dome C, in central Antarctica, from 263 ky BP to 671 ky BP. The new data enable the confirmation of climatic features observed in the most recent glacial cycle, in addition to characterising the variation of Pb isotopes over the past six glacial/interglacial cycles. The data also provide an important contribution to the developing understanding of the variation of continental dust compositions present across Antarctica.

9.1 Sample variability

The data presented here (Table 9.1.1) includes adjacent inner core samples collected from individual sections of ice, which usually display similar Pb and Ba concentrations but occasionally feature quite different Pb isotopic compositions. For each 55 cm piece of ice that was decontaminated, two inner core samples of ~25 cm length were collected and analysed separately. Generally there is only minor variability in Pb and Ba concentrations between each part of the ice core section, but Pb isotopic compositions do vary greatly between adjacent samples.

Samples displaying greatest variability in Pb or Ba concentration occur at 267, 274, 368 and 449 ky BP while the samples with greatest variability in $^{206}Pb/^{207}Pb$ occur at 286, 362, 368, 425 and 631 ky BP. Some of these ages (425, 631 ky BP) correspond to transition periods from glacial maxima to interglacials, periods of rapid climatic variation in which it would be expected that broad changes to dust concentration and provenance would occur on centennial or even decadal scales. For the other periods of variability, these do not consistently correspond to certain stages of climatic variation so it is difficult to find an adequate explanation for why the data from 8 samples vary markedly between adjacent sections but the other 39 samples do not vary to such an extent.

Few data are available representing interglacial periods although the two interglacials best represented (MIS 9.3, 327-335 ky BP and MIS 15.1, 554–574 ky BP) do not indicate any substantial decadal to centennial variation in Pb or Ba concentrations or Pb isotopic composition. During MIS 9.3, $^{206}Pb/^{207}Pb$ values increase from 1.18 to 1.20 from 335 to 327 ky BP while Ba concentrations decrease from 13 to 6 pg/g. Similarly during MIS 15.1, Ba concentrations decrease by approximately 50% and $^{206}Pb/^{207}Pb$ values increase from 574 to 566 ky BP, but no samples are available to demonstrate shorter-term variability on centennial or decadal scales.

Depth (m)	Age (yr BP)	del deuterium (‰)	206Pb/207Pb	± [a]	208Pb/207Pb	± [a]	206Pb/204Pb	± [a]	Pb conc. [b] (pg/g)	Ba conc. [b] (pg/g)	Pb/Ba (by weight)
2368.6	263565	-427,68	1,200	0,004	2,486	0,009	18,4	0,3	2,3	75,6	0,030
2379.6	267392	-437,01	1,190	0,006	2,472	0,015	18,7	0,4	15,1	396,4	0,038
2379.9	267500	-437,05	1,195	0,002	2,474	0,005	18,7	0,2	19,7	587,6	0,034
2396.1	274151	-439,25	1,191	0,002	2,467	0,004	18,5	0,1	18,8	387,5	0,048
2396.4	274268	-439,21	1,193	0,004	2,474	0,008	18,7	0,2	20,7	630,5	0,033
2407.1	278656	-434,66	1,190	0,008	2,472	0,014	18,2	0,4	6,8	125,6	0,054
2407.4	278777	-434,57	1,200	0,004	2,485	0,006	18,8	0,2	4,8	134,8	0,036
2429.1	286327	-420,35	1,232	0,006	2,476	0,010	19,4	0,3	5,7	29,9	0,190
2429.4	286413	-420,35	1,201	0,004	2,463	0,006	18,9	0,2	5,5	35,1	0,156
2550.4	327432	-393,55	1,202	0,010	2,459	0,010	18,8	0,3	0,2	6,2	0,040
2583.4	334762	-383,91	1,181	0,005	2,461	0,007	18,3	0,1	0,5	13,4	0,034
2605.1	343250	-439,58	1,192	0,007	2,480	0,010	18,4	0,4	4,2	124,0	0,034
2605.4	343403	-439,53	1,191	0,009	2,468	0,018	18,9	0,5	6,1	176,7	0,035
2632.9	358947	-437,82	1,197	0,006	2,503	0,014	19,1	0,5	3,5	131,6	0,027
2638.1	361992	-432,74	1,198	0,003	2,474	0,006	18,7	0,2	3,1	85,4	0,036
2638.4	362150	-432,70	1,190	0,007	2,449	0,014	18,0	0,5	4,3	97,6	0,044
2649.1	368148	-429,37	1,202	0,005	2,478	0,008	19,1	0,2	4,0	124,6	0,032
2649.4	368303	-429,28	1,217	0,009	2,483	0,015	18,4	0,7	6,1	248,0	0,025
2682.1	385808	-416,33	1,188	0,007	2,448	0,012	17,7	0,4	0,9	13,3	0,066
2682.4	385942	-416,49	1,190	0,004	2,464	0,007	18,4	0,4	0,7	21,4	0,034
2693.1	391793	-414,43	1,203	0,004	2,470	0,006	18,6	0,2	0,8	16,8	0,047
2693.4	391942	-414,63	1,205	0,007	2,478	0,013	18,4	0,2	0,9	20,6	0,044
2776.6	424905	-404,49	1,195	0,014	2,458	0,026	18,4	1,5	0,4	13,7	0,032
2776.9	425027	-404,75	1,231	0,008	2,497	0,012	19,1	0,3	0,7	15,4	0,046
2786.6	432598	-443,02	1,196	0,002	2,475	0,005	18,4	0,2	15,9	522,2	0,030
2786.9	432870	-443,01	1,195	0,004	2,474	0,006	18,7	0,2	16,0	423,6	0,038
2803.1	449435	-431,54	1,195	0,002	2,476	0,004	18,7	0,1	15,5	479,8	0,032
2803.4	449719	-431,49	1,198	0,004	2,477	0,006	18,4	0,2	8,4	288,2	0,029
2830.6	479361	-416,36	1,197	0,014	2,465	0,022	17,6	0,5	0,8	31,7	0,027
2830.9	479623	-416,27	1,211	0,010	2,477	0,025	18,8	0,6	2,1	44,2	0,048
2875.6	511071	-422,45	1,197	0,006	2,472	0,007	18,9	0,3	0,6	22,8	0,027
2907.6	532571	-429,67	1,205	0,003	2,484	0,008	18,6	0,2	4,1	124,2	0,033
2907.9	532841	-429,67	1,196	0,004	2,485	0,006	18,7	0,2	5,7	139,5	0,041
2913.1	537923	-433,18	1,193	0,003	2,471	0,005	18,7	0,1	7,9	199,2	0,040
2913.4	538194	-433,20	1,198	0,006	2,476	0,011	18,5	0,2	8,4	208,6	0,040
2929.6	554062	-416,86	1,195	0,006	2,477	0,009	18,8	0,3	0,7	25,1	0,030
2929.9	554250	-416,91	1,195	0,005	2,472	0,009	18,8	0,2	0,9	27,8	0,033
2957.1	566577	-401,83	1,201	0,008	2,479	0,014	18,8	0,4	0,4	8,8	0,049
2979.1	574322	-404,11	1,183	0,008	2,465	0,011	18,2	0,3	0,5	20,9	0,026
2979.4	574428	-404,08	1,185	0,010	2,465	0,014	18,8	0,4	0,3	14,1	0,022
3006.6	591058	-421,74	1,188	0,005	2,463	0,009	18,4	0,3	1,0	24,3	0,041
3017.6	603812	-410,59	1,190	0,003	2,463	0,007	18,5	0,1	2,5	99,2	0,025
3040.6	631304	-438,49	1,188	0,003	2,465	0,007	18,5	0,2	6,7	158,1	0,043
3040.9	631964	-438,68	1,203	0,002	2,481	0,006	18,8	0,1	6,3	153,3	0,041
3050.9	655611	-435,34	1,187	0,007	2,465	0,013	18,6	0,4	1,5	56,2	0,027
3061.6	671102	-429,16	1,196	0,004	2,468	0,008	18,6	0,3	3,5	101,5	0,034
3061.9	671706	-429,08	1,190	0,003	2,469	0,006	18,6	0,3	3,3	87,7	0,038

[a] Uncertainties in the isotope ratios are 95% confidence intervals
[b] Concentrations are accurate to ±15% (95% confidence interval)

Table 9.1.1 : *Lead and Ba concentrations and Pb isotopic compositions in Antarctic Dome C ice core from 263 to 671 ky BP*

9.2 Lead and Ba concentrations

Lead and Ba concentrations in the EPICA Dome C ice core are shown in **Figure 9.2.1**. In agreement with previous studies of dust in the EPICA Dome C ice core (Vallelonga et al., 2005, Gabrielli et al., 2005), Pb and Ba concentrations are greater during colder climatic periods.

The relative magnitudes of Ba peaks during interglacial periods are also generally in accordance with those previously reported (EPICA community, 2004), indicating greater dust concentrations during climate stages 7 and 11 and dust concentrations approximately 50% lower during climate stages 5, 9, 13 and 15. The concordance between del deuterium (used here as a climatic temperature proxy) and Ba concentration is effectively composed of two linear relationships which operate about a del Deuterium transition value of approximately -430‰. Hong et al. (2003) noted a significant variation in the ratio of Pb concentration to Al concentration in Vostok ice about a del Deuterium value of -470‰, perhaps reflecting differing surface temperatures at each site for a specific hemispheric climatic regime, or reflecting isotopically lighter snowfall at Vostok as air masses travel toward the centre of the East Antarctic Plateau.

Pb/Ba ratios in EPICA Dome C ice are generally lower and less variable over glacial-interglacial cycles prior to the last (**see Figure 9.2.1**). Over the past glacial cycle, relatively large variations in Pb/Ba ratios were noted from 0.026 to 0.09, with one high value at 0.17 attributed to the input of volcanic Pb. By comparison, the data presented here indicates that over the five glacial cycles from 263 to 671 ky BP, Pb/Ba ratios varied between 0.022 and 0.066 with one core displaying unusually high values of 0.16 and 0.19. This apparent increase in variability of Pb/Ba ratio may be an artefact of sampling at higher resolution toward the top of the ice core, or may indicate a relatively recent increase in climatic variability and/or atmospheric transport and/or volcanic Pb emissions during the past glacial cycle. The generally low value of the Pb/Ba ratio is consistent with Pb/Ba ratios reported for the Earth's bulk crustal composition (Pb/Ba ~0.03, McLennan, 2001) and so confirms the dominance of mineral dust as the primary source of Pb in Dome C ice.

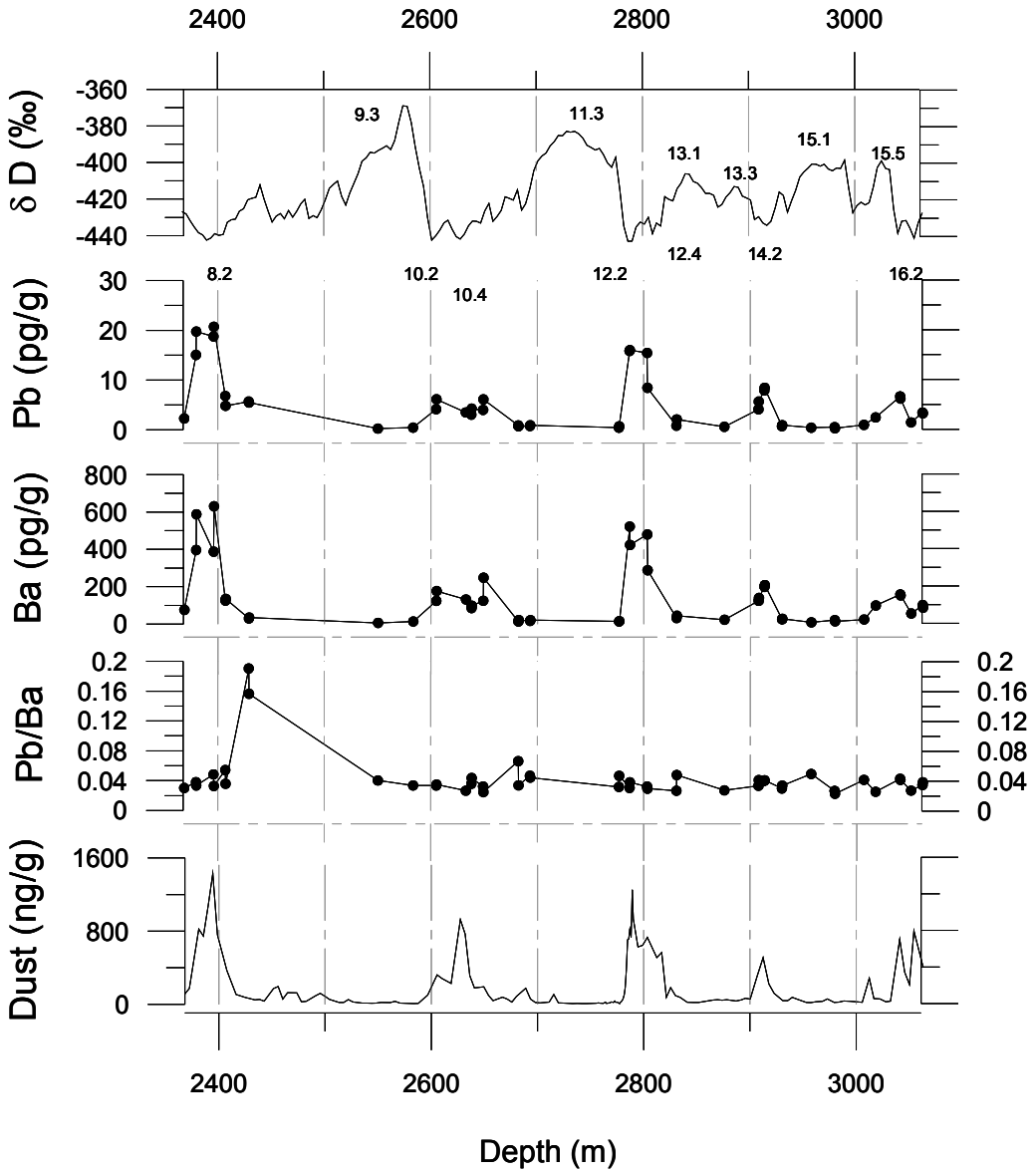

Fig. 9.2.1:*EPICA/Dome C Antarctic ice core: changes in concentrations of Pb and Ba as a function of depth from 2368.6 m to 3061.9 m (263 to 671 ky BP). Also shown at the top of the figure are the variations in deuterium concentrations (expressed in delta per mil) (EPICA Community members, 2004), Marine Isotope Stages (MIS) numbers (Bassinot et al., 1994), and at the bottom of the figure Pb/Ba ratios and changes in dust concentrations (expressed in ng/g) (EPICA Community members, 2004).*

9.3 $^{206}Pb/^{207}Pb$ ratios

Values of $^{206}Pb/^{207}Pb$ reported here (see **Figure 9.3.1**) for deeper sections of the EPICA Dome C ice core are in good agreement with those previously reported for the period 0 – 220 ky BP (Vallelonga et al., 2005). $^{206}Pb/^{207}Pb$ values reported here range between 1.18 and 1.23 although the majority (91%) of samples are within a range of lower values 1.18 – 1.205. This is different to the most recent EPICA samples, which are well distributed within the range 1.19 – 1.26 with only 53% of samples present within the range 1.19-1.205. This gradual increase in Pb isotopic variability may be related to the gradually increasing range of temperatures observed during glacial/interglacial cycles, as represented by δD values. This may also be related to changing dominance of climatic cycles from 40 ky (obliquity) forcing to 100 ky (eccentricity) forcing, according to the Milankovitch theory of climate forcing (Berger et al., 1992).

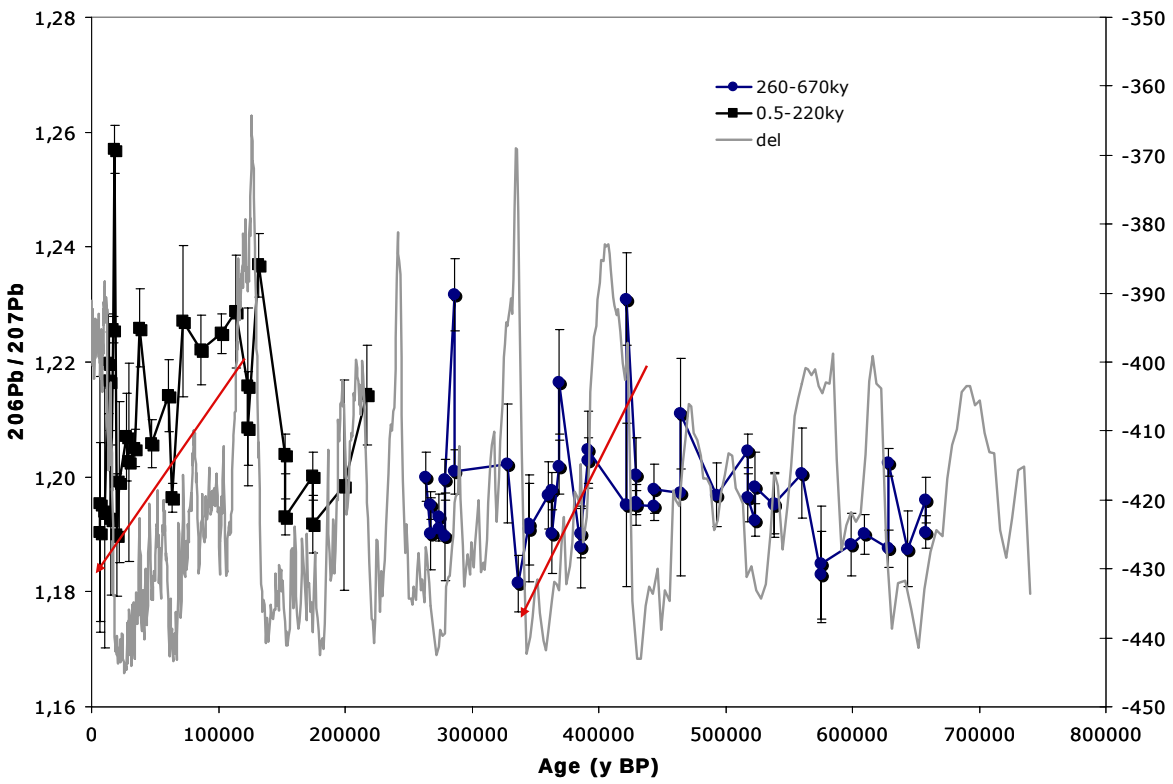

Fig. 9.3.1: *EPICA/Dome C Antarctic ice core: changes in $^{206}Pb/^{207}Pb$ ratios as a function of age over eight climatic cycles. Data for the period from 0.5 to 220 ky BP from Vallelonga et al. (2005). Also shown are the variations in deuterium concentrations (expressed in delta per mil) (EPICA Community members, 2004). Red arrows show decreasing $^{206}Pb/^{207}Pb$ values over cooling glacial periods*

Despite some qualitative evidence to suggest a relationship between $^{206}Pb/^{207}Pb$ value and δD, or temperature, there is no significant statistical correlation that can be drawn from the data presented. As noted earlier by Vallelonga et al (2005), a qualitative link was drawn toward generally decreasing $^{206}Pb/^{207}Pb$ values over the cooling glacial period from the Eemian interglacial to the Last Glacial Maximum. Any such qualitative assessment of a link between del D and $^{206}Pb/^{207}Pb$ cannot be confirmed by the data presented here.

Rather than disproving any potential correlation, this may be due to the nature of the sampling – here 47 samples are used to represent a period of approximately 400,000 years whereas Vallelonga et al. (2005) reported 20 values for the 100,000 year period covering the Eemian-LGM glaciation. Additionally, the smoothing of ice strata in the core will demand that smaller samples are taken at depth to maintain a constant temporal sampling rate. In this work, all samples were approximately similar in depth interval, therefore integrating greater time periods with depth. This increasing integration of δD and $^{206}Pb/^{207}Pb$ values with depth may act to increase the noisiness of any climate-related $^{206}Pb/^{207}Pb$ signal, thus making it more difficult to detect without a commensurate increase in the number of samples taken.

Finally, any correlation between $^{206}Pb/^{207}Pb$ and del value may be impaired by the changing amplitude of the δD cycle – simply δD values corresponding to interglacials MIS 13 or MIS 15 are identical to values observed during glacial maxima MIS 4 or MIS 6. Thus it may be that the gradually increasing amplitude of del D variations impedes the proper correlation of δD and $^{206}Pb/^{207}Pb$ because a single δD value may correspond to a "cold" or "warm" period depending on which Marine Isotopic Stage it happens to appear.

9.4 $^{208}Pb/^{207}Pb$ ratios

Lead isotopic compositions determined in the EPICA Dome C ice core are shown in **Figure 9.4.1**. As with $^{206}Pb/^{207}Pb$ Pb ratios, there is good agreement between the data presented here and that reported previously (Vallelonga et al., 2005) for the most recent part of the EPICA Dome C ice core. $^{206}Pb/^{207}Pb$ values are between 1.18 and 1.23 while $^{208}Pb/^{207}Pb$ values range between 2.45 and 2.50. These ranges are more restricted than those reported for the most recent 220 ky of

ice at Dome C, suggesting less variability in dust sources contributing to Dome C in the past, compared to the most recent glacial cycle.

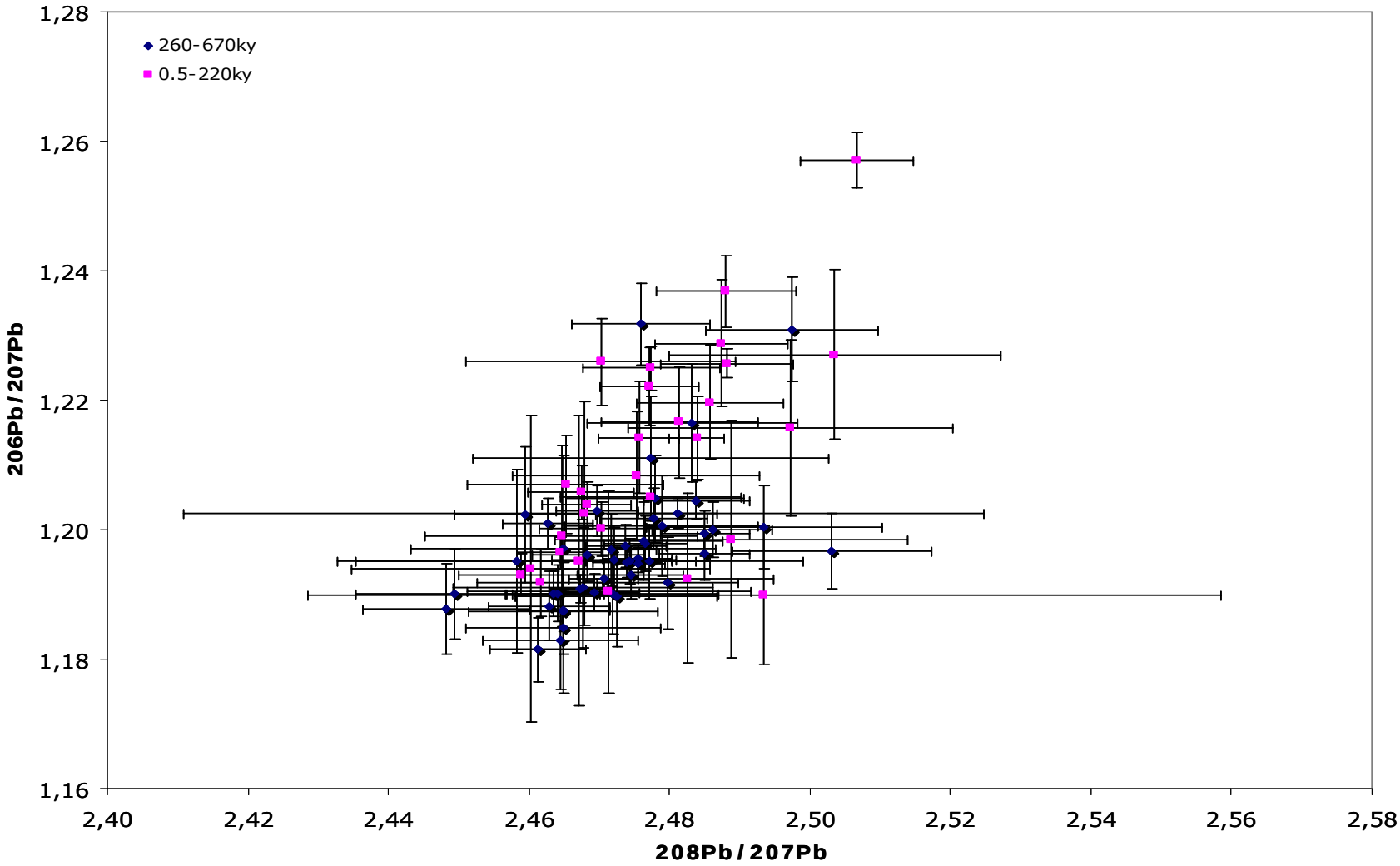

Fig. 9.4.1: *EPICA/Dome C ice core: isotopic composition of lead over eight climatic cycles. Samples used to represent the period from 0.5 to 220 ky BP (Vallonga et al., 2005) are shown as filled pink square whilst samples used for the period from 260 to 670 ky BP (This work) are shown as filled blue ring.*

When compared to other Pb isotopic compositions reported for pre-industrial Antarctic ice, Dome C samples (see **Figure 9.4.2**) are consistently less-radiogenic, confirming that different dominant sources or combinations of sources of dust are present across the Antarctic continent. Lead isotope compositions in Dome C ice are less-radiogenic (lesser $^{206}Pb/^{207}Pb$ and $^{208}Pb/^{207}Pb$ values) than those reported for Law Dome (Vallelonga et al., 2002b) while Taylor Dome ice (Matsumoto & Hinkley, 2001) is generally more-radiogenic than that at Law Dome. It has been argued that this variation in Pb isotopic compositions across Antarctica reflects differences in the influence of local Antarctic sources of volcanic emissions (Vallelonga et al., 2005). These volcanic emissions are highly radiogenic, as evidenced by the Pb isotopic composition of Mt Erebus lava (Sun & Hanson, 1975) (see **Figure 9.4.2**).

Recent studies of Dome C ice based on Sr and Nd isotopes (Delmonte et al., 2004; Revel-Rolland et al., 2006; Gaiero, 2007) have indicated that the arid Patagonian desert steppe is a dominant source of dust transported to Dome C with minor influences from other Southern Hemisphere dust sources including Australia and possibly a local Antarctic source. As mentioned previously, Mt Erebus has been taken as representative of local Antarctic emissions, but currently there are no Pb isotope data available to represent Australian dust sources. Southern South American dust sources can be represented by South Atlantic Ocean pelagic sediments (Chow and Patterson, 1962). The Pb isotopic compositions reported for South American PSAs are generally similar to the less-radiogenic Pb isotopic compositions observed in Dome C ice, thereby confirming a dominant Patagonian/Southern South American origin for the dust transported to Dome C (see **Figure 9.4.2**).

The range of Pb isotopic compositions observed in Dome C, Law Dome and Taylor Dome ice confirms that there are at least two sources of dust transported to Antarctica, of which the less-radiogenic source is compatible with southern South American dust sources. At this stage the only data available to attribute to the more-radiogenic source originates from Antarctica, notably Mt Erebus and other volcanic rock outcrops (Sun & Hanson, 1975; Hart et al., 1997; Hole et al., 1993). Isotopic studies and atmospheric modelling suggest that Australia should be a source of Antarctic dust, but it is impossible to assess the influence of this source using the presented data while PSAs remain uncharacterised for Pb isotopes.

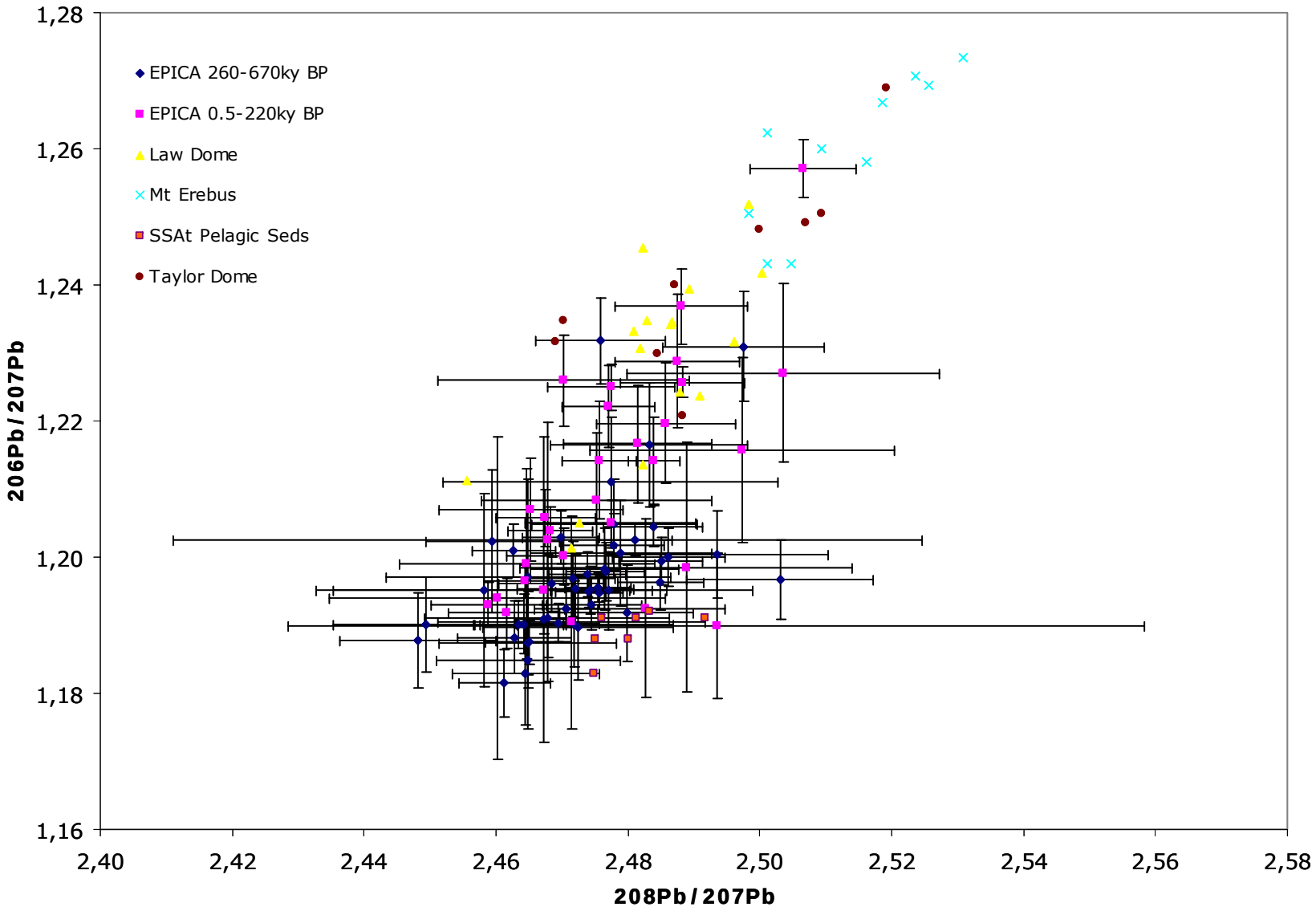

Fig. 9.4.2: *Pb isotopic compositions in ice from Dome C and other Antarctic sites. Also included are Pb isotopic compositions of South Atlantic pelagic sediments (Chow and Patterson, 1962), Ross island basanitoids (Sun and Hanson, 1975).*

Lead isotopic compositions in Dome C samples vary between glacial and interglacial samples (**Figure 9.4.3**), suggesting that the composition of dust sources contributing to Dome C ice varies with climate. Glacial samples generally have Pb isotopic compositions closer to those reported for Southern South American dust, while interglacial samples have values with slightly greater $^{206}Pb/^{207}Pb$ and slightly smaller $^{208}Pb/^{207}Pb$. Such a distribution is in agreement with an intensification of the southern South American dust source(s) during glacial periods, as implied by the modelling of Lunt and Valdes (2001).

Lead isotopes and Pb and Ba concentrations have been reported for the deeper sections of the EPICA Dome C ice core, providing a record of Pb isotopic compositions in central East Antarctica from 7 ky BP to 671 ky BP. The data indicate that Pb isotopic compositions were lower and less variable in earlier glacial-interglacial climate cycles, with 91% of samples $^{206}Pb/^{207}Pb$ values within the range 1.18 – 1.205 before 220 ky BP and 53% of samples with $^{206}Pb/^{207}Pb$ values within the range 1.19-1.205 since 220 ky BP. Variations in Pb and Ba concentrations and Pb/Ba ratios are generally consistent with previously reported data from Dome C. Lead isotope data agree with other studies indicating a dominant southern South American source for dust in central East Antarctica, while indicating that there is at least one other major dust source. Such a dust signature is consistent with local Antarctic volcanic or radiogenic dust sources but cannot be confirmed until Pb isotopic signatures have been reported for potential Australian dust sources. A thorough assessment of Australian PSA signatures is essential to accurately identifying the sources of dust deposited in Antarctica.

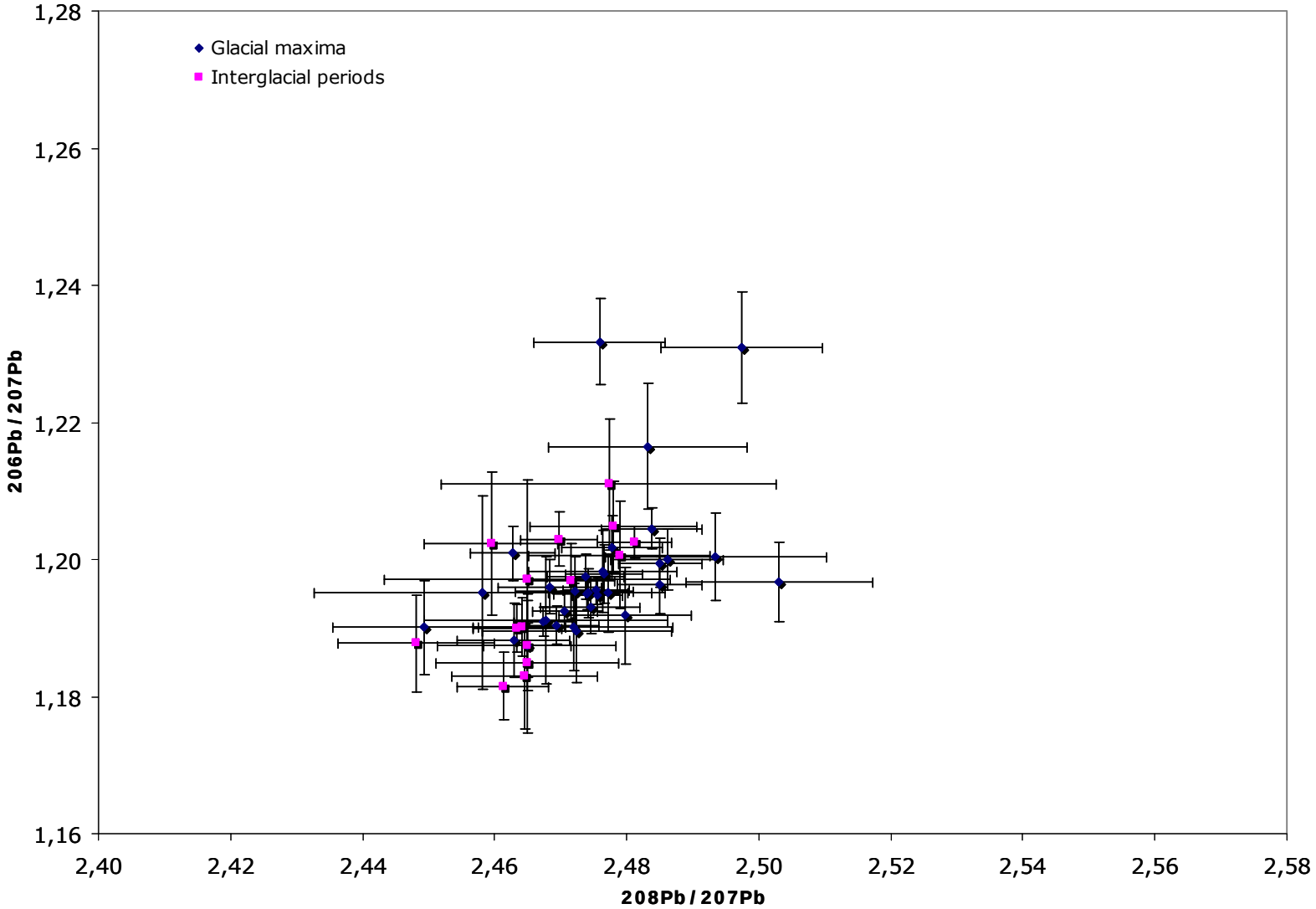

Fig. 9.4.3: *Comparison of Pb isotopic compositions between glacial maxima and interglacial periods in ice from the EPICA/Dome C ice core over eight climatic cycles*

REFERENCES

Bassinot FC, Labeyrie LD, Vincent E, Quidelleur X, Shackleton NJ, Lancelot Y (1994) The astronomical theory of climate and the age of Brunhes-Matuyama magnetic reversal. *Earth and Planetary Science Letters* **126**, 91-108

Berger A, Loutre MF, Laskar J (1992) Stability of the Astronomical Frequencies Over the Earth's History for Paleoclimate Studies. *Science* **255**, 560-566

Candelone JP, Hong S, Boutron CB (1994) An improved method for decontaminating polar snow or ice cores for heavy metal analysis. *Analytica Chimica Acta* **299**, 9 - 16

Delmonte B, Basile-Doelsch I, Petit JR, Maggi V, Revel-Rolland M, Michard A, Jagoutz E, Grousset F (2004) Comparing the EPICA and Vostok dust records during the last 220,000 years: stratigraphical correlation and provenance in glacial periods. *Earth Science Reviews* **66**,573-589

Chow TJ, Patterson CC (1962) The occurrence and significance of lead isotopes in pelagic sediments. *Geochimica et Cosmochimica* Acta **26**, 263-308

EPICA Community members (2004) Eight glacial cycles from an Antarctic ice core. *Nature* **429**, 623-628

Gabrielli P, Barbante C, Boutron C, Cozzi G, Gaspari V, Planchon F, Ferrari C, Turetta C, Hong S, Cescon P (2005) Variations in atmospheric trace elements in Dome C (East Antarctica) ice over the last two climatic cycles. *Atmospheric Environment* **39**, 6420-6429

Gaiero DM (2007) Dust provenance in Antarctic ice during glacial periods: From where in southern South America? *Geophysical Research Letters* **34**. doi:10.1029/2007GL030520

Hart SR, Blusztajn J, LeMasurier WE, Rex DC(1997), Hobbs Coast Cenozoic volcanism: Implications for the West Antarctic rift system. *Chemical Geology* **139**, 223 – 248

Hole MJ, Kempton PD, Millar IL (1993) Trace-element and isotopic characteristics of small-degree melts of the asthenosphere: Evidence from the alkalic basalts of the Antarctic Peninsula. *Chemical Geology* **109**, 51 – 68

Hong S, Kim Y, Boutron CF, Ferrari CP, Petit JR, Barbante C, Rosman K, Lipenkov VY (2003) Climate-related variations in lead concentrations and sources in Vostok Antarctic ice from 65,000 to 240, 000 years BP. *Geophysical Research Letters* **22**, 2138, doi: 10.1029/2003GL018411

Lunt DJ, Valdes PJ (2001) Dust transport to Dome C, Antarctica, at the last glacial maximum and present day. *Geophysical Research Letters* **28 (2),** 295–298

Matsumoto A, Hinkley TK (2001) Trace metal suites in Antarctic pre-industrial ice are consistent with emissions from quiescent degassing of volcanoes worldwide. *Earth and Planetary Science Letters* **186**, 33-43

McLennan SM (2001), Relationships between the trace element composition of sedimentary rocks and upper continental crust. *Geochemistry Geophysics Geosystems* **2**, doi:10.1029/2000GC000109

Murozumi M, Chow TJ, Patterson CC (1969) Chemical concentrations of pollutant lead aerosols, terrestrial dusts and sea salts in Greenland and Antarctic snow strata. *Geochimica et Cosmochimica Acta* **33**, 1247-1294

Revel-Rolland M, De Deckker P, Delmonte B, Hesse PP, Magee JW, Basile-Doesch I, Grousset F, Bosh D (2006) Eastern Australia: A possible source of dust in East Antarctica interglacial ice. *Earth and Planetary Science Letters* **249**, 1– 13

Rosman KJR, Chisholm W, Hong S, Candelone JP, Boutron CF (1997) Lead from Carthaginian and Roman Spanish mines isotopically identified in Greenland ice dated from 600 B.C. to 300 A.D. *Environmental Science of Technology* **31**, 3413-3416

Rosman KJR, Chisholm W, Boutron CF, Hong S, Edwards R, Morgan V, Sedwick PN (1998) Lead isotopes and selected metals in ice from Law Dome, Antarctica. *Annals of Glaciology* **27**, 349-354

Rosman KJR, Ly C, Van de Velde K, Boutron CF (2000) A two century record of lead isotopes in high altitude alpine snow and ice. *Earth and Planetary Science Letters* **176**, 413-424

Rosman KJR (2001) Natural isotopic variations in lead in polar snow and ice as indicators of source regions. In: Caroli S, Cescon P, Walton DWH (Eds.) *Environmental contamination in Antarctica: A challenge to analytical chemistry*, Elsevier Science B.V., New York, 2001, pp. 87-106

Sun SS, Hanson GH (1975) Origin of Ross Island Basanitoids and Limitations upon the Heterogeneity of Mantle Sources for Alkali Basalts and Naphelinites. *Contributions to Mineralogy and Petrology* **52**, 77-106

Vallelonga P, Van de Velde K, Candelone JP, Ly C, Rosman KJR, Boutron CF, Morgan VI, Mackey DJ (2002a) Recent

advances in measurement of Pb isotopes in Polar ice and snow at sub-picogram per gram concentrations using Thermal Ionisation Mass Spectrometry. *Analytica Chimica Acta* **453**, 1-12

Vallelonga P, Van de Velde K, Candelone JP, Morgan VI, Boutron CF, Rosman KJR (2002b) The lead pollution history of Law Dome, Antarctica, from isotopic measurements on ice cores: 1500 AD to 1989 AD. *Earth and Planetary Science Letters* **204**, 291-306

Vallelonga P, Gabrielli P, Rosman KJR, Barbante C, Boutron CF (2005) A 220 kyr record of Pb isotopes at Dome C Antarctica from analyses of the EPICA ice core. *Geophysical Research Letters* **32(1)**, L01706.

Van de Velde K, Vallelonga P, Candelone JP, Rosman KJR, Gaspari V, Cozzi G, Barbante C, Udisti R, Cescon P, Boutron CF (2005) Pb isotope record over one century in snow from Victoria Land, Antarctica. *Earth and Planetary Science Letters* **232**, 95-108

Chapter 10- INTENSE MERCURY SCAVENGING FROM DUST AND SALT LADEN ANTARCTIC ATMOSPHERE DURING THE GLACIAL AGES

Mercury is a globally dispersed pollutant that is emitted into the atmosphere by anthropogenic and natural sources (Mason et al., 1994; Pyle and Mather, 2003). Elemental (gaseous) mercury (Hg^0) is the predominant atmospheric Hg species, with a largely accepted residence time of ~1 year, which means that it can be long-range transported before its deposits on Earth (Shroeder et al., 1998). Nevertheless, the discovery of "Atmospheric Mercury Depletion Events" (AMDEs) has shown that for Hg^0 a much shorter residence time may occur locally in polar areas. During AMDEs, Hg^0 undergoes rapid oxidation into more reactive forms (e.g. Hg^{2+}), which are rapidly removed from the Arctic and Antarctic coastal atmosphere (Schroeder et al., 1998; Ebinghaus et al., 2002) resulting in a sudden Hg accumulation is observed in surface snow (Lindberg et al., 2002). However, it remains unresolved whether substantial Hg deposition processes are linked exclusively to recent AMDEs or may have occurred with the same or a different mechanism in polar areas on even larger spatial or even temporal scales. This is an important point in order to establish whether the polar regions constitute a sink or a source of Hg species, with relevant implications for the understanding of the Hg biogeochemical cycle. For this kind of studies, deep cores retrieved from polar ice caps represent unique environmental archives, which may reveal accurately the behaviors of atmospheric Hg species in ancient times (Vandal et al., 1993).

10.1 Materials and Methods

To date information regarding Hg levels in polar snow/ice is very scarce. A single study reported so far concentrations of inorganic mercury (Hg^{2+}) in Antarctic ice (Vandal et al., 1993) and snow (Capelli et al., 1998) and also scarce data are published for Hg in Greenland ice/snow (Ferrari et al., 2004). In polar ice/snow Hg^{2+} is present generally at the pg g^{-1} levels (Vandal et al., 1993; Capelli et al., 1998) whereas for $MeHg^+$ concentrations <0.1 pg g^{-1} were assessed (Ferrari et al., 2004).

The scarce literature data in terms of Hg levels in polar ice/snow is mainly due to the lack of enough sensitive analytical techniques required for the ultra-trace determination of Hg species.

Other problems arise from sample contamination (Boutron et al., 1998; Ferrari et al., 2000) and from the difficulty of stabilization/preservation of Hg species at ultra-trace levels (Parker and Bloom, 2005; Yu and Yan, 2003). It is therefore mandatory to use ultra-clean protocols and highly sensitive analytical approaches for the accurate determination of Hg species at ultra-trace levels in polar ice.

Decontamination of the ice sections analyzed in this work was thoroughly carried out using the procedure described elsewhere (Planchon et al., 2004; Candelone et al., 1994); the determination of Hg_T in the inner ice core as well in the outer layers demonstrated negligible contamination (Planchon et al., 2004). After decontamination, the ice samples were conserved frozen until analysis either in low-density polyethylene (LDPE) or glass recipients decontaminated in both cases using the procedure reported in a previous work (Boutron, 1990). 36 sections (~2-207 ky B.P.) of the EPICA ice core analyzed here (see Table V, Annexe II) were kept frozen (at -20 ^{o}C) in LDPE recipients (made by Paolo Gabrielli) whereas the other 34 sections (~264-671 ky B.P.) were stored (also at -20 ^{o}C) into decontaminated glass recipients until analysis.

The use of LDPE recipients for storage of Hg solutions at trace levels seems to be questioned by some authors (Parker and Bloom, 2005). However, to our knowledge so far there is no evidence that supports an assumption in terms of negative effects (contamination, loss, etc.) of such recipients for long-term storage (at very low temperature, e.g. below -20 ^{o}C), particularly of ice samples. It appears that for Hg solutions, LDPE bottles may contribute to mercury loss rather than contamination (Yu and Yan, 2003) (the concern that a sample may become contaminated from the atmosphere, *via* transmission of Hg^0 vapor is unfounded unless the storage area itself has significantly greater than ambient concentrations of Hg^0, *e.g.*>30 ng m^{-3}) but the Hg_T levels obtained in our study do not confirm a Hg loss. In addition, as far as mercury species interconversion is concerned, the very low levels of $MeHg^+$ assessed in the ice do not support evidence that such a process took place.

The two datasets obtained in our study using either LDPE and glass recipients for the ice storage are in good agreement and led to similar environmental behavior, with the highest levels obtained during the glacial age and lower levels during interglacial stages.

Simultaneous speciation analysis of Hg^{2+} and $MeHg^{+}$ in the Antarctic ice was carried out by multicapillary gas chromatography (MCGC) coupled to inductively coupled plasma-time of flight-mass spectrometry (ICP-TOFMS) (Jitaru and Adams, 2004) at the University of Antwerp, Belgium (made by Petru Jitaru). In order to be amenable to MCGC separation but also to cope with the ultra-trace levels determination, Hg^{2+} and $MeHg^{+}$ were derivatized by converting them into ethylated derivatives (by using $NaB(C_2H_5)_4$) as derivatization agent) and also pre-concentrated *in situ* (preconcentration factor of ~10^4) by solid-phase micro-extraction just before the MCGC-ICP-TOFMS analysis. The method detection limits (MDL) obtained were 0.03 pg g^{-1} for $MeHg^{+}$ and 0.3 pg g^{-1} for Hg^{2+}. The relative standard deviation (R.S.D.,%) calculated for 10 successive analyses was <4% for both species. The spike recovery factors determined for the estimation of the method accuracy were ~100% for $MeHg^{+}$ and ~104% for Hg^{2+}.

The determination of total mercury (Hg_T) was carried out by inductively coupled plasma-sector field-mass spectrometry (ICP-SFMS) using the method described in detail in a previous work (Planchon et al., 2004). The MDL reassessed just before this session of experiments was ~1 pg g^{-1}. The R.S.D. was ~15% and the spike recovery factor determined for the method accuracy assessment was ~100%.

As already mentioned before, to date there is information only on one series of determinations of Hg in the first deep ice core retrieved near Dome C on the Eastern Antarctic plateau (Vandal et al., 1993). Vandal et al. (1993) determined Hg^{2+} in 14 ice sections, which covered a time period until ~34 ky B.P. The analytical method used in their work employed the reduction of Hg^{2+} to Hg^0 (also known as 'cold vapor') using $SnCl_2$ followed by detection of Hg^0 by atomic fluorescence spectrometry. Our (speciation) method used a derivatization reaction (for reasons mentioned before) of Hg^{2+} (and $MeHg^{+}$) with ethyl groups (provided by $NaB(C_2H_5)_4$). Hg^{2+} measured in both cases ((Vandal et al., 1993) and (Jitaru and Adams, 2004)) represents largely the fraction of soluble inorganic mercury (II) (available either to reduction or to ethylation). The results from the two data sets are generally in good agreement, however, the maximum level of Hg^{2+} obtained in our study during the Last Glacial Maximum (LGM) (~9 pg g^{-1}, 22 ky B.P.) (Table V, Annexe II) is significantly higher than the maximum obtained in the previous study (Vandal et al., 1993). It must be taken into account that these ice samples were not part of the

same section and even the same ice core. Actually, the previous and the recent drilling sites at Dome C are located about 50 km far from each other. The considerable difference in Hg levels between our study and that by Vandal et al. (1993) may have important implications on the understanding the biogeochemical cycle of Hg given that accurate estimation of its levels in Polar areas in important. This might also indicate the importance of short-term monitoring of Hg in such archives. We suggest that the lower number of samples analyzed in the previous work may have resulted in an underestimation of the variability of the mercury concentration during the LGA.

10.2 Changes in concentration during the last eight climatic cycles

Deep ice cores, retrieved from polar ice caps, represent a unique environmental archive which may reveal the past behaviors of atmospheric mercury species (Boutron et al., 1998; Vandal et al., 1993). Thirty-six ice sections were analyzed for methylmercury ($MeHg^{+}$) and inorganic mercury (Hg^{2+}) concentration whilst seventy ice sections were analyzed for total mercury (Hg_T) concentration, in an Antarctic ice core drilled at Dome C (DC) (East Antarctica, 75°06'S; 123°21E; 3233 m a.s.l.) as part of the European Project for Ice Coring in Antarctica (EPICA) (EPICA community members, 2004).

The depths of the ice sections ranged from 86.9 to 2138.4 m, spanning a period from the late Holocene (~2 kyr BP) back to the penultimate glacial age, (~210 kyr BP) for MeHg and Hg^{2+} and from 86.9 to 3061.6 m for Hg_T, spanning a period from the late Holocene back to Marine Isotopic Stage MIS 16.2 (~671 kyr BP) (see Table V, appendix II).

Concentrations of Hg_T and Hg^{2+}were found at the pg g^{-1} level (1 pg g^{-1} = 10^{-12} g g^{-1}), whereas MeHg concentrations were about one order of magnitude lower (see **Figure 10.2.1**). It is remarkable that for all Hg species investigated in this work the concentrations varied considerably with time during the last eight climatic cycles.

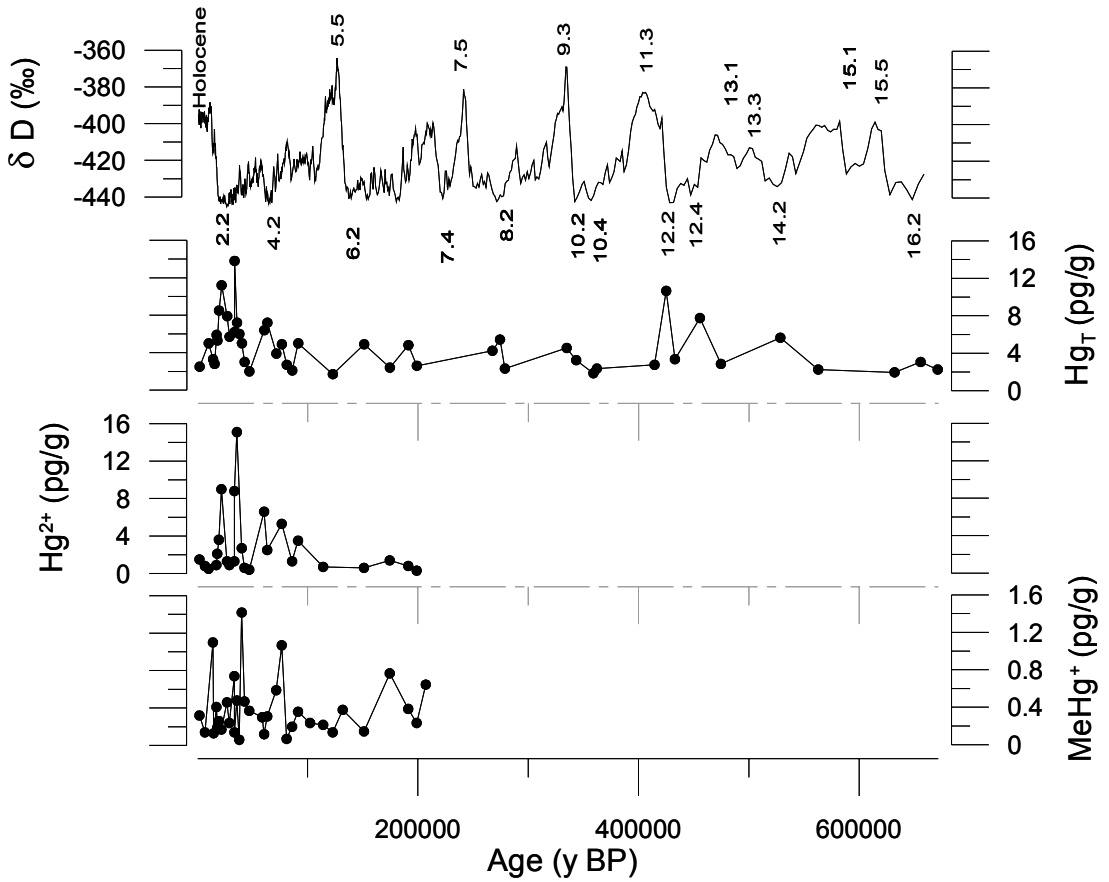

Fig. 10.2.1: *EPICA/Dome C ice core: Concentrations for $MeHg^+$ and Hg^{2+} spanning a period from the late Holocene (~2 kyr BP) back to the penultimate glacial age, (~210 kyr BP) and for Hg_T from 86.9 to 3061.6 m, spanning a period from the late Holocene back to Marine Isotopic Stage MIS 16 (EDC3Beta6 timescale from Parrenin et al, 2007). Also show at the top of the figure are is the deuterium profile and MIS numbers (EPICA Community members, 2004). Concentrations are expressed in pg/g, except for deuterium (delta per mil).*

The Hg^{2+} levels determined in DC ice were generally <1.5 pg g^{-1} during the Holocene, and were below the limit of detection especially during the last glacial-interglacial transition and the last interglacial. The highest levels for Hg^{2+} were determined during the late stages of the LGA, when levels reached ~15 pg g^{-1} (~36 ky B.P.) and during the Last Glacial Maximum (~9 pg g^{-1}, ~22 ky B.P.).

If we want to compare our Antarctic data, to date there is only a single mercury record on a climatic time scale (Vandal et al., 1993), which was obtained from the first deep ice core retrieved at Dome C, covering ~34 kyr. As determined in that work, only the mercury fraction

involved in easily reducible complexes by $SnCl_2$ is comparable to Hg^{2+} concentrations presented in our study. Actually, complexes reactive with $NaBEt_4$ (used as a derivatization reagent in our method (Jitaru et al., 2004)), are easily reducible also by $SnCl_2$ and are therefore quantified in a similar manner by the two procedures. It is remarkable that the maximum level of Hg^{2+} obtained in our study during the Last Glacial Maximum (LGM) (~9 pg g^{-1}, 22 kyr BP) is significantly higher than the maximum mercury concentration obtained by the previous study (Vandal et al., 1993) at approximately the same time (~2 pg g^{-1}, 21 kyr BP). It must be taken into account that these ice samples were not part of the same ice section and even the same ice core. Actually, the old and the recent drilling sites at Dome C are located about 50 km apart. We suggest that the lower number of samples analyzed in the previous work may have resulted in an underestimation of the variability of the mercury concentration during the LGA.

The relevant Hg^{2+} concentration value found at the LGM (~9 pg g^{-1}, 22 kyr BP) is independently confirmed by a noticeable Hg_T level obtained with a different method in the same ice section (~11 pg g^{-1}). In addition, although not in all cases, high Hg^{2+} concentrations, such as those measured in deeper sections (9, 15 and 6.6 pg g^{-1} at 34, 36 and 61 kyr BP respectively), are also supported by particularly high Hg_T levels measured in the same ice sections (14, 7 and 6 pg g^{-1}). However, the higher value of Hg^{2+} than Hg_T at 36 kyr BP remains unexplained. In most of the other cases levels of Hg^{2+} are lower than those of Hg_T. This difference suggests that mercury is present in ice also in insoluble forms such as HgS and/or other strongly bound Hg(II) complexes, which cannot be measured by the speciation method (Jitaru and Adams, 2004). Similar results were found by Ferrari et al. (2002) in which levels of Hg_T up to 100 times higher than those of Hg^{2+} level were assessed in Alpine snow.

Hg_T concentrations were rather low during interglacial and warm interstadials, in general ranging from below the method detection limit (1 pg g^{-1}) up to ~2 pg g^{-1}. Conversely, during the coldest periods of the last glacial ages Hg_T concentrations ranged between ~3 pg g^{-1} up to ~14 pg g^{-1} and hence were up to 7 times higher compared to interglacial and warm interstadials, with particularly high concentrations during marine isotopic stages (MIS) 2.2 and 4.2 (see **Figure 10.2.1**). At ~386 ky B.P. a much higher concentration (65 pg g^{-1}) was obtained for Hg_T, but it is not clear whether this is a real level of Hg_T in Antarctic ice or is caused by contamination.

The pronounced difference in Hg levels during the glacial and interglacial stages cannot be explained by a variation in the snow accumulation rate, which varied in DC by only a factor of 2 between glacial and interglacial periods (EPICA Community members, 2004). Hence, the natural Hg contribution to the Antarctic Dome C mercury budget in ice, as well as the transport and deposition processes of Hg should be considered.

10.3 Contribution from natural sources to mercury budget

The potential natural sources of atmospheric Hg include continental dust, the oceans, and volcanoes (Pyle and Mather, 2003). In order to estimate the Hg contribution from aeolian dust, we have calculated the crustal enrichment factor (EF_c) defined as:

$$EF_c = \{[Hg_T]/[Mn]\}_{ice} / \{[Hg_T]/[Mn]\}_{crust}$$

where $\{[Hg_T]/[Mn]\}_{crust}$ is the concentration ratio in the upper continental crust (Wedepohl, 1995) and $[Mn]_{ice}$ is the Mn concentration, which is used as a dust proxy in the same DC ice samples (Gabrielli et al., 2005). EF_c range from ~30 during cold periods up to ~5000 (Table VI, Annexe II) during interglacials and are evidence of a negligible Hg contribution from continental dust.

The evaluation of the Hg input from volcanoes is based on an estimated Hg/S mass ratio in volcanic emissions of between ~10^{-4}-10^{-6} (Pyle and Mather, 2005) (10^{-5} used in our study) and assuming that ~10% of the sulphate of non sea-salt origin ($nss.SO_4$) in ice ($nss.SO_4=[SO_4]_{ice}-\{[SO_4]/[Na])_{marine}\times[Na^+]_{ice}\}$) is contributed by volcanoes (Vandal et al., 1993) ($[SO_4]_{ice}$ and $[Na^+]_{ice}$ data from ref. (Wolff et al., 2006)). Using this criterion, volcanic Hg contribution accounts for 0.1-5% of Hg_T. Furthermore, given that Hg/Na in sea water is ~10^{-12} (Gill and Fitzgerald, 1987) and assuming that $[Na^+]_{ice}$ (corrected with $[Mn]_{ice}$ for the crustal contribution) originates exclusively from sea salt, the sea-spray Hg contribution is <10^{-7} pg g^{-1} (Table VI, Annexe II). The cumulative input of Hg from continental dust (Hg_{crust}), volcanoes ($Hg_{volcanic}$) and sea-spray ($Hg_{sea\ spray}$) accounts for less than 5% of Hg_T in our study.

It is accepted nowadays that the primary source of Hg in East Antarctica during the LGA was the non sea-salt biogenic oceanic emission of Hg^0 (Vandal et al., 1993). Based on the fact that ~80% of nss.SO_4 results from the oxidation of dimethylsulfide (DMS) of oceanic biogenic origin (Prospero et al., 1991) and also on the basis of an estimated ratio Hg/S of ~4.4×10^{-5} (S from DMS) (Kim and Fitzgerald, 1986; Cline and Bates, 1983), the calculated biogenic marine contribution explains ~ 15-180% (70% at the median) of the Hg_T level. Because the processes driving the emission of DMS and Hg from the oceans might differ, and in addition, the cumulated uncertainties of the determination of Na, Mn and SO_4 in ice (used to calculate the oceanic Hg contribution) a relatively large uncertainty in these estimates is possible. Nevertheless, DMS and Hg are both related to ocean productivity and thus our estimate supports (mostly possibly also during warm periods) a significant direct Hg contribution from oceanic biogenic emissions.

10.4 Contribution of Hg from the Southern Ocean to the Antarctic during glacial periods

A higher biogenic-oceanic Hg_T fallout to the East Antarctic plateau during the coldest periods, compared with the Holocene, may be explained by an increased bio-productivity of the Southern Ocean due to iron fertilization originating from the enhanced dust fallout (Martin, 1990). However, this interpretation is challenged by the recent evidence that the nss.SO_4 flux in Dome C was found to be relatively constant during glacial and interglacial periods (Wolff et al., 2006). Thus, at least in the adjacent coastal Antarctic area of the Southern Ocean where DMS is emitted, there seems to be little change in bio-productivity from glacial periods to Holocene. Alternatively, the higher biogenic-oceanic Hg_T glacial fallout during the coldest periods may be explained by an enhanced glacial productivity, north of the polar front (Kohfeld et al., 2005). In order to investigate whether the strong Hg_T increase recorded during the glacial stages was due to changes in Hg species linked to oceanic bio-productivity, $MeHg^+$ was also determined in the DC ice, given its biogenic production by the Southern Ocean (Mason, 2005).

In most DC ice samples $MeHg^+$ was assessed at levels below 0.5 pg g^{-1} (Table V, Annexe II) but higher levels were also sporadically recorded during the LGA (e.g. ~1.4 pg g^{-1} at ~40 ky B.P.). The origin of $MeHg^+$ in polar environments is still a matter of debate, as it is not clear whether this species is transported onto the polar snow or it is biologically produced on site by bacteria

(Loseto et al., 2004). However, the biomethylation of (inorganic) Hg in Antarctica has not yet been proved. In fact, given the extremely low temperatures at DC and hence very unfavorable climatic conditions for metabolic processes, we suggest that biomethylation of (inorganic) Hg in Antarctic ice is highly unlikely. The determination of $MeHg^+$ in Antarctic ice can therefore be the first *direct* evidence of the contribution of Hg from the Southern Ocean to Antarctica.

The biogenic marine sources can significantly contribute to the atmospheric concentration of some heavy metals, especially of Hg, by means of methylation processes (Pongratz and Heumann, 1998). It was already shown that macroalgae and bacteria produce $MeHg^+$ and dimethylmercury (Me_2Hg) by methylation of Hg^{2+} in the Southern Ocean (Pongratz and Heumann, 1998). The production of Me_2Hg by macro algae seems to be lower compared to $MeHg^+$, but the fully methylated Hg species (Me_2Hg) is preferentially transferred from the ocean into the atmosphere due to its higher volatility and very low solubility compared to $MeHg^+$ (Pongratz and Heumann, 1999).

Given that the atmospheric residence time of Me_2Hg is ~2 days (Heumann, 2001), and that the time needed for oceanic aerosols to reach Central Antarctica from the coast is ~1-2 days (Bodhaine et al., 1986), it is possible that gaseous Me_2Hg is transported from the Southern Ocean to the Antarctic atmosphere, before it is converted to $MeHg^+$ and ultimately to Hg^0 (Heumann, 2001).

The enrichment of $MeHg^+$ in the ocean microlayer makes it also available for transport as sea-spray or sea-ice aerosols (Pongratz and Heumann, 1999) in Antarctica where it could be deposited to some extent in this form before and also converted to Hg^0 and ultimately oxidized to Hg^{2+} before deposition (Heumann, 2001).This can explain the assessment of $MeHg^+$ in the ancient Antarctic ice, which may actually be the first evidence of the *direct* contribution of the Southern Ocean with Hg to Antarctica.

Apart from Hg^0, which is the Hg species most abundantly emitted by oceans (Mason, 2005; Heumann, 2001), the production of Me_2Hg and $MeHg^+$ in the Southern Ocean may have contributed significantly to the atmospheric Hg^0 budget and in turn to the fallout of reactive Hg^{2+}

to East Antarctica. In this context, it is noticeable that Hg^{2+} and Hg_T levels in DC are correlated (r=0.65) and moreover, their maximum levels are highly comparable. This provides evidence that Hg^{2+} contributed significantly to the total Hg budget (Hg_T) in ancient Antarctic ice, especially during coldest periods.

10.5 Insoluble dust versus mercury relationship during coldest climatic stages

Additionally, in spite of a negligible contribution from continental dust, Hg_T and Hg^{2+} match rather well the insoluble dust concentration profile obtained in the same ice core (Delmonte et al., 2004) (see **Figure 10.5.1**). In particular, Hg_T levels are correlated with those of Mn (r=0.65), the proxy for insoluble dust used in this study. These links support the conclusion that, although originating from a different source (indicated by the very high EF_c), Hg_T was deposited concomitantly with the continental particles and often as Hg^{2+} onto the East Antarctic plateau during the coldest climatic stages.

The contemporaneous deposition of dust and Hg^{2+}, possibly of biogenic oceanic origin, cannot, however, be ascribed to an intensified meridional transport of aerosol (Wolff et al., 2006). Recent findings have shown that the increase in dust and sea salt fallouts recorded in glacial times were mostly caused by higher Aeolian dust production in Patagonia and a larger sea ice extent around Antarctica during cold periods, rather than increased meridional transport (Wolff et al., 2006). Thus, another process must have produced the higher Hg accumulation in DC ice during the coldest climatic periods.

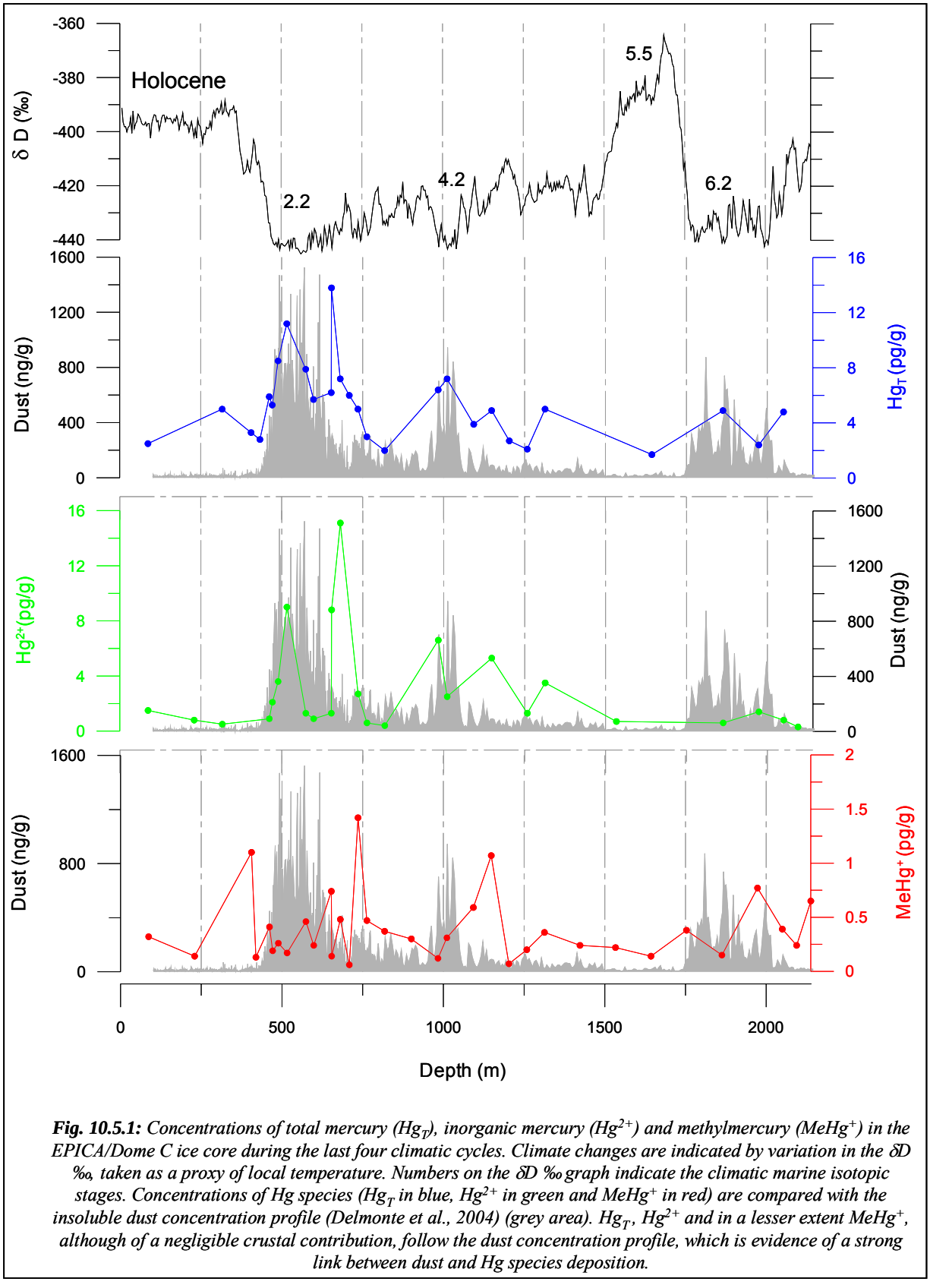

Fig. 10.5.1: *Concentrations of total mercury (Hg_T), inorganic mercury (Hg^{2+}) and methylmercury ($MeHg^+$) in the EPICA/Dome C ice core during the last four climatic cycles. Climate changes are indicated by variation in the δD ‰, taken as a proxy of local temperature. Numbers on the δD ‰ graph indicate the climatic marine isotopic stages. Concentrations of Hg species (Hg_T in blue, Hg^{2+} in green and $MeHg^+$ in red) are compared with the insoluble dust concentration profile (Delmonte et al., 2004) (grey area). Hg_T, Hg^{2+} and in a lesser extent $MeHg^+$, although of a negligible crustal contribution, follow the dust concentration profile, which is evidence of a strong link between dust and Hg species deposition.*

10.6 Modeling of the enhanced Hg accumulation during glacial stages

The enhanced Hg accumulation during the coldest periods can be explained by the following simple model (J.MC.Plane, University of Leeds, pers. comm.). Rapid Hg scavenging in polar coastal areas (AMDEs) is driven by halogen (mainly bromine) chemistry. Br_2 and BrCl are emitted from frozen surfaces such as snow (McConnell et al., 1992), frost flowers (Rankin et al., 2002), aerosol (Vogt et al., 1996) and ice clouds (Gauchard et al., 2005) after oxidation of the sea-salt derived bromine ions (Foster et al., 2001).

Subsequently, Br atoms are produced through photolysis and the BrO radical is generated by the reaction of Br with O_3. Iodine, produced from the biogenic emission of iodo-carbons and I_2, may also play a role in the activation of bromine (Brooks et al., 2006). Once bromine is activated in the form of Br and BrO radicals, and atmospheric temperatures drop below ~253 K, Hg^0 is converted to the very stable Hg^{2+} state, forming Reactive Gaseous Mercury (RGM), which is then scavenged to the snowpack.

However, there is recent evidence that a significant fraction of the snowpack RGM is photochemically reduced back to Hg^0, and then re-emitted to the atmosphere (Brooks et al., 2006). We assume here that RGM, which first adsorbs onto fine mineral aerosol before being deposited is permanently removed to the snowpack. This is consistent with observations of Hg bound to sub-micron dust particles (Milford and Davidson, 1985; Keeler et al., 1995) and is supported by our observation that dust deposition is closely linked to Hg_T and Hg^{2+} fallout during the coldest climatic stages 2.2, 4.2 and 6.2 (see **Figure 10.2.1** and **Figure 10.5.1**).

Recent observations of the seasonal behavior of BrO and IO at Halley Bay (about 15 km from the present sea ice edge) show that these radicals are present throughout the sunlit part of the year, with average concentrations of ~6 parts per trillion (ppt). This study also showed that these halogen oxides are present at levels of around 3 ppt in air masses that had originated from the interior of Antarctica, indicating that the halogens remain active in the gas phase for several days. Here we assume average IO and BrO concentrations of 5 ppt in air transiting from coastal

Antarctica to DC. During the sunlit period, the corresponding concentrations of Br and I are then ~0.6 and 2.4 ppt (Saiz-Lopez et al., 2007).

The rates of oxidation of Hg^0 to Hg^{2+} (i.e. $HgBr_2$ and HgBrI) can then be estimated using a formalism we have derived recently (Saiz-Lopez et al., 2007; Goodsite et al., 2004). Assuming that the average Antarctic boundary layer temperature was 206 K during the coldest periods compared with 216 K during interglacial periods (EPICA Community members, 2004), and that the halogen levels were unchanged, then the rate of oxidation of Hg^0 to Hg^{2+} would have varied from 4.8×10^{-3} to 4.3×10^{-3} s^{-1} i.e. an e-folding lifetime of ~6 hours, with little change over a climatic cycle.

This lifetime is short compared to the transit time from coastal Antarctica to the East Antarctic plateau (>one day), so that effectively all the Hg^0 in the boundary layer would be oxidized to RGM well before reaching DC. This calculation shows that even if halogen levels were higher during the coldest periods because of the greater extent of sea ice (Wolff et al., 2006), the gas-phase oxidation rate of Hg^0 alone would not explain the increased rate of Hg^{2+} deposition in the DC ice.

Instead, a more important factor appears to be the dramatic variation in the fine dust loading over a climatic cycle. The dust surface area in the boundary layer at DC ranged between 1.2×10^{-8} and 6×10^{-8} m^2 m^{-3} during the Holocene and 30×10^{-8} and 150×10^{-8} m^2 m^{-3} during LGM. For our model we considered the median specific surface area of 3.6×10^{-10} cm^2 cm^{-3} during the Holocene and 90×10^{-8} cm^2 cm^{-3} for the LGM, respectively. Assuming a deposition velocity of 0.2 cm s^{-1}(Brooks et al., 2006) for an efficient uptake of RGM on mineral dust and subsequent deposition of the Hg-rich dust, causes permanent removal of Hg from the atmosphere because the dust particles act as a stabilizing agent in the snow mantle; RGM is also deposited directly to the snowpack (with a deposition velocity of 0.2 cm s^{-1} and a boundary layer height of 350 m (King et al., 2006)); however, 60% of this is recycled photochemically to Hg^0 (Brooks et al., 2006). The e-folding lifetime of Hg^0 against permanent deposition as RGM is then 41 hours in the dusty atmosphere of the LGM, compared with 128 hours during the Holocene. This is consistent with the three-fold increase in the flux of Hg^{2+} and the doubled flux of Hg_T recorded in Antarctic ice

during the coldest and dusty period (MIS 2.2) (on average ~7 pg cm^{-2} y^{-1} of Hg^{2+} and 12 pg cm^{-2} $y^{-1}$of Hg_T), compared with the interglacial periods (~2 pg cm^{-2} y^{-1} of Hg^{2+} and 6 of Hg_T pg cm^{-2} y^{-1}) (Table VII, Annexe II).

A final important point is that significantly higher concentrations of sea salt and dust have been found in ice from the Antarctic coastal regions during the coldest climatic stages, compared with Dome C (Wolff et al., 2006). Thus, it is likely that there was much higher Hg fallout to the coastal areas than that detected in Dome C, which is situated on the high and remote East Antarctic plateau. Coastal polar regions would then have acted as an important sink for Hg during the LGA, modulating its abundance in the Earth's atmosphere and consequently its biogeochemical cycle during the last climatic cycles. Additional evidence to test this hypothesis will likely be provided by measuring the concentrations of Hg_T, $Hg^{2+}$and $MeHg^{+}$ in coastal Antarctic ice records such as those obtained at Dronning Maud Land (EPICA) and Talos Dome (TALDICE).

REFERENCES

Bassinot FC, Labeyrie LD, Vincent E, Quidelleur X, Shackleton NJ, Lancelot Y (1994) The astronomical theory of climate and the age of Brunhes-Matuyama magnetic reversal. *Earth and Planetary Science Letters* **126**, 91-108

Bodhaine BA, Deluisi JJ, Harris JM, Houmere P, Bauman S (1986) Aerosol measurements at the South Pole. *Tellus* **38B**, 223-235

Boutron CF (1990) A clean laboratory for ultralow concentration heavy metals analysis. *Fresenius Journal of Analytical Chemistry* **337,** 482-491

Boutron CF, Vandal GM, Fitzgerald WF, Ferrari C (1998) A forty year record of mercury in central Greenland snow. *Geophysical Research Letters* **25**, 3315-3318

Brooks SB, Saiz-Lopez A, Skov H, Lindberg SE, Plane JMC, Goodsite ME (2006) The mass balance of mercury in the springtime arctic environment. *Geophysical Research Letters* **33**, L13812, doi: 10.1029/2005GL025525

Candelone JP, Hong S, Boutron CF (1994) An improved method for decontaminating polar snow or ice cores for heavy metals analysis. *Analytica Chimica Acta* **299**, 9-16

Capelli R, Mingianti V, Chiarini C, De Pellegrini R (1998) Mercury in snow layers from Antarctica. *International Journal of Environmental Analytical Chemistry* **7**, 245-253

Cline JD, Bates TS (1983) Dimethyl sulfide in the equatorial pacific ocean: a natural source of sulfur to the atmosphere. *Geophysical Research Letters* **10**, 949-952

Delmonte B, Basile-Doelsch I, Petit JR, Maggi V, Revel-Rolland M, Michard A, Jagoutz E, Grousset F (2004) Comparing the EPICA and Vostok dust records during the last 220,000 years: stratigraphical correlation and provenance in glacial periods. *Earth Science Reviews* **66**,573-589

Ebinghaus R, Kock HH, Temme C, Einax JW, Löwe AG, Richter A, Burrows JP, Shroeder WH (2002) Antarctic springtime depletion of atmospheric mercury. *Environmental Science and Technology* **36**, 1238-1244

EPICA Community members (2004) Eight glacial cycles from an Antarctic ice core. *Nature* **429**, 623-628

Ferrari C, Moreau AL, Boutron CF (2000) Clean conditions for the determination of ultra-low levels of mercury in ice and

snow samples. *Fresenius Journal of Analytical Chemistry* **366**, 433-437

Ferrari C, Dommergue A, Veysseyre A, Planchon F, Boutron CF (2002) Mercury speciation in the French seasonal snow cover. *Science of the Total Environment* **287**, 61-69

Ferrari C, Dommergue A, Boutron CF, Jitaru P, Adams FC (2004) Profiles of mercury in the snow pack at Station Nord, Greenland shortly after polar sunrise. *Geophysical Research Letters* **31**, 10.1029/2003GL018961

Foster KL, Plastridge LA, Bottenheim JW, Shepson PB, Finlayson-Pitts BJ, Spicer CW (2001) The role of Br_2 and BrCl in surface ozone destruction at polar sunrise. *Science* **291,** 471-474

Gauchard PA, Aspmo K, Temme C, Steffen A, Ferrari C, Berg T, Ström J, Kaleschke L, Dommergue A, Bahlmann E, Magand O, Planchon F, Ebinghaus R, Banic C, Nagorski S, Baussand P, Boutron C (2005) Study of the origin of atmospheric mercury depletion events recorded in Ny-Alesund, Svalbard, spring 2003. *Atmospheric Environment* **39**, 7620-7632

Gill GA, Fitzgerald WF (1987) Picomolar mercury measurements in seawater and other materials using stannous chloride reduction and two-stage gold amalgamation with gas phase detection. *Marine Chemistry* **20**, 227-243

Goodsite M, Plane jmc, Skov H (2004) A theoretical study of the oxidation of Hg^0 to $HgBr_2$ in the troposphere. *Environmental Science of Technology* **38**, 1772-1776.

Heumann KG (2001) Biomethylation in the Southern Ocean and its contribution to the geochemical cycle of trace elements in Antarctica. In: Caroli S, Cescon P, Walton D (Eds) *Environmental Contamination in Antarctica: A Challenge to Analytical Chemistry*. Elsevier, Amsterdam, 2001

Jitaru P, Adams FC (2004) Solid-phase microextraction and multicapillary gas chromatography hyphenated to inductively coupled plasma –time-of-flight-mass spectrometry. *Journal of Chromatography A*. **1055**, 197-207

Keeler GJ, Glinsorn G, Pirrone N (1995) Particulate mercury in the atmosphere: its significance, transport, transformation and sources. *Water Air and Soil Pollution* **80**, 159-168

Kim JP, Fitzgerald WF(1986) Sea-air partitioning of mercury in the equatorial Pacific Ocean. *Science* **231**, 1131-1133

King C, Argentini SA, Anderson PS (2006) Contrasts between the summertime surface energy balance and boundary layer structure at Dome C and Halley stations,

Antarctica. *Journal of Geophysical Research* **111**, D02105, doi: 10.1029/2005JD006130

Kohfeld KE, Le Quere C, Harrison SP, Anderson RF (2005) Role of marine biology in glacial-interglacial CO_2. *Science* **308**, 74-78

Lindberg SE, Brooks S, Lin CJ, Scott KJ, Landis MS, Stevens RK, Goodsite M, Richter A (2002) Dynamic oxidation of gaseous mercury in the Arctic troposphere at polar sunrise. *Environmental Science and Technology* **36**, 1245-1256

Loseto LL, Lean DRS, Siciliano SD (2004) Snowmelt sources of methylmercury to high Arctic ecosystems.*Environmental Science of Technology* **38**, 3004-3010

Martin JH (1990) CO glacial-interglacial. *Paleoceanography* **5**, 1-13

Mason RP, Fitzgerald WF, Morel FM (1994) The biogeochemical cycling of elemental mercury: anthropogenic influences. *Geochimica et Cosmochimica Acta* **58**, 3191-3198

Mason RP (2005) Air-sea exchange and marine boundary layer atmospheric transformations of mercury and their importance in the global mercury cycle. In : Pirrone N, Mahaffey KR (Eds) *Dynamics of mercury pollution on regional and global scales: Atmospheric Processes and Human Exposures Around the World,* Springer, New York

Mc Connell JC, Henderson GC, Barrie L, Bottenheim J, Niki H, Langford CH, Templeton EMJ (1992) Photochemical bromine production implicated in Arctic Boundary –layer ozone depletion. *Nature* **355**, 150-152

Milford JB, Davidson CI (1985) The sizes of particulate trace elements in the atmosphere. *Journal of the Air Pollution Control Association* **35**, 1249-1260

Parker JL, Bloom NS (2005) Preservation and control techniques for low-level aqueous mercury speciation. *Science of the Total Environment* **337**, 253-263

Planchon F, Gabrielli P, Gauchard PA, Dommergue A, Barbante C, Cairns WRL, Cozzi G, Nagorski SA, Ferrari CP, Boutron CF, Capodaglio G, Cescon P, Varga A, Wolff EW (2004) Direct determination of mercury at the sub-picogram per gram levels in polar snow and ice by ICP-SFMS. *Journal of Analytical Atomic Spectrometry* **19**, 823-830

Pongratz P, Heumann KG (1998) Production of methylated mercury and lead by polar macroalgae - a significant natural source for atmospheric heavy metals in clean

room compartments. *Chemosphere* **36 (9)**, 1935-1946

Pongratz R, Heumann KG (1999) Production of methylated mercury, lead, and cadmium by marine bacteria as a significant natural source for atmospheric heavy metals in polar regions. *Chemosphere* **39 (1),** 89-102

Prospero JM, Savoie DL, Saltzman ES, Larsen R (1991) *Nature* **350**, 221-

Pyle DM, Mather TA (2003) The importance of volcanic emissions for the global atmospheric mercury cycle.*Atmospheric Environment* **37**, 5115-5124

Rankin AM, Wolff EW, Martin S (2002) Frost flowers: implications for tropospheric chemistry and ice core interpretation. *Journal of Geophyical. Research* **107**, 4683-4697

Saiz-Lopez A, Plane JMC, Mahajan AS, Anderson PS, Bauguitte SJB, Jones AE, Roscoe HK, Salmon RA, Bloss WJ, Lee JD, Heard DE (2007) On the vertical distribution of boundary layer halogens over coastal Antarctica: implications for O3, HOx, NOx and the Hg lifetime. *Atmospheric Chemistry and Physics Discussions* **7**, 9385–9417

Schroeder W., Anlauf K, Barrie LA, Lu J, Steffen A, Schneeberger D, Berg T (1998) Measurements of atmospheric mercury species at a coastal site in the Antarctic and over the south Atlantic ocean during polar summer. *Nature* **394**, 331-332

Vandal GM, Fitzgerald WF, Boutron CF, Candelone JP (1993) Variations in mercury deposition to Antarctica over the past 34,000 years. *Nature* **362**, 621-623

Vogt R, Crutzen PJ, Sander R (1996) A mechanism for halogen release from sea-salt aerosol in the remote marine boundary layer. *Natur*e **383**, 327-330

Wedepohl KH (1995) The composition of the continental crust. *Geochimica et Cosmochimica Acta* **59**, 1217-1232

Wolff EW, Fischer H, Fundel F, Ruth U, Twarloh B, Littot GC, Mulvaney R, Röthlisberger R, de Angelis M, Boutron CF, Hansson M, Jonsell U, Hutterli MA, Lambert F, Kaufmann P, Stauffer B, Stocker TF, Steffensen JP, Bigler M, Siggaard-Andersen ML, Udisti R, Becagli S, Castellano E, Severi M, Wagenbach D, Barbante C, Gabrielli P, Gaspari V (2006) Southern Ocean sea-ice extent, productivity and iron flux over the past eight glacial cycles. *Nature* **440**, 491-496

Yu LP, Yan XP (2003) Factors affecting the stability of inorganic and methylmercury during sample storage. *Trends in Analytical Chemistry* **22**, 245-253

CHAPTER 11: CONCLUSIONS AND OUTLOOKS

After an introduction to the Quaternary climate system (Chapter 1), preceding chapters have provided a literature review of studies of trace elements, REE, determination of lead isotopic composition and mercury in polar snow and ice today and in the past (Chapters 2, 3, 4 and 5). Special precautions were undertaken to ensure the minimisation of contamination entrained in the samples prior to the measurement by ICP-SFMS (Inductively Coupled Plasma Sector Field Mass Spectrometry; trace elements, REE and mercury) and TIMS (Thermal Ionisation Mass Spectrometry; lead isotopic compositions) (Chapter 5).

This work has allowed investigating trace elements (crustal elements, metals, metalloids, REE, mercury species) and Pb isotopes variations in EPICA/Dome C ice core from 263 to 671 ky BP, taking advantages of ultra clean samples preparation procedure and the high sensitivity of Mass spectrometry techniques. They cover 400 ky BP which corresponds to 6 climatic cycles, from MIS 8.2 to MIS 16.2. Concentrations and fallout fluxes show in most cases large variations, with very low values during warm periods and much higher values during the coldest periods.

11.1 Conclusions

11.1.1 Crustal trace elements in the EPICA/Dome C ice core

Among the trace elements, crustal trace elements such as V, Cr, Mn, Fe, Co, Rb, Ba and U have been extensively measured. For V, Fe, Rb, Ba and U, the atmospheric cycle of these elements in the remote areas of the Southern Hemisphere was dominated by crustal dust, both during glacial and interglacial periods. The situation is more complex for Co and Cr. The atmospheric cycles of these two elements were dominated by crustal dust during the cold dust climatic stages while contribution from additional sources such as volcanoes was probably significant during warmer periods, especially interglacials.

Moreover, the advection of crustal trace elements to the East Antarctic plateau is found to occur when a well-defined critical value of δD (~ - 430 ‰) was reached.

Finally; previous studies has noticed that the glacial cycles display smaller amplitudes (McManus, 2004), which it was confirmed by our data. The most recent glacial maxima such as MIS 2.2 and 4.2 are indeed well pronounced, while the maxima are much less pronounced for the oldest glacial maxima such as MIS 14.2 and 16.2. Then, one possible explanation for the changes in the amplitude of the maxima in concentrations could be linked with changes in the size distribution of dust particles transported from mid-latitude areas such as Patagonia to the Antarctica ice cap, with a decreasing trend in the dust size over the last 500 ky (Lambert et al., 2007).

11.1.2 Metals and metalloids in the EPICA/Dome C ice core

Cu, Zn, As, Cd, Pb, Bi and U have been extensively measured in the EPICA/Dome C ice core samples from 263 to 671 kyr BP. The analysis of these that affected our atmosphere over 6 glacial/interglacial cycles has provided unique insight on the past natural changes of these elements without anthropogenic inputs.

For Cu, Pb and Bi, concentrations appear to be closely linked with climate conditions with high values during the coldest periods and low values during interglacial periods. The situation appears to be less clear for As, Cd and possibly Zn with observed variations which are less clearly linked with deuterium changes. Moreover, for Cu, Pb and Bi, the amplitude of the variations appears to be larger during the most recent climatic cycles than during the oldest ones whilst the situation is less clear for As and Cd.

The metals and metalloids can be separated into two groups. The first group consists of Cu, Zn and Pb. Cu, Zn and Pb mainly derived from rock and soil dust during glacial maxima, while contributions from other sources (volcanoes) were significant during interglacials. The second group consists of As, Cd and Bi. Rock and soil dust was a minor source of As and Cd during the past 671 ky whatever the period and that they mainly derived from other sources (volcanoes). Bi

shows a climatic-dust behaviour but shows also a volcanic contribution, which is most important during interglacials. Moreover, sea-salt spray is not a significant source for heavy metals and metalloids during glacial maxima and interglacials.

11.1.3 REE in the EPICA/Dome C ice core

Hereafter the most innovative scientific knowledge produced by this work is the study of Rare Earth Elements, which is the first time that such type of analyses are realized in a deep ice core. Rare Earth Elements (REE) which can be divided in three groups of elements: Light Rare Earth Elements (La to Nd); Middle Rare Earth Elements (MREE; Sm to Tb) and Heavy Rare Earth Elements (HREE; Er to Lu) correlate with the particle concentration. Dust materials being delivered from the EPICA/Dome C ice core exhibit different REE signature during glacial and interglacial periods.

Crustal trace elements provenance in glacial and interglacial epochs from 263 to 671 ky BP has been identified through a comparison, between the REE signature of the EPICA/Dome C ice core and sediments from the Potential Source Areas (PSA) of the Southern Hemisphere (South America, South Africa, Australia and Transantarctic Mountains).

More pronounced glacial maxima (MIS 8.2, MIS 10.2, MIS 10.4 and MIS 16.2) clearly suggests a dominant South American contribution whilst less pronounced glacial maxima (MIS 12.2, MIS 12.4 and MIS 14.2) show tiny changes in source mixing compared to more pronounced glacial maxima. The Eastern Australian contribution could be more important during less pronounced glacial maxima. These results suggest that the relatively greater contribution of Eastern Australian dust inferred for Antarctic less pronounced glacial maxima ice compared with more pronounced glacial maxima ice is not directly reflective of changes in dust transport, but instead it could be related to a differential weakening of South American sources during less pronounced glacial maxima time with respect to the Eastern Australian sources.

The interglacials from MIS 9.3 to MIS 15.5 are characterized by an REE signature different from that of glacial maxima. For these East Antarctic interglacial samples, crustal trace elements

suggest a mixed origin from South American regions, Eastern Australia and Transantarctic Mountains.

11.1.4 Pb isotopes in the EPICA/Dome C ice core

Pb and Pb isotopes composition have been investigated in the EPICA/Dome C ice core from 263 to 671 ky BP. In agreement with previous studies of dust in the EPICA/Dome C ice core (Vallelonga et al., 2005, Gabrielli et al., 2005a; 2005b) Pb concentrations are greater during colder climatic stages.

Values of $^{206}Pb/^{207}Pb$ reported here for deeper sections of the EPICA/Dome C ice core are in good agreement with those previously reported for the period 0-220 ky BP (Vallelonga et al., 2005). However gradually increase range of Pb isotopic variability was observed from 671 up to the Holocene. It may be related to the gradually increasing range of temperatures observed during glacial/interglacial cycles, as represented by del Deuterium values. This may also be related to changing dominance of climatic cycles from 40 ky (obliquity) forcing to 100 ky (eccentricity) forcing, according to Milanlovitch theory of climate forcing.

As with $^{206}Pb/^{207}Pb$ ratios, lead isotopic compositions are in good agreement with that reported previously for the most recent part of the EPICA/Dome C ice core (Vallelonga et al., 2005). These ranges are more restricted than those reported for the most recent 220 ky of ice at Dome C, suggesting less variability in dust sources contributing to Dome C in the past, compared to the most recent glacial cycles.

Glacial samples generally have Pb isotopic compositions closer to those reported for Southern South American dust, while interglacial samples have values with slightly greater $^{206}Pb/^{207}Pb$ and slightly smaller $^{208}Pb/^{207}Pb$. It could be explain by additional sources like Australia but currently there is no Pb isotope data available to represent Australian dust sources.

11.1.5 Mercury species in the EPICA/Dome C ice core

It is the first time total mercury and mercury species (methylmercury and inorganic mercury) have been determined in deep Antarctic ice over eight climatic cycles. The results obtained shows much stronger mercury deposition during the coldest climatic stages (~20, ~60 and ~150 kyr BP). This occurred in close concurrence with the highest atmospheric dust load. We propose that the oxidation of atmospheric mercury by halogens was enhanced in the comparatively cold, sea-salt rich atmosphere, resulting in the transfer of gaseous mercury onto crustal particle surfaces followed by rapid scavenging into the snowpack. This implies that the polar ice caps have acted as an important sink for mercury during the coldest climatic stages, and that rapid mercury deposition events are not a phenomenon of recent origin.

11.2 Outlooks

It will be interesting in the future to work with other ice cores which can be divided in two groups. The first group of ice cores correspond to coastal ice cores with higher annual snowfall to provide a detailed record of events over the last glacial cycle. The second groups of ice cores which have a low snow accumulation allow changes over several glacial cycles to be recorded at a lower resolution.

The EDML and Talos Dome ice cores correspond to the first group of ice cores. A glacial climate record derived from an ice core from Dronning Maud Land (EDML), Antarctica, which represents South Atlantic climate at a resolution comparable with the Greenland ice core records, can allow a better knowledge of the phase relationship between climate changes in the two hemispheres which is a key for understanding the Earth's climate dynamics (EPICA Community members, 2006). The Talos Dome project aims to obtain on that specific site an ice core down to the bedrock (1500 m). It will give access to a detailed record of climatic and environmental parameters in the Ross Sea area, covering the Holocene, the last deglaciation and, with a reduced temporal resolution, down to the penultimate glaciation (Frezzoti et al., 2004).

The deepest part of the EPICA/Dome C ice core will be analysed by Sungmin Hong (Korea Polar Research Insitute) in order to extend the record of trace elements and Pb isotopes to MIS 20 (~ 800 ky BP). Moreover, the Project IPICS (International Partnerships in Ice Core Sciences) will allow to obtain the oldest ice cores (up to 1.5 million year record of climate and greenhouse gases from Antarctica) (Brook and Wolff, 2006). An ice core reaching back to or towards 1.5 Ma ago would be a major step forwards an understanding Quaternary climate, and would further our understanding of the relationship between trace elements and climate. In parallel, a similar project is planned by the Scientific China Community in Dome A, East Antarctica.

In the future, it will be essential to focus the investigations on other elements such as Ir, Pt and Os, which are considered as evidence of the past fallout vaporization and re-condensation products of meteoroids, the "meteoric smoke", to the polar ice caps. Thus, using the meteoritic smoke influx, we could estimate the past accretion rate of interplanetary dust particles to the Earth and identify ancient changes in the Antarctic atmospheric circulation.

Moreover, it will be also interesting to develop a new analytical methodology in order to measure organoselenium in ice, using an ICP-SFMS. The aim of this study is to use organoselenium as a oceanic proxy. Effectively, organoselenium is considered as an element derived from ocean processes (Steinnes et al., 2005).

11.2.1 Metal and Metalloids

Currently due to the lack of data on the abundances of metals and metalloids in aerosols product by biogenic activity, it is impossible to evaluate the contribution in metals and metalloids in ice cores coming from biogenic sources. So, in the future, it will be essential to focus the investigations on the study of metals and metalloids in sea ice in Antarctica as well as in the region of the Ross Sea and the Weddell Sea in order to have a better knowledge of the trace elements emissions coming from biogenic activity in these areas of high productivity.

It could be also interesting to compare metals and metalloids variations in Antarctica over 800 kyr BP. Such a study could be done with the Dome A ice core which could cover 1,000 ky BP and the EPICA/Dome C ice core. Currently only the 671 ky have been analyzed for these

elements on the EPICA/Dome C ice core, the bottom part of EPICA/Dome C ice core (from the beginning of MIS 16 to MIS 20) is still unanalyzed.

11.2.2 Crustal trace elements and Rare Earth Elements

Much effort has to be done in order to study variations of crustal trace elements and rare earth elements with a high-resolution mode during various periods, for example the Holocene and the Last Glacial Maximum, in different Antarctic ice cores (Dome C, Dome Fuji, Dronning Maud Land, Law Dome, Thalos Dome, Vostok, etc.). So, results about crustal trace elements and rare earth elements variability within the Holocene and the Last Glacial Maximum at different sites could be discussed as well as possible phenomena of regionalisation of the transport mode in Antarctica.

11.2.3 Lead isotopes

It will be interesting in the future to determine lead isotopes in Antarctica over 800 kyr BP. Such a study could be done with the Dome A ice core and the EPICA/Dome C ice core. For doing that, it is also necessary to extend the Pb isotope record obtained by Vallelonga et al. (2005) and in this work to the last eight climatic cycles covered by the EPICA/Dome C ice core, back to ~ 800 ky BP. To taking full advantage of such data, much effort has to be done for lead isotopes measurements in different potential source areas in Australia in order to characterise sediments and aeolian deposits from the large and arid Australian continent in better detail. Also, it will be important to combine the Pb isotopes data with REE data and Sr/Nd data for a good characterization of the provenance of dust material during glacial and interglacial epochs over such a long time period.

11.2.4 Mercury species

In the future, it will be important to focus the investigations on Dome A, Vostok and the entire EPICA/Dome C ice core. In this way, comparisons can allow to have a better knowledge on the mechanism regulating the past deposition of Hg on the continental part of Antarctica. A

comparison of study of mercury species with GRIP and GISP ice cores located in Greenland could be interesting for a good understanding of the Mercury Depletion Events recently registered in both polar remote areas.

It could be also interesting to do a one dimensional thermodynamic model developed to calculate the frost flower coverage (Kaleshke et al., 2004) during various glacial and interglacial periods over the 671 ky period studies in this PhD. This model could be associated with the Hg data found over the same time period and thus helping for the understanding of mechanism regulating the deposition of Hg in Antarctica during 8 glacial/interglacial cycles.

REFERENCES

Brook E, Wolff EW (2006) The future of ice core science. *EOS Trans*. **87**, 39

EPICA Community members (2006) One-to-one coupling of glacial climate variability in Greenland and Antarctica. *Nature* **444**, 195-198

Frezzotti M, Bitelli G, de Michelis P, Deponti A, Forieri A, Gandolfi S, Maggi V, Mancini F, Remy F, Tabacco I, Urbini S, Vittuari L, Zirizzottl A (2004) Geophysical survey at Talos Dome, East Antarctica: the search for a new deep-drilling site. *Annals of Glaciology* **39**, 423-432

Gabrielli P, Barbante C, Boutron C, Cozzi G, Gaspari V, Planchon F, Ferrari C, Turetta C, Hong S, Cescon P (2005a) Variations in atmospheric trace elements in Dome C (East Antarctica) ice over the last two climatic cycles. *Atmospheric Environment* **39**, 6420-6429

Gabrielli P, Planchon FAM, Hong S, Lee KH, Hur SD, Barbante C, Ferrari CP, Petit JR, Lipenkov VY, Cescon P, Boutron CF (2005b) Trace elements in Vostok Antarctic ice during the last four climatic cycles. *Earth and Planetary Science Letters* **234**, 249-259

Grousset FE, Biscaye PE, Revel M, Petit JR, Pye K, Joussaume S, Jouzel J (1992) Antarctic (Dome C) ice-core dust at 18 k.y. B.P.: isotopic constraints and origins. *Earth and Planetary Science Letters* **111**, 175– 182

Kaleschke L, Richter A, Burrows J, Afe O, Heygster G, Notholt J, Rankin AM, Roscoe HK, Hollwedel J, Wagner T, Jacobi HW (2004) Frost flowers on sea ice as a source on sea salt and their influence on Tropospheric halogen chemistry. *Geophysical Research Letters* **31**, doi: 10.1029/ 2004GL020655

Lambert F, Delmonte B, Petit JR, Bigler M, Kaufmann PR, Huttterli MA, Stocker TF, Ruth U, Steffensen JP, Maggi V (2007) New constraints on the aeolian dust cycle and climatic implications from an 800 ka ice core record, submitted to *Nature*

McManus JF (2004) A great grand-daddy of ice cores. *Nature* **429**, 611-612

Steinnes E, Hvatum OØ, Bølviken B, Varskog P (2005) Atmospheric supply of trace elements studied by peat samples from ombotrophic bogs. *Journal of Environmental Quality* **34**, 192-197

Vallelonga P, Gabrielli P, Rosman K, Barbante C, Boutron CF (2005) A 220 ky record of Pb isotopes at Dome C Antarctica from analyses of the EPICA ice core. *Geophysical Research Letters* **32**, L01706

APPENDIX I

List of publications outcome from this work

Papers

Gabrielli P, Barbante C, Turetta C, **Marteel** A, Boutron C, Cozzi G, Cairns W, Ferrari C, Cescon P (2006) Direct determination of Rare Earth Elements at the sub-picogram per gram level in Antarctic ice by ICP-SFMS using a desolvatation system. *Analytical Chemistry* **78 (6)**, 1883-1889

Marteel A, Gaspari V, Boutron CF, Barbante C, Gabrielli P, Cescon P, Cozzi G, Ferrari CP, Dommergue A, Rosman K, Hong S, Hur SD (2007) Climate-related variations in crustal trace elements in Dome C (East Antarctic) ice during the past 671 ky. Submitted to *Climatic Change*.

Marteel A, Boutron CF, Barbante C, Gabrielli P, Cozzi G, Gaspari V , Cescon P, Christophe Ferrari CP, Dommergue A, Rosman K, Hong S, Hur SD (2007) Changes in atmospheric heavy metals and metalloids in Dome C (East Antarctica) ice back to 671 ky BP (Marine Isotopic Stage 16.2). Submitted to *Earth and Planetary Science Letters*.

Marteel A, Boutron CF, Barbante C, Gabrielli P, Cozzi G, Gaspari V , Cescon P, Christophe Ferrari CP, Dommergue A, Rosman K, Hong S, Hur SD (2007) Crustal trace elements provenance through REE signature in Dome C (East Antarctica) ice from 263 to 671 ky BP. To be submitted to *Geochimica et Cosmochimica Acta*.

Vallelonga P, **Marteel** A, Gabrielli P, Rosman KJR, Barbante C, Boutron CF (2007) Eight glacial cycles of Pb isotopic compositions in the EPICA Dome C ice core. Submitted to *Earth and Planetary Science Letters*.

Jitaru P, Gabrielli P, **Marteel** A, Plane JMC, Barbante C, Boutron CF, Adams CF, Planchon FAM, Gauchard PA, Cescon P, Ferrari CP (2007) Intense mercury scavenging from the dust and salt laden Antarctic atmosphere the glacial ages. To be submitted to *Science*.

APPENDIX II

Table I - EPICA/Dome C Antarctic ice core: V, Cr, Mn, Fe, Co, Rb, Ba and U concentrations measured in ice from 78 depth intervals from 2368.6 to 3061.9m. The length of each sample is about 20 cm and the depth given in the table is the depth for the top of the sample. The age of the ice is from the EDC3Beta6 timescale from Parrenin et al., 2007. Concentrations are expressed in pg/g, except for Fe (ng/g).

Table II - EPICA/Dome C Antarctic ice core: crustal enrichment factor (EFc) for V, Cr, Fe, Co, Rb, Ba and U in ice from 78 depth intervals, using Mn as crustal reference element. The length of each sample is about 20 cm, and the depth given in the table is the depth for the top of the sample. The age of the ice is from the EDC3Beta6 timescale from Parrenin et al., 2007.

Table III - EPICA/Dome C Antarctic ice core: Cu, Zn, As, Cd, Pb and Bi concentrations measured in ice from 77 depth intervals between 2368.6 m (age of 263 ky BP) and 3061.9 m (age of 671 ky BP). The length of each sample is about 20 cm, and the depths given in the table are the depths for the top of the samples. The age of the ice is estimated using the EDC3Beta6 timescale from Parrenin et al., 2007. Concentrations are expressed in pg/g.

Table IV - EPICA/Dome C Antarctic ice core: La, Ce, Pr, Nd, Sm, Eu, Gd, Tb, Dy, Ho, Er, Tm, Yb and Lu concentrations measured in ice from 77 depth intervals from 2368.6 to 3061.9m. The length of each sample is about 20 cm, and the depth given in the table is the depth for the top of the sample. The age of the ice is from the EDC3Beta6 timescale from Parrenin et al., 2007. Concentrations are expressed in pg/g.

Table V – Concentrations of Hg_T, Hg^{2+} and $MeHg^+$ concentrations in EPICA/Dome C ice core. The age of the ice is from the EDC3Beta6 timescale from Parrenin et al., 2007. Concentrations are expressed in pg/g.

Table VI – Crustal enrichment factors (EFc) and calculated natural Hg contribution to the Antarctic Dome C mercury budget in ice.

Table VII – Fluxes of Hg_T, Hg^{2+} and $MeHg^+$ to Antarctic Dome C ice

Table VIII – Detection Limits (DL) and Relative Standard Deviation (RSD) for all trace elements

Table I

Section number	Depth (m)	Age (yr)	Concentration							
			V	Cr	Mn	Fe	Co	Rb	Ba	U
4308	2368.6	263565	11	9	212	1	4	21	73	0.2
	2368.9	263649	9	9	243	1	< 22	19	76	0.4
4328	2379.6	267392	33	16	894	17	14	46	225	1.2
	2379.9	267500	30	15	627	12	9	34	144	0.9
4358	2396.1	274151	59	25	1252	28	21	67	271	1.3
	2396.4	274268	42	29	896	22	15	48	204	1.7
4378	2407.1	278656	10	9	313	4	6	17	67	0.3
	2407.4	278777	16	13	496	6	11	21	92	0.4
4418	2429.1	286327	3	5	88	0.8	2	7	26	< 0.1
	2429.4	286413	3	5	69	1.1	1	8	20	0.1
4638	2550.1	327365	2	5	31	0.6	1	3	8	0.02
	2550.4	327432	0.7	3	15	0.2	0.5	3	5	< 0.02
4658	2561.1	330017	1	3	24	0.3	0.9	3	7	0.03
	2561.4	330083	0.8	4	21	0.3	0.9	3	7	0.02
4678	2572.1	332601	2	16	20	0.3	0.6	3	8	< 0.02
	2572.4	332653	7	4	56	1	2	3	11	0.07
4698	2583.1	334702	0.9	4	13	0.2	0.4	3	7	< 0.02
	2583.4	334762	4	6	50	1	2	3	14	0.05
4738	2605.1	343250	21	10	387	2	6	26	121	0.6
	2605.4	343403	25	13	458	3	10	25	102	0.5
4788	2632.6	358780	19	12	563	3	10	25	125	1.1
	2632.9	358947	18	12	483	2	9	22	118	0.6
4798	2638.1	361992	15	12	230	4	5	16	58	0.4
	2638.4	362150	19	11	368	5	7	27	88	0.6
4818	2649.1	368148	21	13	524	7	7	31	109	1.1
	2649.4	368303	21	9	246	4	5	20	73	0.4
4878	2682.1	385808	2	4	49	0.4	0.9	5	16	0.06
	2682.4	385942	2	4	39	0.3	1	4	10	0.03
4898	2693.1	391793	2	4	58	0.6	1	5	17	0.05
	2693.4	391942	1	5	51	0.8	3	5	14	0.04
4948	2720.6	402652	2	4	19	0.3	0.8	3	7	< 0.05
	2720.9	402741	0.7	3	20	0.2	2	3	7	< 0.05
5008	2753.6	414265	0.8	6	12	0.1	1	3	4	< 0.04
	2753.9	414392	1	8	19	0.1	2	4	9	0.13
5028	2765.6	419265	0.6	4	24	0.3	0.6	4	7	0.15
	2765.9	419398	1.8	3	25	0.3	1	4	11	< 0.02
5048	2776.6	424905	3	4	44	0.5	1	4	14	0.03
	2776.9	425027	1	3	24	0.3	1	4	9	< 0.03
5068	2786.6	432598	48	22	965	21	14	45	282	1.2
	2786.9	432870	48	21	400	14	9	34	140	0.7
5098	2803.1	449435	22	14	714	11	10	27	127	0.6
	2803.4	449719	41	22	980	20	14	45	194	0.7
5108	2808.6	455259	25	10	319	2	5	30	112	0.6
	2808.9	455550	48	27	1162	7	21	25	261	0.6
5138	2825.1	474273	13	8	175	1	5	12	57	0.7
	2825.4	474576	7	9	115	1	3	10	42	0.5
5148	2830.6	479361	5	4	141	2	4	12	36	0.2
	2830.9	479623	6	5	110	1	2	10	30	0.2
5178	2847.1	491650	1	5	19	0.2	0.6	4	6	0.04
	2847.4	491845	1	4	25	0.3	0.6	4	7	0.05
5228	2875.6	511071	3	3	55	0.6	2	6	14	0.03
	2875.9	511267	4	6	64	0.7	2	6	19	< 0.05
5278	2902.1	528239	3	8	61	0.3	2	15	40	0.3
	2902.4	528422	3	9	73	0.4	4	15	40	0.3
5288	2907.6	532571	15	8	337	7	5	17	72	0.4
	2907.9	532841	17	7	104	5	-	12	41	0.2
5298	2913.1	537923	29	21	248	8	5	23	62	0.4
	2913.4	538194	16	10	416	8	7	24	64	0.3
5328	2929.6	554062	2	5	68	0.8	2	6	20	0.08
	2929.9	554250	2	5	91	1.3	2	7	27	0.1
5358	2946.1	562690	2	6	35	0.1	2	4	11	0.1
	2946.4	562799	2	3	35	0.0	8	4	6	< 0.2
5378	2957.1	566577	1	5	14	0.0	1	4	5	0.09
	2957.4	566671	1	4	19	0.0	1	3	4	0.03
5418	2979.1	574322	1	10	31	0.2	2	5	10	0.08
	2979.4	574428	1	3	29	0.1	1	4	9	0.06
5468	3006.6	591058	3	8	74	0.7	6	17	43	0.3
	3006.9	591301	5	8	130	0.8	4	19	55	0.5
5488	3017.6	603812	2	3	50	0.5	1	4	12	0.03
	3017.9	604150	2	3	45	1.0	0.8	9	47	0.2
5508	3028.6	615972	2	6	31	0.1	1	5	9	0.08
	3028.9	616273	2	3	32	0.3	1	5	9	0.06
5528	3040.6	631304	15	10	529	8	7	20	86	0.5
	3040.9	631964	14	10	576	8	8	21	88	0.5
5548	3050.6	655109	10	8	232	2	5	22	80	0.4
	3050.9	655611	8	7	155	1	4	18	62	0.6
5568	3061.6	671102	23	10	328	2	5	28	109	0.9
	3061.9	671706	19	10	453	2	< 40	25	102	0.7

Table II

			EFc						
Section number	Depth (m)	Estimated Age (yr)	V	Cr	Fe	Co	Rb	Ba	U
4308	2368.6	263565	0.5	0.7	0.1	0.8	0.5	0.3	0.2
	2368.9	263649	0.4	0.5	0.1	4	0.4	0.2	0.3
4328	2379.6	267392	0.4	0.3	0.3	0.7	0.2	0.2	0.3
	2379.9	267500	0.5	0.4	0.3	0.7	0.3	0.2	0.3
4358	2396.1	274151	0.5	0.3	0.4	0.8	0.3	0.2	0.2
	2396.4	274268	0.5	0.5	0.4	0.8	0.3	0.2	0.4
4378	2407.1	278656	0.3	0.4	0.2	0.9	0.3	0.2	0.2
	2408.4	278777	0.3	0.4	0.2	1.0	0.2	0.1	0.2
4418	2429.1	286327	0.3	0.8	0.2	0.9	0.4	0.2	0.2
	2429.4	286413	0.4	1	0.3	0.9	0.6	0.2	0.3
4638	2550.1	327365	0.5	2	0.3	1	0.5	0.2	0.1
	2550.4	327432	0.5	3	0.2	2	0.8	0.3	0.3
4658	2561.1	330017	0.5	2	0.2	2	0.7	0.2	0.2
	2561.4	330083	0.4	3	0.3	2	0.7	0.3	0.2
4678	2572.1	332601	1.0	12	0.3	1	0.7	0.3	0.2
	2572.4	332653	1.1	1	0.4	2	0.2	0.1	0.3
4698	2583.1	334702	0.7	4	0.3	1	1.2	0.4	0.3
	2583.4	334762	0.9	2	0.4	1	0.3	0.2	0.2
4738	2605.1	343250	0.5	0.4	0.1	0.7	0.3	0.2	0.4
	2605.4	343403	0.5	0.4	0.1	0.9	0.3	0.2	0.2
4788	2632.6	358780	0.3	0.3	0.1	0.8	0.2	0.2	0.4
	2632.9	358947	0.4	0.4	0.1	0.9	0.2	0.2	0.3
4798	2638.1	361992	0.7	0.8	0.3	1	0.3	0.2	0.3
	2638.4	362150	0.5	0.5	0.2	0.9	0.3	0.2	0.3
4818	2649.1	368148	0.4	0.4	0.2	0.6	0.3	0.2	0.4
	2649.4	368303	0.8	0.6	0.3	0.9	0.4	0.2	0.3
4878	2682.1	385808	0.3	1	0.1	0.8	0.5	0.3	0.2
	2682.4	385942	0.4	2	0.1	1	0.5	0.2	0.1
4898	2693.1	391793	0.4	1	0.2	0.9	0.4	0.2	0.2
	2693.4	391942	0.2	1	0.3	3	0.5	0.2	0.2
4948	2720.6	402652	1.1	3	0.3	2	0.7	0.3	0.5
	2720.9	402741	0.4	2	0.2	5	0.7	0.3	0.6
5008	2753.6	414265	0.7	8	0.1	4	1.4	0.2	0.7
	2753.9	414392	0.6	7	0.1	4	1.1	0.4	1.4
5028	2765.6	419265	0.2	2	0.2	1	0.7	0.2	1.3
	2765.9	419398	0.7	2	0.2	2	0.7	0.4	0.2
5048	2776.6	424905	0.6	1	0.2	1	0.4	0.3	0.1
	2776.9	425027	0.5	2	0.2	2	0.8	0.3	0.3
5068	2786.6	432598	0.5	0.3	0.4	0.7	0.2	0.2	0.3
	2786.9	432870	1.2	0.8	0.6	1	0.4	0.3	0.4
5098	2803.1	449435	0.3	0.3	0.3	0.7	0.2	0.1	0.2
	2803.4	449719	0.4	0.3	0.3	0.7	0.2	0.2	0.2
5108	2808.6	455259	0.8	0.5	0.1	0.8	0.4	0.3	0.4
	2808.9	455550	0.4	0.4	0.1	0.8	0.1	0.2	0.1
5138	2825.1	474273	0.8	0.7	0.1	1	0.3	0.3	0.9
	2825.4	474576	0.6	1	0.1	1	0.4	0.3	0.9
5148	2830.6	479361	0.4	0.5	0.2	1	0.4	0.2	0.3
	2830.9	479623	0.5	0.7	0.2	0.8	0.4	0.2	0.3
5178	2847.1	491650	0.6	4	0.2	1	1.0	0.3	0.4
	2847.4	491845	0.5	2	0.2	1	0.8	0.2	0.4
5228	2875.6	511071	0.6	0.9	0.2	1	0.5	0.2	0.1
	2875.9	511267	0.6	1	0.2	1	0.5	0.2	0.2
5278	2902.1	528239	0.4	2	0.1	2	1.2	0.5	1.0
	2902.4	528422	0.4	2	0.1	2	1.0	0.4	1.0
5288	2907.6	532571	0.4	0.3	0.4	0.7	0.2	0.2	0.2
	2907.9	532841	1.7	1	0.9	39	0.6	0.3	0.4
5298	2913.1	537923	1.2	1	0.5	0.8	0.4	0.2	0.3
	2913.4	538194	0.4	0.4	0.3	0.7	0.3	0.1	0.2
5328	2929.6	554062	0.2	1	0.2	1	0.4	0.2	0.2
	2929.9	554250	0.3	0.8	0.3	1	0.4	0.2	0.3
5358	2946.1	562690	0.5	3	0.05	3	0.6	0.2	0.9
	2946.4	562799	0.5	1	0.01	11	0.5	0.1	1.2
5378	2957.1	566577	0.5	5	0.01	3	1.4	0.3	1.4
	2957.4	566671	0.6	3	0.02	3	0.8	0.2	0.4
5418	2979.1	574322	0.4	5	0.1	3	0.8	0.3	0.5
	2979.4	574428	0.3	2	0.03	2	0.7	0.2	0.5
5468	3006.6	591058	0.4	2	0.2	4	1.1	0.5	1.0
	3006.9	591301	0.4	0.9	0.1	1	0.7	0.3	0.8
5488	3017.6	603812	0.3	1	0.2	1	0.4	0.2	0.1
	3017.9	604150	0.5	1	0.4	0.8	0.9	0.8	0.9
5508	3028.6	615972	0.6	3	0.1	1	0.8	0.2	0.5
	3028.9	616273	0.5	2	0.1	2	0.7	0.2	0.4
5528	3040.6	631304	0.3	0.3	0.3	0.6	0.2	0.1	0.2
	3040.9	631964	0.2	0.3	0.2	0.7	0.2	0.1	0.2
5548	3050.6	655109	0.5	0.7	0.1	1	0.6	0.3	0.8
	3050.9	655611	0.4	0.5	0.1	0.9	0.5	0.3	0.3
5568	3061.6	671102	0.7	0.5	0.1	0.8	0.4	0.3	0.6
	3061.9	671706	0.4	0.3	0.1	4	0.3	0.2	0.3

Table III

Section number	Depth (m)	Estimated Age (yr)	Concentration					
			Cu	Zn	As	Cd	Pb	Bi
4308	2368.6	263 565	7	44	14	0.4	4	0.03
	2368.9	263 649	7	47	4	0.3	5	0.10
4328	2379.6	267 392	22	72	18	0.5	17	0.33
	2379.9	267 500	28	74	18	0.4	11	0.25
4358	2396.1	274 151	33	111	18	0.6	27	0.55
4378	2407.1	278 656	8	29	5	0.3	6	0.14
	2408.4	278 777	11	47	11	0.4	7	0.22
4418	2429.1	286 327	4	162	4	0.3	6	0.15
	2429.4	286 413	4	186	5	0.2	7	0.08
4638	2550.1	327 365	4	12	4	0.3	1	0.10
	2550.4	327 432	2	10	1	0.2	1	0.15
4658	2561.1	330 017	2	8	1	0.2	1	0.03
	2561.4	330 083	2	10	1	0.2	1	0.07
4678	2572.1	332 601	2	10	1	0.2	1	0.04
	2572.4	332 653	4	12	15	0.3	1	0.02
4698	2583.1	334 702	2	8	8	0.3	1	0.09
	2583.4	334 762	5	11	4	0.3	1	0.10
4738	2605.1	343 250	9	52	9	0.4	5	0.05
	2605.4	343 403	7	56	11	1.3	5	0.04
4788	2632.6	358 780	10	60	5	1.5	5	0.05
	2632.9	358 947	8	50	5	1.4	4	0.02
4798	2638.1	361 992	11	25	15	0.3	4	0.12
	2638.4	362 150	12	37	22	0.3	5	0.12
4818	2649.1	368 148	16	49	15	0.5	9	0.24
	2649.4	368 303	10	32	19	0.3	5	0.29
4878	2682.1	385 808	3	17	7	0.3	1	0.06
	2682.4	385 942	2	12	5	0.3	1	0.05
4898	2693.1	391 793	4	18	5	0.4	1	0.11
	2693.4	391 942	5	10	1	0.4	1	0.07
4948	2720.6	402 652	3	10	9	0.2	1	0.06
	2720.9	402 741	2	9	1	0.1	1	0.10
5008	2753.6	414 265	4	54	1	0.4	1	0.02
	2753.9	414 392	6	31	13	0.3	3	0.04
5028	2765.6	419 265	2	10	16	0.2	1	0.09
	2765.9	419 398	5	10	30	0.2	1	0.08
5048	2776.6	424 905	4	12	8	0.3	1	0.21
	2776.9	425 027	2	11	21	0.3	1	0.07
5068	2786.6	432 598	22	78	14	0.5	16	0.40
	2786.9	432 870	18	57	9	0.4	9	0.16
5098	2803.1	449 435	16	41	15	0.3	10	0.22
	2803.4	449 719	25	82	14	0.3	17	0.28
5108	2808.6	455 259	9	61	6	0.4	8	0.08
	2808.9	455 550	14	69	0	1.8	18	0.20
5138	2825.1	474 273	8	27	3	1.1	17	0.12
	2825.4	474 576	8	49	28	1.5	23	0.07
5148	2830.6	479 361	5	22	21	0.4	2	0.13
	2830.9	479 623	4	18	13	0.5	1	0.07
5178	2847.1	491 650	2	8	1	0.2	0.4	0.04
	2847.4	491 845	3	9	3	0.1	1	0.07
5228	2875.6	511 071	2	17	14	0.3	1	0.04
	2875.9	511 267	5	15	24	0.3	1	0.07
5278	2902.1	528 239	6	47	-	0.2	2	0.03
	2902.4	528 422	5	49	11	1.3	2	0.03
5288	2907.6	532 571	10	30	13	0.2	7	0.11
	2907.9	532 841	11	27	13	0.2	4	0.10
5298	2913.1	537 923	11	44	11	0.2	6	0.10
	2913.4	538 194	9	80	10	0.2	9	0.13
5328	2929.6	554 062	3	10	5	0.2	1	0.21
	2929.9	554 250	5	18	2	0.2	2	1.08
5358	2946.1	562 690	5	18	13	0.4	2	0.11
	2946.4	562 799	4	38	12	0.3	2	0.04
5378	2957.1	566 577	4	37	3	0.2	0	0.01
	2957.4	566 671	4	70	_	0.5	1	0.04
5418	2979.1	574 322	3	13	_	0.4	1	0.04
	2979.4	574 428	3	43	23	0.4	1	0.02
5468	3006.6	591 058	6	51	11	1.6	2	0.02
	3006.9	591 301	7	51	26	0.5	3	0.05
5488	3017.6	603 812	5	13	6	0.2	1	0.10
	3017.9	604 150	6	38	20	0.3	4	0.20
5508	3028.6	615 972	4	60	5	0.5	1	-
	3028.9	616 273	4	35	5	0.7	1	-
5528	3040.6	631 304	10	33	7	0.4	7	0.13
	3040.9	631 964	8	32	7	0.4	7	0.12
5548	3050.6	655 109	6	47	11	0.5	3	0.03
	3050.9	655 611	9	53	16	0.4	4	0.11
5568	3061.6	671 102	9	53	14	0.5	7	0.09
	3061.9	671 706	8	58	13	1.6	6	0.06

Table IV

			Concentrations														
Section number	Depth (m)	Age (yr)	La	Ce	Pr	Nd	Sm	Eu	Gd	Tb	Dy	Ho	Er	Tm	Yb	Lu	Th
4308	2368.6	263565	5.5	12.8	1.6	5.9	1.4	0.3	1.4	0.2	1.1	0.2	0.6	0.09	0.5	0.07	1.3
	2368.9	263649	3.2	7.7	0.9	3.4	0.9	0.2	0.9	0.1	0.7	0.1	0.4	0.05	0.3	0.04	0.6
4328	2379.6	267392	19.3	47.0	5.3	19.7	4.6	1.0	4.3	0.6	3.3	0.6	1.7	0.2	1.4	0.2	6.1
	2379.9	267500	12.8	29.6	3.9	12.7	3.1	0.7	3.0	0.4	2.3	0.4	1.1	0.2	1.0	0.1	4.0
4358	2396.1	274151	21.0	48.3	5.7	20.3	4.7	1.0	4.4	0.6	3.3	0.6	1.6	0.2	1.3	0.2	7.1
	2396.4	274268	26.9	63.3	7.5	26.2	6.2	1.3	5.8	0.8	4.4	0.8	2.1	0.3	1.8	0.2	9.0
4378	2407.1	278656	6.2	14.1	1.6	5.8	1.3	0.3	1.3	0.2	1.0	0.2	0.5	0.06	0.4	0.05	1.6
	2408.4	278777	8.2	18.9	2.3	8.1	1.8	0.4	1.9	0.2	1.4	0.3	0.7	0.1	0.6	0.07	1.9
4418	2429.1	286327	1.8	3.8	0.4	1.5	0.3	0.08	0.3	0.04	0.2	0.04	0.1	0.02	0.09	0.01	0.5
	2429.4	286413	1.4	3.3	0.4	1.3	0.3	0.08	0.3	0.04	0.2	0.04	0.1	0.01	0.08	0.01	0.4
4638	2550.1	327365	2.3	3.5	0.3	1.0	0.4	0.3	0.2	0.02	0.1	0.02	0.06	0.01	0.05	0.009	2.0
	2550.4	327432	0.2	0.5	0.05	0.2	0.08	0.02	0.05	0.006	0.03	0.005	0.02	0.003	0.02	0.002	0.1
4658	2561.1	330017	0.4	0.8	0.08	0.3	0.09	0.03	0.06	0.007	0.05	0.006	0.02	0.003	0.02	0.003	0.1
	2561.4	330083	0.4	0.8	0.08	0.3	0.09	0.05	0.05	0.006	0.03	0.007	0.01	0.003	0.02	0.002	0.2
4678	2572.1	332601	0.3	0.4	0.04	0.1	0.06	0.03	0.03	0.003	0.02	0.003	0.008	0.002	0.009	0.002	0.1
	2572.4	332653	1.2	2.6	0.3	1.1	0.3	0.1	0.2	0.03	0.2	0.03	0.08	0.01	0.06	0.008	0.1
4698	2583.1	334702	1.8	2.7	0.2	0.6	0.2	0.2	0.1	0.01	0.06	0.02	0.03	0.005	0.05	0.005	1.4
	2583.4	334762	6.0	11.9	1.3	4.3	1.0	0.4	0.8	0.08	0.4	0.07	0.2	0.02	0.1	0.02	11.0
4738	2605.1	343250	5.1	12.1	1.4	5.4	1.3	0.3	1.3	0.2	1.1	0.2	0.6	0.08	0.5	0.09	1.0
	2605.4	343403	5.0	11.8	1.5	5.5	1.3	0.3	1.3	0.2	1.0	0.2	0.5	0.07	0.5	0.06	1.1
4788	2632.6	358780	6.0	14.7	1.8	6.7	1.7	0.4	1.6	0.2	1.4	0.3	0.7	0.1	0.6	0.08	1.4
	2632.9	358947	4.7	11.0	1.3	5.1	1.2	0.3	1.2	0.2	1.0	0.2	0.5	0.07	0.5	0.06	0.8
4798	2638.1	361992	5.6	12.6	1.5	5.1	1.2	0.3	1.1	0.1	0.8	0.2	0.4	0.06	0.4	0.05	1.7
	2638.4	362150	7.9	17.9	2.1	7.3	1.6	0.4	1.6	0.2	1.2	0.2	0.6	0.09	0.5	0.07	2.4
4818	2649.1	368148	30.5	64.9	7.4	24.7	5.2	1.1	5.1	0.7	3.9	0.7	2.0	0.3	1.7	0.2	4.6
	2649.4	368303	7.1	15.3	1.9	6.3	1.4	0.3	1.3	0.2	1.0	0.2	0.5	0.07	0.5	0.06	2.1
4878	2682.1	385808	0.7	1.6	0.1	0.5	0.1	0.03	0.1	0.01	0.07	0.01	0.04	0.006	0.03	0.004	0.3
	2682.4	385942	0.5	1.2	0.1	0.3	0.09	0.02	0.06	0.008	0.04	0.009	0.03	0.004	0.02	0.003	0.2
4898	2693.1	391793	1.1	2.4	0.2	0.8	0.2	0.07	0.2	0.02	0.1	0.03	0.07	0.01	0.06	0.009	0.4
	2693.4	391942	3.2	6.1	0.6	2.0	0.5	0.3	0.4	0.06	0.3	0.06	0.1	0.02	0.1	0.02	1.3
4948	2720.6	402652	0.4	0.8	0.08	0.3	0.1	0.03	0.07	0.009	0.05	0.009	0.02	0.004	0.02	0.003	0.2
	2720.9	402741	0.3	0.6	0.06	0.2	0.09	0.03	0.05	0.006	0.04	0.007	0.02	0.003	0.02	0.0023	0.1
5008	2753.9	414392	0.3	0.6	0.05	0.2	0.06	0.02	0.06	0.006	0.04	0.005	0.03	0.004	0.02	0.003	0.07
5028	2765.6	419265	0.3	0.5	0.05	0.2	0.06	0.02	0.03	0.004	0.02	0.005	0.02	0.003	0.02	0.003	0.1
	2765.9	419398	0.4	0.8	0.09	0.3	0.09	0.03	0.06	0.01	0.05	0.01	0.02	0.004	0.02	0.003	0.1
5048	2776.6	424905	0.8	1.8	0.2	0.6	0.2	0.05	0.1	0.02	0.1	0.02	0.06	0.009	0.05	0.008	0.1
	2776.9	425027	0.2	0.7	0.04	0.1	0.05	0.02	0.02	0.003	0.02	0.004	0.009	0.002	0.01	0.001	0.1
5068	2786.6	432598	24.7	57.4	7.0	24.8	5.8	1.3	5.5	0.8	4.3	0.8	2.2	0.3	1.8	0.2	7.1
	2786.9	432870	13.2	26.0	2.8	9.8	2.3	0.5	2.1	0.3	1.6	0.3	0.8	0.1	0.7	0.09	3.5
5098	2803.1	449435	13.8	31.1	3.6	12.4	2.8	0.6	2.8	0.4	2.1	0.4	1.1	0.2	0.9	0.1	4.2
	2803.4	449719	22.1	50.5	5.8	20.3	4.7	1.0	4.6	0.6	3.5	0.7	1.8	0.2	1.6	0.2	7.3
5108	2808.6	455259	6.4	15.0	1.8	6.4	1.5	0.3	1.6	0.2	1.2	0.2	0.7	0.1	0.6	0.08	1.5
	2808.9	455550	7.1	16.5	2.0	7.3	1.9	0.4	1.7	0.3	1.5	0.3	0.8	0.1	0.7	0.08	1.7
5138	2825.1	474273	4.2	9.0	1.0	4.0	1.3	0.3	0.6	0.1	0.7	0.1	0.4	0.05	0.4	0.04	0.9
	2825.4	474576	3.9	8.2	1.0	3.8	1.2	0.3	0.6	0.09	0.6	0.1	0.4	0.04	0.4	0.03	1.01
5148	2830.6	479361	5.4	12.4	1.3	4.3	0.9	0.1	0.8	0.1	0.6	0.1	0.4	0.05	0.3	0.05	0.7
	2830.9	479623	1.1	2.4	0.3	0.9	0.2	0.06	0.2	0.03	0.2	0.03	0.09	0.01	0.08	0.009	0.3
5178	2847.1	491650	0.2	0.4	0.03	0.1	0.05	0.02	0.02	0.003	0.01	0.003	0.009	0.002	0.01	0.001	0.08
	2847.4	491845	0.3	0.8	0.07	0.2	0.07	0.02	0.03	0.005	0.03	0.006	0.01	0.003	0.02	0.003	0.1
5228	2875.6	511071	0.8	1.7	0.2	0.6	0.2	0.04	0.1	0.02	0.1	0.02	0.05	0.008	0.05	0.007	0.2
	2875.9	511267	1.1	2.3	0.2	0.8	0.2	0.05	0.1	0.02	0.1	0.02	0.06	0.008	0.06	0.008	0.3
5278	2902.1	528239	0.7	1.6	0.2	0.6	0.1	0.03	0.1	0.02	0.09	0.02	0.05	0.009	0.04	0.005	0.2
	2902.4	528422	0.7	1.6	0.2	0.6	0.1	0.04	0.1	0.02	0.1	0.02	0.07	0.01	0.05	0.006	0.1
5288	2907.6	532571	8.3	17.6	2.0	7.2	1.7	0.4	1.6	0.2	1.2	0.2	0.6	0.09	0.5	0.07	2.2
	2907.9	532841	4.0	7.3	0.8	2.7	0.6	0.1	0.6	0.08	0.4	0.07	0.2	0.03	0.2	0.02	1.2
5298	2913.1	537923	6.7	13.1	1.3	4.4	1.0	0.2	1.0	0.1	0.7	0.1	0.3	0.04	1.6	0.03	1.7
	2913.4	538194	6.5	14.2	1.5	5.3	1.2	0.3	1.2	0.1	0.9	0.2	0.4	0.06	0.3	0.05	1.8
5328	2929.6	554062	1.2	2.4	0.3	0.9	0.2	0.05	0.2	0.02	0.1	0.02	0.07	0.01	0.06	0.009	0.3
	2929.9	554250	1.7	4.1	0.4	1.5	0.4	0.09	0.3	0.04	0.2	0.05	0.1	0.02	0.1	0.02	0.5
5358	2946.1	562690	0.3	0.6	0.06	0.2	0.09	0.02	0.05	0.008	0.04	0.007	0.02	0.005	0.02	0.003	0.08
	2946.4	562799	0.3	0.7	0.07	0.2	0.1	0.03	0.06	0.008	0.05	0.009	0.03	0.005	0.03	0.003	0.1
5378	2957.1	566577	0.2	0.4	0.04	0.2	0.06	0.02	0.04	0.006	0.03	0.004	0.01	0.003	0.01	0.002	0.04
	2957.4	566671	0.2	0.4	0.04	0.1	0.06	0.01	0.05	0.006	0.02	0.004	0.01	0.003	0.01	0.002	0.06
5418	2979.1	574322	0.4	0.8	0.08	0.3	0.1	0.04	0.07	0.009	0.08	0.01	0.05	0.007	0.03	0.004	0.1
	2979.4	574428	0.2	0.4	0.05	0.2	0.04	0.01	0.04	0.006	0.03	0.005	0.01	0.003	0.02	0.001	0.04
5468	3006.6	591058	0.9	2.0	0.2	0.7	0.2	0.04	0.2	0.02	0.1	0.03	0.07	0.01	0.06	0.008	0.2
	3006.9	591301	1.5	3.4	0.4	1.5	0.3	0.1	0.3	0.05	0.3	0.05	0.1	0.02	0.1	0.02	0.3
5488	3017.6	603812	0.7	1.6	0.2	0.6	0.1	0.04	0.1	0.02	0.1	0.02	0.07	0.03	0.06	0.007	0.2
	3017.9	604150	0.5	1.9	0.1	0.4	0.1	0.04	0.08	0.01	0.06	0.01	0.03	0.007	0.03	0.006	0.1
5508	3028.6	615972	0.5	1.0	0.1	0.4	0.1	0.04	0.08	0.01	0.08	0.01	0.04	0.007	0.03	0.004	0.1
	3028.9	616273	0.5	1.0	0.1	0.3	0.1	0.03	0.07	0.009	0.07	0.01	0.03	0.007	0.03	0.003	0.1
5528	3040.6	631304	9.7	23.7	2.9	10.4	2.3	0.5	2.2	0.3	1.7	0.3	0.9	0.1	0.8	0.09	3.0
	3040.9	631964	10.0	26.2	3.3	12.4	2.7	0.6	2.7	0.4	2.1	0.4	1.1	0.1	0.9	0.1	3.1
5548	3050.6	655109	3.7	8.9	1.1	3.9	0.9	0.2	0.9	0.1	0.8	0.1	0.4	0.05	0.3	0.04	0.7
	3050.9	655611	2.4	5.6	0.6	2.4	0.5	0.1	0.6	0.08	0.5	0.09	0.2	0.04	0.2	0.03	0.4
5568	3061.6	671102	4.9	11.9	1.4	5.2	1.2	0.3	1.2	0.2	0.9	0.2	0.5	0.07	0.4	0.06	1.1
	3061.9	671706	4.7	12.0	1.4	5.2	1.2	0.3	1.2	0.2	1.0	0.2	0.5	0.07	0.5	0.06	0.8

Table V

No	Depth [m]	Age [ky B.P.]	Hg_T [pg g^{-1}]	SD (n=3)	Hg^{2+} [pg g^{-1}]	SD (n=3)	$MeHg^{+}$ [pg g^{-1}]	SD (n=3)
1.	86.9	2,015	2.5	1.2	1.5	0.5	0.32	0.03
2.	229.4	6,949	≤MDL	-	0.8	0.1	0.14	0.01
3	316.3	10,280	5.0	1.5	0.5	0.2	≤MDL	-
4	405.6	14,204	3.3	1.3	≤MDL	-	1.1	0.1
5	419.4	14,910	≤MDL	-	≤MDL	-	0.13	0.01
6	432.9	15,626	2.8	1.2	≤MDL	-	≤MDL	-
7	461.5	17,400	5.9	1.7	0.9	0.1	0.41	0.03
8	471.1	18,133	5.3	1.6	2.1	0.1	0.19	0.01
9	488.7	19,627	8.5	2.1	3.6	0.3	0.26	0.01
10	515.9	21,967	11.2	2.5	9.0	1.3	0.17	0.01
11	574.2	27,033	7.9	2.0	1.3	0.1	0.46	0.06
12	598.4	29,117	5.7	1.6	0.9	0.1	0.24	0.04
13	653.1	33,661	6.2	1.7	1.3	0.3	0.74	0.06
14	654	33,729	13.8	2.9	8.8	0.8	0.14	0.06
15	680.9	35,967	7.2	1.9	15.1	1.2	0.480	0.003
16	708.7	38,135	6.0	1.7	≤MDL	-	0.060	0.004
17	735.6	40,375	5.0	1.5	2.7	0.1	1.42	0.05
18	763.1	42,801	3.0	1.2	0.6	0.1	0.47	0.07
19	818.1	47,175	2.0	1.1	0.40	0.05	0.37	0.05
20	900.9	58,853	≤MDL	-	≤MDL	-	0.3	0.05
21	983.4	60,674	6.4	1.7	6.6	0.5	0.120	0.003
22	1010.9	63,453	7.2	1.9	2.5	0.3	0.31	0.08
23	1093.1	71,637	3.9	1.4	≤MDL	-	0.59	0.07
24	1148.4	76,601	4.9	1.5	5.3	0.8	1.07	0.16
25	1203.1	81,050	2.7	1.2	≤MDL	-	0.070	0.002
26	1258.4	86,028	2.1	1.1	1.3	0.4	0.200	0.003
27	1313.4	91,456	5.0	1.5	3.5	0.5	0.36	0.09
28	1423.4	102,283	≤MDL	-	≤MDL	-	0.24	0.04
29	1533.4	114,142	<MDL	-	0.7	0.2	0.22	0.03
30	1643.4	122,832	1.7	1.0	≤MDL	-	0.14	0.05
31	1753.4	131,892	≤MDL	-	≤MDL	-	0.38	0.05
32	1863.1	151,184	4.9	1.5	0.6	0.03	0.15	0.03
33	1973.4	174,491	2.4	1.1	1.4	0.1	0.77	0.08
34	2050.1	191,286	4.8	1.5	0.8	0.0	0.39	0.09
35	2094.4	198,944	2.6	1.2	0.3	0.1	0.24	0.13
36	2138.4	207,225	≤MDL	-	≤MDL	-	0.65	0.02
37	2368.9	263,649	≤MDL	-				
38	2379.9	267,500	4.2	0.1				
39	2396.4	274,268	5.4	0.5				
40	2407.4	278,777	2.3	0.1				
41	2429.4	286,413	≤MDL	-				
42	2550.4	327,432	≤MDL	-				
43	2561.4	330,083	≤MDL	-				
44	2572.4	332,653	≤MDL	-				
45	2583.4	334,762	4.5	0.2				
46	2605.4	343,403	3.2	0.1				
47	2632.9	358,947	1.8	0.2				
48	2638.4	362,150	2.3	0.1				
49	2649.4	368,303	≤MDL	-				
50	2682.4	385,942	65*	8				
51	2693.4	391,942	≤MDL	-				
52	2720.9	402,741	≤MDL	-				
53	2753.9	414,392	2.7	0.1				
54	2765.9	419,398	≤MDL	-				
55	2776.9	425,027	10.6	1.1				
56	2786.9	432,870	3.3	0.2				
57	2808.9	455,550	7.7	0.4				
58	2825.4	474,576	2.8	0.1				
59	2830.9	479,623	≤MDL	-				
60	2847.4	491,845	≤MDL	-				
61	2875.9	511,267	≤MDL	-				
62	2902.4	528,422	5.6	0.1				
63	2907.9	532,841	≤MDL	-				
64	2929.9	554,250	≤MDL	-				
65	2946.4	562,799	2.2	0.1				
66	2979.1	574,322	≤MDL	-				
67	3017.9	604,150	≤MDL	-				
68	3040.9	631,964	1.9	0.1				
69	3050.9	655,611	3.0	0.1				
70	3061.6	671,102	2.2	0.1				

Table VI

No	Depth [m]	Age [ky B.P.]	EFc	Hg [pg g^{-1}]			
				Hg_{crust}	$Hg_{volcanic}$	$Hg_{sea\ spray} \times 10^8$	Hg_{marine}
1.	86.9	2,015	487	0.001	0.04	2	2.2
2.	229.4	6,949	-	0.001	0.02	2	1.3
3	316.3	10,280	4695	0.001	0.03	1	1.4
4	405.6	14,204	800	0.001	0.04	3	2.0
5	419.4	14,910	-	0.001	0.03	3	1.4
6	432.9	15,626	506	0.002	0.03	3	1.8
7	461.5	17,400	258	0.03	0.05	6	3.0
8	471.1	18,133	146	0.02	0.10	8	5.2
9	488.7	19,627	151	0.10	0.06	7	3.2
10	515.9	21,967	208	0.04	0.05	7	2.8
11	574.2	27,033	155	0.02	0.08	8	4.3
12	598.4	29,117	111	0.04	0.06	6	3.3
13	653.1	33,661	332	0.02	0.05	8	2.5
14	654	33,729	499	0.02	0.06	7	3.2
15	680.9	35,967	338	0.003	0.08	8	4.2
16	708.7	38,135	548	0.003	0.05	6	2.6
17	735.6	40,375	205	0.01	0.05	6	2.5
18	763.1	42,801	223	0.01	0.08	7	4.3
19	818.1	47,175	115	0.01	0.06	7	3.1
20	900.9	58,853	-	0.01	0.06	6	3.2
21	983.4	60,674	222	0.04	0.06	7	3.0
22	1010.9	63,453	132	0.10	0.06	7	3.3
23	1093.1	71,637	925	0.004	0.04	5	2.3
24	1148.4	76,601	359	0.01	0.04	4	2.0
25	1203.1	81,050	503	0.002	0.03	3	1.6
26	1258.4	86,028	176	0.01	0.05	5	2.6
27	1313.4	91,456	1530	0.001	0.04	5	1.9
28	1423.4	102,283	-	0.005	0.03	3	1.7
29	1533.4	114,142	-	0.001	0.03	3	1.5
30	1643.4	122,832	608	0.001	0.03	1	1.7
31	1753.4	131,892	-	0.01	0.05	5	3.0
32	1863.1	151,184	96	0.03	0.05	6	2.9
33	1973.4	174,491	93	0.01	0.05	6	2.9
34	2050.1	191,286	260	0.01	0.05	5	2.5
35	2094.4	198,944	2060	0.001	0.04	3	2.1
36	2138.4	207,225	-	0.001	0.04	3	2.1
37	2368.9	263,649	-		0.04	5	2.3
38	2379.9	267,500	52		0.07	6	3.8
39	2396.4	274,268	47		0.07	4	4.1
40	2407.4	278,777	53		0.07	7	3.6
41	2429.4	286,413	-		0.04	8	2.3
42	2550.4	327,432	-		0.03	2	1.7
43	2561.4	330,083	-		0.03	2	1.8
44	2572.4	332,653	-		0.03	1	1.4
45	2583.4	334,762	1361		0.03	1	1.5
46	2605.4	343,403	70		0.06	7	3.1
47	2632.9	358,947	32		0.06	6	3.2
48	2638.4	362,150	71		0.06	7	3.2
49	2649.4	368,303	-		0.06	5	3.2
50	2682.4	385,942	13910		0.04	3	2.0
51	2693.4	391,942	-		0.04	4	2.3
52	2720.9	402,741	-		0.03	2	1.6
53	2753.9	414,392	1604		0.03	2	1.6
54	2765.9	419,398	-		0.03	2	1.9
55	2776.9	425,027	2953		0.03	2	1.6
56	2786.9	432,870	45		0.07	7	3.8
57	2808.9	455,550	98		0.06	5	3.1
58	2825.4	474,576	179		0.04	5	2.3
59	2830.9	479,623	-		0.04	4	2.0
60	2847.4	491,845	-		0.04	4	2.3
61	2875.9	511,267	-		0.05	5	2.6
62	2902.4	528,422	776		0.05	4	2.5
63	2907.9	532,841	-		0.05	6	2.9
64	2929.9	554,250	-		0.03	3	1.9
65	2946.4	562,799	582		0.04	3	2.3
66	2979.1	574,322	-		0.03	2	1.7
67	3017.9	604,150	-		0.04	4	2.2
68	3040.9	631,964	32		0.06	8	3.3
69	3050.9	655,611	148		0.06	7	3.3
70	3061.6	671,102	52		0.05	5	2.6

Table VII

No	Depth [m]	Age [ky B.P.]	Flux [pg yr^{-1} cm^{-2}]		
			Hg_T	Hg^{2+}	$MeHg^{+}$
1.	86.9	2,015	7	4	0.9
2.	229.4	6,949	-	2	0.4
3	316.3	10,280	16	2	-
4	405.6	14,204	7	-	2.3
5	419.4	14,910	-	-	0.3
6	432.9	15,626	6	-	-
7	461.5	17,400	11	2	0.8
8	471.1	18,133	8	3	0.3
9	488.7	19,627	12	5	0.4
10	515.9	21,967	16	13	0.2
11	574.2	27,033	11	2	0.6
12	598.4	29,117	9	1	0.4
13	653.1	33,661	9	2	1.1
14	654	33,729	21	13	0.2
15	680.9	35,967	11	23	0.7
16	708.7	38,135	10	-	0.1
17	735.6	40,375	7	4	2.0
18	763.1	42,801	4	1	0.7
19	818.1	47,175	3	1	0.6
20	900.9	58,853	-	-	0.5
21	983.4	60,674	10	10	0.2
22	1010.9	63,453	10	4	0.4
23	1093.1	71,637	7	-	1.0
24	1148.4	76,601	9	10	2.1
25	1203.1	81,050	6	-	0.2
26	1258.4	86,028	4	3	0.4
27	1313.4	91,456	10	7	0.7
28	1423.4	102,283	-	-	0.5
29	1533.4	114,142	-	2	0.6
30	1643.4	122,832	6	-	0.5
31	1753.4	131,892	-	-	0.8
32	1863.1	151,184	8	1	0.2
33	1973.4	174,491	4	2	1.2
34	2050.1	191,286	8	1	0.7
35	2094.4	198,944	6	1	0.6
36	2138.4	207,225	-	-	1.6
37	2368.9	263,649	-		
38	2379.9	267,500	16		
39	2396.4	274,268	20		
40	2407.4	278,777	8		
41	2429.4	286,413	-		
42	2550.4	327,432	-		
43	2561.4	330,083	-		
44	2572.4	332,653	-		
45	2583.4	334,762	13		
46	2605.4	343,403	9		
47	2632.9	358,947	5		
48	2638.4	362,150	6		
49	2649.4	368,303	-		
50	2682.4	385,942	168		
51	2693.4	391,942	-		
52	2720.9	402,741	-		
53	2753.9	414,392	7		
54	2765.9	419,398	-		
55	2776.9	425,027	25		
56	2786.9	432,870	8		
57	2808.9	455,550	17		
58	2825.4	474,576	6		
59	2830.9	479,623	-		
60	2847.4	491,845	-		
61	2875.9	511,267	-		
62	2902.4	528,422	11		
63	2907.9	532,841	-		
64	2929.9	554,250	-		
65	2946.4	562,799	4		
66	2979.1	574,322	-		
67	3017.9	604,150	-		
68	3040.9	631,964	3		
69	3050.9	655,611	5		
70	3061.6	671,102	3		

Table VIII

	D.L (ppt)	RSD (%)
V	0.20	22
Cr	0.51	15
Fe	40	9
Co	0.17	12
Rb	0.10	5
Ba	0.08	5
U	0.02	30
Cu	0.46	16
Zn	2.21	8
As	0.95	26
Cd	0.07	21
Pb	0.04	8
Bi	0.04	6
La	0.001	3
Ce	0.001	4
Pr	0.001	5
Nd	0.002	5
Sm	0.004	6
Eu	0.002	6
Gd	0.001	7
Tb	0.001	7
Dy	0.002	6
Ho	0.003	7
Er	0.001	7
Tm	0.001	7
Yb	0.002	9
Lu	0.0004	5

Detection limits ranged from 0.0004 pg/g for Lu to 40 pg/g for Fe. Overall procedural blanks were determined by processing an artificial ice core, made by freezing ultrapure water in which the concentrations of the different elements were known beforehand (Vallelonga et al., 2002). The corresponding contribution was found to be extremely small. Typical precisions in terms of relative standard deviations were found to range from 3% for La to 30% for U.